

DISSERTATION

submitted to the
Combined Faculties for the Natural Sciences and for Mathematics
of the Ruperto-Carola University of Heidelberg, Germany
for the degree of
Doctor of Natural Sciences

presented by
Diplom-Physicist Tobias Kluge
born in Heilbronn

Oral examination:
22.10.2008

Fluid inclusions in speleothems as a new archive for the noble gas palaeothermometer

Referees:

Prof. Dr. Werner Aeschbach-Hertig

Prof. Dr. Augusto Mangini

Zusammenfassung

Fluideinschlüsse in Speläothemen stellen ein einzigartiges Archiv für Paläowässer dar. Diese Arbeit beschäftigt sich mit der Untersuchung der Fluideinschlüsse in Speläothemen bzgl. deren Verwendbarkeit als Paläotemperaturarchiv. Anhand der temperaturabhängigen Löslichkeit verschiedener Edelgase (He, Ne, Ar, Kr und Xe) können Edelgastemperaturen gewonnen werden. Dazu ist die Bestimmung von Edelgaskonzentrationen unerlässlich, welche neben der Bestimmung absoluter Gasmengen auch die Messung der freigesetzten Wassermenge voraussetzt. Es werden zwei Möglichkeiten vorgestellt, mit denen die sehr kleinen, aus dem Gestein extrahierten Wassermengen ($\leq 1 \mu\text{l}$) mit ausreichender Genauigkeit gemessen werden können. Darüberhinaus wurden verschiedene Verfahren zur Extraktion von Edelgasen aus Speläothemen untersucht und in Bezug auf die angestrebte Anwendung analysiert. Als besonders geeignet hat sich das Zerkleinern in einem Stahlzylinder unter Hochvakuum mittels einer magnetisch bewegten Stahlkugel erwiesen. Außerdem werden die Edelgasaufbereitung sowie das auf sehr kleine Gasmengen spezialisierte massenspektrometrische Messverfahren erläutert.

Abschließend wird anhand von 6 Proben aus einer Wachstumsschicht des Stalagmiten BU-U aus der Bunkerhöhle (Sauerland) aufgezeigt, dass es möglich ist, reproduzierbare und glaubwürdige Temperaturen zu berechnen. Die Messungen an weiteren Stalagmiten der Bunkerhöhle (BU-1 bzw. BU-2) ergaben darüber hinaus Temperaturen, die mit den erwarteten klimatischen Bedingungen übereinstimmen. Typische Temperaturunsicherheiten liegen bei diesen Probenstücken zwischen $< 1 \text{ }^\circ\text{C}$ und $2 \text{ }^\circ\text{C}$. An den Stalagmiten BU-U und BU-1 wurden über die Messung von Edelgaskonzentrationen Paläotemperaturverläufe erstellt und in Verbindung mit den stabilen Isotopendaten diskutiert. Diese exemplarischen Anwendungen machen das große Potential der hier vorgestellten Methode deutlich.

Abstract

Fluid inclusions in speleothem constitute a unique archive for palaeo-waters. This thesis deals with the investigation of fluid inclusions in speleothems and their possible use as a palaeotemperature archive. The main objective focuses on the calculation of noble gas temperatures, which can be derived from the temperature-dependent solubility of the noble gases He, Ne, Ar, Kr and Xe. An essential requirement is the determination of noble gas concentrations, which implies measuring the absolute gas amounts as well as determining the amounts of water released. Two ways of measuring the tiny water amounts ($\leq 1 \mu\text{l}$) extracted from the speleothems are presented and will be discussed with regard to the required precision. Furthermore, various techniques for the extraction of noble gases from the speleothems are investigated and analysed in terms of the intended application. It turned out that crushing under vacuum in a steel cylinder by milling with a magnetically movable steel ball is the most suitable technique. Additionally, the noble gas preparation and the mass spectrometric procedure, optimized for the measurement of tiny gas amounts, will be discussed.

Finally, it is demonstrated that it is possible to determine reliable temperatures from fluid inclusions in speleothems and that the acquired results can be reproduced to a certain extent. From the stalagmite BU-U (Sauerland, NW Germany) six samples from one growth period were extracted and measured. Their results agree within the uncertainties although the samples are not totally identical. Measurements on other stalagmites (BU-1, BU-2) from the same cave revealed temperatures corresponding to the expected climatic conditions in the respective growth period. Typical uncertainties for these samples range from $\leq 1 \text{ }^\circ\text{C}$ to $2 \text{ }^\circ\text{C}$ at most. From the stalagmites BU-U and BU-1 a temperature record has been established by noble gas concentrations and will be discussed in combination with the stable isotope data. These exemplary applications reveal the high potential of the method presented.

Contents

1	Introduction	5
2	Theory and basics	9
2.1	Speleothems as a climate archive	9
2.1.1	Speleothem formation and types	9
2.1.2	The importance of speleothems in climate research and possible applications	13
2.1.3	Limitations	15
2.2	Fluid inclusions	16
2.2.1	Definition, origin, properties	16
2.2.2	Applications	18
2.3	Noble gases and common applications	19
2.3.1	Noble gases - occurrence and solubility	19
2.3.2	Temperature determination using noble gas concentrations	21
2.3.3	Further applications	22
2.3.4	Limitations	23
2.4	Noble gases from speleothems as a proxy	24
2.4.1	Studies using noble gases in fluid inclusions of speleothems and minerals	24
2.4.2	Basic idea of climate reconstruction from noble gases in speleothems	25
2.4.3	Objective	26
2.4.4	Constraints	26
2.5	Diffusion of noble gases in speleothems	28
2.5.1	Theoretical background	29
2.5.2	Literature values	31
2.6	Adsorption effects	31
2.7	Goals of this study	35
3	Working with speleothems	37
3.1	Sample selection	37
3.1.1	Optical methods	37
3.1.2	Summary of the thin-section analysis	42
3.2	Water determination	43
3.2.1	Water determination by weighing	44
3.2.2	Water determination by pressure	46
3.2.3	Precision and limits	48
3.2.4	Summary	50
3.3	Extraction of water and noble gases	51
3.3.1	Design of the extraction line	51
3.3.2	Extraction using a metal crusher	54

3.3.3	Extraction by crushing in a copper tube	56
3.3.4	Extraction by microwave heating	60
3.3.5	Extraction by thermal decrepitation	65
3.3.6	Summary	69
3.4	Separation techniques	71
3.4.1	Stepwise crushing	71
3.4.2	Stepwise heating	72
3.4.3	Combined stepwise procedures	75
3.4.4	Summary	78
3.5	Mass spectrometry	78
3.5.1	Gas separation and purification	78
3.5.2	Measurement sequences	79
3.5.3	Calibration	80
3.5.4	Reproducibility and uncertainties	81
3.5.5	Sensitivity	82
3.5.6	Blank values	83
3.5.7	Measurement automation	85
3.6	Mass spectrometric procedures and data evaluation	85
3.6.1	He and Ne measurement	85
3.6.2	Argon measurement	92
3.6.3	Magnet stability and implications for data evaluation	93
3.6.4	Data evaluation	95
3.7	Test of the measurement procedure with an artificial standard	96
4	Results	99
4.1	Cave air and dripwater measurements	99
4.1.1	Investigation of the cave air	99
4.1.2	Dripwater measurements	104
4.2	Extraction	114
4.2.1	Sample selection	114
4.2.2	Water determination and water content	114
4.2.3	Air/water volume ratio	116
4.2.4	Applications	117
4.2.5	Theory of fluid inclusion origin and frequency	124
4.3	Separation techniques	127
4.4	Noble gas fractionation and enrichment	130
4.5	Dating via Helium	134
4.6	Case studies	142
4.6.1	Reproducibility and uncertainties	142
4.6.2	Case study BU-1	148
4.6.3	Case study BU-U	153
5	Summary and outlook	161
	References	164
	Appendix	179
	Abbreviations	179
	List of figures	182
	List of Tables	185

Chapter 1

Introduction

The ten warmest years since 1880 have occurred from 1995 to 2007, of which since 2001 every year has been one of the ten warmest (DWD, 2008; WMO, 2008). Such an accumulation of extraordinary mean annual air temperatures encourage the discussion about global warming and climate change. Not only temperatures are rising significantly compared to the beginning of the last century, but also the content of climate-relevant gases in the atmosphere. The CO₂ concentration is now (2008) at about 385 ppm which is considerably above the highest values at interglacial times (280 ppm) and of the glacial periods (180 ppm) as reconstructed from ice cores from Antarctica (Siegenthaler et al., 2005). Other greenhouse gases like methane are as well far above the values of the last 650 000 years. Today a methane concentration of about 1750 ppb is reached. In glacial and interglacial times the methane level was oscillating between 400 and 770 ppb (Spahni et al., 2005). Such a strong modification of the natural conditions is assumed to cause effects in the whole climate system. To estimate the impact of man-made changes an immense number of climate models has been created and is used to make projections with different greenhouse gas emission scenarios (e.g., HADCM3 - used in IPCC TAR 2001, NCAR-CCSM and the today frequently used ECHAM5 - described by Roeckner et al., 2003).

To achieve plausible results it is necessary to describe the complex climate system as precisely as possible. Therefore, we have to know stable states, unstable transition states, interconnections between the different compartments, the magnitude of the connection and especially the forcings of the system.

Instrumental weather records, in general, only date back to 1850 (Jones and Moberg, 2003) and in exceptional cases back to the 18th century. The instrumental records started e.g. in Austria in some places in the year 1767, s. Auer et al. (2001). Furthermore weather chronologies can be extracted from historical notes, from some hundred to up to some thousand years back in the past (Brázdil et al., 2005). However, the information gets scarce the further we go back in history. For modelling purposes the time span covered by instrumental records is by far not sufficient and additionally it is difficult to derive, from the certainly subjective notations, information about interconnections, stable states and transitions in the historical time scale. Therefore it is imperatively necessary to resort to palaeoclimate data derived from different archives as for example ice cores, marine and lacustrine sediments, stalagmites and tree rings. The more precise this data, the more the archives cover the whole earth and the more it extends over sufficiently large time scales, the better the past climate and especially the climate changes together with forcings and triggers can be inferred and used for future projections.

Although much is known about the interaction between forcings and climate change in principle, its details are mostly left in the dark. Exact timing, temporal and spatial development

and magnitude of such events are basically unknown. For example, most archives sustain dating problems and often it is not possible to transfer the (stable isotope) signals into unambiguous and sufficiently precise temperature information. Speleothems can be dated rather precisely, but often it is also difficult to assign temperatures to the measured isotope data. In this work, supported in the context of the scientific group DAPHNE, we are trying to introduce a new method to determine absolute temperatures using physical principles based on noble gas concentrations in liquids which will overcome the problems of stable isotope data interpretation.

The basic idea

The idea of temperature determination via noble gas measurements (He, Ne, Ar, Kr and Xe) on fluid inclusions (air-, water- or partially water-filled cavities) in calcite precipitates is based on the temperature-dependent solubility. Low temperatures are correlated with a high solubility and a corresponding high gas concentration in the water. Increasing temperatures lead to a decreased solubility and gas concentrations. As noble gases are not affected by chemical reactions, the noble gas concentrations in water are a direct proxy for temperature.

In the case of groundwater the temperature determination using noble gas concentration is a well established method with precise results (uncertainty $<1^{\circ}\text{C}$), but lacks a good temporal resolution as well as a precise dating. In contrast, calcite precipitates in caves, as e.g. stalagmites or stalactites, summarized under the term speleothems, are precisely datable up to 500 kyr with U-Th and further with U-Pb and enable in some cases even seasonal resolution. Due to the commonly present inclusions speleothems constitute a unique archive for palaeowater. In the fluid inclusions, there exist small water amounts which contain noble gases corresponding to the climatic conditions during growth. Measurements of the water amount as well as the dissolved noble gases can give information about palaeotemperatures using the well-known solubility temperature dependence.

In the past some effort has been made to use this promising archive. So far no successful data has been obtained with regard to this objective. However, we have been able to develop a suitable extraction procedure for noble gases and water as well as a sufficiently precise measurement method for the released water and the extracted noble gases, which allowed temperature determination at selected speleothems with an uncertainty of 1°C or even less. The water is determined with a manometrical method and the noble gases are measured by a sector-field mass spectrometer.

The major complication is the presence of air-filled inclusions. In general, they contain noble gases with the typical mixing ratio of atmospheric air delivering no information about palaeotemperatures. Stepwise extraction procedures may enable the application of this method also to samples with a larger air content as it separates air- and water-filled inclusions to a certain extent.

Case studies on samples from Bunker cave in North-Western Germany resulted in reproducible temperatures for a growth layer and yielded reasonable temperature differences between the Early Holocene ($\Delta T - 4.2^{\circ}\text{C}$, 11-12 kyr BP), a warm period during the last Glaciation ($\Delta T - 2.6^{\circ}\text{C}$, 53 kyr BP), and the Eemian ($\Delta T + 3^{\circ}\text{C}$, 125 - 134 kyr BP) compared to more recent values (1.3 kyr BP).

This study shows the potential of noble gas measurements on fluid inclusions for temperature determination and presents methods to achieve the aimed resolution in temperature of better than 1°C .

The experiments

The key to precise temperatures is a suitable extraction. A high extraction efficiency is necessary to obtain water and gas amounts in a measurable range. In addition, low background values as well as a small air contribution to the total noble gas signal have to be achieved. Gases from air-filled inclusions mask the temperature information of the dissolved noble gases. An investigation of different procedures like squeezing in copper tubes, heating with micro waves and crushing with a steel ball under vacuum, revealed that crushing in a cylinder with a steel ball to be the best method. It offers a high efficiency and enables to partially separate the water- and air-filled inclusions by a stepwise crushing procedure in combination with heating. Furthermore the blank can be reduced by preheating and is in general better controllable compared to squeezing in copper tubes.

With regard to the water determination two methods have been investigated. Highest precision in the typical scale (0.1 - 1 mg) can be achieved by a manometrical method, measuring the water vapour pressure in adequate and calibrated volumes.

Outline

First an overview over the different forms of speleothems and their importance in climate research is given. The fluid inclusions are of major importance in this project and are presented in the subsequent section. The second part of the first chapter focuses on noble gases, their occurrence, their solubility as well as possible applications in the different research fields. Especially, we discuss the constraints for precise temperature determination via noble gas measurements. Diffusion and adsorption can influence the results and are also briefly discussed.

In the third section of this work the main elements for successful noble gas studies on speleothems are presented. The first part explains which samples are suitable and how they can be selected in advance using simple inspection by eye and microscopy. The following part investigates two ways of water determination in the mg range and their advantages as well as their disadvantages. The main part presents several methods for gas and water extraction as well as stepwise procedures. Finally an overview on the basics of gas processing, mass spectrometric measurement and data evaluation is given. Problems related to the mass spectrometric measurement and the use of artificial standards are briefly discussed.

The last section presents the main results covering sample selection and extraction methods. In a special section the results of noble gas measurements of cave air, drip water and water from a cave pond are described. The effect of stepwise extraction for separation of water- and air-filled inclusions is discussed on exemplary data. Radiogenic He and the water content exhibit interesting features with regard to dating, respectively paleoclimate and are also presented in this chapter. The main part is focused in the temperature determination and discusses several case studies. The first gives an overview over repeated measurements on a growth layer with regard to reproducibility of temperature. The second case study presents temperature values over a large part of the Holocene and compares them with published data. Finally, paleotemperatures are given for the Eemian, a period during the last Glaciation and the Early Holocene, and are compared to published studies. Furthermore, they are discussed in combination with the stable oxygen and carbon isotopes obtained from the same stalagmite. The chapter is closed with a short summary and a brief outlook for future research related to this topic.

Chapter 2

Theory and basics

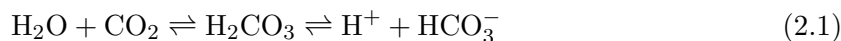
2.1 Speleothems as a climate archive

In the last decade the importance of speleothems as a climate archive has strongly increased. Due to new techniques such as laser ablation and improved detection processes even annual resolution can be achieved for stable isotopes and trace elements. Their use in the climate reconstruction as well as advantages and limits will be discussed in the following sections.

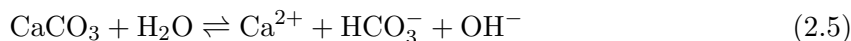
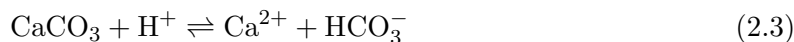
2.1.1 Speleothem formation and types

In caves not only stalactites and stalagmites are abundant, there also exist flowstones, soda straws and lots of other types of precipitated calcite (Fig. 2.2). In this chapter the different species of speleothems together with their formation will be presented.

Speleothems are formed by precipitation of carbonates inside the cave. Rain water can absorb large amounts of CO₂ while percolating through the soil, as the CO₂ partial pressure is very high (about 0.1 atm, see White, 1976) in the soil air. Meanwhile carbonic acid is produced according to the following balance reactions, the first one is important for low pH-values, where the second equation is valid for pH ≥ 7 (see Buhmann and Dreybrodt, 1985):



The elevated content of carbonic acid in the water dissolves calcium carbonate from the host rock and soil material. This process can be described by the so-called Plummer-Wigley-Parkhurst equation (Plummer et al., 1978):



In the cave itself the CO₂ partial pressure is higher than in ambient air, e.g. 1.5 · 10⁻³ atm like in Obir Cave (Spoetl et al., 2005), but in general rarely above 3 · 10⁻³ atm (White, 1976) and thus significantly lower than in the soil air. Therefore, reactions are shifted towards the left side. The water is supersaturated in carbonate and precipitation of calcite occurs.

According to growth conditions and water composition different crystals are formed. The most common type is calcite, other more rare forms are aragonite and dolomite. Aragonite is

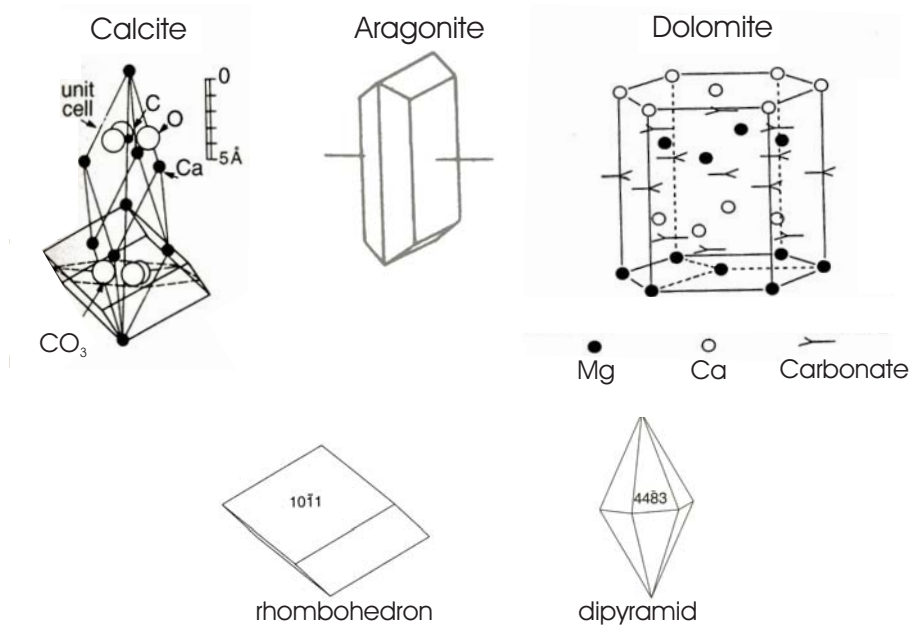


Figure 2.1: In the upper row the unit cell configuration of calcite and dolomite as well as the form of an aragonitic crystal is shown (adapted from Ford and Williams, 2007). Below, possible ideal configurations of calcite as e.g. the rhombohedron and the dipyramidal configuration are displayed. Three others configurations are also possible: pinacoid, prism and scalenohedron (adapted from Ford and Williams, 2007). Images of crystals which grew under laboratory conditions and in cave environment can be found in Fig.2.3 and Fig.2.6 respectively.

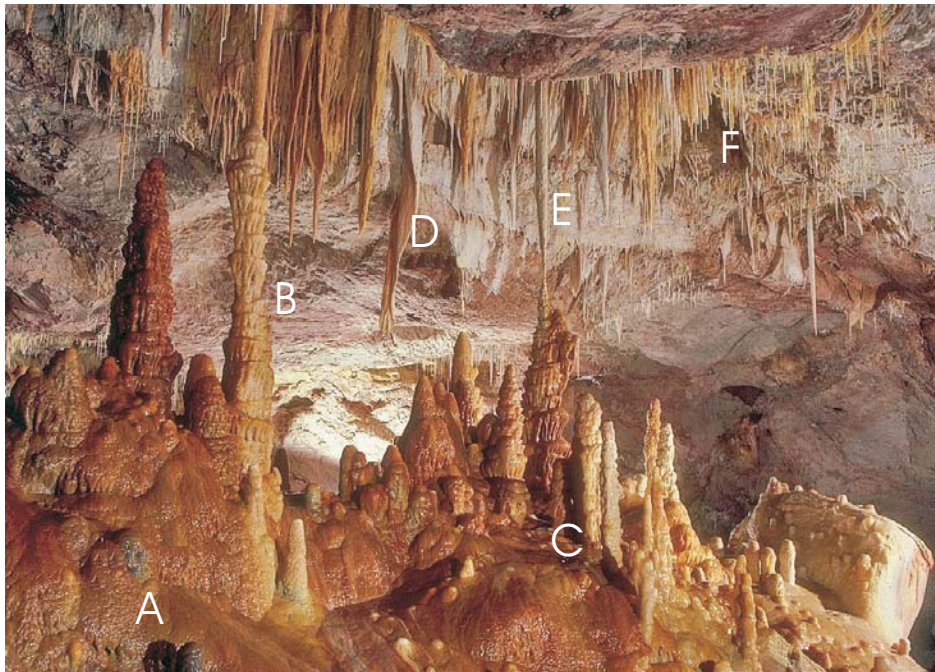


Figure 2.2: Selection of common speleothem forms in a cave. A: flowstone, B: stalagmite column, C: stalagmites, D: drapery, E: stalactites, F: soda straws. Modified from a photo of Bunnell (2006).

the high-pressure polymorph of CaCO_3 and is supposed to be the third most common cave mineral (the second being gypsum, White, 1976). At typical cave temperatures, its solubility is about 11% higher than for calcite. Dolomite is an ordered structure in close relation to calcite, but with alternating layers of magnesium and calcium (White, 1976). Actively forming dolomite has rarely been observed. Therefore, in the following we focus on the most common type, the calcite minerals.

Typical properties of the three carbonates are listed in Table 2.1 and the according mineral forms are displayed in Fig. 2.1.

Table 2.1: Properties of the carbonate species calcite, aragonite and dolomite. Data from Ford and Williams (2007).

mineral	chemical composition	specific weight (g/cm^3)	hardness (Mohs scale)	crystal type
Calcite	CaCO_3	2.71	3	rhombohedral
Aragonite	CaCO_3	2.95	3.5 - 4	orthorombic, dypramidal
Dolomite	$\text{CaMg}(\text{CO}_3)_2$	2.85	3.5 - 4	hexagonal, rhombohedral

Speleothems can be distinguished in 3 different groups:

- dripstone and flowstone forms
 - stalactites
 - stalagmites
 - draperies
 - flowstone sheets
- erratic forms
 - shields
 - helictites
 - botrioidal forms
 - anthodites
 - moonmilk
- sub-aqueous forms
 - rimstone pools
 - concretions
 - pool deposits
 - crystal linings

The most important group is the first one. Stalagmites are the most prominent speleothems due to their simple stratigraphy. They are built on ground by water dripping on top and thus growing up to the cave ceiling. The older parts are always below the younger layers. The stalagmite growth is strongly correlated to temperature and the amount of carbon dioxide available in the soil (Kaufmann, 2003) as well as the content of calcium in the dripwater (Genty et al., 2001). In a cave in England growth rates ranging from 0.04 to 0.16 mm yr^{-1} are reported with a mean of 0.077 mm yr^{-1} , in a cave in France 0.2 - 0.9 mm yr^{-1} and in a artificial tunnel in Belgium of up to 1.3 mm/a (Baker et al., 1998). Genty et al. (2001)

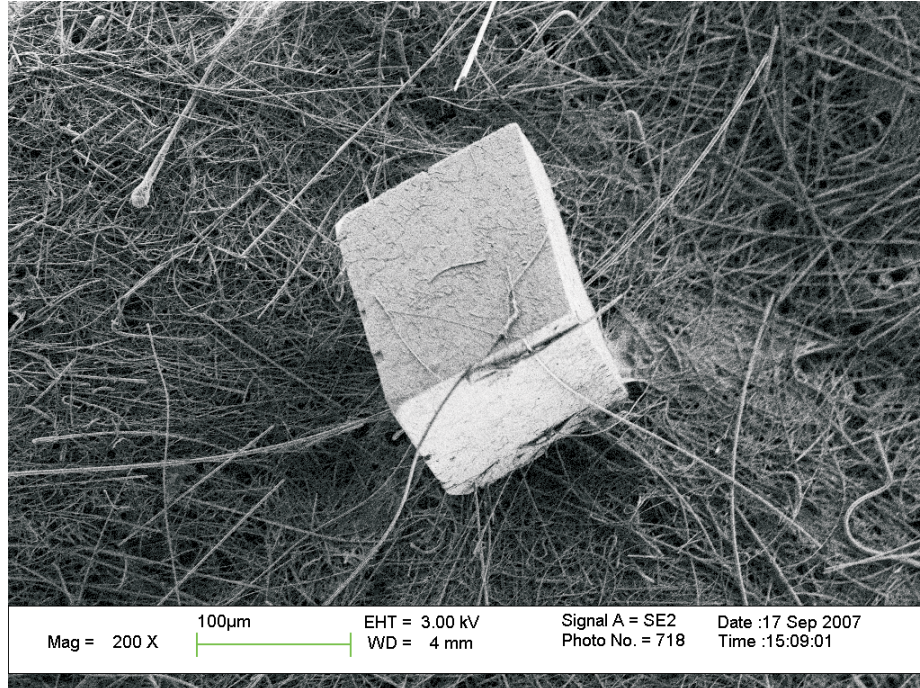


Figure 2.3: SEM image of a calcite which grew in a channel experiment under controlled and constant laboratory conditions. The image was made at the Faculty of Chemistry of the University of Heidelberg.

reported similar values from six caves in Europe with a maximum growth rate of 1.5 mm yr^{-1} . The stalagmite shape varies due to the calcite deposition process. An increased drip rate leads to a larger stalagmite diameter (Franke, 1965). For drip intervals $\geq 1000 \text{ s}$ a minimum equilibrium diameter of about 4 cm is established (Kaufmann, 2003; Curl, 1973). Other effects like drip fall height (Gams, 1981) also influence the shape as well as temperature and soil CO_2 variations. A uniform diameter implies constant growth conditions over a long time period. Terraces suggest periodic variations and a conical style implies a decrease in drip rate (White, 1976). However, due to the complex interdependence of stalagmite stratigraphy and palaeoclimate it is not possible to infer the climate information only from shape- and growth information (Kaufmann, 2003).

The inverse form of stalagmites, which grow from the top of the cave to the bottom, are stalactites. As sometimes the water is flowing through the stalactite core, it is difficult to estimate the age of different growth layers. Sections cut perpendicular to the growth axis usually show structures analog to tree rings which is due to the additional flow at the outside of the stalactite. As the water flow channels are quite large, sand grains and other material can be transported as well. Blockage due to this matter transport can form stalactites with a complicated growth history. The size of stalactites is limited by weight.

Soda straws or soda stalactites are long and thin calcite tubes. The water percolates through these tubes, and a small amount of mineral material is deposited as a ring similar to the drop diameter. The soda straw is growing downwards and also on the outside, because water can seep between boundary layers. If the central channel is blocked, the water is forced to flow on the outer side and a conical stalactite may be formed.

Another group of speleothems which can be dated rather well are flowstones. They form in places where water is flowing over cave walls. According to the pathways different shapes like

flowstone cascades, draperies and "bacon-strip" forms can occur. Growth rates reported from three sites in southeastern England range from 0.009 to 0.05 mm yr⁻¹ (Baker and Smart, 1995), which is about one order of magnitude less than the mean of most stalagmites.

Subaqueous forms, like pool deposits may be a very well suited speleothem for inclusion measurement, as they grew below the water surface. Therefore, few air-filled inclusions can be expected. The water-filled inclusions may be predominant. Due to CO₂ loss from the pool surface, water can be supersaturated and lead to calcite precipitation. Growth is most rapid near the water surface as this is where the loss of CO₂ and the strongest supersaturation occur.

Due to their shapes, the erratic forms can hardly be used for palaeoclimatic purposes. It will be rather difficult to address representative ages to such a speleothem. However, these special calcites show interesting forms. The helictites for instance grow in curved respectively spiraled paths. In case of helictites the crystal growth is dominant. The crystallization follows the fast growing mineral axis of the calcite. The rapid changes in growth directions are caused by blockage of the drip channel through clastic material. Similar but larger as the helictites are eccentric stalactites. Botryoidal forms are globular protuberances on the cave walls. Anthodites are chunks of crystalline aragonite growing radially.

2.1.2 The importance of speleothems in climate research and possible applications

Speleothems constitute a unique archive for climate information on continents due to their properties and also due to the environment in which they grow. The cave itself is protected against direct human influence and against fast erosion, and is therefore able to conserve information about the past climate even in urbanized or heavily polluted areas.

Speleothems offer a variety of environmental tracers like stable isotopes, trace elements and trapped pollen grains as well as parameters such as inter-annual thickness variation of growth-laminae, growth rate changes, organic acid content and dust layers. Mostly, stable isotope signals are used in combination with precise dating to estimate the onset and duration of climate events, such as the transition from glacial to interglacial, Dansgaard-Oeschger oscillations or short-term climate changes with high amplitudes like the 8.2 kyr event. Even growth rates provide information about the climate. In glacial times the growth rate slows down and, for instance, during Marine Isotope Stage 2 no calcite precipitation is found on the Northern Hemisphere ($\geq 35^\circ$ N). Often slower growth rates can be related to a cooler climate (compare review of McDermott, 2004).

This data gains importance with the increasing use of global circulation models. The information from speleothems can be added to the data from ice-cores, marine and lacustrine sediments, pollen and tree rings to test and validate the models. Well dated speleothems exhibit a high potential in refining the chronology of high-latitude ice-cores, as many of the stable isotope features are also found in speleothems (Spoetl and Mangini, 2002). Furthermore, they can give insight into forcing and feedback mechanism of the global climate system. Short-term changes like the 8.2 kyr event or the Medieval Warm Period as well as major climate changes are saved in the isotopic composition of the growth layers. As there has been proven annual lamination in some stalagmites (Frisia et al., 2003), it is possible to derive high resolution data from speleothems. With laser-ablation gas chromatography isotope ratio mass spectrometry (LA-GC-IRMS) a spatial resolution of 250 μm can be achieved (McDermott et al., 2001), which corresponds to 4 years at a mean annual growth rate of 80 μm . Even better resolution was achieved by Frappier et al. (2002) with about 20 μm using micro-milling. Similar resolution can be obtained by ion microprobe techniques (Kolodny et al., 2003). In addition, this archive provides samples over time spans of thousands of years up to some

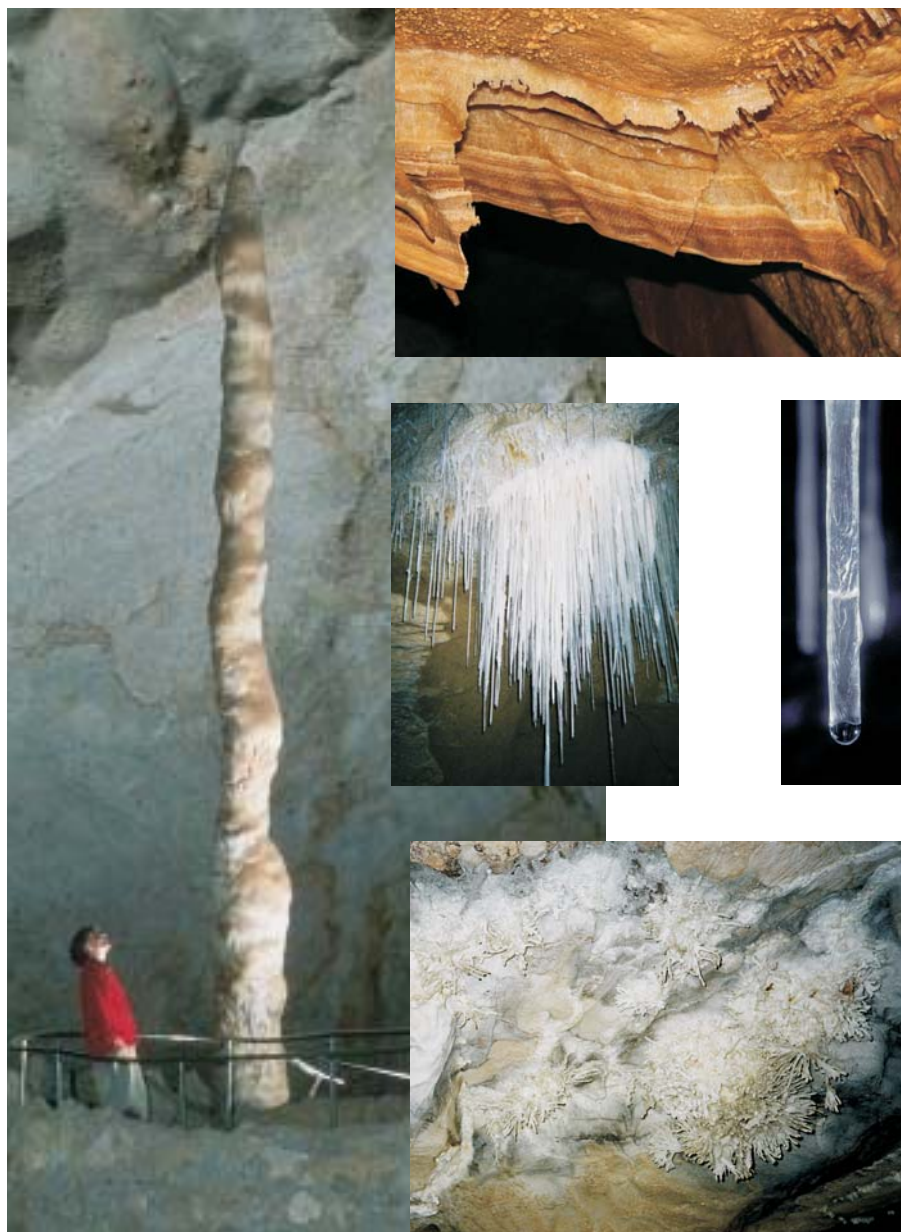


Figure 2.4: Picture of different speleothem forms. On the left side a huge stalagmite ('witchs finger' in the Carlsbad Cavern) can be seen. The upper picture on the right side shows a flowstone drapery, in the middle soda straws and on the bottom some helictites have been photographed.

hundred thousand years. So in principle speleothems can cover the whole range of the earth's climate, which is governed by the glaciation - deglaciation pattern with a 100 kyr period.

In caves the temperature is typically rather constant throughout the year. The recorded temperature signal reflects the mean annual air temperature of the cave region (McDermott, 2004; Genty et al., 2002). However, common studies focus on the precise estimation of timing and duration of major stable isotope-defined climatic events as it is hardly possible to achieve unambiguous temperatures due to kinetic fractionation effects and difficult relations between the absolute values of stable isotopes and environmental parameters at a certain sample site. As a new and independent proxy, noble gases in fluid inclusions of speleothems will be used to determine absolute temperatures and temperature differences between different climatic periods. Speleothems can become one of the most important climate archives as they can provide precise dating and unambiguous temperatures using noble gas measurements. In combination with the high-resolution stable isotope data it may be possible to reconstruct the past climate in a complete way.

2.1.3 Limitations

The use of stable isotopes and to some extent that of trace elements is restricted as the reason for changes in isotope data sometimes is difficult to figure out. Some solutions are ambiguous, and only in very few cases it is possible to assign a signal change in stable isotopes directly to a change in temperature. The change in stable isotopes could be caused by a set of factors e.g. changes in the isotopic composition of the precipitation or changes in the isotope fractionation during calcite deposition. $\delta^{18}\text{O}$ and δD can be influenced by changes in the moisture source, changes in the $\delta^{18}\text{O}$ value of the ocean surface due to increased or decreased continental ice volume, changes in the fraction of non-oceanic precipitation or by an increased or decreased amount effect (McDermott, 2004). Even if vegetation changes above the cave, a feedback in isotope data can be expected.

However, with an independent temperature calculation, using noble gases from fluid inclusions, it should become feasible to derive the different components of the total isotope signal, to assign a certain signal variation to the temperature change and to changes in the moisture source and the type of precipitation as well as to modifications of land cover and calcite precipitation.

For very old stalagmites the archive is limited in dating. The uranium - thorium method can only be used for up to 500 000 years. If the stalagmite is older than 300 kyrs or 400 kyrs, the precision in dating gets smaller or it even gets impossible to determine a reliable age. Nevertheless, using the helium data from the noble gas measurements, a rough age estimation may be possible. Furthermore, geochronological methods like U/Pb (Richards et al., 1998; Polyak et al., 2008) and possibly U/He may be applied as well.

2.2 Fluid inclusions

In this section origin, composition and properties of fluid inclusions in stalagmites are explained. Furthermore, possible and actually performed applications are presented.

2.2.1 Definition, origin, properties

Fluid inclusions are microscopic cavities within a crystal, filled with gas or liquids or with a mixture of both. Fluid inclusions are present in approximately all minerals as they formed mostly in presence of liquids or came into contact with liquids when fractures were built or healed (Roedder, 1984). Even in certain meteorites liquid inclusions are reported (Zolensky et al., 1999; Bodnar and Zolensky, 2000).

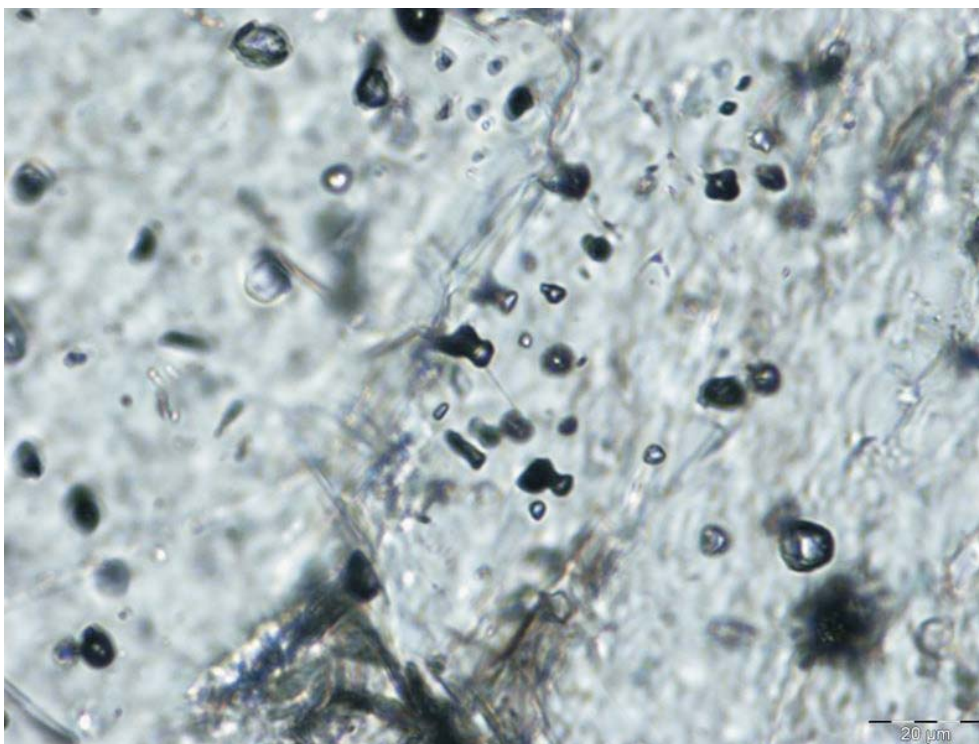


Figure 2.5: Thin section of a sample from the stalagmite H12 from Oman. The dark irregular shaped inclusions are assumed to be only air-filled. The light-reflecting, round or ellipsoidal inclusions are water-filled.

Fluid inclusions are in general very small, about some μm and in rare cases up to $50 \mu\text{m}$. Generally they are ellipsoidal or sausage shaped and are frequently distributed inhomogeneously (Schwarcz et al., 1976). Zones with a high abundance of water-filled inclusions are milky white (Genty et al., 2002), especially in the case of a coarse crystalline type. In these samples about 10^9 inclusions/ cm^3 are assumed (Roedder, 1984). Fluid inclusions typically constitute trace amounts up to 3 ‰ of the total speleothem sample weight (Serefiddin et al., 2002), written as ‰ wt. In addition to the liquids in fluid inclusions, water molecules can be trapped along grain boundaries or even in the calcite matrix and may contribute to the released water in special extraction steps like, for example, strong heating.

Water-filled fluid inclusions in speleothems are typically generated by entrapment of water in voids inside the crystal granules. Scheidegger et al. (2007a) reported that they found water-filled inclusions always to be located inside the calcite crystals. Furthermore, most

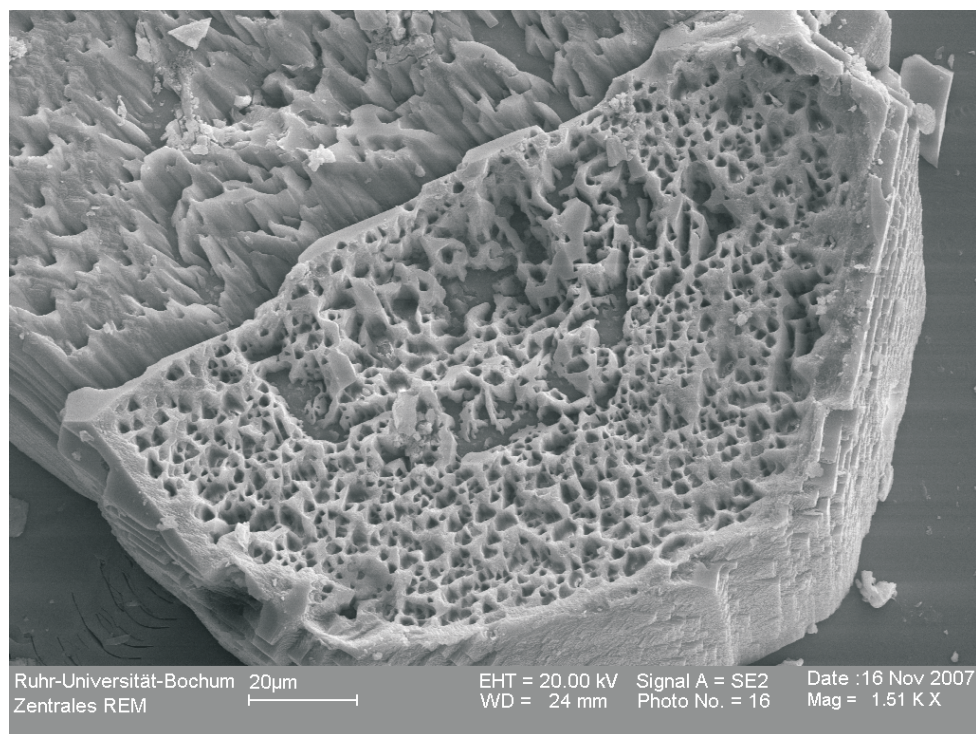


Figure 2.6: SEM image of a single calcite crystal, which grew in the Bunker Cave on a glass plate within one year. Picture with courtesy by Dr. R. D. Neuser / D. Riechelmann.

of the water-filled inclusions seem to contain a gas-filled bubble. As air-filled inclusions are different in their location (in general between the calcite crystals) and size (20-60 µm, Scheidegger et al., 2007a) it may be possible to separate the two fractions by adequate extraction techniques (Scheidegger et al., 2007b).

The speleothem is formed due to the degassing of CO₂ from the carbon saturated water (further details: see Schwarcz (1986); Ford and Williams (1989)). Typically, the cave interior shows a high humidity and therefore evaporation can be neglected. Thus, the enclosed water in fluid inclusions reflects the characteristics of dripwater. As the dripwater normally shows negligible salinity this can be assumed as well for fluid inclusions.

A considerable difference of calcite growth under laboratory conditions and natural conditions can be seen with regard to the shape the calcite establishes and the deviation from the expected shape. In laboratory very regular crystals with a precisely defined shape are detectable (Fig.2.3), whereas in the cave the crystals show strongly different behaviour. As it can be seen on the SEM image of a calcite sample from Bunker Cave (s. Fig.2.6) there is an overall crystalline feature combined with an unexpected crater type pattern, possibly referring to micro-crystalline growth. The little holes are in general very small (some µm) and scattered over the whole surface. Comparing their size to the typical inclusion dimension, it gives the impression that these holes might be the preceding structure responsible for the amount and size of the fluid inclusions.

With respect to the spatial distribution of fluid inclusions, thin section analysis is a useful tool. In many thin sections a sequence of inclusion-rich and inclusion-free layers can be detected. In Fig. 3.2 we can see on the upper left side a significant change in the inclusion pattern from an area with few and large inclusions to an area dominated by bands of rather small inclusions. A similar pattern showing a change between inclusion-rich and inclusion-free layers can be seen in Fig. 3.3.

According to this, the reason for such patterns is an interesting question. Brook et al. (1999) investigated two stalagmites which showed a strong layered pattern. By using Sr isotopes they proved that inclusion-poor layers are correlated with a slow calcite precipitation and inclusion-rich layers with faster precipitation. In accordance with this data, they derived a similar correlation using the MgCO_3 content of the calcite. Inclusion-poor layers are correlated with low MgCO_3 and the inclusion-rich parts with a higher MgCO_3 - value. Higher MgCO_3 content is related with a faster precipitation caused by an increase in the saturation state (Goldstein and Reynolds, 1994). Brook et al. (1999) concluded from their data, that the inclusion-rich layers are deposited during dry seasons and the inclusion-poor layers during wet seasons. Similarly, Genty and Quinif (1996) interpreted couplets of dark and light laminae as annual cycles caused by differences in the water excess. Thus, it is possible to derive information about the climatic conditions from the chronology of different layers. Furthermore, this argument can be turned around and can be used for the search for adequate samples with a high content of inclusions.

2.2.2 Applications

As the fluid inclusions preserve information about the environment at time of enclosure, they are used to derive this unique data from the past.

In stratigraphy and sedimentation they are used to identify the provenance of detrital grains in sandstone, quartzite and conglomerate; in geology for studies concerning the petrogenesis and the tectonics, for instance to trace erosion and uplift; in astrophysics to reconstruct extraterrestrial or possible early terrestrial processes from lunar and meteoritic samples. Furthermore, fluid inclusions are applied in the search for oil as they can provide information about the tectonics and pressure-temperature evolution of the oil-bearing basin. Even in security investigations of nuclear waste and nuclear reactor sites they can provide data about the properties of the underlying rocks, for instance, the last movement of faults at this site (for more detail see Roedder, 1984).

In the field of climate research some attempts have been made to derive information about precipitation and temperature. Most of the studies focused on stable isotope signals in fluid inclusions and not on noble gases. In the last decade remarkable advances in extraction and measurement techniques had been achieved with regard to the stable isotopes. Therefore, it was possible to derive reliable stable isotope data from fluid inclusions (Matthews et al., 2000; Dennis et al., 2001; Genty et al., 2002; Serefiddin et al., 2002; McGarry et al., 2004; Zhang et al., 2008). However, it is rather difficult to extract and especially to collect the released water entirely, if the extraction is not performed under vacuum conditions. Due to adsorption of water molecules significant fractionation of the stable isotopes can occur. Furthermore, the measured isotopic signal may not only reflect undisturbed dripwater, but can also be influenced by a post-depositional isotopic exchange with the host calcite (Schwarcz et al., 1976; Wilkinson, 2001).

Some pilot projects have been performed to assess the potential of entrapped air in fluid inclusions in order to reconstruct palaeoclimatic conditions. Scheidegger et al. (2007b) and Badertscher et al. (2007) investigated N_2 , O_2 , N_2O and Ar as well as the gases methane and carbon dioxide using dynamic mass spectrometry. Methane and the CO_2 -concentration may be of special interest in the air-filled inclusions. As they have been closely related to the climatic cycles, their concentration development along the growth axis may give valuable insights into timing and evolution of the signals as well as the connection between temperature change and variations in the methane respectively CO_2 level.

With regard to noble gas measurements on fluid inclusions aiming at temperature determination few studies have been published (Böhlke and Irwin, 1992b; Stuart and Turner, 1992; Scheidegger, 2005) or presented on conferences (Scheidegger et al., 2007b, 2006). This may be due to the fact that nobody has successfully derived absolute noble gas temperatures with palaeoclimatic implication from speleothem fluid inclusions so far. In this thesis, the method for a successful noble gas analysis and temperature calculation as well as the results of the most striking measurements are presented.

2.3 Noble gases and common applications

In this section the basics about noble gases and their applications in the research field of palaeoclimatology will be presented. Noble gases are widely used in groundwater research in order to investigate flow regimes and residence times on the one hand and on the other hand to deduce information about the past climate.

2.3.1 Noble gases - occurrence and solubility

Noble gases owe their name due to their chemical inert behaviour. They build only very few real compounds, otherwise they normally exist in atomic form. The commonly used noble gas isotopes in palaeoclimate and dating studies are ^3He and ^4He , ^{20}Ne and ^{22}Ne , ^{36}Ar , ^{40}Ar , Kr- and Xe-isotopes with high abundances like ^{84}Kr and ^{132}Xe and the short-lived ^{222}Rn .

The standard and reference for noble gas measurements is the terrestrial atmosphere. Typical atmospheric mixing ratios, which are assumed to have stayed constant over the last million years, are shown in Table 2.2. Water samples in equilibrium with the atmosphere yield noble gas concentrations corresponding to these values and the solubility of each isotope. However, in some samples different values can be found. ^3He , ^4He and ^{222}Rn are formed by radioactive decay or other nuclear processes and can therefore show an excess in older samples compared to equilibrium values. Radon itself is also radioactive and decays further; the other mentioned noble gases are stable.

Beyond the atmospheric abundance, neon can be formed by nucleogenic reactions in the crust or mantle (Yatsevich and Honda, 1997). The fraction of neon due to this source is related to the radio-element and target-element concentration. The present-day production rate for ^{20}Ne lies at about $1.4 \cdot 10^{-23}$ ccSTP $\text{yr}^{-1}\text{g}^{-1}$ in mantle and $1.5 \cdot 10^{-21}$ ccSTP $\text{yr}^{-1}\text{g}^{-1}$ in crustal material and in the case of ^{22}Ne $1.5 \cdot 10^{-24}$ ccSTP $\text{yr}^{-1}\text{g}^{-1}$ in mantle-, respectively $5.2 \cdot 10^{-21}$ ccSTP $\text{yr}^{-1}\text{g}^{-1}$ in crustal material (Leya and Wieler, 1999).

As in the case of neon, argon may have contributions beyond the atmospheric reservoir. ^{40}Ar production is dominated by ^{40}K decay and therefore proportional to the potassium concentration. About 102 atoms ^{40}Ar are produced in this way per μg of K and year (Ballentine and Burnard, 2002). ^{36}Ar production can be neglected compared to the background of ambient ^{36}Ar .

Krypton and xenon are rare noble gases in the environment and are typically dominated by the constant atmospheric abundance. However, ^{84}Kr and ^{132}Xe can also be produced to a very small extent by fission of ^{238}U . Besides this dominant process, fission of ^{232}Th and ^{235}U can be a further production path. The present day crustal production rate for ^{84}Kr ($2.1 \cdot 10^{-23}$ ccSTP $\text{yr}^{-1}\text{g}^{-1}$) is about 10 orders, for ^{132}Xe ($5.2 \cdot 10^{-22}$ ccSTP $\text{yr}^{-1}\text{g}^{-1}$) about 9 orders of magnitude smaller compared to the production rate of ^4He of $3.3 \cdot 10^{-13}$ ccSTP $\text{yr}^{-1}\text{g}^{-1}$ (g referred to one gram of crustal material). Even compared with ^{40}Ar it is about 10 respectively 8 orders of magnitude smaller (Ballentine and Burnard, 2002). In the case of samples with no extraordinary composition (e.g. high uranium contents) and a moderate age, all nucleogenic as well as the fissiogenic contributions to the measured signals can be neglected.

Table 2.2: Atmospheric mixing ratios of noble gases (compare Ozima and Podosek (2001) or Porcelli et al. (2002))

isotope	volume mixing ratio
^3He	$7.33 \cdot 10^{-12}$
^4He	$5.24 \cdot 10^{-6}$
^{20}Ne	$1.645 \cdot 10^{-5}$
^{21}Ne	$4.872 \cdot 10^{-8}$
^{22}Ne	$1.678 \cdot 10^{-6}$
^{36}Ar	$3.14 \cdot 10^{-5}$
^{40}Ar	$9.30 \cdot 10^{-3}$
^{84}Kr	$6.50 \cdot 10^{-7}$
^{132}Xe	$2.34 \cdot 10^{-8}$
^{222}Rn	$\sim 6 \cdot 10^{-20}$

As the atmospheric noble gas mixing ratio is constant, valuable information can be deduced from noble gases dissolved in water, for instance from groundwater or even from fluid inclusions in speleothems. At equilibrium, the dissolved concentration (C_i^{water}) of a noble gas i in water is proportional to the concentration in the gas phase (C_i^{gas}) as it is described by Henry's law:

$$C_i^{\text{gas}} = H_i(T, S) \cdot C_i^{\text{water}} \quad (2.6)$$

The proportionality factor H_i , called Henry coefficient, inversely describes the solubility of the gaseous element in the fluid and depends on temperature T and salinity S and is different for each gaseous element i . Furthermore the equilibrium concentration $C_{i,\text{eq}}^{\text{water}}$ of water in contact with air is dependent on the atmospheric pressure p . Therefore the atmospheric equilibrium concentration C_i^* is often used, which is the dissolved concentration of a gas i in water at equilibrium with vapour saturated air at a total pressure of $p_0 = 1$ atm:

$$C_i^* = \frac{p_i^{\text{atm}}|_{p=p_0}}{H_i(T, S)} = \frac{(p_0 - e) \cdot z_i}{H_i(T, S)} \quad (2.7)$$

p_i^{atm} is the partial pressure of the corresponding noble gas i , e the saturation vapour pressure and z_i the volume fraction of the gas in dry air (s. Table 2.2). The Henry coefficient H_i is not dependent on the pressure p , but as mentioned above the equilibrium concentration $C_{i,\text{eq}}^{\text{water}}$ changes with pressure. The complete formula is then:

$$C_{i,\text{eq}}^{\text{water}} = \frac{(p_0 - e) \cdot z_i}{H_i(T, S)} \cdot \frac{p - e}{p_0 - e} = \frac{(p - e) \cdot z_i}{H_i(T, S)} \quad (2.8)$$

The solubility strongly depends on temperature. As temperature increases the solubility decreases. This effect is most pronounced for the heavy noble gases. A temperature change from 0°C to 30°C reduces the solubility of e.g. He by only 11%, whereas it is about 63% in case of Xe.

Normally the salinity plays a minor role as typical groundwater has a negligible salt content. The effect of salinity on the solubility is also stronger for the heavier noble gases, but the difference between light and heavy elements is less pronounced. He solubility is reduced by about 0.5% per g of salt in 1 kg water, in case of xenon it is about 0.67 % per g of salt in 1 kg water.

As described in the last equation, $C_{i,\text{eq}}^{\text{water}}$ is directly proportional to the ratio of the actual pressure and to p_0 in case of dry air. The pressure p changes according to the barometric

Table 2.3: Noble gas concentrations of water equilibrated with atmospheric air at a pressure of 1013.25 mbar and no salinity. Data calculated using solubilities of Weiss (1971) for He and Ne, of Weiss (1970) for Argon and of Weiss and Kyser (1978) for Kr. Xenon concentrations are calculated using the data presented by Clever (1979). Rn - values are corresponding to an air activity concentration of 1 Bq/m³ and solubilities given by Weigel (1978).

isotope	noble gas concentration in cc/g at			
	0°C	10°C	20°C	30°C
³ He	6.66·10 ⁻¹⁴	6.32·10 ⁻¹⁴	6.09·10 ⁻¹⁴	5.94·10 ⁻¹⁴
⁴ He	4.90·10 ⁻⁸	4.65·10 ⁻⁸	4.48·10 ⁻⁸	4.36·10 ⁻⁸
²⁰ Ne	2.04·10 ⁻⁷	1.83·10 ⁻⁷	1.68·10 ⁻⁷	1.56·10 ⁻⁷
²² Ne	2.08·10 ⁻⁸	1.86·10 ⁻⁸	1.71·10 ⁻⁸	1.59·10 ⁻⁸
²¹ Ne	6.03·10 ⁻¹⁰	5.41·10 ⁻¹⁰	4.96·10 ⁻¹⁰	4.61·10 ⁻¹⁰
³⁶ Ar	1.68·10 ⁻⁶	1.30·10 ⁻⁶	1.05·10 ⁻⁶	8.74·10 ⁻⁷
⁴⁰ Ar	4.96·10 ⁻⁴	3.85·10 ⁻⁴	3.11·10 ⁻⁴	2.59·10 ⁻⁴
⁸⁴ Kr	7.07·10 ⁻⁷	5.19·10 ⁻⁸	3.97·10 ⁻⁸	3.15·10 ⁻⁸
¹³² Xe	5.18·10 ⁻⁹	3.54·10 ⁻⁹	2.56·10 ⁻⁹	1.93·10 ⁻⁹
²²² Rn	9.03·10 ⁻¹⁵	6.22·10 ⁻¹⁵	4.50·10 ⁻¹⁵	3.45·10 ⁻¹⁵

height formula. At 1000 m above sea level the p/p_0 ratio is 0.886 and leads to a correspondingly reduced noble gas concentration in the liquid phase.

With regard to fluid inclusions of speleothems it is assumed that the salinity is in a first order approximation related to the dripwater. As in most cases the dripwater shows no significant values the salinity is in general negligible. Niggemann (2000) made an intensive monitoring of different caves in north-western Germany. Dripwater always showed electrical conductivities in the range of groundwater. Similar values have been reported by Galdenzi and Maruoka (2003). They measured a value of 0.2 - 0.4 g/l in case of water from the vadose zone and even in rather rare sulfidic groundwater values did not exceed 2 g/l. In an intensive monitoring of gypsum karst waters Krawczyk and Ford (2007) could emphasize this finding, as almost all water samples showed salinities below 4 g/l.

However, data derived by microthermometry of fluid inclusions indicate that in some special cases a considerable salinity may have built (Scheidegger et al., 2007b). Thus, prior to noble gas data analysis this point has to be investigated.

2.3.2 Temperature determination using noble gas concentrations

Using the temperature dependent solubility we are able to derive temperatures from measured noble gas concentrations. The so-derived values are called noble gas temperatures (NGTs). The noble gas concentrations are the total extracted noble gas amounts related to the corresponding water volume.

The simplest case, water in equilibrium with the ambient air, the so-called air-equilibrated water (AEW), only consists of the dissolved atmospheric noble gas component. Typical noble gas concentrations of water in equilibrium with the atmosphere are shown in Table 2.3. However, in case of groundwater an additional component, referred to as excess-air, is found (Heaton and Vogel, 1981, 1979; Andrews and Lee, 1979). Through fluctuations of the water table bubbles may be included and partially or totally dissolved afterwards (Holocher et al., 2002). This causes in groundwater the additional excess-air contribution to the equilibrium noble gas concentrations, which in general consists of a certain amount of atmospheric air. If the bubbles are only partially dissolved an elemental and isotopic fractionation may occur. The excess-air contribution is handled with an additional parameter, the air-water volume ratio A ($= V_{\text{air}}/V_{\text{water}}$), respectively the Ne-excess ΔNe . An air/water volume ratio of 0.1

indicates that the measured noble gases originated from a ten times larger water volume compared to the air volume, e.g. 0.1 μl air and 1 μl water. If fractionation plays a role, another parameter (F) is included in the calculation. Nevertheless, all these complications can be managed with sufficient precision due to adequate inverse modeling concepts developed by Aeschbach-Hertig et al. (1999) and Ballentine and Hall (1999). By using the whole dataset of neon, argon, krypton and xenon it is possible to derive all unknown parameters such as temperature T , excess-air A and fractionation F .

With respect to the speleothems, the pressure parameter p can be fixed according to the height above sea level, as the location of the cave as well as the position of the speleothem is known. Fractionation can be excluded due to the incorporation process of water in the speleothem. The water gets equilibrated before being closed-off in calcite. The excess-air consists of air-bubbles inside the water inclusions, respectively of totally air-filled inclusions. As free parameters for the inverse modelling temperature T and excess air A are remaining. They can be well fitted in the over-determined system by using neon, argon, krypton and xenon. The simplest model approach consists of the unfractionated excess-air model (UA-model):

$$C_i = C_{i,\text{eq}} \cdot (1 + A \cdot H_i(T)) \quad (2.9)$$

In this equation, C_i describes the modeled concentration, $C_{i,\text{eq}}$ the volumetric concentration of the noble gas i in air-equilibrated water (AEW), H_i is the dimensionless Henry's law coefficient and A the volume ratio of enclosed air to water. This model is used in the following for the speleothem samples to derive NGTs.

In contrast to this, groundwater studies have to take into account the possible fractionation processes and use therefore more sophisticated models, such as the partial re-equilibration model (PR-model, Stute et al., 1995) or the closed-system equilibration model (CE-model, Aeschbach-Hertig et al., 2000). Fitting the neon, argon, krypton and xenon concentrations in groundwater samples to the model by χ^2 -minimization, reasonable temperature differences between distinct climatic periods (Aeschbach-Hertig et al., 2002) with small errors, usually well below 1 $^\circ\text{C}$ (Aeschbach-Hertig et al., 1999), can be obtained. Furthermore, Stute and Sonntag (1992) and Stute and Schlosser (1993) could show, that the NGTs are related to the ground temperature during recharge. As cave temperatures, like ground temperatures, are closely related to the mean annual air temperature (Gascoyne, 1992; McDermott, 2004), the fluid inclusions and therein dissolved noble gases provide information about the past climate. Thus, the idea concerning temperature reconstruction via the solubility is expanded to speleothems and discussed in the following chapters.

2.3.3 Further applications

Noble gases can be used for a widespread set of applications, from tracing of flows to dating purposes and investigation of palaeoclimatic conditions. In the following, some exemplary applications related to the work with speleothems are presented.

^3He , ^4He and ^{222}Rn are well suited for dating purposes. ^{222}Rn is a short-lived radio-isotope with a half-life of 3.82 d. It can be used to trace submarine groundwater discharge (Cable et al., 1996; Corbett et al., 2000) and infiltrating groundwater in lakes due to the strong concentration gradients between the two reservoirs (Kluge et al., 2007) or it can be used to estimate the travel time of artificially recharged water in aquifers as well as the flow velocity of the groundwater body (Hoehn and von Gunten, 1989). Because of the short half-life the applications are limited to a maximum of two to three weeks. Afterwards the signal is lost due to natural decay. Applied in caves radon can be a useful tool to investigate the ventilation (Hakl et al., 1996) or to control the dripwater whether a degassing has just occurred.

^4He can be used at least as a semi-quantitative tool for dating of old groundwater (Andrews and Lee, 1979; Mazor and Bosch, 1992). ^4He accumulates in groundwater traveling in the aquifer due to α decay of radioactive elements like uranium. However, an important requirement for a robust age calculation is a well-known value for the Helium flux from the aquifer and neighbouring layers to the groundwater body.

This idea can be expanded to the age determination of speleothems. If all the helium has stayed inside the calcite and the inclusions, the ^4He built up by radioactive decay can be used as an internal clock. In the case of minerals this method is already used (Lippolt et al., 1994; Wernicke and Lippolt, 1994). Some attempts for speleothem dating are discussed in chapter 4.5.

The combination of ^3He and tritium (^3H) can be used to date young groundwater (Szabo and Rice, 1996; Solomon et al., 1992; Schlosser et al., 1988) and to trace mixing in the ocean (Andrié et al., 1988). The naturally occurring tritium is formed in the atmosphere by a nuclear reaction of nitrogen atoms induced by cosmic rays. The tritium decays through β -decay into ^3He with a half-life of 12.32 years (Lucas and Unterweger, 2000). If both isotopes, ^3He and tritium are used, an age determination without knowing the tritium-input function is possible. After a certain residence time t the tritium content is:

$$^3\text{H}(t) = ^3\text{H}(0) \cdot e^{-\lambda t} \quad (2.10)$$

The amount of ^3He formed during this time t due to the decay of tritium is:

$$^3\text{He}(t) = ^3\text{H}(0) - ^3\text{H}(t) = ^3\text{H}(0)(1 - e^{-\lambda t}) \quad (2.11)$$

Therefore it is sufficient to measure ^3He and tritium at one certain point of time to determine the residence time of e.g. water in the aquifer. A complication are other sources of ^3He in the water sample. A water sample contains an excess-air component $^3\text{He}_{\text{ex}}$, an equilibrium component $^3\text{He}_{\text{eq}}$, a possible terrigenic component (reaction of Li with neutrons) and the tritogenic component (Aeschbach-Hertig, 1994). The equilibrium and the excess-air component can be estimated by measuring all noble gases. The terrigenic component can be deduced from ^4He , which has also a radiogenic component. The tritogenic helium $^3\text{He}_{\text{trit}}$ is calculated from the total ^3He ($^3\text{He}_{\text{tot}}$) in the following way:

$$^3\text{He}_{\text{trit}} = ^3\text{He}_{\text{tot}} - (^3\text{He}_{\text{eq}} + R_{\text{ex}} \cdot L_{\text{ex}} \cdot \text{Ne}_{\text{ex}} + ^4\text{He}_{\text{rad}} \cdot R_{\text{rad}}) \quad (2.12)$$

R_{ex} means the ratio of excess-air ^3He to the corresponding ^4He value. R_{rad} is the radiogenic ^3He - ^4He ratio. L_{ex} describes the $^4\text{He}/\text{Ne}$ ratio of excess air. Thus the penultimate term in the equation describes the excess-air and the last term the terrigenic component.

With regard to caves and fluid inclusions in speleothems, it is not known a priori how long it takes the water to percolate through the vadose zone down to the stalagmites. In some cases, few weeks or less are necessary for the water to move from the surface to the dripping site due to fissures and fractures. However, in deep caves and caves with quasi-saturated layers above, considerable delay can be present. Therefore the dating via ^3H - ^3He has been applied to dripwater in an exemplary site and is discussed in chapter 4.1.2.

2.3.4 Limitations

The main objective of this thesis is to investigate the possibility of using noble gases in speleothems as a new climate proxy. Therefore, it is suggestive to compare the available data, its quality and the limitations in case of speleothems with the information that can be derived from groundwater, where noble gases are originally used to determine palaeotemperatures.

The groundwater constitutes a reliable and unique palaeoclimate archive, but is nevertheless limited because of signal dispersion, mixing between aquifers and dating constraints.

If there has been a sudden temperature change with a duration of only some 100 years this signal will become smaller and will disappear in some thousand years due to the diffusion of the noble gases according to the concentration gradients (Stute and Schlosser, 1993). So, high frequency fluctuations like the 8.2 ka event (Alley et al., 1997; Alley and Ágústsdóttir, 2005) can hardly be seen in the groundwater archive. Nevertheless, substantial changes in the climate system are very well recorded, for instance the transition from the last glaciation to the holocene (Stute et al., 1995; Aeschbach-Hertig et al., 2002; Stute and Deák, 1989).

A strong constraint in the use of groundwater as a palaeoclimate archive is dating. Usually ^{14}C is used to determine the age of the water samples. Unfortunately, the ^{14}C content is influenced by various constituents as, e.g. the dissolution of ^{14}C -active CO_2 from the soil gas, ^{14}C in the soil layer and dissolution of mostly ^{14}C -free carbon from rock and aquifer materials (the so-called dead carbon fraction). In addition to this, chemical reactions of water flowing through the aquifer may change the ^{14}C content and can furthermore influence the ^{14}C value by fractionation. Determining the different constituents as well as the initial ^{14}C concentration is difficult, but can be managed by an additional measurement of the $\delta^{13}\text{C}$ -value (Fontes and Garnier, 1979). In general, dating is restricted to a timespan of about 40 000 years, as the half life of ^{14}C is only 5730 years.

Furthermore, mixing of groundwater bodies may result in misleading data. Different proxies can, for instance, show totally different ages which complicates the data interpretation (Mazor, 1997). With the use of chemical parameters and an intensive isotope study the end members of mixing can still distinguished, however with rather high uncertainties.

In case of the speleothems, most of these problems are of minor importance or do not exist. Mixing and dispersion does not occur and dating is possible up to 500 000 yrs with a rather small uncertainty when using the U-Th-disequilibrium method. Thus, noble gas measurements on fluid inclusions of speleothems would provide an ideal tool for palaeoclimate reconstruction.

2.4 Noble gases from speleothems as a proxy

Now, the advantages of noble gas measurements in liquids, the calculation of absolute temperatures, shall be combined with the precise dating of stalagmites. In this section the idea is explained in detail and the constraints on a feasible application are discussed. Furthermore, published studies using noble gases in fluid inclusions are presented and interpreted with focus on the NGT calculation.

2.4.1 Studies using noble gases in fluid inclusions of speleothems and minerals

Noble gases are of widespread use in geological applications, especially the $^3\text{He}/^4\text{He}$ measurements as well as the Ar measurements for dating. However, in the past (before the 1980s) they have rarely been measured in combination with fluid inclusions.

One of the early studies refers to Kelley et al. (1986), who attempted to apply the ^{40}Ar - ^{39}Ar dating method to fluid-inclusion bearing vein quartz. Similarly, Turner and Bannan (1992) tried to apply this method to fluid inclusions in quartz and fluorite veins. Another early study was conducted by Stuart and Turner (1992), who investigated noble gases from fluid inclusions in quartz, fluorite, mantle materials and also minerals that precipitated in equilibrium with

the atmosphere (a flowstone sample). They did not measure the amount of released water and thus were not able to derive noble gas concentrations. However, they calculated noble gas ratios which at least could indicate a temperature range for the equilibration of the inclusions fluids as well as the contribution of air. They concluded this air contribution to be an unfractionated addition of atmospheric air.

Böhlke and Irwin (1992a) introduced a system for high resolution studies on fluid inclusions using tiny sample amounts and a laser microprobe system. Based on microstandards and synthetic inclusions they demonstrated the possibility for precise and reproducible measurements in the range of these very small samples (down to 10^{-11} l). The new system was applied to high-salinity hydrothermal fluid inclusions from the lead-fluorite-barite deposits at Hansenburg (New Mexico). The combined measurements on noble gases as well as on halogens yielded an equilibration temperature of $(20 \pm 5)^\circ\text{C}$ for these samples (Böhlke and Irwin, 1992b). They used the obtained noble gas and halogen data primarily to derive conclusions about the origin of hydrothermal fluids and dissolved salts.

Burnard et al. (1994) used CO_2 , He and Ar isotopes in fluid inclusions of a dunite nodule to distinguish different inclusion types and to infer some information about the mantle history. Norman and Musgrave (1994) used N_2 , Ar and He to distinguish the source of the inclusion fluids in different hydrothermal systems. Stuart et al. (1995) also made a study on hydrothermal fluids. They used helium and argon isotopes to constrain mantle and crustal components in the fluids and to derive information about crust and mantle behaviour of the Pacific plate in the late Cretaceous. Newman et al. (1996) attempted to use the N_2 , Ar, He, CH_4 and CO_2 values, gained from fluid inclusions of different calcites, to understand the processes and environmental conditions which control the calcite precipitation.

Scarsi (2000) performed a detailed study on olivine and phenocrysts focused on the crushing technique under vacuum. He detected the fluid inclusions to be opened in the first steps and a second source to be responsible for gases released in further steps. The second source may be related to the mineral matrix or to secondary inclusions.

Recently, some groups started investigations concentrating on fluid inclusions of speleothems. Scheidegger (2005) investigated different ways to separate noble gases from air- and water-filled inclusions based on noble gas ratios: Rice (2004) built an extraction system for speleothems using crushing in a steel cylinder and Träumner (2005) tested several stalagmites with regard to noble gases from fluid inclusions. All samples showed ratios close to atmospheric values. All of these first attempts to use noble gases in fluid inclusions as a temperature proxy lack the water determination which rules out the possibility of meaningful temperature calculation.

2.4.2 Basic idea of climate reconstruction from noble gases in speleothems

The solubility of noble gases in water is, amongst other effects, dependent on temperature. Therefore, the noble gas concentrations in water that has not been in contact with the atmosphere after the close-off, can be used to derive the temperature at time of enclosure, if other effects like salinity and pressure are known. Fluid inclusions are small residuals of the water dripping on the speleothems. As they are growing, the fluids are embedded between grains, inside grains or in the calcite lattice. The cave's temperature at this time is crucial for the noble gas concentrations in the trapped fluid parcel volume. After including the fluid in the calcite a change in noble gas composition is unlikely as the diffusion is extremely small (s. chapter 2.5). Only the helium concentration can be modified by radioactive decay or by diffusive loss at high temperatures.

Hence, long-term temperature changes in the environment, for instance during the transition from a cold period, like the last glaciation to a warmer period, like the Holocene, should be well

conserved in the noble gases from fluid inclusions. Even changes with a smaller duration (for example Dansgaard-Oeschger events) should be detectable as diffusion is strongly suppressed or negligible. So a climate signal remains in the fluid inclusion of different layers.

2.4.3 Objective

The main objective of this work is the calculation of absolute temperatures from speleothems with the highest possible resolution. Special extraction techniques have been developed so that even stalagmites with an inappropriately high amount of air-filled inclusions in an untreated case can be used for this purpose. Altogether, palaeotemperatures with an uncertainty of about 1 °C should be achieved. By comparison with other proxies like stable isotopes and trace elements, information about precipitation and other climate parameters will be derived. Similarly, the NGT data may be used to disentangle the different effects provoking changes in the stable isotope values of the calcite.

2.4.4 Constraints

The determination of minute quantities of water from the inclusion fluids may be difficult. In a simple approach it is also possible to determine temperatures with noble gas ratios only, which can already be obtained by noble gas measurements without water amount determination. However, these temperatures yield uncertainties of at least 2 °C (Aeschbach-Hertig and Kluge, 2006). This is too large for high precision climate studies and rejects the use of noble gas ratios only. Thus, we are forced to determine also the according amount of water for the calculation of noble gas concentrations. The achievable uncertainties for the temperature calculation based on noble gas concentrations can be derived from Fig. 2.7. This plot was generated by synthetic data varying the air/water volume ratio as well as the analytical error originating from the measurement process. The temperature uncertainty was calculated by the application of the inverse modeling method (Aeschbach-Hertig et al., 1999) on the synthetic data.

At first, measurement precision has to be better than 3 % to achieve temperature uncertainties lower than 1 °C. This requires a clean extraction line and very low or at least reproducible and stable background values. Secondly, it is necessary to reduce the air/water volume ratio to below 0.1 in the case of a 2% analytical error. At higher values temperature uncertainty is too large for useful interpretation. A simple estimation based on e.g. 1‰ error in the air-water volume ratio A already shows this effect. Assuming an A of 1, we get about $1.83 \cdot 10^{-13}$ ccSTP Ne from 1 µl of water and $1.65 \cdot 10^{-11}$ ccSTP Ne from 1 µl of atmospheric air. The total signal consists of $1.67 \cdot 10^{-11}$ ccSTP Ne. If we would subtract the air-derived part to obtain the equilibrium component, a 1 ‰ error in A would result in an uncertainty of 9 % in the case of the remaining Ne equilibrium fraction. Larger A values provoke even higher uncertainties and show that this is a crucial value for the aimed precision.

Furthermore, the cave air composition should be atmospheric and not changing with time. If the noble gas mixing ratio would be different between the caves, representative air samples would be necessary beyond the speleothem samples. Moreover, in this case it is not sure whether the noble gas composition is constant over time. However, there are few reasons for such situations as noble gases (except helium) have no significant sources over the investigated time scales of some thousand to 100 000 years. To investigate this aspect, cave air samples have been taken and measured (see chapter 4.1.1: cave air measurements).

Another important point for this technique is the retention of noble gases inside the fluid inclusions. The temperature signal would be modified if considerable diffusion occurred. High diffusion constants would also influence sampling and the preparation in the laboratory.

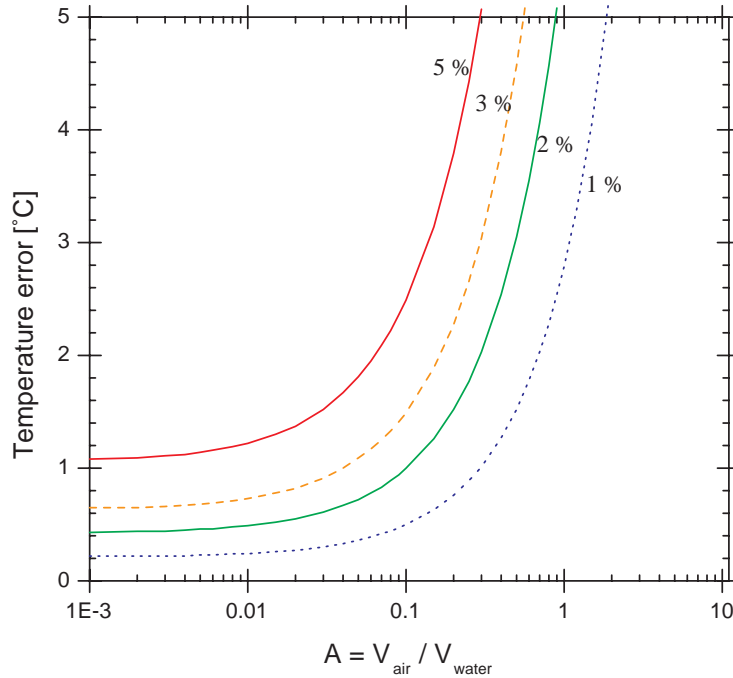


Figure 2.7: Maximum precision achievable at a certain analytical error and various air/water volume ratios. Fitting parameters are temperature and excess air. The pressure is known from the location of the speleothem inside the cave, salinity is assumed to be zero and also fractionation is supposed to be negligible.

Calculations and a discussion are summarized in chapter 2.5 .

In the case of water samples excess air and fractionation play an important role. As water-filled inclusions sometimes also contain some bubbles, it is possible that fractionation has to be considered in the calculation. However, considering growth history of speleothems this can almost be ruled out. The process of embedding liquid drops in calcite takes a long time (typical growth of a stalagmite is about some tens of μm per year), so that a very good equilibrium with the surrounding atmosphere is achieved. Additional air bubbles only possess a composition according to the cave atmosphere. As the pressure inside the fluid inclusions does not increase essentially, the bubble stays with an unchanged mixing ratio and no fractionation is supposed to occur. Even if fractionation between water and gas occurs, no separation takes place. As we extract the total noble gas amount, including the fractions from bubbles as well as from water, both parts are measured. The total gas amount itself is only influenced by conditions during growth, in particular the temperature governing the solubility. Changes after the close-off do not alter the total noble gas amount.

Furthermore, the precision will be limited by the sample size and water content. If we assume a speleothem with a water content of 1 ‰ wt and negligible air-filled inclusions we will get 1 μl water from 1 g speleothem. If the speleothem has grown at a temperature of 10 °C 4.64 · 10⁻¹¹ cc He, 2.02 · 10⁻¹⁰ cc Ne, 3.85 · 10⁻⁷ cc Ar, 9.10 · 10⁻¹¹ cc Kr and 1.32 · 10⁻¹¹ cc Xe are contained in this sample. This corresponds to about 10¹³ atoms in case of ⁴⁰Ar and 9.5 · 10⁷ atoms in the case of ¹³²Xe. To achieve a signal with an uncertainty of less than 5 % at least some 10⁷ atoms should be available in a sample for each noble gas isotope. The minimum number depends on the ionization efficiency and the background for each isotope. The limiting case is ¹³²Xe, which is the less frequent noble gas isotope measured with our mass spectrometer. Thus the sample size is limited to 0.1 g at a water content of 1 ‰ wt.

However, speleothems with an advantageous air/water volume ratio sometimes only contain 0.05 ‰ wt water. In this case the minimum sample size is 2 g.

Böhlke and Irwin (1992a) showed that it is possible to measure noble gas abundances and isotopic compositions by laser microprobe noble gas mass spectrometry down to 10^{-11} l of inclusion fluids. In fact they did not measure the water amount of the water-filled inclusions opened by laser. However, they were able to assign a temperature to fluid inclusions samples from hydrothermal brines with a mean value of 20 ± 5 °C using the ratio of ^{84}Kr to ^{36}Ar vs Cl to ^{36}Ar (Böhlke and Irwin, 1992b).

An important practical problem is the abundance of air-filled or at least partially air-filled inclusions (Kluge and Aeschbach-Hertig, 2007; Scheidegger et al., 2006). They often contribute much more noble gases than the water and mask noble gas signals from the water-filled inclusions. This will therefore limit the NGT determination to a small number of speleothems if a simple one-step extraction is used. In the case of our method all the noble gases are measured together and separated afterwards via inverse modelling. As the air-filled inclusions are supposed to contain only unfractionated atmospheric noble gases (Stuart and Turner, 1992; Böhlke and Irwin, 1992b) it is feasible to model the total gas amount with regard to the interesting water-referring signal. In contrast to the results of Stuart and Turner and Böhlke and Irwin we observed fractionation or enrichment patterns in some special samples (see chapter 4.4). In this case a more sophisticated procedure and data analysis is necessary.

2.5 Diffusion of noble gases in speleothems

Is the calcite tight for noble gases at typical cave temperatures? This is one of the crucial questions concerning this method. If the diffusion coefficient of the noble gases in the calcite is too high, not only for helium, but also for heavier noble gases, the method can not be applied to speleothems, because gases and the temperature signals will be affected severely in the same way.

Copeland et al. (2007) investigated the diffusion of He in calcite and dolomite. Their results indicate that the speleothems are closed for He and therefore also for the heavier noble gases at typical cave temperatures. Furthermore, our own measurements affirm these results. Some pieces of one growth layer of the stalagmite BU-U(we) (chapter 4.6.3) were measured. From the mean surplus-He an age was calculated via α decays in the decay chain using the measured uranium and thorium content. The age obtained by fitting the time parameter to the measured radiogenic He concentration is about 16 500 yrs. Unfortunately, the uncertainty is rather high and in the order of some thousand years, as the extraction was not 100 % efficient in the copper tubes. However, the uranium-thorium dating, which resulted in a time span from 10 500 to 12 100 yrs, is not very far from this rough estimation (s. chapter 3.7). To substantiate this result and to prove the diffusion behaviour of the different noble gases, heating experiments have been performed.

Furthermore, the investigation of diffusion gains importance with regard to background control and reduction. In geological applications the extraction line and the extraction device including the sample is heated some days up to ≥ 100 °C to remove the superficially absorbed and adsorbed gases (baking overnight at 150-200 °C: Yamamoto et al., 2004; baking overnight at 150 °C: Matsubara et al., 1988 and Podosek et al., 1980). In the case of the calcite it was not known to which temperature the preheating could be extended without losing the gases from inside the calcite and from inside the fluid inclusions. The heating experiments should also deliver information about this topic.

2.5.1 Theoretical background

Usually the diffusion coefficient is written according to the Arrhenius law, where T_0 is the reference temperature in Kelvin, D_0 the diffusion coefficient at temperature T_0 and E the activation energy:

$$D = D_0 \cdot \exp\left(\frac{-E}{kT}\right) \quad (2.13)$$

The diffusive flux of gases is proportional to the diffusion constant, driven by the concentration gradient $\left(\frac{\partial C}{\partial x}\right)$ and can be written according to Fick's law in one dimension:

$$J = -D \cdot \left(\frac{\partial C}{\partial x}\right) \quad (2.14)$$

Using the continuity equation we get Fick's second law:

$$\frac{\partial C}{\partial t} = \frac{\partial}{\partial x} \left(D \frac{\partial C}{\partial x} \right) \quad (2.15)$$

If the diffusion constant does not depend on the position parameter x , the equation can be simplified to the following form:

$$\frac{\partial C}{\partial t} = D \frac{\partial^2 C}{\partial x^2} \quad (2.16)$$

The one-dimensional solution for an initial pulse with a fixed total tracer amount is given by

$$C(x, t) = \frac{C_0}{\sqrt{4\pi Dt}} \cdot \exp\left(-\frac{x^2}{4Dt}\right) \quad (2.17)$$

C_0 refers to the initial concentration at $x = 0$. For calculating concrete numbers the diffusion length x_d is a helpful parameter. x_d corresponds to the variance of the Gaussian distribution (compare equation 2.17 and Fig. 2.8).

$$x_d^2 = 2 \cdot D \cdot t \quad (2.18)$$

If the speleothem sample is pumped inside the vacuum chamber, the boundary conditions are different. Outside the speleothem the gas concentration is strongly reduced due to the pumping process and compared to atmospheric values inside air-filled inclusion by about 10 orders of magnitude smaller. Therefore, the value outside can be fixed to 0 for a first order approximation. The solution of the diffusion equation is in this case given by one branch of the error function for the concentration inside the speleothem and 0 outside:

$$C(x, t) = \begin{cases} C_0 \cdot \operatorname{erfc}\left(\frac{x-x_1}{\sqrt{4Dt}}\right) & \text{for } x \geq x_1 \\ 0 & \text{for } x \leq x_1 \end{cases} \quad (2.19)$$

C_0 is the initial concentration. x_1 is the point where the concentration is fixed to 0. The temporal evolution is displayed in an exemplary case in Fig.2.9 for one side, and the assumption that this part is not influenced by the diffusion from the other side. A detailed discussion of solutions for the diffusion equation can be found for example in Barrer (1941) and Crank (1994). A similar problem occurs in the case of ice cores. Noble gas measurements on ice core samples also require pumping in a vacuum chamber prior to the measurement to avoid contamination by ambient air. The description of the diffusive behaviour leads in one dimension also to eq.(2.19). The three-dimensional solution is discussed e.g. by Friedrich (2003) or Gölzhäuser (2008).

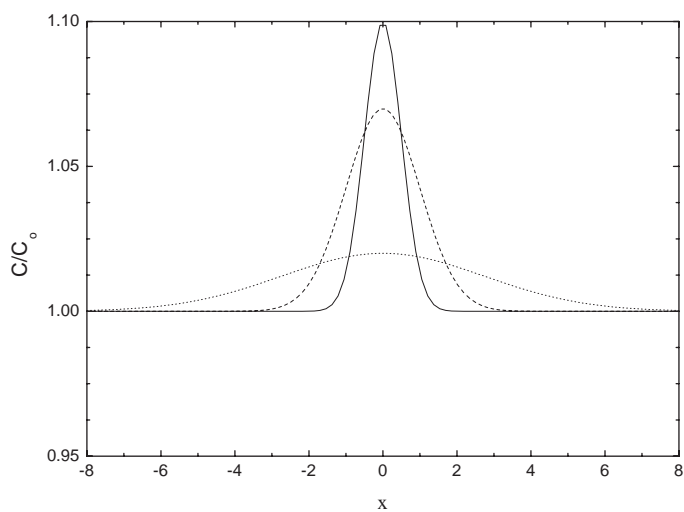


Figure 2.8: Evolution of an initial pulse (continuous line) in one dimension at three different points in time (dotted and dashed line). The signal was caused for example by cooling and therefore more noble gases are stored in the water-filled inclusions. With time these higher values are reduced by diffusion and the concentrations in nearby points are slightly increased.

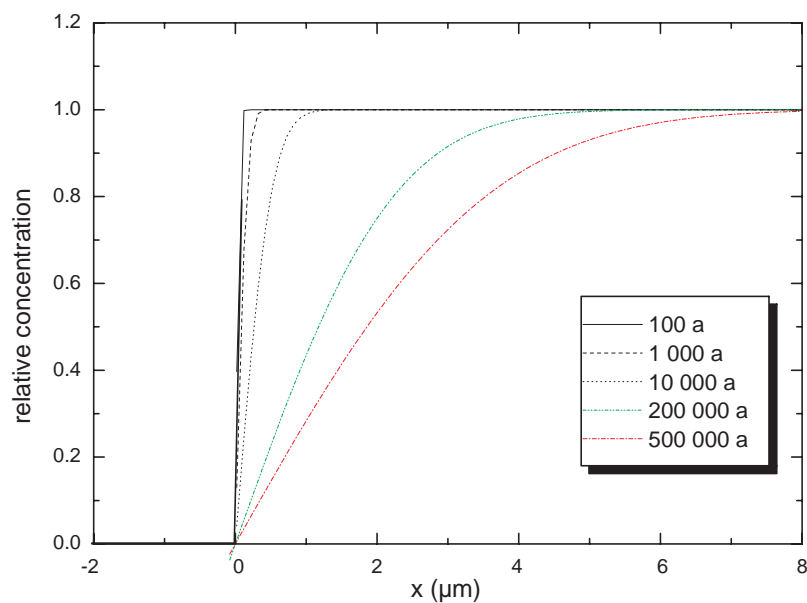


Figure 2.9: Diffusion from a calcite cube in one dimension. The concentration outside the calcite is set to 0. As diffusion coefficient the literature value of $2.4 \cdot 10^{-25} \text{ m}^2/\text{s}$ at $30 \text{ }^\circ\text{C}$ (Copeland et al., 2007) was used for calculation.

2.5.2 Literature values

So far, little systematic research on noble gas diffusion in calcite was performed. Therefore, only few data is available in literature. For a rough estimation of magnitude, diffusion coefficients from other minerals can be used. Musset (1968) investigated the diffusion of argon in feldspar, sanidine, microcline and other minerals. In all cases the extrapolation of the diffusion coefficient at room temperature led to a value for argon in the order of 10^{-24} to 10^{-26} m²/s. Assuming a mean value of 10^{-25} m²/s to be a good estimation for speleothem calcite, the time for diffusion by 1 µm would be 160 000 years. In 10 000 years the diffusion would broaden the argon signal by 250 nm. As the annual growth of a stalagmite is in the order of some µm even an annual signal should be preserved very well in the case of a holocene stalagmite or a calcite grown during the last glaciation.

A recent publication confirms this data. Copeland et al. (2007) investigated the diffusion of helium in calcite. Step heating experiments led to a closure temperature of $70 \pm 10^\circ\text{C}$ at a cooling rate of $10^\circ\text{C}/\text{Myr}$. They get a weighted average of the activation energy for the treated samples of 29.3 ± 0.7 kcal/mol. Based on the presented data, a mean value for the diffusion constant D of $2.4 \cdot 10^{-25}$ m²/s at 30°C respectively $3.5 \cdot 10^{-19}$ m²/s at 150°C can be calculated. At 30°C this would implicate a helium diffusion of about 1 µm in ≈ 70 000 years. As the cave temperature is normally below this value, even higher timescales for the same diffusion length can be assumed. In consideration of the mean annual growth rates of stalagmites, the diffusive loss of significant multi-annual events becomes even more unlikely. With regard to the preparation of the samples at e.g. 150°C the timescale for diffusion of 1 µm is about 400 hours. About 50 % of the speleothem sample stays larger than 200 µm after being crushed 60 times with the steel ball. Therefore, the diffusive loss of noble gases during pumping of the samples, prior to the measurements, can be neglected as additionally the pumping time normally does not exceed 24 hours.

Heating measurements on a cube of the H12-stalagmite revealed no significant diffusive loss or fractionation after a pumping period of more than 12 days with temperatures of up to 250°C (s. chapter 2.3.5). A subsequent crushing step of the heated and for a long time pumped sample yielded a well measurable water content as well as Ne and Ar ratios (9.92 ± 0.08 , 295 ± 3) close to atmospheric air and noble gas concentrations in correspondence with air-equilibrated water. Thus the diffusive loss of noble gases during pumping and mild heating can be neglected.

Helium is the lightest noble gas with the highest diffusion constant, the heavier noble gases are better retained in the calcite with respect to diffusion. Therefore it can be stated recapitulatory that a diffusive loss of noble gases is unlikely to occur in the cave or after sampling and that pumping with mild heating $\leq 150^\circ\text{C}$ does only marginally affect the noble gases.

2.6 Adsorption effects

Gas molecules can be "bound" to solid surfaces by adsorption. Adsorption consists of two different types, physical adsorption by Van-der-Waals forces and chemical adsorption by orbital overlap or charge transfer. The physical adsorption is a long-range bonding, but relatively weak with a bond energy of less than 50 kJ/mol. The chemical adsorption has a bond energy of 50 kJ/mol up to 500 kJ/mol, but is only acting on short distances. The chemisorption is surface specific, whereas the physisorption takes place on any surfaces at adequate low temperatures. Physisorption can generate multi-layers of adsorbed atoms, which can be described by the BET-isotherm. In case of chemisorption mono-layers are expected, which can be described by the Langmuir isotherm in the adsorption equilibrium state.

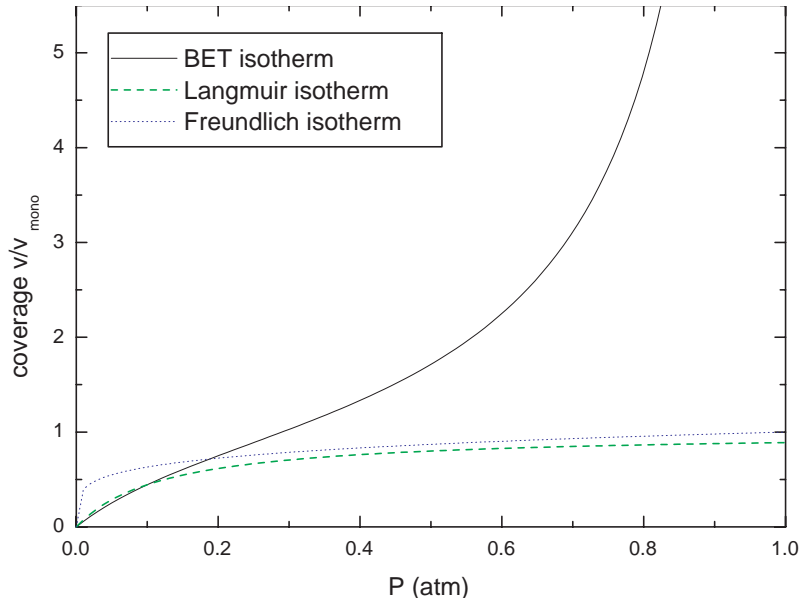


Figure 2.10: Freundlich, Langmuir and BET isothermes. The isotherms describe how well certain molecules or atoms are bond to the adsorbing solid. The isotherm displays the surface concentration of the adsorbed material in dependence of the equilibrium concentration (liquid), respectively the gas pressure or the volume ratio.

The isotherm is a function which connects the number of adsorbed atoms or molecules on the adsorbent with the pressure in the gas phase. A first empirical approach has been made by Küster (1894) and Freundlich (1907):

$$\frac{x}{m} = k \cdot P^{\frac{1}{n}} \quad (2.20)$$

x describes the adsorbed quantity, m the adsorbent quantity, P refers to the pressure. k and n are empirical constants for a given temperature.

Langmuir expanded this approach to a larger range including high pressures and low temperatures (Langmuir, 1916, 1918):

$$\Theta = \frac{\alpha P}{1 + \alpha P} \quad (2.21)$$

Θ describes the percent coverage of the surface. α is the Langmuir adsorption constant, which increases with the strength of adsorption and decreases with temperature. P is the gas pressure.

The Langmuir isotherm is restricted to the case of monolayers. Uniform surface, no interaction between the adsorbed molecules and the same mechanism for adsorption of all molecules and atoms are assumed. For the more general case Brunauer et al. (1938) developed a modified formula (BET-isotherm):

$$\frac{x}{v(1-x)} = \frac{1}{v_{\text{mono}}C} + \frac{x(C-1)}{v_{\text{mono}}C} \quad (2.22)$$

where x is ratio of the equilibrium to the saturation pressure of the adsorbate at a given temperature. v is the adsorbate volume at standard conditions (STP), C is an empirical constant at the given temperature. v_{mono} is the volume in STP necessary to form a monolayer. The BET-isotherm describes the physisorption, whereas the Langmuir formula is better suited for the chemisorption.

von Antropoff (1954) investigated the adsorption of N_2 and Ar at different pressures and temperatures on charcoal. He found a strong dependence on the concentration in the gas phase. The adsorbed Ar amount is about 3 orders of magnitude smaller at room temperature compared to $-76\text{ }^\circ\text{C}$, whereas the effect of increased temperature gets smaller at higher temperature values. The adsorption of noble gases was also investigated by Gvozdev and Tovbin (1997). They found a strong decrease of the adsorbed gas at a decreasing pressure in agreement with the behaviour of the Freundlich, respectively the Langmuir isotherm at low pressures. Munakata et al. (2003) measured the adsorption of Kr and Xe on different materials (charcoal, molecular sieves, mordenite) with the objective to remove radioactive noble gases from the exhaust air of nuclear power plants and reprocessing units by adsorption. The adsorbed amount is strongly dependent on the adsorbent material and shows differences up to two orders of magnitude. Ag mordenite yielded the highest ability for adsorption and a special molecular sieve the lowest ability amongst the investigated materials. At a Xe partial pressure of 10 Pa 10^{-6} mol Xe per g of adsorbate are adsorbed on the molecular sieve, whereas it is about 10^{-4} mol Xe in the case of the Ag mordenite. For Kr the values are between 10^{-6} and 10^{-7} mol Kr per g in the case of this two materials. These values indicate that a considerable amount of noble gases can be adsorbed on certain materials. Typically the pressure in the preparation and extraction line is considerably lower (8-9 orders of magnitude) and therefore a smaller contribution from adsorbed noble gases, released from the walls during extraction, can be expected. However, regarding calcite growth, a gas addition with preferential adsorption of heavy noble gases may occur in correspondance with the higher ability of certain materials to adsorb the heavy gases.

For very low range noble gas measurements (total sample gas amount: Ar $\leq 10^{-6}$ ccSTP, Xe $\leq 10^{-10}$ ccSTP) a clean line and an adequate sample preparation are necessary. As the signals are very low, even adsorption of atmospheric gases on the surfaces of the line, the crushing device and the sample after venting of the system play a role.

Measurements have revealed a long pumping time for the heavier noble gases and show substantial values of adsorbed Xe remaining before thermal decrepitation (s. Marx, 2008). Thus, it can be assumed that Xe has a higher coefficient of adsorption on solid surfaces compared to the light noble gases. A similar conclusion can be extracted from the studies of Podosek et al. (1980) and Matsubara et al. (1988). They revealed a progressive enrichment of the heavier noble gases and especially Xe in sediments. Torgersen et al. (2002) detected noble gases to physisorb rapidly on natural rocks. They also suggest a quick modification of this weak physisorption into a strong chemisorption mode. This finding is in good agreement with our laboratory experience, as we need temperatures remarkably above room temperature to release the adsorbed component efficiently. E.g. at 120°C a peak was found for all noble gases likely caused by desorption from the copper tube walls (Fig. 3.38). The physisorption yields a bond-energy of up to 50 kJ/mol which corresponds to about 0.5 eV per atom or molecule. For chemisorption the bond energy per atom or molecule is even up to 5 eV . The thermal energy is about 0.025 eV at $20\text{ }^\circ\text{C}$ and therefore too low to release the adsorbed components.

The sorption isotherms show a dependence of the adsorbed component on the partial pressure, respectively the concentration. Thus, the two possibilities - low partial pressure due to pumping and high temperatures through heating - are combined for reducing the adsorption. In order to remove adsorbed noble gases from the crusher surface, it has been heated at least overnight (minimum 8 hours) at temperatures between $70\text{ }^\circ\text{C}$ in the case of the simple steel cylinder and at $150\text{ }^\circ\text{C}$ with the new crusher system including the external sample pocket in a modified valve. The pumping procedure is orientated to the preparation process used in geology. E.g., Matsubara et al. (1988) baked the samples at $150\text{ }^\circ\text{C}$ overnight.

With regard to the noble gases in the sample itself, the adsorption on the calcite surface during the speleothem growth may play a role for the final noble gas concentration. As the calcite surface is typically not absolutely plane (s. Fig.2.6) a large surface for adsorption exists. In the case of samples with a very small number of water- or air-filled inclusions the adsorbed noble gas components may alter the noble gas concentrations towards higher values, indicating apparent cooler temperatures like in the case of the CG-stalagmite (water content: ≈ 0.03 wt%, low gas amount, fitted temperature about 5 to 10 °C below expected values) or the two Spannangel samples (SPA 12, water content: 0.08 wt%; SPA 52, water content: 0.1 wt%, fitted temperature in both cases below 0°C). This effect is amplified by the smaller mobility of the heavy noble gases Kr and Xe, which are more likely adsorbed and less easily removed from the calcite surface. Thus, the water content of the speleothem samples as well as the total gas amount can indicate the influence of adsorption. If there is a large number of inclusions, a possibly adsorbed component will be of minor importance.

To get an impression of theoretically adsorbed molecules or atoms on a typical surface we made a simple estimation. On a surface of 5 mm x 5 mm, which corresponds to typical dimensions of the measured pieces, about $5.4 \cdot 10^7$ Xe atoms could be placed in one monolayer assuming a mean atomic radius of 1 Å, atmospheric air and typical mixing ratios. This is a rather large number compared to the Xe content in an inclusion-poor stalagmite. In 0.1 µl of water, equilibrated at 10°C, about $3.5 \cdot 10^7$ Xe atoms are abundant. Actually, polar molecules like H₂O will be adsorbed preferentially and hamper the adsorption of other atoms and gases. In detailed experiments Marx (2008) found crushed calcite to adsorb water vapour very efficiently. The too low NGTs obtained from the CG as well as the Spannangel samples may at least partially be explained by an underestimated water amount due to the adsorption of water on the crushed calcite. Underestimated water amounts or an enhanced noble gas content lead in both cases to higher noble gas concentrations indicating apparent low temperatures. In most samples we found no indication of increased noble gas content for the heavier isotopes. This may be an important hint that adsorption of noble gases during growth plays only a minor role, at least for the majority of the samples.

2.7 Goals of this study

The main objective of this study is to establish the determination of noble gas temperatures from speleothem fluid inclusions.

To achieve this goal different points have to be considered and examined accurately:

- **sample selection:** for reconstruction of the palaeoclimate only well datable samples are useful. Speleothem types with adequate properties for noble gas measurement and also dating purposes have to be figured out. A procedure for a simple sample selection has to be developed.
- **sample preparation:** to achieve maximum time resolution, samples have to be sufficiently thin, but with regard to the extraction line and the crusher they should possess certain dimensions, e.g. a not too big cross sectional area. An optimum sample preparation should be figured out.
- **sample treatment prior to extraction:** this is one of the most critical points as the results of the measurement can strongly depend on the preparation and pumping, which influences the blanks in the same way. A procedure has to be developed, which reduces the blank by pumping of the sample and the whole extraction line in high vacuum at either moderate heating or at room temperature.
- **development of a noble gas extraction line for speleothems.** The extraction line should be built with regard to the lowest blanks possible and a convenient line control via pressure gauges to monitor the extraction process or detect possible leaks. The line should possess connections which provide the possibility for a high sample throughput and special line parts for water determination including cold fingers, pressure gauges and expansion volumes. For maintaining a high vacuum ($\approx 10^{-8}$ mbar), an adequate pumping line including turbo-molecular and scroll pumps for cleaning should be available.
- **development of a system for water determination in the low μl -range.** Speleothem samples rarely contain more than 1 μl of water in 1 g of carbonate. For NGT calculation these low water amounts have to be determined with sufficient precision of better than 3 % to achieve an overall uncertainty in the range of 3 %.
- **development of an appropriate extraction method.** In general all of the noble gases from opened water-filled inclusions should be released. Additionally an extraction procedure to separate the noble gases from the air-filled part should be developed. The extraction has to yield a low air/water volume ratio. As a constraint for the procedure, the extracted water amount should normally be above 0.1 μl , so that the noble gases can be measured with sufficient precision.
- **development of an adequate noble gas preparation procedure.** The separation of heavy and light noble gases as well as the purification process should be designed in such way that the largest part of the released noble gases are being transferred to the mass spectrometer. By this way very small samples can be measured also.
- **development of a special speleothem measurement procedure.** Speleothem samples can not be measured like water samples as they deliver about 3 orders of magnitude less noble gases. In some cases the ion multiplier has to be used instead of the faraday cup for measurements in the mass spectrometer. Furthermore, the ion source tuning has to be changed to achieve maximum efficiency and the actual measurement procedure has to be adapted concerning peak centering, magnet precycling and ion source tuning changes to achieve a good signal stability and mass resolution.

- development of a measurement procedure for diluted calibration standards. For calculation of absolute noble gas amounts, measured signals from speleothems have to be compared with a known standard. A diluted standard has to be prepared which yields gas amounts comparable to the samples. Furthermore, scripts for the automatic calibration measurement have to be established. Using automation it is possible to run the measurements 24 hours and 7 days a week.
- development of a sophisticated background control. As the sample signal is rather low, blank contributions are of critical importance. The relevant background fraction has to be figured out and scripts for automatic measurements have to be established. Furthermore, scripts for contribution control of double ionized atoms to the measured signals have to be written. This is of importance especially in case of ^{20}Ne due to the possible double ionisation of ^{40}Ar .
- development of an appropriate data evaluation. In one measurement run several hundred of single noble gas measurements are performed. Data evaluation by hand would take some weeks and would be quite error-prone. Instead, an automatic evaluation routine would be less time consuming and in general less error charged.
- optimization of calibration. The calibration measurements should show reproducible values, low scattering, as little as possible non-linear behaviour with regard to gas amounts and small uncertainties for all noble gases (at best below 1 %).
- **test of the obtained noble gas data** - reasonable results? At first, tests samples from a certain site and from known climatic periods should deliver reasonable values. Holocene samples, for instance from a cave with a present-day cave temperature of about 10 °C should at least give NGTs between 7 °C and 13 °C. Permanent shifts above or below this range would indicate systematic problems either in extraction and measurement or in data evaluation.
- test of data reproducibility: to establish this new method for palaeoclimate reconstruction reliable data have to be produced. A speleothem sample, which could be measured with low overall uncertainties (including sample, line and preparation blanks, calibration and water determination uncertainties) in the range of few percent and an acceptable air-water volume ratio below 0.1 should reproduce within 1 °C.
- comparison with stable isotopes. Assuming all the preceding points had been achieved and reliable as well as precise data can be derived, measurements along a stalagmite growth axis can be performed. In this case the NGTs should be compared to the stable isotope data. As the temperature is known from the noble gas concentrations, it should be attempted to infer information about precipitation or soil cover changes from the temperature corrected isotope data.
- development of a measurement **procedure for routine work**. In the final phase a larger number of samples should be measured in a short time. To reach this goal an adequate procedure has to be developed. According to the sample property a typical extraction method has to be used and the extraction line has to be prepared for a high sample throughput. This can be achieved with a set of three or more crushers, as for example one is pumped via turbo-pump connection, one used for sample crushing and the third is in the measurement stage at the same time.

Chapter 3

Working with speleothems

In this chapter the basics about deriving noble gas data from speleothems will be presented. At first, the sample selection will be discussed. This is of special interest as the noble gas composition, especially the fraction from air-filled, respectively water-filled inclusions is dependent on the type and structure of the stalagmite. Investigation of thin sections play a major role with regard to this task.

Noble gas temperatures with low uncertainties can only be obtained from noble gas concentrations. Therefore, it is necessary to determine the water amount which corresponds to the measured gas signal. In the following section a method is presented and discussed of how to determine the tiny water amounts with sufficient precision. Additionally, different extraction techniques have been investigated with regard to the efficiency and the gas background. High air/water volume ratios complicate the precise temperature determination. Using stepwise procedures may yield better conditions and is discussed briefly. Finally, the subtle noble gas measurements with the mass spectrometer and the sophisticated data analysis is presented.

3.1 Sample selection

An ideal sample for the calculation of noble gas temperatures has to accomplish several constraints. Primarily, the ratio of noble gases from air-filled inclusions to the noble gases from water-filled inclusions has to be sufficiently small (air/water volume ratio ≤ 0.3). Secondly, the sample should provide enough water and noble gases in order to be measured with the necessary precision. The total uncertainty including water determination and noble gas signal uncertainty should be smaller than 3 %. In this section the properties of the measured samples are discussed using microscopic analysis of thin sections. Based on this data a conclusion can be drawn which samples can be assumed to be useful for NGT measurements with the above described properties.

3.1.1 Optical methods

A good impression of the speleothem structure can be obtained from thin sections. They offer the possibility to connect the noble gas signals and other properties like the air/water-volume ratio and the water content to the structure. Furthermore, they give insight into distribution, size and type of inclusions.

The preparation was successfully realized in the laboratories of the Institute of Mineralogy. Several steps have to be taken in order to get a good thin section. Small parts (≤ 3 cm x 5 cm x 0.3 cm) are cut of the speleothem, embedded to a grinding plate with cold-embedding material like Epofix or Caldofix and polished with SiC-paper in a way that the sides are totally plane without any grooves. Subsequently the speleothem piece is attached to a microscope



Figure 3.1: Investigated speleothems are from different parts of the Earth. Caves, from which samples have been taken are marked with a flag. BC Bear Cave, BU Bunker Cave, CG Dos Anas Cave, H Hoti Cave, MA Marcelo Arevalo Cave, OBI Obir Cave, SPA Spannagel Cave.

slide, grinded roughly down to 500 - 100 μm and lapped afterwards with SiC powder with grain size F150, F400 or F600 to a thickness of about 35 μm . To achieve a high reflecting surface and to remove deformations caused by the fine-grinding step, the sample is diamond- or oxide-polished.

Afterwards, the microscopic analysis was done in the Institute of Geology and Paleontology with support of Dr. Glasmacher using a special automated transmitting- or reflecting-light microscope.

Inclusions may be larger than 30 μm and can be destroyed during the thin-section preparation. Therefore, usually thick sections are prepared to avoid the damage of larger inclusions and the loss of a three-dimensional perspective. For sedimentary rocks a thickness of 40 to 60 μm is sufficient (Goldstein and Reynolds, 1994). In the case of speleothems up to 150 μm may be appropriate. However, all the data presented here refers to thin-sections with a thickness of 35 μm . The smaller inclusions (<20 μm) are assumed not to be affected by the preparation and thus the thin-section can give a rough overview of the inclusion distribution and its general dimensions.

A set of samples with significantly different noble gas signals has been investigated using microscopic inspection of thin sections. The samples were taken from caves with different climatic conditions (Fig.3.1):

- OBI5, stalagmite from the Obir Cave in Austria (Spoetl et al., 2005). The cave is situated at about 1100 m above sea level with a mean annual air temperature of about 6 °C.

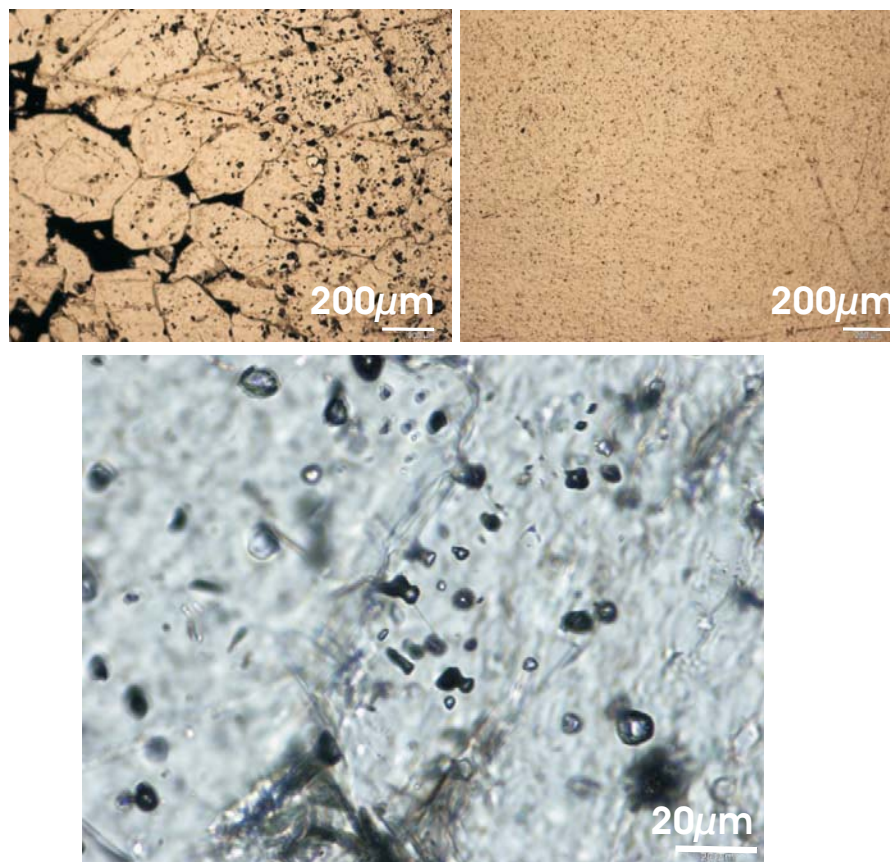


Figure 3.2: Thin sections of stalagmites H12 and OBI5. The upper pictures are displayed with the same magnification. The upper left picture is a thin section of H12, the right of OBI5. The scale bar is in both cases $200\mu m$. The lower picture illustrates the fluid inclusions of H12 with a higher magnification - the scale bar corresponds to $20\mu m$.

- H12, stalagmite from the Hoti Cave in Oman (Neff, 2001). The cave is located 950 m above sea level. In this cave temperature ranges between $23\text{ }^{\circ}\text{C}$ and $26\text{ }^{\circ}\text{C}$. The investigated stalagmite H12 reflects arid to semiarid climatological conditions of the Holocene and is younger than 6000 years. The about 80 cm long H12 stalagmite shows layering and in general a grey appearance with highly porous zones and denser milky white parts.
- flowstone H8Z, extremely pronounced layered speleothem from the Hoti Cave in Oman. Small brownish up to black layers are alternating with thicker as well as brighter layers.
- CG, 72 cm tall whitish stalagmite from Cuba from the Dos Anas cave in the Majaguas-Cantera cave system (Pajon et al., 2006). This sample has grown at 90 - 100 m above sea level in a tropical environment with typical precipitation values of 1600 - 1800 mm/yr and a mean cave air temperature between 21 and $22\text{ }^{\circ}\text{C}$. The cave chamber from which the sample was taken is at 1.2 - 1.3 km distance from the entrance area.
- BU-U, stalagmite from the Bunker Cave in Sauerland (NW Germany). The cave is located 180 m above sea level. The recent mean annual air temperature is about $9.5\text{ }^{\circ}\text{C}$ (1960-1990). The region is characterized by a temperate climate with regular precipitation. The investigated thin section from the about 10 cm long stalagmite originate from a milky white Early Holocene growth layer.

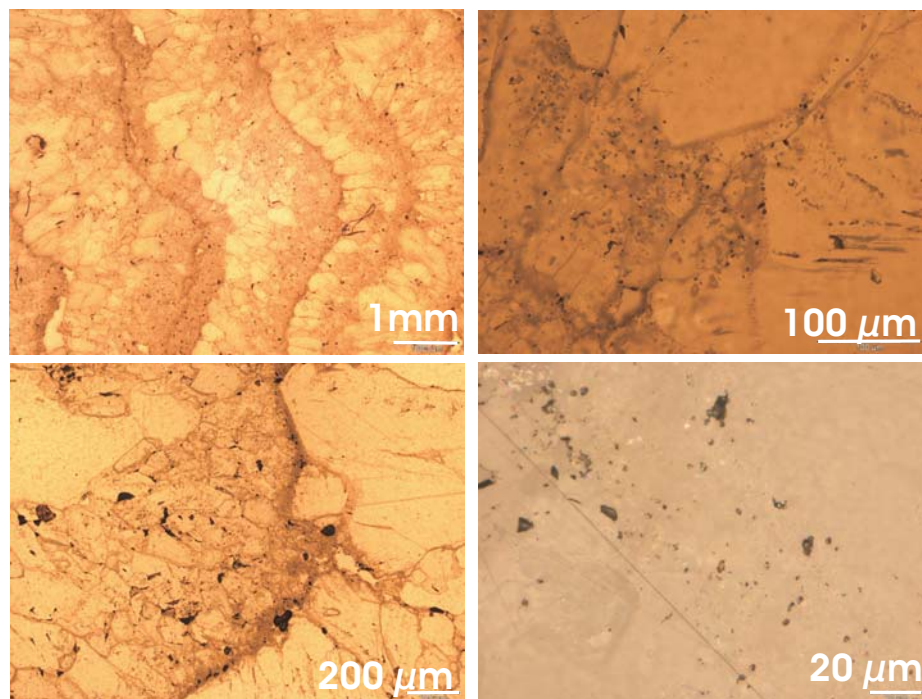


Figure 3.3: Thin sections of the flowstone H8Z from Hoti cave (Oman) using different magnifications.

The thin-section of stalagmite H12 (Fig. 3.2) shows a microsparitic fabric without a clear c-axis orientation under polarized light. Furthermore, the thin section is characterized by many small and also some large inclusions. They are distributed with a certain pattern over the whole thin-section, which may reflect seasonality as found e.g. by Genty and Quinif (1996). Two denser lines of fluid inclusions are visible on the right side. On the left side grains and large inclusions can be seen. The large inclusions with irregular forms are air-filled. Water-filled inclusions are rarely larger than $20\ \mu\text{m}$ (s. Fig. 3.2, lower picture). Due to the huge amount of inclusions this speleothem has a considerable noble gas signal. However, the large air-filled inclusions contribute overwhelmingly to the signal. The change in structure and also the alternation of zones with a higher fluid inclusion density with areas exhibiting few inclusions, may be due to the frequent and strong changes in precipitation and growth conditions in the Hoti Cave, which was marginally influenced by the Asian monsoon (Neff et al., 2001; Burns et al., 2001).

This speculation can be verified by the following samples from the Obir Cave and also from Bunker cave. OBI5 from Obir Cave (right side of Fig. 3.2) shows large columnar crystals, which are mostly orientated in the same direction. In contrast to H12, we found randomly distributed inclusions which were significantly smaller than in the case of H12. Even using a higher magnification, no grains are visible, but a layered structure became visible. As the dimension and amount of inclusions is obviously smaller, the noble gas signal is also strongly reduced compared to H12. However, the ratio of noble gases from the air-filled inclusions to noble gases from water-filled inclusions is even worse. The uniform distribution of inclusions in the shown thin section may be related to more constant growth conditions as the cave is situated in the west-wind zone, where precipitation is provided over the whole year.

The flowstones are formed by a water flow over substrate. As there is normally a constant water film above the speleothem, the growth conditions are rather constant. Therefore, a similar appearance as in case of OBI5 should be expected. However, Figure 3.3 shows a



Figure 3.4: Thin sections of the stalagmite CG from Cuba.

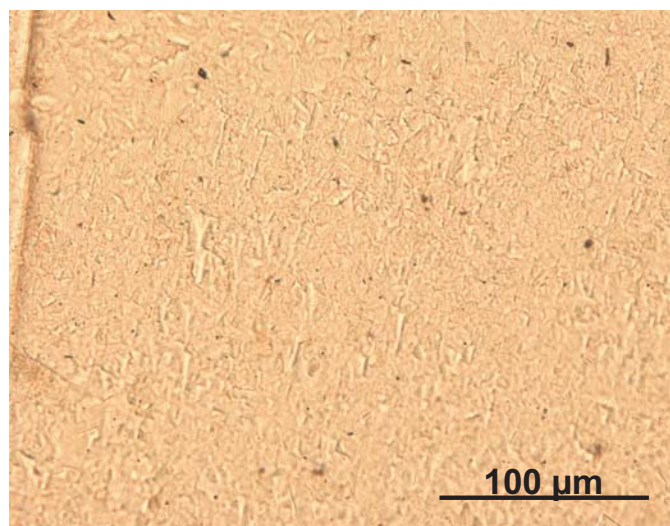


Figure 3.5: BU-U thin section. Most of the inclusions are very small, round and randomly distributed over the displayed photo.

pronounced layered structure with large grains and a high amount of inclusions in certain areas. Similarly, the distinct layers can be seen with polarized light. Bands with dendritic fabric alternate with layers of columnar crystals. The flowstone originates from the same cave system as the stalagmite H12 and is similarly influenced by the monsoon. Dry periods deliver less water and can therefore cause a change in the saturation state of dripwater and influence the calcite development. Otherwise, a very fast dripping site with low or no supersaturation may provoke a stop in growth or even calcite dissolution. These changes in growth conditions generate also different amounts of inclusions. In large grains few inclusions are visible whereas at the layer boundary and between small grains a huge number can be detected.

The age-model of the stalagmite from Cuba shows that it was a fast and constantly growing speleothem (0.5 mm per year). As in the case of OBI5, the constant conditions led to randomly distributed inclusions and furthermore to a hardly layered structure without visible smaller grains (≤ 0.5 mm). Similarly to the thin-section OBI5 we can see large crystals, but with an erratic shape and irregularly interspersed small crystals. In the case of the highest

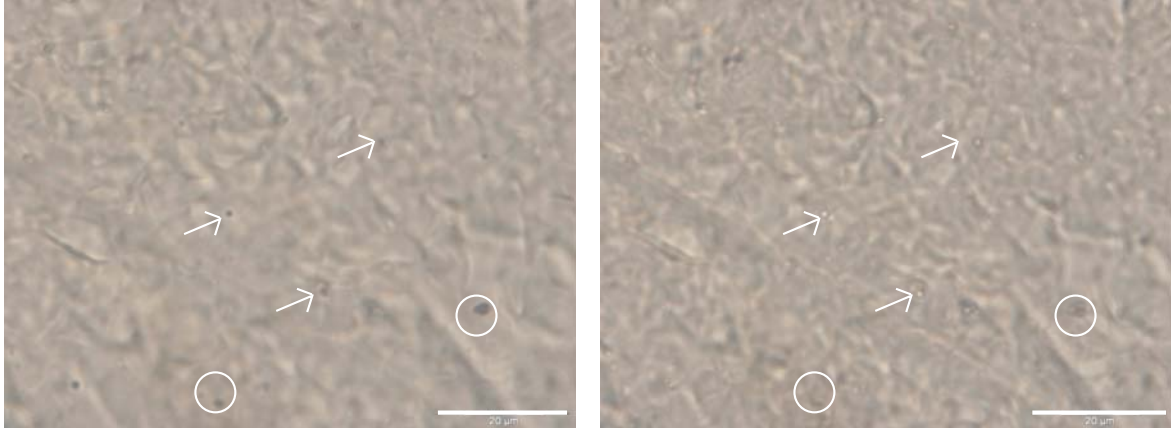


Figure 3.6: BU-U thin section on a closer view. Most of the inclusions are water-filled. They have a round form and appear white in the translucent light image (see places marked by arrows), if the distance of the lenses to the object is adequate. This can be seen in the right photo. The left photo shows the same detail, but with different distance object-lenses. Scale bar 20 μm .

magnification only few inclusions, which are at least partially water-filled (light reflecting points), and no purely air-filled inclusion (should be dark) are visible (Fig. 3.4). Furthermore, the inclusions are extremely small ($\ll 1\mu\text{m}$) compared to the inclusions shown in the other thin sections. The noble gas signal and fortunately also the air/water volume ratio was accordingly small. Thus, most of the noble gases originate from the water-filled inclusions.

With regard to the Bunker Cave, a very low air/water volume ratio A was measured in stalagmite BU-U. A mean value, calculated from noble gas fitting, was about 0.035. In Figure 3.5 a thin-section is taken through the microscope at a low magnification. There, a large number of generally very small inclusions can be seen. Larger inclusions may have been destroyed during the thin-section preparation. A closer look on the photograph reveals a structure which reminds of a gravel deposition in river valley. In general, very large columnar crystals (from some mm up to several cm) with a uniform orientation are prevailing.

In another thin-section of BU-U (Fig. 3.6), recorded at higher magnification, the size of the water-filled inclusions can be estimated. Compared to the scale bar with a total length of 20 μm they, at best, have a diameter of 1 μm . Another interesting point is the change in behaviour if the focus setting is varied a bit. If the inclusion is totally air-filled, no reflection can be expected; whereas the water-filled inclusions can show a white glow due to the optical behaviour of a water drop. Varying the focus settings, the water-filled inclusion on the shown pictures can be detected (indicated by arrows). Comparing the two pictures of Fig. 3.6 only the two largest inclusions (marked by circles) do not show reflections and are therefore assumed to be only filled with air. Recapitulatory, few air-filled inclusions with moderate diameters ($\leq 10\ \mu\text{m}$) and a large number of water-filled inclusions with a small diameter ($\leq 1\ \mu\text{m}$) have been found.

3.1.2 Summary of the thin-section analysis

Samples with a high amount of inclusions often show a grain-type feature as e.g. the Oman samples. In contrast to these samples, the milky white speleothems provide a smaller total amount of inclusions and also less large (air-filled) inclusions. An example is the BU-U stalagmite or the CG speleothem. Both show a milky white appearance with large columnar crystals and are similar in the inclusion distribution. Very few large inclusions can be found,

whereas the mostly water-filled and in general tiny inclusions ($\leq 1 \mu\text{m}$) are distributed randomly. A milky colour can mostly be related to an advantageous air/water volume ratio, as e.g. demonstrated by the CG and the BU-U stalagmite. In contrast, the brownish or grey appearance of stalagmite H12 or the samples from Chile (MA), is associated with a huge number of inclusions, which are dominated by a high contribution of extremely large air-filled inclusions. Interestingly, both H12 and MA are affected by monsoon or high monsoon-like precipitation.

Another interesting parameter is the water content, which is determined through crushing. If a structure with large columnar crystals is prevailing, then the total water amount decreases in the way the speleothem gets more translucent. A very translucent sinter-piece with large crystals yields e.g. a low water content, whereas the more milky soda straw yields a water content about one order of magnitude higher.

Noble gas studies should focus on inclusion-rich speleothems which are dominated by water-filled inclusions. They can be selected primarily by their colour, which should be in general milky white and not too translucent, and additionally by thin sections, which should show few large air-filled inclusions and a great number of small (water-filled) inclusions.

3.2 Water determination

Temperature calculation with uncertainties $<2 \text{ }^\circ\text{C}$ is not possible using only the noble gas ratio. The only way towards precise palaeotemperatures is given by the noble gas concentrations. To determine these concentrations it is necessary to know the water amount from which the noble gases originate. Moreover, an interesting issue is the survey of special techniques like stepwise heating and stepwise crushing in consideration of therein opened water-filled inclusions. Similarly, the released water is an important parameter for the different methods and can give information about the extraction efficiencies.

Dennis et al. (2001) and McDermott et al. (2006) say, that water amounts are typically in the range of 0.6 - 1.9 ‰wt, but in this study we found out to vary them considerably more (0.001 to 4 ‰wt). Therefore a precise measurement down to the submicrolitre range is necessary for speleothem samples with a typical weight of about 1 gram. To solve this problem, two methods have been developed. First, a relatively precise balance can be used to determine the amount of extracted water, and second, the relationship between water vapour pressure and water amount, derived from a special calibration curve is useful. In the microlitre range a measurement with an uncertainty of 2 - 3% can be achieved by both methods. The objective was to reduce the uncertainty to less than 1% in the microlitre range ($\approx \text{mg}$), to 1 - 2 % at 0.1 μl (100 μg) and in maximum to 10 % in the range from 0.1 to 0.01 μl .

To determine the released water from speleothems two different methods have been used. One with acceptable precision is weighing of water in the mg range. The disadvantage is the high time consumption (at least 1 hour per sample). A practicable method, especially for small samples, is the water determination by pressure. There are only 10 - 15 minutes necessary for one sample.

Beyond these two methods, the absorption of light may be used to determine the water amount. Perhaps this method can be used in the range of extremely low water amounts, because the laser can be tuned to a special H_2O -absorption line. However, this method still awaits its testing. FTIR spectroscopy has just been used to control the presence of liquid water in crushed stalagmite samples (McDermott et al., 2006), but not with the objective to determine water amounts.



Figure 3.7: High precision balance (Mettler Toledo) with a precision of 2 μg . The sample is put on the small roundish dish inside a chamber which is protected from air motion by sliding windows.

3.2.1 Water determination by weighing

The weighing tests have been performed using samples prepared at the extraction line of Rice (2004). To test the efficiency and the effects of different handling, artificial samples have been built. Glass-capillaries (Hirschmann Laborgeräte, 12.5 cm length, 0.3 mm inner diameter, 0.03 μl reading accuracy, see Fig. 3.8) have been filled with tap water. The water is sucked into the glass tube by the capillary effect or the use of a pipette. Afterwards the two ends of the glass tubes are flame-sealed. Then the filled capillaries are opened in a copper tube by crushing under high vacuum conditions (before crushing $\leq 1 \cdot 10^{-7}$ mbar). The released water is frozen into a copper cold finger (Fig. 3.8) using dry ice. After 30 minutes the cold finger is closed by squeezing. The closed copper tube part and the rest of the copper tube as well as the gaskets are weighed using a special balance (Mettler Toledo, maximum weight: 19.99 g, reading accuracy: 2 μg). For comparison the empty copper tube as well as the gaskets are measured before the experiment. Moreover a buoyancy-correction is performed. The weight is reduced by 1000 μg , because of the lower pressure inside the tube. The weight difference of the empty copper tube and the gaskets to the weight after freezing of the water, including the corrections, leads to the amount of water captured in the cold finger.

The application of the weight method requires a very attentive handling. One careless movement can influence the results substantially. Several points have been tested in this context and should be taken into account in the weight calculation (s. Fig. 3.10).

Rubbing the copper tube several times with a paper results in a large reduction of the weight. In contrast to this, there is no deviation detectable if the copper tube is slightly rubbed once with a sand paper. One finger-touch increases the total weight because of the adsorbed grease or other particles. Hence, the sample can only be touched carefully with tweezers. Squeezing in order to close the water-containing part of the tube leads to a weight reduction in the order of (105 ± 10) μg . Because this effect can not be avoided, it is included in the correction of the weight calculation. Carrying the copper tube parts with tweezers is difficult and sometimes provokes them to fall off to the ground. However, falling tests did not reveal a deviation of the expected value.

In consideration of all the effects that have to be taken into account (buoyancy correction due to lower pressure inside the squeezed copper part, mass-changes by different handling, drifts of the high-precision balance), it is fairly time-consuming to reach the maximum precision. Additionally, the uncertainty can not be reduced in the necessary order of magnitude as the correction uncertainty alone is about 50 μg . This would cause a total uncertainty of at least 50 % in the case of 0.1 μl of water, which is by far too high for a meaningful NGT calculation.

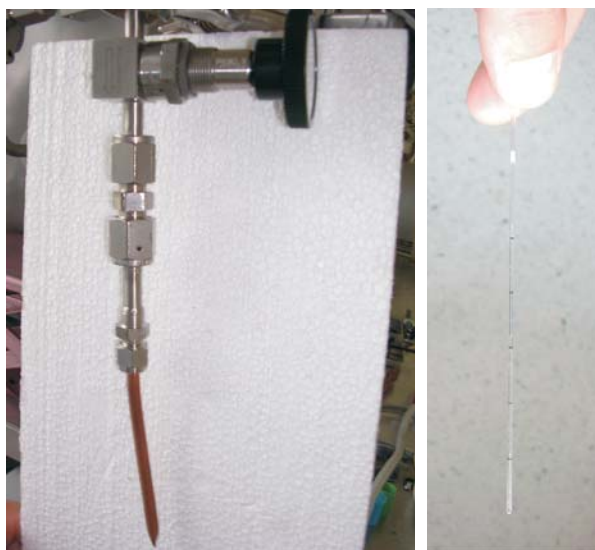


Figure 3.8: Copper tube freezing finger attached with gaskets. Only the lowermost part of the finger is cooled by dry ice for 30 minutes to freeze out the water. The copper tube is squeezed directly below the attachment point by a special pincer to enclose the water. Then the valve is closed and the two copper tube parts are weighed. Right picture: glass capillary filled with a known water amount for calibration purposes. Between two black rings 1 μl of water is contained.

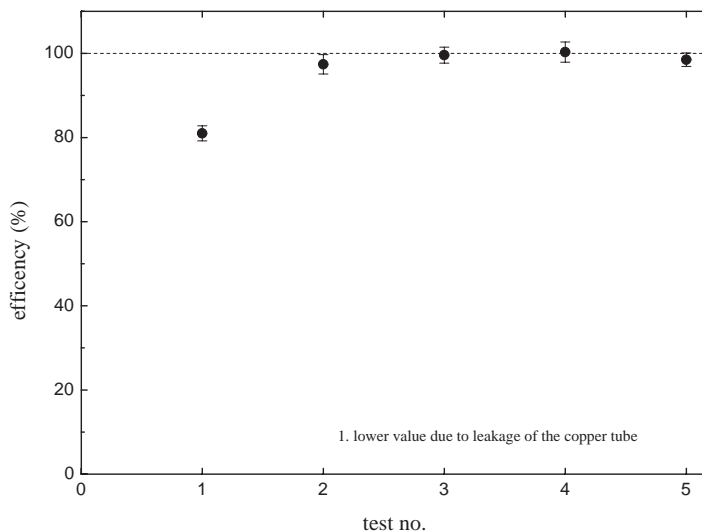


Figure 3.9: Result of five efficiency tests. The water amount measured by weighing is compared to the water input before the extraction (recovery in % of the input value). The first value is lower due to incomplete freezing and a leak in the copper tube. The other four measurements show that the water can be well collected and detected with an overall recovery of $(99.0 \pm 1.3) \%$ (first value not included). Therefore we can assume that the water recovery of this method is complete.

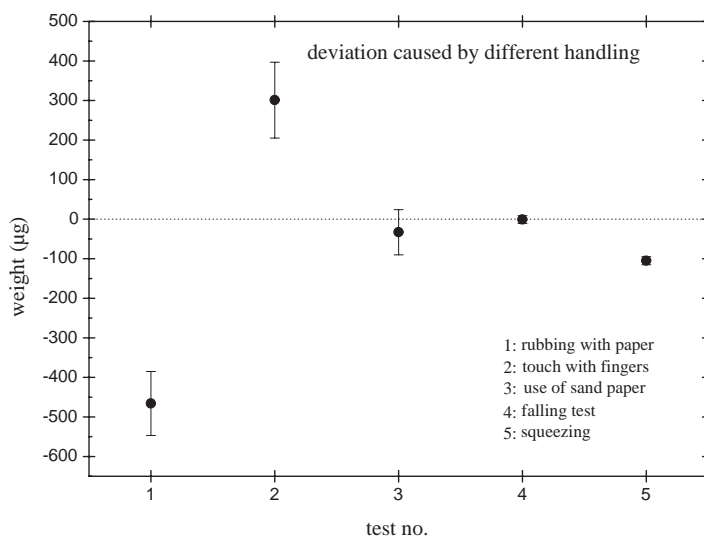


Figure 3.10: Effects of different handling on the determined weight. The deviations are given in μg with statistical uncertainties resulting from the weight determination (no.1 - no.4) respectively from repeated measurements (no.5).

3.2.2 Water determination by pressure

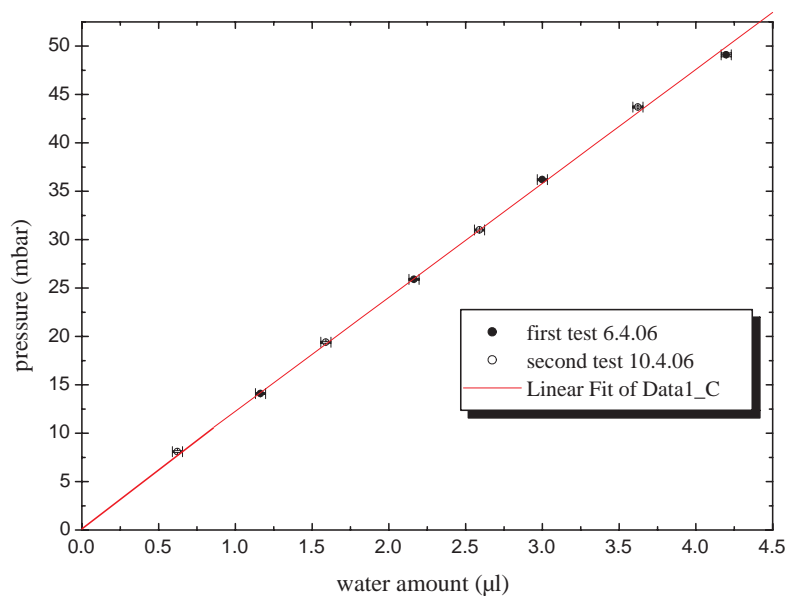
Motivated by the large effort applying the weight method, some other ways have been considered to solve the problem of a precise water determination. Due to the rather high precision which can be achieved with special pressure gauges (Keller Lex1, precision 0.01 % full scale, range 0 to 3000 mbar and Pfeiffer CMR 263, 2 ‰ accuracy, range 10^{-3} to 11 mbar, both are capacitance pressure sensors), we tried to determine the water amount by the pressure of the water vapour in certain line volumes. Unless the water does not condensate (saturation water vapour pressure at different temperatures: s. Table 3.1) the pressure can be used to calculate the corresponding water amount. 1 mg of water corresponds to 1.25 ccSTP of water vapour, whereas it only contains dissolved atmospheric gases on the order of 10^{-5} ccSTP. Thus, the pressure in the different volumes is almost totally produced by the water vapour. Knowing the volume, the determined pressure can be transferred into a gas volume using the equation for ideal gases or the Van-der-Waals gas, and finally be transferred into a water amount. However, we did not follow this way of water determination.

Another possibility is given by the use of calibration curves. These curves are prepared using known water amounts sealed in glass capillaries. The capillary consists of a fixed total volume, wherein certain water amounts are filled. The remaining volume contains air. The sealed glass capillaries are inserted into a copper tube, where they are pumped until a sufficient low pressure is reached. Then the glass capillaries are opened by squeezing of the surrounding copper tube. The released water leads to a certain pressure, which is noted manually.

The results of the first attempt using the calibrated pressure curve at the line of Rice (2004) can be seen in Figure 3.11. For pressure determination a Keller Lex1 gauge has been used. Until a pressure of about 60 mbars the relation between pressure and water amount remained quite linear. The condensation point was about 60 mbars, because the line was heated to

Table 3.1: Saturation vapour pressure of water respectively ice at different temperatures.

temperature ($^{\circ}\text{C}$)	p_{ice} (mbar)	p_{water} (mbar)
-100	$1.4 \cdot 10^{-5}$	$3.6 \cdot 10^{-5}$
-78	$7.5 \cdot 10^{-4}$	$1.62 \cdot 10^{-3}$
0	6.1115	6.1121
20	-	23.39
21	-	24.87
22	-	26.44
23	-	28.10
24	-	29.85
36	-	59.5
37	-	62.8
40	-	73.8
60	-	199.3
100	-	1013.25

**Figure 3.11:** Calibration curve prepared at the line constructed by Rice (2004). Two test series showed a good linear relationship up to 60 mbar at a temperature of 36 $^{\circ}\text{C}$. This calibration curve was used to determine the water amount in the first crushing and heating experiments

about 36 °C. Further heating to shift the condensation point to higher values is not possible, because this would damage the electronics of the pressure gauge. A second series of tests reproduced the results of the first tests with regard to the linearity. A linear fit of the data led to the following result:

$$p(v) = 0.49(\pm 0.6) + 11.78(\pm 0.25)v \quad (3.1)$$

The pressure p is given in mbar as function of the water amount v in μl . If the fitting error is taken into account, a stalagmite sample with a total amount of opened water inclusions of about 4 μl has an uncertainty of 2.4 % according to this calibration-curve.

The extraction line has been rebuilt and different expansion volumes have been attached with the purpose to achieve higher precision in the case of different sample amounts. In the final stage, the calibration curves were prepared using three different expansion volumes to detect very small water amounts in the range of 0.1 μl as well as larger water amounts up to 1.5 μl with a typical precision of 2 - 3 %. The glass capillaries had been prepared in the same way as explained above. After squeezing of the capillaries, the water is frozen to the cold finger for 20 min. Subsequent to line pumping the freezing finger is warmed up to room temperature, which is held quite constant by air-conditioning to $(23 \pm 1)^\circ\text{C}$. Then the water vapour is expanded to the first volume (detailed description see Fig. 3.15), where the pressure is determined 5 min after expansion by the capacitance pressure sensor CMR 263. Subsequently, the water vapour is expanded to the next volume where the pressure is determined again after 5 min.

The results are displayed in Fig. 3.12 for all three volumes. For speleothem samples all three volumes are used and an average is calculated from these three measurements. The uncertainty is calculated using simple error propagation from measurement errors and fitting uncertainty. Therefore a typical sample with a water amount of 0.5 μl yields an uncertainty of about 2 %, a water sample of 0.1 μl an uncertainty of 6 %. The error increases to about 10 % if the released water amount is less than 0.06 μl .

3.2.3 Precision and limits

- Weighing method

The relative error of water determination by weighing is in the range of 2 % in case of 4 μl -samples. As typical stalagmite samples (0.5 - 1 g) provide only 0.1 to 1 μl of water, the relative error is significantly higher. The uncertainty is dominated by the uncertainty of the correction terms and, therefore, difficult to reduce. The weight itself can be determined with a higher precision. The overall absolute uncertainty including the correction terms can hardly be reduced below 50 μg which results in an uncertainty of at least 50 % if only 0.1 μl water is released.

- Manometric method

In this case the precision is limited by the uncertainty of the calibration curve and the precision of the pressure gauge.

The main uncertainty derives from scattering in the calibration curve. One part belongs to the slope error and the other part to the error of the intersection point at the y-axis. These errors can be reduced if the number of calibration samples is increased. The relative slope error is, in the case of the first attempt (Fig. 3.11) 2 %, and in the final state for the expansion volume 2 about 1 % (Fig. 3.12). Thus, the uncertainty due to the calibration curve can be reduced to about 1 %. The uncertainty of the

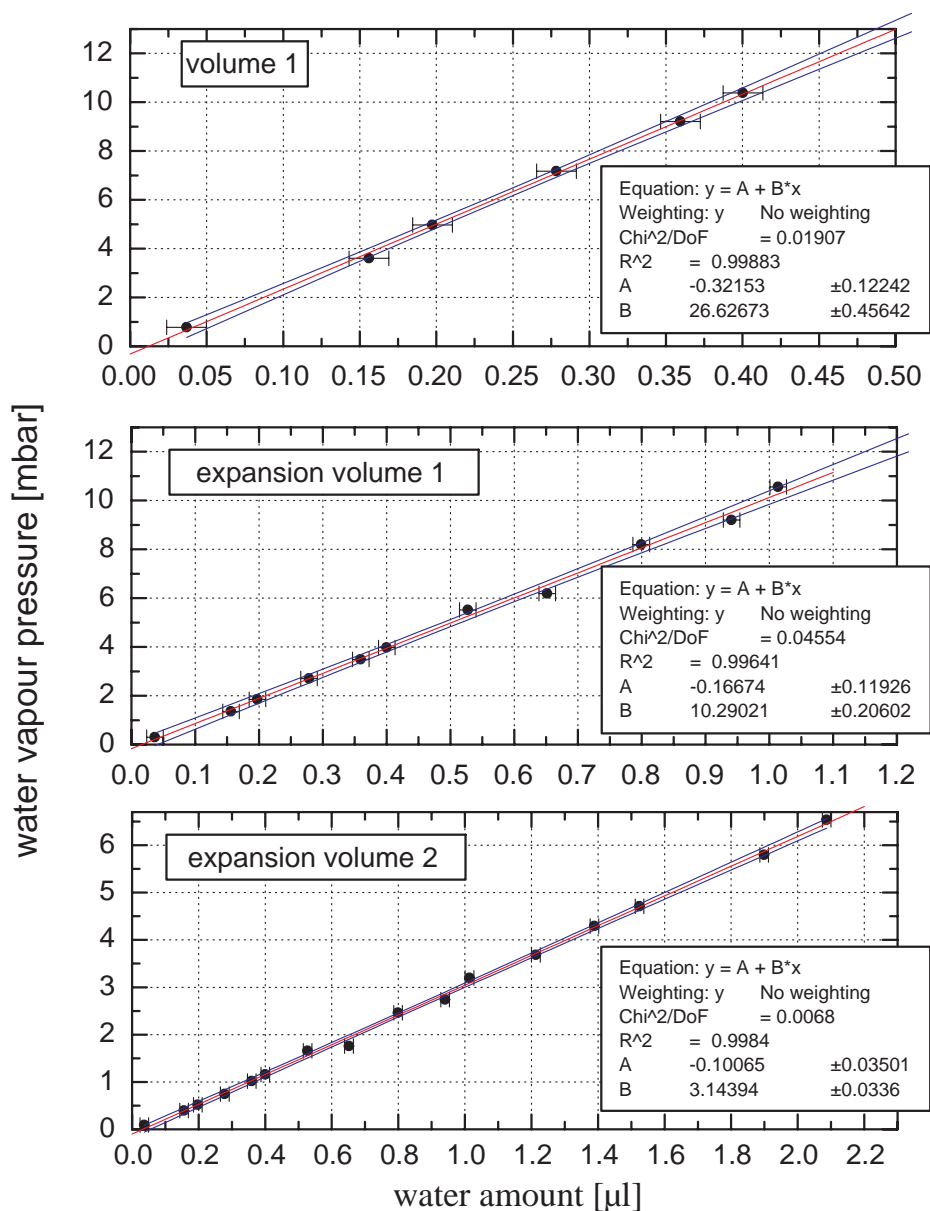


Figure 3.12: Water determination at the extraction line using different expansion volumes (increasing from top to bottom). The calibration curve was derived via artificial standard samples. The volumes are not heated during the water determination, but kept at room temperature (about 23.0 °C), which is stabilized by an air-conditioning system. In each case a linear relation is obvious. The fitting results are given in the small box at the right side. These calibration curves were used to determine the water amount of all speleothem samples measured beginning with measurements in December 2007.

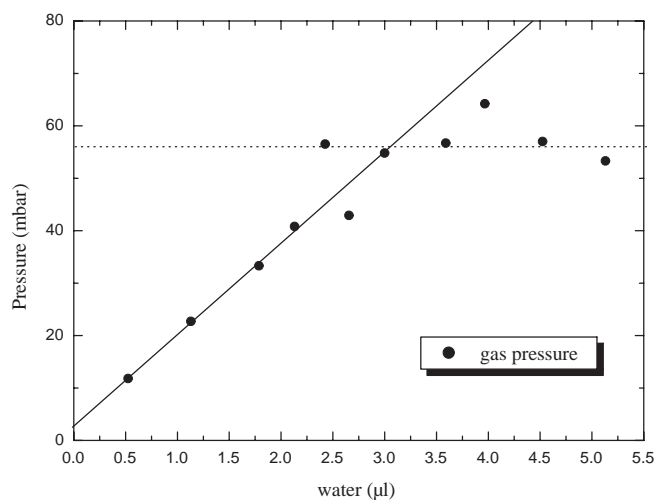


Figure 3.13: The relation between pressure and water amounts stays linear until 55 - 60 mbar, when the line is heated to about 35 °C. Then the water condensates at the coldest part of the line and no further pressure rise can be detected. The method is limited by this effect and therefore adequate expansion volumes have to be chosen to prevent condensation. In the final state the line is held at about 23 °C which corresponds to a saturation vapour pressure of 27.2 mbar.

pressure gauge (0.1 mbar using the Keller Lex1 and 0.005 mbar using the CMR 263 gauge) plays a minor role, if the line volume is adapted for smaller water amounts. For instance, a sample with 0.1 µl water produces a pressure of about 2.2 mbar in the case of volume 1 used in Fig. 3.12. Then, the relative error due to the CMR pressure gauge is 2 ‰. However, measuring smaller water amounts is limited as it is difficult to prepare standard water amounts smaller than 0.04 µl for calibration. Precision and calibrated range could potentially be improved by precise volume determination (can be calibrated to ± 0.3 ‰) and calculation of the water amount using the ideal gas laws (corrections due to Van-der-Waals behaviour of water are small).

3.2.4 Summary

In most cases the released water amount is in the range of submicroliters (0.1 - 0.7 µl) and can be even less than 0.1 µl for some special techniques like stepwise extraction procedures or samples with an extremely low water content (≤ 0.1 ‰wt). The uncertainty is at least about 50 µg with regard to the weighing and, therefore, results in a total uncertainty larger than 50 % in the case of 0.1 µl water. However, using the pressure-based water determination via calibration curves, the total uncertainty is about 6 % even at 0.1 µl. For NGT calculation the total uncertainty should not exceed 5 % to achieve meaningful results. Therefore, the water determination via weighing has to be rejected. The noble gas concentrations are derived using the water vapour pressure as the uncertainty is in most cases below 5%.

3.3 Extraction of water and noble gases

In this section different extraction methods like crushing in copper tubes, milling with a steel ball, thermal decrepitation and extraction by microwave heating will be introduced and discussed. Of special interest is the separation of gases from the air- and water-filled inclusions, which can only be implemented with adequate extraction techniques.

3.3.1 Design of the extraction line

The extraction line built by Rice (2004), which was used in a modified version at the beginning, is displayed in Fig. 3.14. In the basic version, a vessel with degassed water was attached instead of the pressure gauge. It was intended to provide a constant gas flow from the stalagmite crusher to the sample container. The sample container was therefore cooled with liquid nitrogen to establish the gas flow from the crusher to the gas container. However, this did not work very well as it resulted to be difficult to prepare degassed water in the necessary quality. The vessel was filled with about 250 ml of water, which needs to be degassed to more than 99.99995 % to prevent a major influence on the speleothem results. Even in the case of this efficiency a significant noble gas amount will derive from the degassed water as it is about 500 000 times more than the water typically released from speleothems. Therefore this design was rejected.

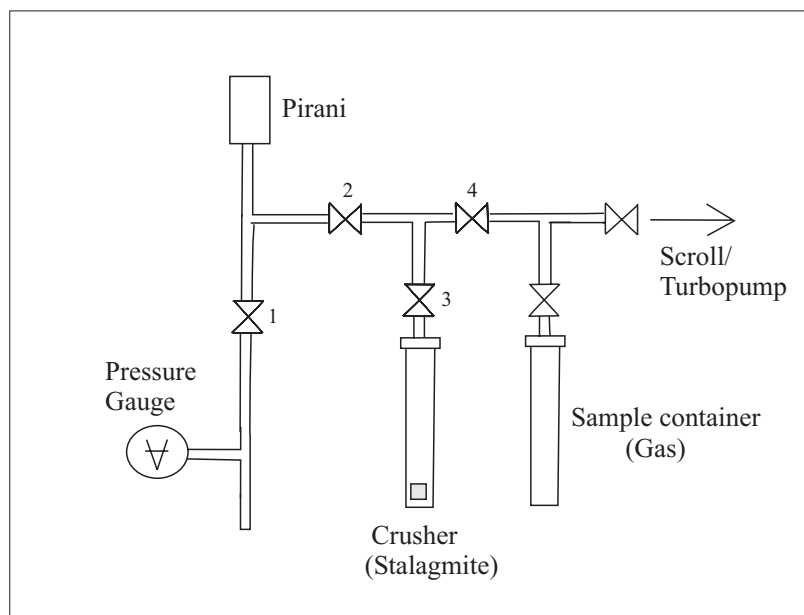
In the modified version a freezing finger and a capacitance pressure gauge (Keller Lex1) were attached instead of the water vessel. The speleothems were crushed either in a steel cylinder respectively in a copper tube, which had been evacuated. Before crushing the hand valve 4 is closed, valve 1,2 and 3 are opened to freeze the water at the lowest end of the left side. Then valve 1 is closed and the line is heated to determine the water amount using the water vapour pressure. Afterwards the gases are expanded to the whole line including the sample container, which is closed off after a certain time. The gas-filled sample container is attached to the preparation line of the mass spectrometer for noble gas measurements. However, using this procedure not all noble gases can be transferred to the mass spectrometer due to the volume splitting at the extraction line, which cuts off about 50 % of the total gas amount. This setup was used for some samples in the first test runs ("run August" and "run November").

At the same time a simplified extraction was implemented directly at the mass spectrometer preparation line, which is also shown in Figure 3.14. At first, the sample is crushed in a copper tube and then the water vapour pressure is determined in the unheated line using a capacitance pressure gauge (Keller Lex1). Afterwards the gases are frozen totally into the cryogenic traps without any splitting. This setup was used for most samples in the first two measurement runs.

The final extraction line (shown in Fig. 3.15) is designed to enable the extraction of at least one sample per day including 24 hours pumping time. Therefore the crushing devices (steel cylinder as well as copper tubes and the cracking device for glass ampuls) can be attached at the extraction system at three different inlet points. One sample can be pumped by the scroll pump, the second sample can be pumped with the turbo-molecular pump and the third can be extracted and its gases being frozen to the traps at the same time. If a shorter pumping time is used (e.g. 12 hours), it is even possible to measure two samples a day.

The pre-vacuum of the extraction line is established by a scroll pump (Varian SHO 1001 UNIV) and is controlled by a pirani pressure gauge (Pfeiffer compact pirani TPR 261). To avoid longer operation times of the scroll pump, an expansion volume (≈ 1 l) is used to

Extraction modified stalagmite line



Extraction on line

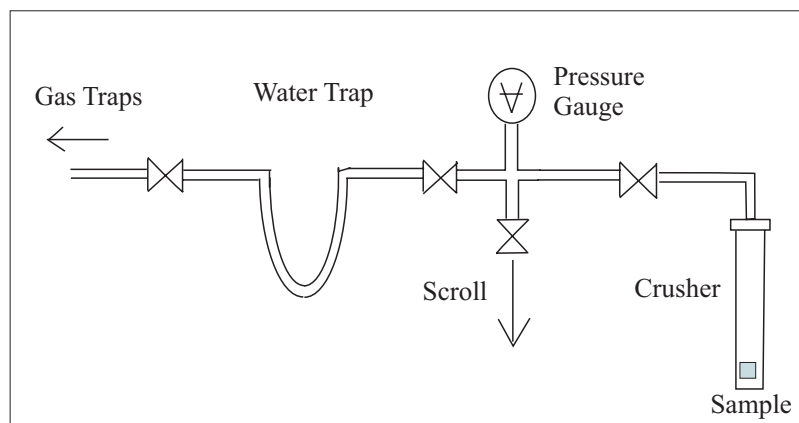


Figure 3.14: Design of the two extraction lines, used in the first measurement runs. The upper drawing presents the external extraction at the modified line of Rice (2004), the lower one shows the extraction at the preparation line of the mass spectrometer. In each case the sample is crushed (or heated) and then the water vapour pressure is controlled by the pressure gauge. The gases are entirely transferred to the mass spectrometer in the case of the direct extraction. If the sample is prepared at the line of Rice, a volume splitting was necessary. The gases have been expanded to the sample container with a volume of about 100 cm^3 , so that the main part is in the sample container. Nevertheless, about 47 % are lost due to this splitting.

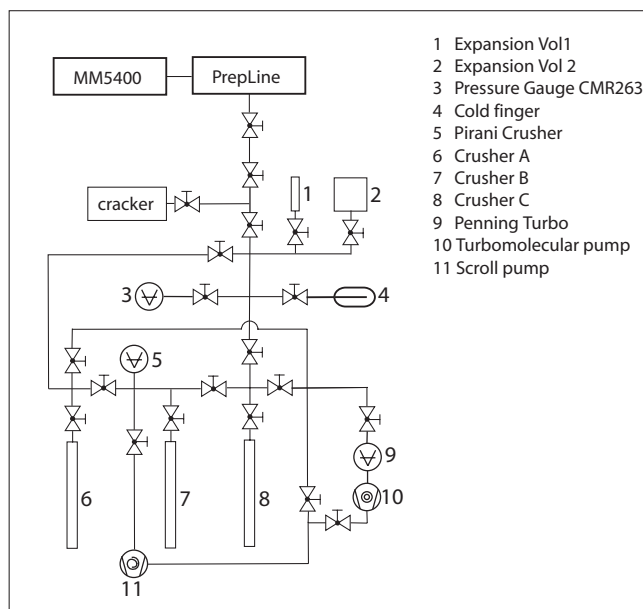


Figure 3.15: Design of the extraction line used in November 2007 and in subsequent measurements, e.g. run Gamma and run Delta. For higher throughput and longer pumping times the number of crushers has been increased (no. 6-8) and additional pump lines have been established. Number 1 and 2 indicates the expansion volumes for water determination. The water is frozen into the cold finger (no.4) and then expanded to the line between 3 and 4 in the first step. Subsequently, the expansion volumes are attached.

preserve a good pressure (10^{-3} - 1 mbar) for at least 2 days. If the prevacuum is worse or if samples have to be pumped, the scroll is switched on manually. There are two inlets designated for pumping with the scroll.

The high vacuum is established using a turbo-pump (Pfeiffer TMU 071 P) at 1500 Hz, which is operating all the time and which can be used via two different pathways for sample pumping. The pressure is controlled above the turbo pump using a compact cold cathode gauge (Pfeiffer IKR 250) with a range of $2 \cdot 10^{-9}$ to $1 \cdot 10^{-2}$ mbar. Typically, the line pressure is in the 10^{-8} mbar range. Additionally, the line pressure is controlled by a pirani gauge (Pfeiffer compact pirani TPR 261) with an operating range down to $5 \cdot 10^{-4}$ mbar to separately control the extraction of the samples. Another pressure gauge (Pfeiffer compact capacitance gauge CMR 263) with a higher precision (2 %) is used for the water determination via water vapour pressure.

The water released during the extraction is frozen for 20 minutes into the cold finger (no.4, see Fig. 3.15) using a dry-ice alcohol slush. Afterwards, the cold finger is closed off from the line by a hand valve and the gases in the line are transferred to the gas traps. The gas loss due to the splitting is in the low permil range as the volume of the freezing finger is about 2 ml and the rest of the line including the crusher more than 750 ml. The water vapour pressure is measured using different expansion volumes (≈ 100 ml and ≈ 275 ml) to prevent condensation and to achieve maximum precision by ideal utilization of the working range ($1 \cdot 10^{-3}$ - 11 mbar) of the pressure gauge.

Before the manometric water determination, the gases are transferred to the noble gas preparation and separation line (for detailed description see Friedrich, 2007). The first trap, a naked steel cryogenic trap, is held at 25 K so that all gases except He and Ne are condensed. After 20 min the connection to the second cryogenic trap, held at about 10 K and filled with activated charcoal, is opened for 20 min in order to condense He and Ne there. Subsequently, the

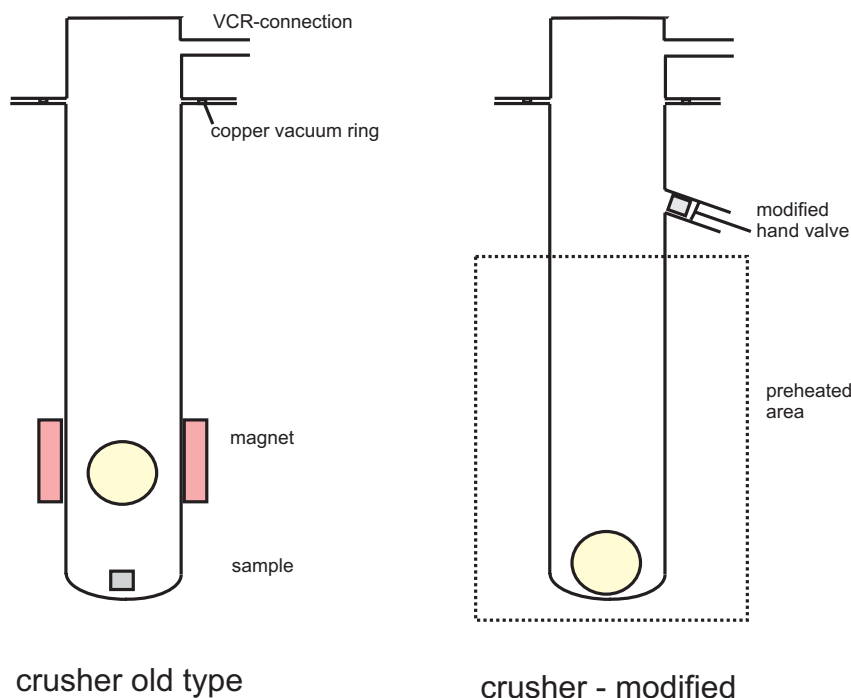


Figure 3.16: Extraction by crushing in a steel cylinder. On the left side the original crusher is depicted. The modified version is displayed on the right. As the sample is located for pumping in the storage space offered by the modified hand valve, the lower part of the crusher can be baked out without affecting the sample.

gases are released from the traps in discrete steps and admitted to a GV 5400 noble gas mass spectrometer for analysis. In the first step the charcoal trap is heated to 45 K to release the He fraction. Next, the trap is set to 90 K to release Ne. Finally the naked steel trap is heated to 130 K to release the heavy noble gases (Ar, Kr, Xe) as well as nitrogen and most other gases that may be present in the sample. The reactive gases in this fraction are removed by a heated SAES GP50 W2F getter and a cold SAES AP10N getter, before the purified Ar-Kr-Xe mixture is admitted to the mass spectrometer. The cold getter is also used for the He and Ne fraction and for the rather pure calibration gases (so-called fastcals), which are measured to correct short-term drifts of the mass spectrometer.

3.3.2 Extraction using a metal crusher

The noble gases can be extracted from the stalagmites by crushing or heating. A well-known setup is the use of a stainless steel cylinder, which is common in geological investigations. The sample is put inside, pumped until a high vacuum is reached and then the inclusions can be opened by crushing with a steel ball (Dennis et al., 2001; Rozanski and Dulinski, 1987; Schwarcz et al., 1976). First test series with a similar extraction system showed unacceptably high background values (Rice, 2004). Therefore, this method was not used at the beginning of this project. It turned out that the high background was caused by small leaks or problems with the vacuum fittings and not by the crusher itself or the crushing procedure.

In a second attempt, the extraction in a steel cylinder by crushing with a steel ball was investigated more closely. Detailed information can be found in the thesis of Marx (2008). In the following, the setup as well as the main results are presented briefly. A schematic drawing (Fig 3.16) shows the two types of crushers. The first one is a simple 33 cm long steel cylinder

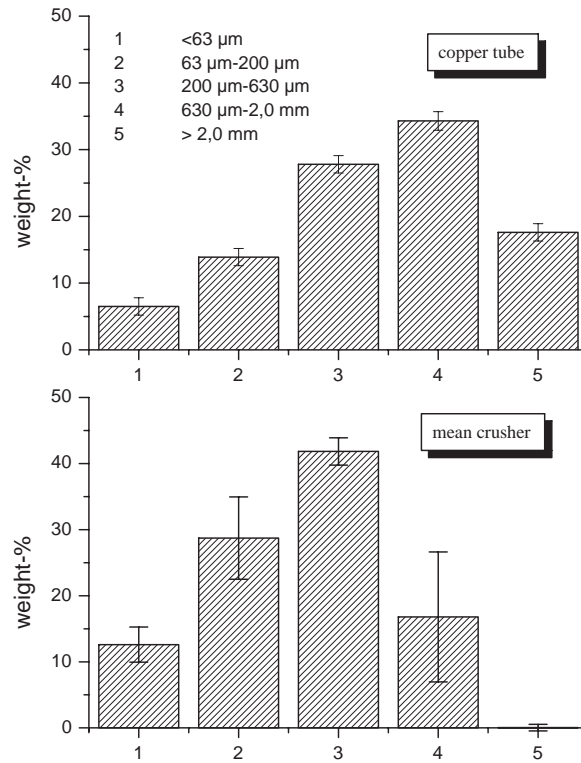


Figure 3.17: Grain size distribution of crushing in the steel cylinder and copper tubes. The copper tube plot refers to speleothems which are squeezed one time inside the tube by a vice. The distribution was determined from a BU-U sample and shows a typical pattern for squeezing in copper tubes. The crusher distribution was determined from several BU-U pieces by calculation of a mean. The stalagmite pieces have been hit 60 times with the steel ball.

with an inner diameter of 26 mm containing a 23 mm steel ball. The cylinder is attached by a copper vacuum ring to a flange, which is welded to a VCR-fitting.

The second crusher type is similar to the basic version, but additionally offers a place for sample storage during bake-out of the crusher at high vacuum, preventing the speleothem to heat to the same extent. This special place for sample storage is constructed from a modified hand valve with an inner diameter of 14 mm and a length of 10 mm. The sample is placed in the attachment by tweezers. Due to this storage the cylinder can be baked out at higher temperature (150 - 250 °C) without affecting the sample. Subsequent to the cleaning and pumping process, the steel ball, which is also baked out, is moved above the sample inlet connection, so that the sample can be thrown down to the bottom of the cylinder by moving the valve. Afterwards the sample is crushed in high-vacuum by the magnetically moveable ball.

According to the number of strokes a corresponding grain size distribution was achieved. The fraction of fine grains ($\leq 200 \mu\text{m}$) is about 40 % wt in the case of 60 hits and even larger than 85 % wt if the sample was hit 400 times. Compared to crushing in copper tubes (see Fig. 3.17) a higher fraction of small crystals can be obtained. Using copper tubes, the fraction of fine grains ($\leq 200 \mu\text{m}$) consists only of about 15 % wt. Furthermore, the extraction is better reproducible with regard to the grain size distribution as well as the background contribution. The grain size distribution is of special interest regarding the separation of noble gases from air and water-filled inclusions as well as for the extraction efficiency. Water-filled inclusions

are supposed to be smaller than 10 μm and mainly even smaller than 1 μm , whereas the air-filled inclusions are in general larger. Crushing with the steel ball enables stepwise separation and extraction techniques, which are discussed in section 3.4.

A further advantage of the modified steel crusher is the possibility of preheating the system. Especially for thermal decrepitation as well as for simple crushing the blank values can be reduced with this method. To investigate the effect of preheating, the steel crusher was vented for 20 minutes with atmospheric air, then pumped for 20 minutes with the scroll pump and afterwards 4 hours with the turbo pump at different temperatures. Subsequent to this pumping procedure the hot-blank was determined. For thermal decrepitation the whole system, except the crusher, is heated to 100 $^{\circ}\text{C}$ and the crusher itself to about 150 $^{\circ}\text{C}$ for 2 hours. Three steps have been tested, preheating at 70 $^{\circ}\text{C}$, which is common in the case of the original steel cylinder, preheating at 250 $^{\circ}\text{C}$ and 350 $^{\circ}\text{C}$.

With little preheating (70 $^{\circ}\text{C}$) the hotblank signal (2h extraction at 150 $^{\circ}\text{C}$) on the multiplier consists of 90 counts per second (cps) in Xe and 340 cps in Kr, whereas it is about 30 cps for Xe and 160 cps for Kr if the crusher is preheated at 350 $^{\circ}\text{C}$ using the same pumping time. Only with this reduced hotblank values reasonable results can be obtained using thermal decrepitation.

3.3.3 Extraction by crushing in a copper tube

A second possibility for noble gas extraction is the use of collapsible materials like copper for crushing (Roedder et al., 1964; Harmon et al., 1979; Scheidegger, 2005). The sample is cut into elongated or cubic pieces and afterwards put into the copper tube (8 mm inner diameter, about 30 cm length), which was welded on one side and attached to the extraction line by a UHV-tight connection (Swagelok tube fitting) on the other end. The tube with the sample is pumped until a good pressure is reached (about $2\text{-}5\cdot 10^{-8}$ mbar). Then the part of the copper tube where the sample is located is squeezed with a vice. To avoid disruption of the copper, it is never squeezed at the same parts. Bottlenecks have been prepared with pliers to enable a multi-stage extraction. The sample is filled into the upper part, squeezed once, then the first narrow part is opened with special pliers, so that the crushed pieces fall down to the next stage and can afterwards be squeezed again (s. Fig. 3.19). This procedure is repeated several times.

The extraction of noble gases from speleothems by crushing in copper tubes is a rather simple method, but it is difficult to obtain a stable and well-defined background. As the pressure of the vice on the copper tube and the stalagmite samples is not strictly reproducible, the background values for the noble gases as well as other parameters like the grain size distribution are variable.

Empty copper tubes have been squeezed several times to examine the relationship between blank signal and squeezing steps (s. Fig. 3.20). All noble gases show a clear trend. Towards a higher number of steps the amount of released atoms from the copper increases in an almost exponential way. Therefore it was attempted to reduce the squeezing steps to a minimum number, that means mostly one or two squeezing steps.

It has to be noted, that the displayed results consist of a summary of different runs, in which different methods have been used. Additionally, the results are influenced by blank problems due to the not UHV-tight pressure gauge in the very first measurement. Therefore the results are not strictly comparable. However, the points which are located on the exponential curve were measured in one run. The rest is displayed to give an impression of the signal scattering (see results at two squeezing steps), which depends on the number of steps and

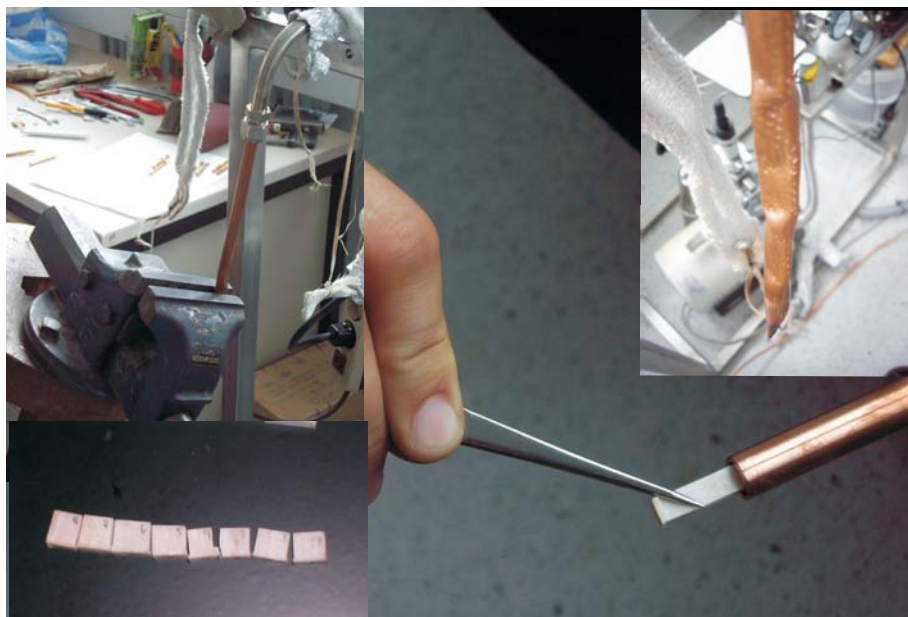


Figure 3.18: Extraction using copper tubes. The picture in the middle shows how an elongated speleothem piece is inserted in the one-side welded tube. On the left side the vice is displayed, which was used to squeeze the tubes. On the right, a copper tube after squeezing is shown. In the lower left picture pieces of the stalagmite H12 are displayed, which were extracted using copper tubes.

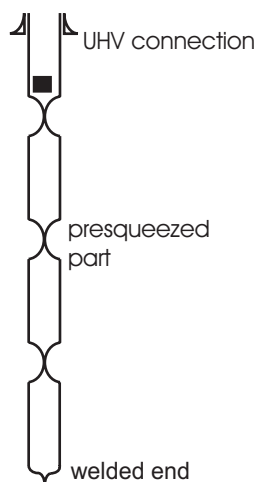


Figure 3.19: Squeezing technique used in the case of copper tubes. The sample (black square) is inserted in the upper part of the precrimped tube, where it is squeezed for the first time, then the first crimped point is opened by special pliers. The crushed sample pieces fall down on the second stage, where the procedure is repeated.

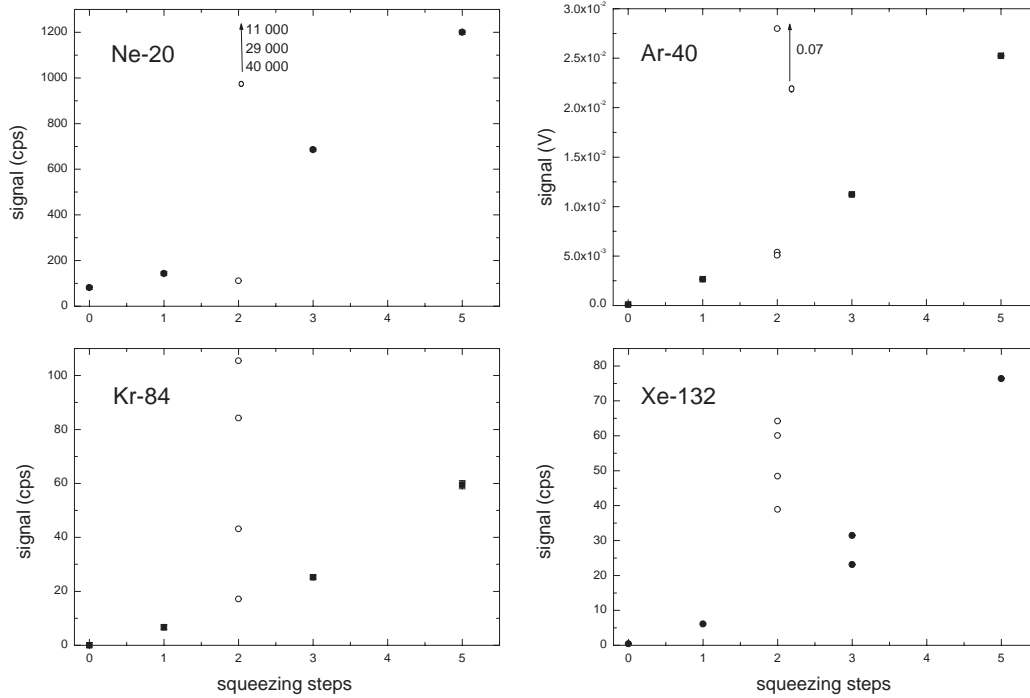


Figure 3.20: Copper tube squeezing blanks. The tests have been carried out with empty copper tubes using the multi-stage extraction explained above. The tests at 0, 1, 3 and 5 squeezing steps refer to one measurements series (filled black circles), whereas the test at 2 squeezing steps (open circles) have been determined earlier using different methods and setup.

also on the measurement run due to changed gas preparation and sensitivities. For the blanks shown at two squeezing steps, Xe yields about 53 cps with an uncertainty of 12 cps. These measurements belong to the older test series, which were influenced by the leaking pressure gauge. Prior to the last runs the copper tubes were preheated to about 200 °C to reduce the background and scattering. By preheating the copper tubes and replacing the pressure gauge a background of 15 cps with an uncertainty of 8 cps was obtained and used for Xe correction of the two-squeezing steps extraction. As the samples mostly yield signals below 100 cps for Xe (except in the last two runs, Delta and Gamma), this background contribution and especially the uncertainty is not acceptable with regard to the aimed precision. An overview of the influence of the crushing uncertainty on the sample signal precision is given in Table 3.2.

For separation of noble gases from air- and water-filled inclusions different techniques are suggested to achieve this objective. One idea is based on the heating of the crushed sample. However, heating can release noble gases not only from the sample itself, but also from the copper material. Therefore some heating measurements of empty copper tubes have been performed.

Empty copper tubes were attached and pumped for at least 8 hours and up to 48 hours, before a blank of the cold tube was performed. Afterwards, measurements of the copper tube at 100°C and 200°C have been made. Precedent to the 200°C - blank the tube was pumped at 100°C for more than 3 hours. All measurements in one run have been performed with the same copper tube and without venting the system in between. This procedure was repeated twice to check the representativeness of the results.

The measurements revealed significant background values (s. Fig. 3.21). The ^{132}Xe blank, e.g. rises from signals below 100 cps up to 400 - 600 counts during heating at 100°C and drops back to significantly better values after the 100°C measurement and the subsequent

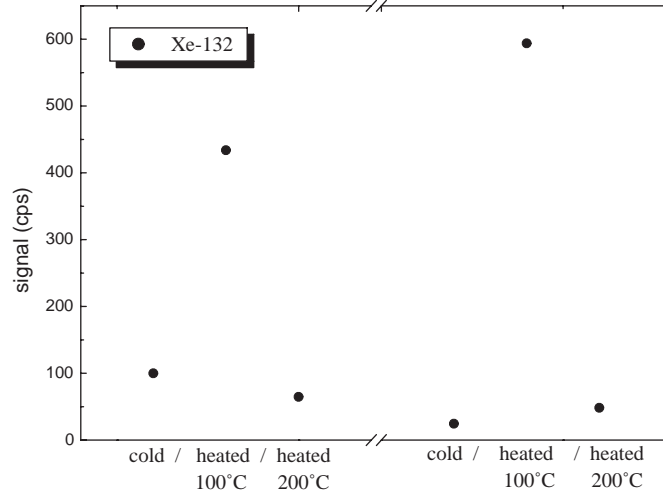


Figure 3.21: Blank of empty copper tubes determined at different temperatures. The copper tubes have not been exposed to the atmosphere between the heating steps, but instead pumped at room temperature and 100°C respectively before the start of the next measurement.

pumping step at the same temperature. Even if the temperature is higher in the last heating measurement, better blank values can be achieved. This behaviour is similar for all noble gases, but is most pronounced in the case of the heavier ones.

This problem may be due to the adsorption of noble gases in the copper tube or even to higher noble gas concentrations in the copper material compared to the normal atmospheric composition, caused by the production and purification process of the copper tubes. The extremely high xenon-blanks at 100°C may not be fully assigned to the adsorption. Otherwise longer pumping should be able to remove these gases. In the second test, the copper tube was pumped 4 times longer (48 hours) than the first copper tube, but nevertheless the signal during heating was comparable. However, this test may also show that it is necessary to use higher temperatures to enable the desorption of Xe from the surfaces. Heating under vacuum can remove a certain part of the noble gases and prepare the system in a more defined way.

Table 3.2: Corrections used for the last copper tube measurements (June 07, run Beta). In the row 'crushing once' the mean blank with the estimated uncertainty based on the preceding blank measurements is displayed. The blank values refers to the interpolation from step 5 to zero of the squeezing measurements. The sample 'uncertainty due to the blank' refers only to the crushing uncertainty.

sample type	^4He (cps)	^{20}Ne (cps)	^{40}Ar (V)	Kr (cps)	^{132}Xe (cps)
crushing once (mean)	38 ± 4	410 ± 40	$(6.9 \pm 3) \cdot 10^{-3}$	16 ± 8	15 ± 8
typical sample signal	1500 - 6000	7000 - 20000	0.4	400-1000	40 - 90
uncertainty due to blank	$\ll 1\%$	$\ll 1\%$	$\leq 1\%$	$\leq 2\%$	$\leq 20\%$

The effect of preheating has not been tested with a sample inside the tube, because diffusive loss of noble gases has to be suspected. Thus, the copper tubes have been preheated under vacuum conditions, cooled down, opened and then the speleothem piece was inserted. It can be expected that a certain amount of gases gets adsorbed during the filling. So we pumped the tube including the sample again during mild heating (70 °C). As we do not know and are not able to determine the blank in this case exactly, we can only use the values of the empty tubes as a first-order estimation. In the case of hot sample extractions the blanks turned out to be by far too imprecise to achieve meaningful results. Due to this background problems the use of copper tubes was rejected.

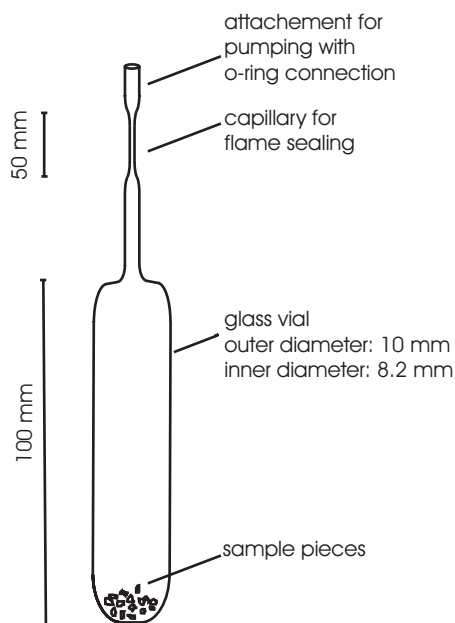


Figure 3.22: Glass vial for microwave extraction of noble gases. The sample pieces are inserted before the capillary is built by the workshop. Then the glass vial is pumped using an o-ring connection on the upper part. The pumped sample is closed off by flame sealing.

3.3.4 Extraction by microwave heating

Noble gases from water-filled inclusions can also be extracted by heating stalagmite samples in the vacuum system. A sophisticated method for opening of the water-filled inclusions is microwave heating. The sample is crushed into small parts, put into a glass vial and then pumped for a certain time. When a sufficient pressure ($\approx 10^{-8}$ mbar) is reached, the vial is flame sealed and afterwards put into a common microwave oven. The microwave-treated sample is opened at the mass spectrometer in a special o-ring-free device (explained below). Due to the microwave heating especially the (small) water-filled inclusions are supposed to be opened, because of an increase in pressure. The air-filled inclusions are assumed to remain closed.

In Figure 3.22 the glass vial is displayed. It is about 10 cm long and has an inner diameter of 8.2 mm in the lower part and is made of a low helium permeability glass. Due to a capillary at the top part it is not possible to fill in the sample directly. It has to be put inside the glass vial before the capillary is manufactured.

The vial is attached at the extraction system via an o-ring connection for pumping. The upper part is divided into two sections by the small capillary area, which is needed for sealing. Using a small gas blowpipe the capillary is warmed up first and then pulled down slowly with a circular motion, when the glass is glowing reddish. After the sample is pumped and sealed, it is put into a common microwave oven (Lunik 340) and heated typically for 5 min at 800 W. Unfortunately, the samples were not only influenced by the microwaves itself but also heated thermally by the hot rotary disc of the oven. To prevent this effect in later experiments the sample was put on ceramics. In some cases condensation of water could be seen at the sharp end of the capillary (Fig. 3.24). In the case of a flowstone with a slightly brownish colour and a set of red stripes, a gas discharge with a whitish or light blue flash has been seen during microwave treatment.



Figure 3.23: Glass vials for microwave extraction. On the left side a vial including a speleothem sample is displayed, which is attached to the preparation system using an o-ring connection. On the right side two pumped and by flame-sealing closed vials as well as one original glass vial are shown.

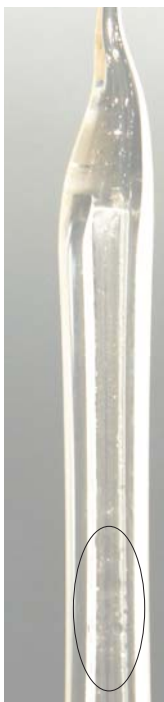


Figure 3.24: The effect of (microwave) heating on a speleothem sample, which consists of fine powder, is obvious on the sharp end of the glass vial. In the lower part of the picture condensation of water vapour inside the capillary part of the glass vial can be seen (black circle). The water vapour is produced by the cracked water-filled inclusions in the milled stalagmite parts.

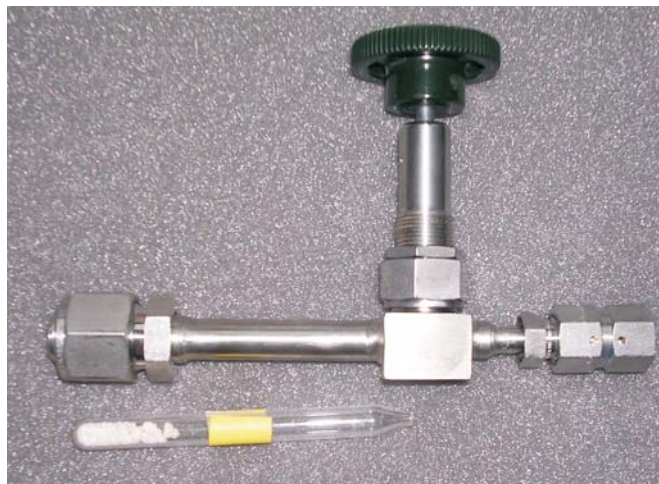


Figure 3.25: System for extraction of microwave treated glass vials. The vial can be inserted totally in the cracker system. Thus, contamination by leaking atmospheric air, as it is present in the case of an o-ring connection, can be prevented. The hand valve is used for moving of a plunger, which cracks the capillary and releases the gases from the vial. Below the cracker an opened sample is displayed.

The flame-sealed and microwave-heated samples are then opened in a special extraction system (Fig. 3.25). A steel tube with a diameter of about 12 mm was provided with typical VCR - fittings at each end. The glass vial can be put totally inside the tube, closed by a fitting (blind flange) and is pumped afterwards. The glass is broken by a modified hand valve at the capillary part, which was scored before. The released gases are frozen into the cryogenic traps for further preparation.

To control the background, empty glass vials have been prepared and treated the same way as real samples. The measurements show that the blank signal depends on the pressure during flame sealing (Fig. 3.26). For ^{40}Ar an almost linear trend is visible, which is comparable to the trend for the other noble gases. To achieve a lower background the glass and the capillary is preheated three times. During the twisting off this results in a lower pressure of $3 \cdot 10^{-8}$ mbar to $2 \cdot 10^{-7}$ mbar compared to values in the 10^{-6} mbar range without this procedure. The glass background values counted in the first microwave run are comparable to the extraction line blank, except at a pressure above $1 \cdot 10^{-6}$ mbar during flame sealing. Typical line blanks have been for instance 0.3 to 0.6 V in case of ^{40}Ar in the first microwave run. This rather high value was reached due to the connection of the glass via an o-ring to the noble gas measurement line. In the following run the o-ring connection was replaced by the above explained special extraction system, which enables the opening of the vial totally included in a vacuum chamber.

The comparison of an empty and microwave-treated glass vial with the lower line blank in the second run, using the modified setup with preheating prior to flame sealing, showed the two signals to be comparable. Therefore, it was assumed that the microwave treatment does

Table 3.3: Mean line blank and sample signals for the two microwave test series.

sample type	^4He (cps)	^{20}Ne (cps)	^{40}Ar (V)	^{132}Xe (cps)
1. run, line blank	$3 \cdot 10^5$	$6 \cdot 10^4$	$3.5 \cdot 10^{-1}$	65
1. run, samples	$3 \cdot 10^5$ to $3 \cdot 10^6$	$7 \cdot 10^4$ to $2 \cdot 10^6$	0.6 to 7.7	80 - 1400
2. run, line blank	$3 \cdot 10^2$	$2 \cdot 10^2$	$1 \cdot 10^{-3}$	2.5
2. run, samples	$1 \cdot 10^3$ to $2 \cdot 10^5$	$7 \cdot 10^2$ to $1 \cdot 10^6$	$7 \cdot 10^{-3}$ to 1.3	1.4 - 1100

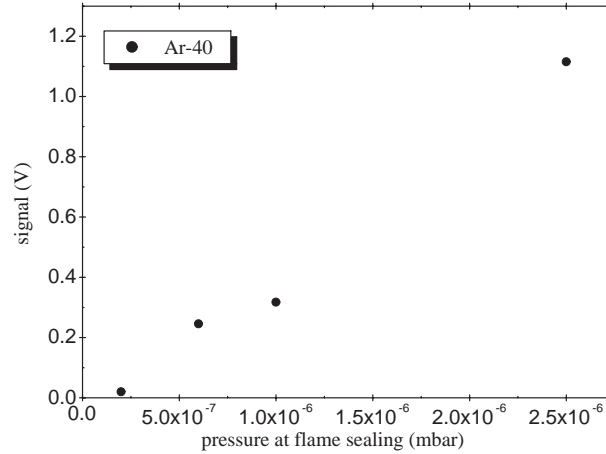


Figure 3.26: ^{40}Ar blank values in the case of the microwave extraction. The blanks have been determined by the measurement of empty glass vials, which have been prepared and processed in the same way as the speleothem sample. An almost linear relation between pressure during flame sealing and the mass spectrometric noble gas signal can be detected. A similar trend has been observed for the other noble gases.

not release additional noble gases from the glass. Furthermore, the background of the line could be reduced considerably due to the new extraction system, for instance down to the range of $8 \cdot 10^{-4}$ to $2 \cdot 10^{-3}$ V for ^{40}Ar respectively 1 to 5 cps for ^{132}Xe .

Table 3.4: Samples measured in the second microwave run. All samples are from not previously measured material. They were chopped into coarse grains before they were filled into the glass vials. 'crush' indicates the samples from which the noble gases were extracted by simple crushing. They are mentioned for comparison and refer to the mean of all crushing measurements.

sample	released water (μl)	water content (wt%)	air/water volume ratio <i>A</i>
H12-I	not detectable	-	-
H12-II	1.14	0.58 ± 0.02	2.9
H12-crush	0.2 - 1.4	2.6	1.8
CG-I	not detectable	-	-
CG-II	$1.6 \cdot 10^{-3}$	$6 \cdot 10^{-3} \pm 6 \cdot 10^{-3}$	2.2
CG-crush	$1.7 \cdot 10^{-2}$ to $1.6 \cdot 10^{-1}$	0.005 up to 0.07	0.35
flowstone	$1.5 \cdot 10^{-1}$	0.119 ± 0.001	0.91
flowstone-crush	$3.4 - 5.1 \cdot 10^{-1}$	0.20 - 0.29	1.1 - 7.7

In the first microwave extraction test four samples have been investigated. All vials have been filled with pieces of the H12 stalagmite from the Hoti Cave. To test the extraction efficiency, the stalagmites pieces were prepared in different ways. Two parts were crushed to coarse grains prior to the pumping and microwave heating. One sample consisted of fine powder from already measured samples and the fourth sample of a simple cube. During flame sealing rather high pressure values occurred (mostly $2 - 3 \cdot 10^{-6}$ mbar, one sample up to $1 \cdot 10^{-5}$ mbar). All glass vials including the speleothem samples were heated for 5 min at 800 W in the microwave oven, then connected with an o-ring to the mass spectrometer line and opened after the line was pumped sufficiently (final pressure $5 \cdot 10^{-8}$ - $1 \cdot 10^{-7}$ mbar).

The noble gas measurements did not yield the results we hoped for. Although it was not possible to determine the released water amount, the three-isotope-plots (Kr/Ar vs. Ne/Ar or

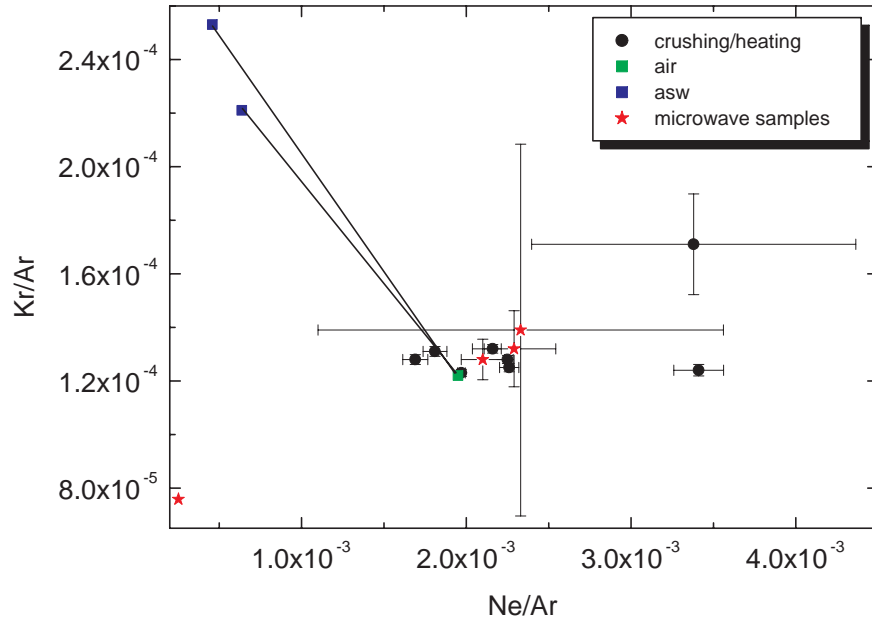


Figure 3.27: Kr-Ar-Ne plot of samples measured in the first microwave test run. For comparison samples from H12 and MA (Chile) are displayed, from which the noble gases have been extracted by crushing. They are indicated by black circles in the figure. The microwave sample in the lower left edge is displayed without error bar. The errors extend over the whole plot.

Kr/Ar vs. Xe/Ar, s. Fig. 3.27) provide some information about the air/water volume ratio. Unfortunately, the samples extracted with microwaves did not differ from pieces extracted by normal crushing methods. The air/water ratio is similar and not significantly better as has been assumed before.

The microwave measurement with the lowest excess-air belongs to the stalagmite powder. Although this powder consists of the remaining part of preceding measurements, an obvious water amount (Fig. 3.24) and the according gases could be extracted. This sample resulted in a slightly improved air/water ratio compared to normally crushed samples.

The difference between the coarse grains and the uncrushed cube was not significant. The coarse grains, which have been measured in a previous run, were totally away from the rest (lowest red star on the left side) and therefore showed that most of the water and also the noble gases have been extracted in the previous run and few water and gases could be released with the microwave treatment. Furthermore, the error was considerably elevated in this case due to the comparatively high o-ring-blank as the vacuum cracker was not usable yet.

Concluding from the first microwave tests, this method does not yield significantly lower air/water volume ratios, but shows that, at least in the case of fine powder, a certain improvement may be possible compared to the crushing. Furthermore, the measurements indicate that it is feasible to open tiny inclusions ($\leq 1 \mu\text{m}$) by microwave heating. The already measured powder, which was crushed and pumped under vacuum in a previous test series, released again water and noble gases due to the microwaves.

In the second run five samples from different stalagmites were investigated using the microwave method. One from a flowstone from the Hoti Cave in Oman, two pieces from the H12 stalagmite and two parts from the stalagmite CG from Cuba. The speleothem samples were crushed to coarse grains before they have been put into the vials. The glass vials were prepared using the modified flame sealing process with preheating of the capillary and were

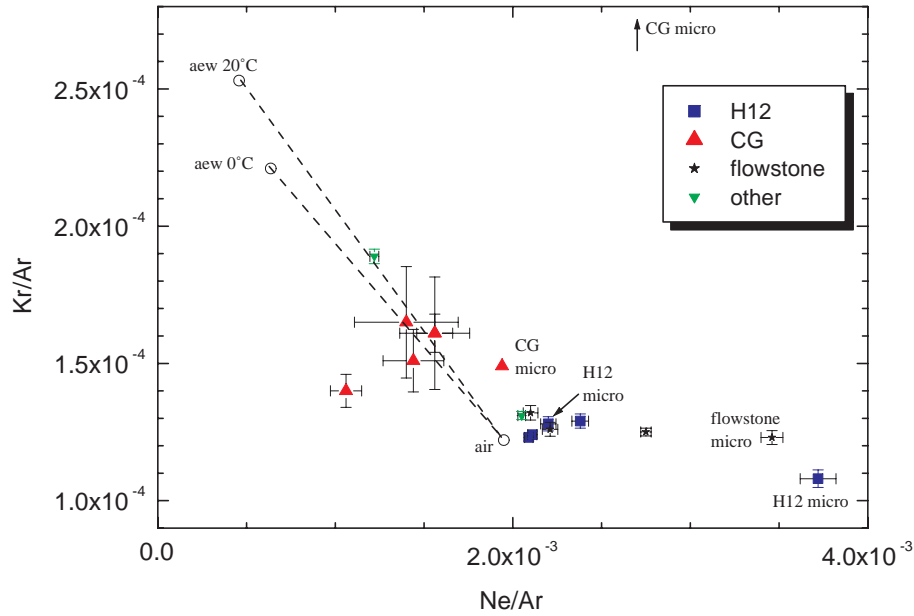


Figure 3.28: Kr-Ar-Ne plot of samples measured in the second microwave run. The samples scattering in the region between AEW and air belong to measurements of pieces from the stalagmite CG extracted by simple crushing and are given for comparison. The microwave sample "CG micro" in the middle of the plot is displayed without error bars. The errors extend over the whole plot.

opened totally included in the vacuum system (Fig. 3.25). Therefore, the blanks could be reduced substantially. The blank signals were up to three orders of magnitude lower in this test series compared to the first microwave run (Table 3.3).

The second run confirmed the results from the first microwave test series. The samples extracted by microwaves showed in general a worse air/water-volume ratio compared to similar speleothem pieces crushed within copper tubes. If the released water is referred to the sample amount in g, the content of water-filled fluid inclusions can be calculated. In general this value of microwave extraction is significantly below the numbers of crushing. As the extraction via copper tube is not 100% efficient, even higher amounts of water will be released in case of milling with a steel ball and therefore the extraction by microwave heating appears especially poor. However, in the second microwave run the speleothems have not been milled to powder, which might yield in general better values.

The uncertainties are much higher in the case of microwave extraction compared to simple crushing as the total amount of noble gas and water is in general rather small. Therefore, it will be inappropriate to use this method for calculation of noble gas concentrations and subsequent fitting. Microwave treatment of milled stalagmite powder may yield some potential. However, it requires an extremely low background and a precise water determination at the lower limit of the method.

3.3.5 Extraction by thermal decrepitation

A further possibility to extract noble gases from speleothems is a simple heating process as already investigated by Yonge (1982), Matthews et al. (2000) and Scheidegger (2005). The sample is heated under vacuum to a certain temperature, either crushed before to a smaller fraction or used as a whole cube. Due to heating, the pressure in the water-filled inclusions will increase and crack the calcite. Thereby the noble gases are released. Matthews et al.

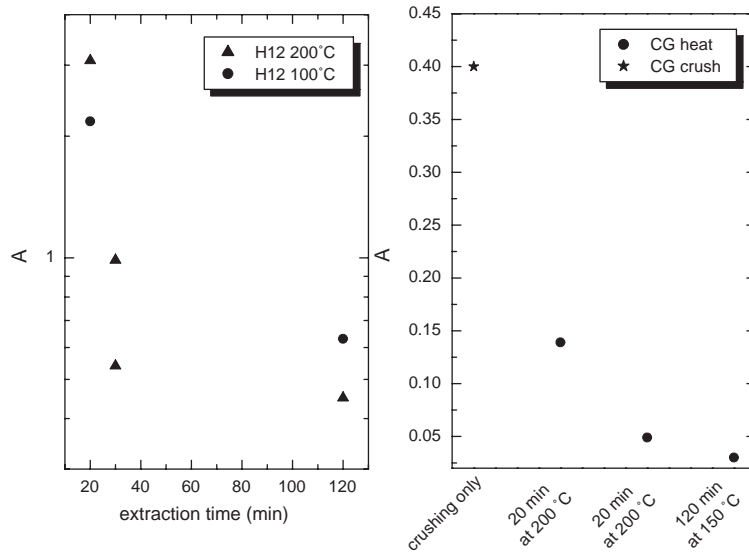


Figure 3.29: Effect of the heating duration on the air/water-volume ratio. On the left side H12 samples are displayed, which were heated between 20 and 120 minutes. The two H12 samples extracted at 200°C with a duration of 20 and 30 minutes were crushed to small pieces prior to the measurement. The rest was extracted subsequent to a crushing step under vacuum. The first CG data point at 20 min and 200°C belongs to a combined extraction of crushing and heating. The second point at 200°C reflects the result of a single heating step after two crushing extractions under vacuum.

(2000) investigated thermal decrepitation at 900°C, whereas Scheidegger (2005) limited the heating steps to about 600°C to avoid decomposition of the calcite.

Different test series have been performed to investigate the potential of thermal decrepitation. For the first measurements small pieces of the stalagmite H12 have been milled into grains with diameters below 2 mm. Subsequently, they were inserted into the copper tubes for pumping and thermal decrepitation. The hot extraction was carried out 20 min respectively 30 min at 200°C. One measurement consisted of a combination of crushing under vacuum and a subsequent heating step, which was performed 20 min at 200°C. In the beginning of 2007 a series of heating tests have been performed, in which the stepwise crushing extraction followed by the 20 min lasting thermal decrepitation at 200°C was investigated. Every sample was squeezed up several times, analysed and pumped after the initial crushing steps. Subsequently, the speleothems were heated for 20 min to 200°C for gas release. The effect of this treatment is displayed in plot 3.29.

In the case of the H12 stalagmite, a heating of 20 minutes at 100°C, respectively 200°C did not yield better *A* values compared to the crushing data. However, a significantly improved result was obtained for the CG stalagmite. In general, the effect of reducing *A* by thermal decrepitation is most pronounced at longer heating times. An exposure time of 20 minutes of the crushing devices to the heat coils does not seem not to be sufficient to heat up the whole setup. With regard to the temperature a lower *A* value was obtained for the H12 sample at 200°C. For pieces from H12 the released water amount was larger in case of the higher temperatures as well as for longer heating times. 30 minutes heating at 200°C released 0.13 and 0.048 $\mu\text{l/g}$, whereas at the 120 minutes heating step 0.14 (100°C) and 0.21 $\mu\text{l/g}$ (200°C) were released. A similar trend was found for the CG pieces with 0.001 $\mu\text{l/g}$ at 20 min and 200°C and 0.042 $\mu\text{l/g}$ at 120 minutes heating with 150°C. However, longer heating periods and higher temperatures bear the problem of increased noble gas desorption from the crusher walls as well as the diffusive release of noble gases from the calcite matrix. In geological

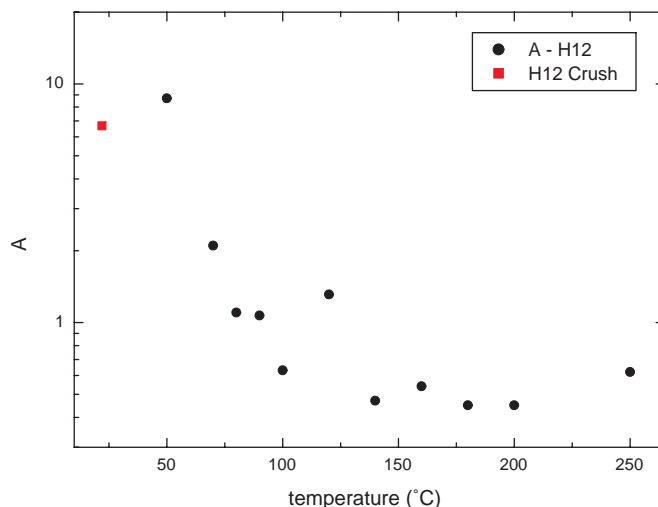


Figure 3.30: Stepwise heating experiment on one H12 sample. The first data point refers to a different sample extracted by crushing only. The subsequent data points have been obtained by heating of one sample at different temperatures, but using always the same extraction time of 120 minutes.

applications heating periods for minerals range from 20 to 30 minutes at high temperatures of e.g. 200 - 1500 °C (Podosek et al., 1980; Stuart et al., 1995).

In "run Beta" (2007) the effect of different temperatures on the extraction efficiency as well as the air/water volume ratio was tested. One sample was inserted into a copper tube, cleaned from superficially adsorbed noble gases by pumping and extracted in subsequent heating steps at various temperatures. In each case the extraction time was fixed to 120 minutes. A clear trend towards a lower air/water volume ratio can be observed at higher temperatures (Fig. 3.30). The best values are obtained between 140 and 200°C and are about 0.4 to 0.5. At 250°C a small increase can be observed, which may be due to noble gases released from the copper tube walls or the calcite matrix. The amount of water was easily measurable as it ranged between 0.15 and 0.5 μl (except at the first step at 50°C).

Heating may influence the noble gas concentration by diffusion. Therefore, deviations from noble gas ratios corresponding to air-equilibrated water and as well deviations from the excess-air line in the two-isotope-plots should be observable. In Fig. 3.31 all samples which have been extracted by thermal decrepitation are displayed. Most of them are lying on the the excess-air line of water equilibrated at about 30°C.

The pattern is more complex concerning the Xe and Ne concentrations. In Fig. 3.32 the same samples as in the Kr-Ar plot 3.31 are displayed. However, some deviations from the expected line can be observed. Most samples are located on a parallel below the excess-air line at 30°C, which indicates an excess in Ne. Points above the expected excess-air range belong to samples from the Cuban stalagmite CG and to the two samples from H12, which have been measured in the very first runs. A location above the excess-air line indicates surplus-Xe. This excess in Xe can be explained for the H12 samples by the release of adsorbed Xe from the copper tube walls. A correction for this effect was not possible. The Xe-excess may be explained in the same way for the CG samples, but it may be influenced additionally by a matrix component, which is enriched in Xe.

Despite the rather high and uncertain hotblanks of the copper tubes, the deviations from the expected concentrations can not always be explained by systematic errors or technical problems. E.g. the Ne-excess in case of the H12 samples occurs also using the crushing extraction. Thus, it is not related to the extraction procedure, but rather to the calcite

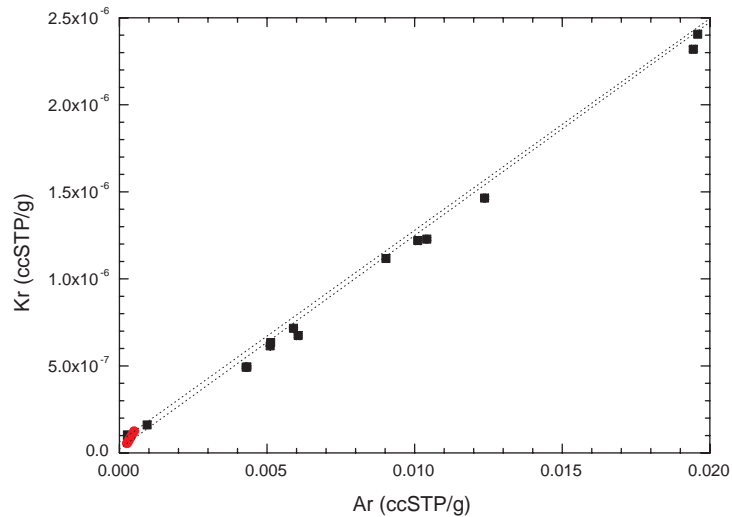


Figure 3.31: Kr and Ar noble gas concentrations of all samples extracted by thermal decrepitation. The values are given in ccSTP per g of water. The red points indicate air-equilibrated water. The upper dashed line refers to water equilibrated at 0°C with addition of various air amounts. The lower line represents the excess-air line corresponding to water equilibrated at 30°C.

and its inclusions. This assumption can be approved by the examination of the Ne- and the Ar-isotope ratios. They are displayed in two small boxes in the same plot. In the case of the $^{40}\text{Ar}/^{36}\text{Ar}$ -ratio most of the data is scattering very close to the value of atmospheric air. The deviations can be explained by the measurement uncertainty of the noble gases, which is below 1 % for ^{40}Ar and some % for ^{36}Ar . Only one measurement exceeds this range with an ratio of about 4800. This value belongs to a heating measurement at 50 °C with a very low amount of released water, but a relatively high noble gas signal. The gases are supposed to be mainly desorbed from the walls as well as from the calcite surface.

The neon ratios scatter in the range of the atmospheric ratio of 9.80. The deviations are in general lower than 2 %, which corresponds to the measurement uncertainty of ^{20}Ne and ^{22}Ne . Taking into account the Ne- and Ar-isotope ratios, no fractionation due to the thermal decrepitation at temperatures below 250°C and 2 hours duration occurs. Therefore, it is feasible to use thermal decrepitation as an extraction method or in a stepwise procedure without alternating or fractionating the noble gas concentrations of the fluid inclusions.

Measurements of other samples confirm the ability of reducing the air/water volume ratio by a heating step. A set of samples is displayed in a three-isotope plot (Fig. 3.33) including the extraction by crushing. The crushing results of two samples (Spa12, Spa 52b) from Spannagel Cave (Vollweiler et al., 2006) and a sinter plate from Bunker Cave scatter around the air point in the same area as the H12 samples. Subsequent heating improves the air/water volume ratio, which is indicated by a position closer to the equilibrated water points. In principle, a fitting of the noble gas concentrations with regard to temperature determination becomes possible using this stepwise procedure, as it gets easier to subtract the air contribution from the total signal. However, the large disadvantage, so far, was the strong increase in uncertainty, which made a meaningful fitting of the data impossible. This occurs due to a significant background during heating which often exceeds 10 % of the sample signal. Additionally, the water amount decreases similarly to the noble gas signal. Therefore, the uncertainty of water

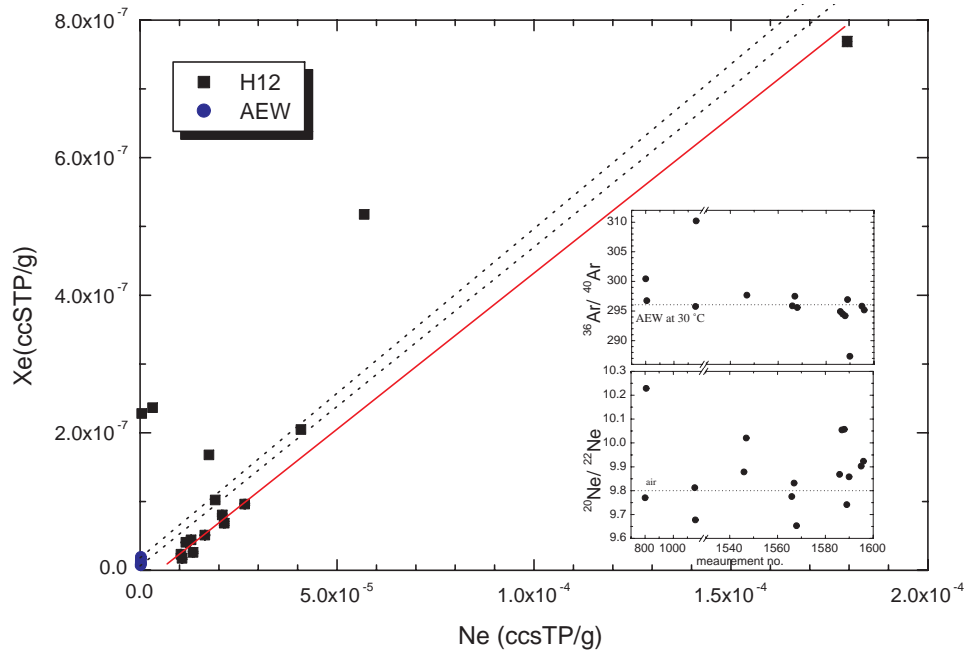


Figure 3.32: Xe and Ne noble gas concentrations of all samples extracted by thermal decrepitation. The values are given in ccSTP per g of water. The blue points indicate air-equilibrated water. The upper dashed line refers to water equilibrated at 0 °C with addition of various air amounts. The lower line represents the excess-air line corresponding to water equilibrated at 30 °C. In the small-sized inserts the corresponding isotope ratios of Ne and Ar are displayed.

determination also increases to higher values, which makes it difficult, in combination with the elevated uncertainties in the noble gas measurements, to push the total uncertainty of the temperature determination below 10°C. The most difficult step is related to the background control. It is not possible to perform an ideal and representative hotblank measurement with the real sample. A measurement without the sample is not practicable as well, as the crusher has to be opened to insert the speleothem sample. In this case noble gases will be adsorbed on the surfaces and the measured blank will not reflect the real conditions. A hotblank measurement including the unheated sample inside the vacuum system bears the disadvantage of outgassing from the sample, which results in an overestimation of the actual hotblank. The blank values are discussed in detail in chapter 3.5.6.

However, combined methods using a sophisticated procedure based on low background values may help to overcome these problems.

3.3.6 Summary

Four different methods have been tested for the extraction of noble gases from fluid inclusions in speleothems. The most exotic procedure using microwave heating did not keep the promise of preferential and especially efficient opening of water-filled inclusions. It may be of interest using very fine powder and a more powerful microwave oven, but so far no convincing results have been achieved.

Squeezing of speleothems in copper tubes showed some success, but difficulties with the background as well as problems to reproduce extraction excluded this method for advanced studies. Thermal heating in copper tubes releases too much noble gases from the copper walls and therefore increases the total uncertainty due to difficult hotblank corrections. Furthermore, it is not possible to perform preheating of the sample or to measure a hotblank including the sample. Reproducible extraction is laborious or even impossible, as the pressure of the

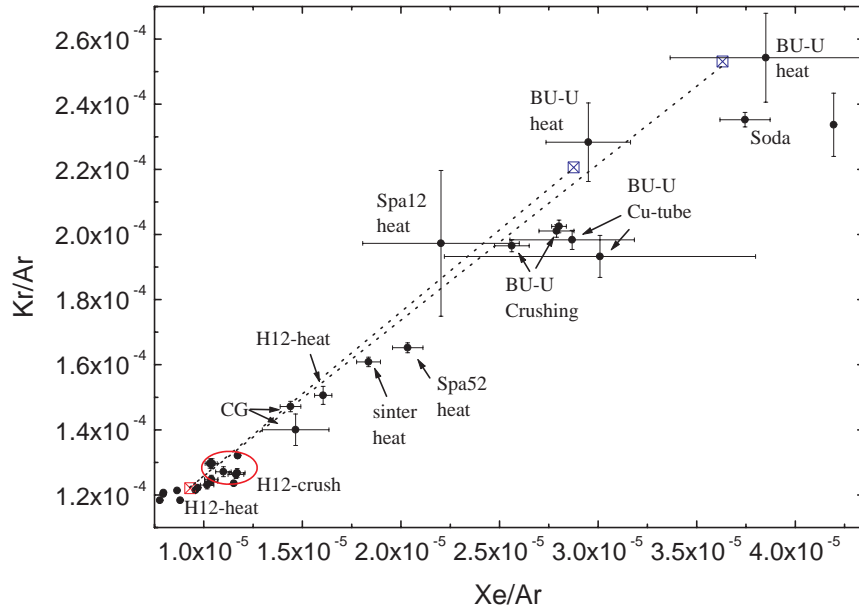


Figure 3.33: Three-isotope plot of samples measured in a speleothem run in 2007 (run Beta). The crushed samples of Spa12, Spa 52b from the Spannagel Cave and a sinter piece from Bunker Cave are scattering around the atmospheric value (red square). Subsequent heating led to a reduced air/water volume ratio indicated by a position more close to the air-saturated water points (indicated by blue squares - left point 25°C, right point 0°C).

vice on the sample during squeezing can not be controlled. The crushing steps are limited to a rather small number (≤ 5) to prevent the formation of leaks. Another disadvantage is the varying and low extraction efficiency. The achieved grain size distribution shows a high variation with a small fraction of small grains ($< 200 \mu\text{m}$).

Thermal decrepitation seems to be very efficient as a tool for the reduction of the air/water-volume ratio and can release considerable water amounts from small grains, whereas further crushing would not yield such results. However, extraction by thermal decrepitation is very laborious as the background signal is rather high. Without a sophisticated preheating process, too much desorbed gases will alter the measured values. The hotblank signal is high compared to the extraction signal and therefore the total uncertainty is in general situated above the aimed values. Another problem is the sometimes low water amount.

The most efficient method for noble gas extraction turned out to be crushing inside a steel cylinder by a magnetically movable steel ball. The blank values are sufficiently low, in both the empty crusher and the moving steel ball inside the crusher with and without calcite. The steel cylinder enables a stepwise crushing procedure and leads to a reproducible extraction efficiency. In general, the grain size distribution yields a large fraction ($\geq 40 \%$ wt) of very small grains ($\leq 200 \mu\text{m}$) and is thus suitable for combined extraction procedures, which are specialized on different inclusion dimensions. The crushing inside the steel cylinder as well as a comparison with the copper tube squeezing and the achieved grain size distributions are discussed by Marx (2008).

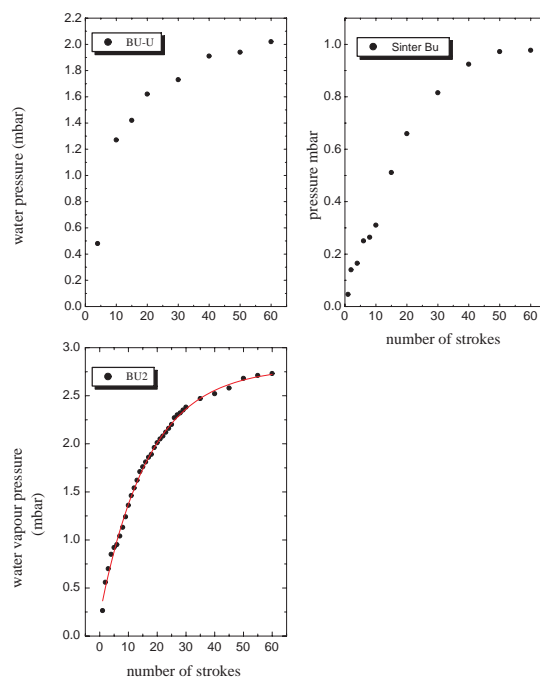


Figure 3.34: Pressure increase due to the water vapour during crushing of different samples from Bunker Cave. Most of the water is released in the first crushing steps. The red curve is a fit with an exponential growth model.

3.4 Separation techniques

Many speleothems do not exhibit a favorable air/water volume ratio A and are mostly dominated by air-filled inclusions. In such cases no meaningful temperature can be calculated. Stepwise procedures are assumed to reduce A (Scheidegger, 2005) by separation of noble gases from air- and water-filled inclusions and thus this technique may enable the calculation of temperatures with sufficiently low uncertainties.

3.4.1 Stepwise crushing

One of the crucial points, the separation of noble gases from air- and water-filled inclusions, may be solved by a combination of several techniques or by stepwise procedures. We first focus on the stepwise crushing and stepwise heating and then discuss the combined technique. To investigate the extraction by crushing with a steel ball, the pressure in the extraction line was recorded for a number of crushing steps. The pressure refers mainly to the released water from the fluid inclusions. $0.1 \mu\text{l}$ of water corresponds to 0.125 ccSTP of water vapour, whereas it contains only on the order of 10^{-6} ccSTP of dissolved atmospheric gases.

Three samples from Bunker Cave have been extracted by crushing in a steel cylinder in the same way. With regard to the water vapour pressure, they show a similar behaviour, which can be described by a strong pressure increase in the first steps and only a small rise in pressure or even stagnation at more than 30 - 50 hits (Fig. 3.34). As the pressure increase during crushing indicates that the main part of water is released in the first steps, it is not feasible to mill the speleothem to fine powder first, to pump the gases and to take an additional extraction step afterwards (by crushing or heating) to release the gases from the smaller water-filled inclusions. However, by applying reasonable steps, as for instance 5 hits followed by 15 and finally 30 additional hits, stepwise crushing can lead to a reduced air/water volume ratio and easily measurable water amounts.

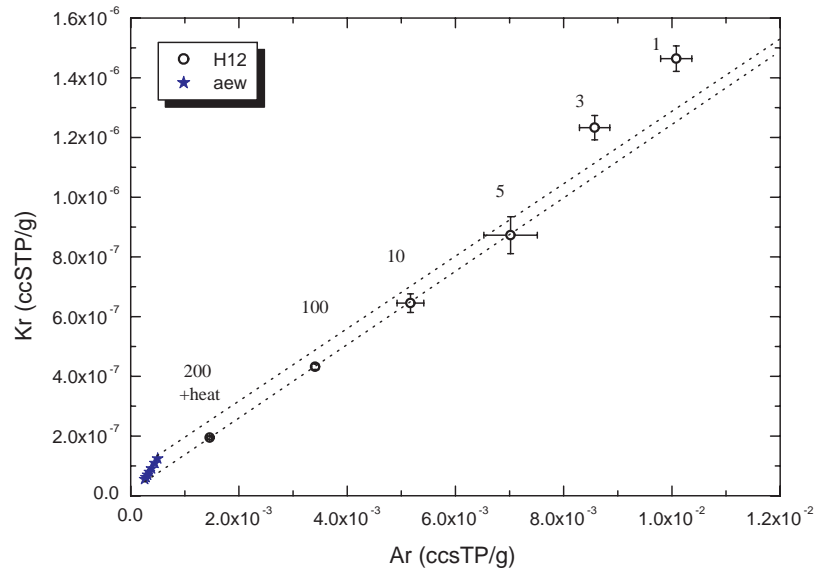


Figure 3.35: Effect of stepwise crushing on a sample from H12. The first crushing step resulted in the most distant values from air-equilibrated water. In each crushing step the air contribution could be reduced. All steps were performed by crushing (total number of strokes indicated in the figure), except the last step, which refers to a combination of 100 additional strokes and heating at 150 °C .

Test measurements with a piece of the H12 stalagmite showed that each crushing step leads to a reduction of A , which starts at about 1.1 at hitting the sample once (Fig. 3.35). In the last step A was reduced by one order of magnitude to about 0.13. The released water amount was about 0.2 μl in the first step and 0.18, 0.08, 0.12, 0.29 and 0.21 μl in the following steps. A disadvantage of the stepwise procedure may be the preferential opening of inclusions of a certain type. During the first hits (≤ 10) the larger inclusions ($\varnothing \geq 1 \mu\text{m}$) are supposed to be opened, whereas in the subsequent steps smaller and mainly water-filled inclusions are cracked. This can lead to an alteration of the noble gas signals (Fig. 3.36). In run Delta a sample from MA and H12 was extracted by stepwise crushing. Hitting the speleothems few times under vacuum resulted in each case in an extreme offset in Ar. This offset became smaller in the subsequent steps and finally ended in the expected range of air-equilibrated water with addition of atmospheric air. Additionally, a systematic offset for Xe and Kr was found for high crushing numbers. This may be due to diffusion of the lighter noble gases from the very small water-filled inclusions ($\varnothing \ll 1 \mu\text{m}$) in the precedent steps, but can also be influenced by noble gases from the calcite matrix. This effects needs to be investigated in the future.

3.4.2 Stepwise heating

A further possibility for the separation of noble gases according to their provenance is a heating process as already stated by Scheidegger (2005) and Scheidegger et al. (2006). The sample is heated to a certain temperature, either crushed before to a smaller fraction or used as a whole cube. Stepwise heating can reduce A by more than one order of magnitude. The results of a stepwise heating run is displayed in Fig. 3.30. A stalagmite sample from H12 was inserted as a whole uncrushed cube and pumped for about 1 day. The thermal decrepitation in each step lasted 120 min. The temperature was varied between 50°C and at maximum 250°C. Between the thermal decrepitation steps, two blanks for background control have been measured. Alternatively, the time was used for pumping the copper tube including the sample up to several days.

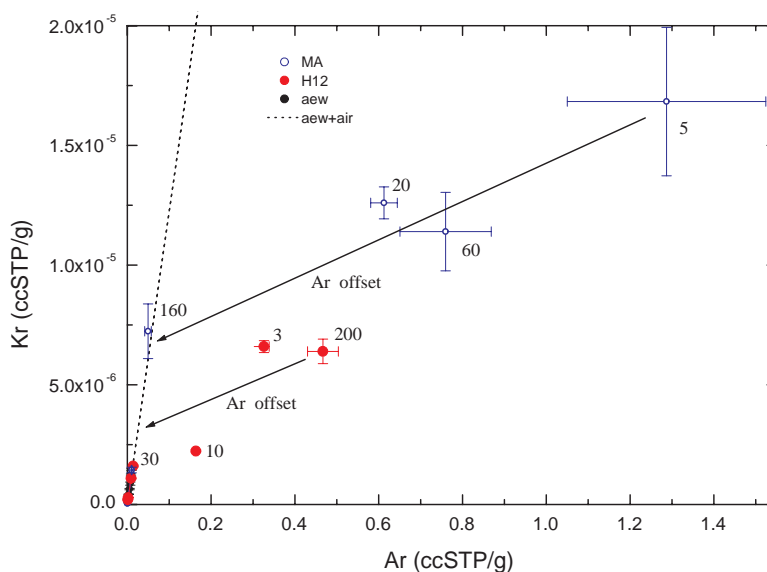


Figure 3.36: Ar offset measured during stepwise crushing procedures (numbers refer to the total of applied strokes). The first crushing steps of two samples, one from H12 and one from MA2, led to extremely high Ar values, which are far from an atmospheric contribution. In subsequent steps the noble gas concentration tended towards air-equilibrated water with addition of atmospheric air.

Low temperature extraction yields high A values comparable to simple crushing. In each of the subsequent steps A was reduced, except at 120°C and 250°C. Between 150°C and 200°C an optimum is achieved. At 50°C a measurable water amount ($\approx 0.05 \mu\text{l}$) was released from the calcite (Fig. 3.37). The stalagmite was pumped prior to the extraction for about 1 day and reached a pressure of about $1 \cdot 10^{-8}$ mbar. Despite this sample preparation a certain amount of water seems to rest inside the surface-near pore space. A relatively high water amount is released at 70°C and at 160°C, respectively 250°C. The first maximum may be due to the opening of larger surface-near inclusions. From 50°C to 160°C a trend towards increasing water release persists. At 180°C and 200°C only a small number of water-filled inclusions are opened additionally. Therefore we focused in the subsequent measurement runs on the extraction at 150°C which integrates over all the temperature steps from 50°C to 150°C and liberates a significant fraction of the inclusion water. At higher temperatures the additional water gain is small and furthermore the contribution of the blanks becomes significant.

The water release at 50°C and 70°C is an important discovery with regard to the sample preparation. As only 70°C is sufficient to release a rather high percentage of the included water, it should be avoided to preheat the sample at too high temperatures. However, a certain part of this water fraction may be related to adsorption and has to be investigated further.

Investigating of the gas concentrations shows a similar pattern for all noble gases (Fig. 3.38). A peak at 120°C is followed by a minimum between 150°C and 200°C and a slight increase at 250°C. The high concentrations at 120°C are most likely due to the release of noble gases from the copper tube walls (compare hotblanks of copper tubes, chapter 3.3.3). The increase at 250°C may be an artefact of the background correction, as a hotblank at 200°C was used for the blank correction. Higher temperatures may enable an increased desorption from the walls.

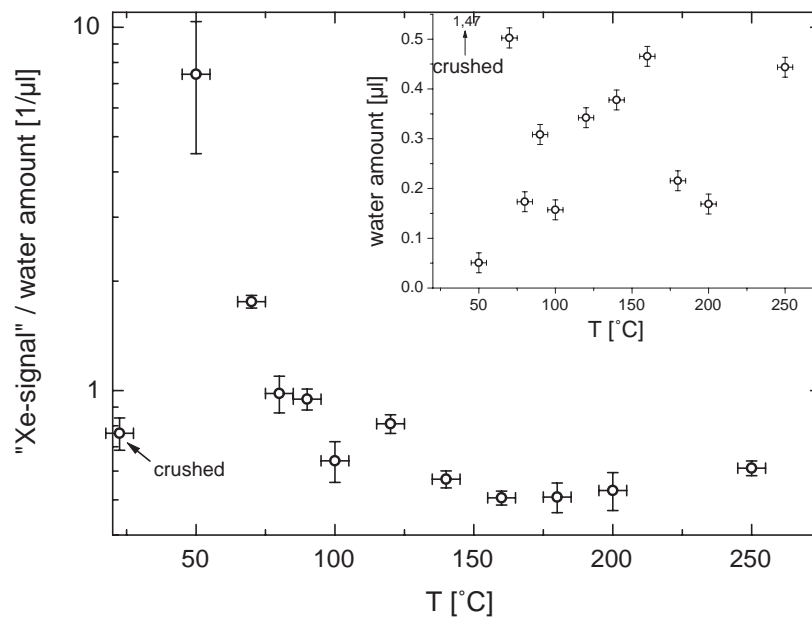


Figure 3.37: Xe signal per water amount for a stepwise heated sample (H12, 1.14g). The result of a final crushing step after the stepwise heating procedure is given for comparison.

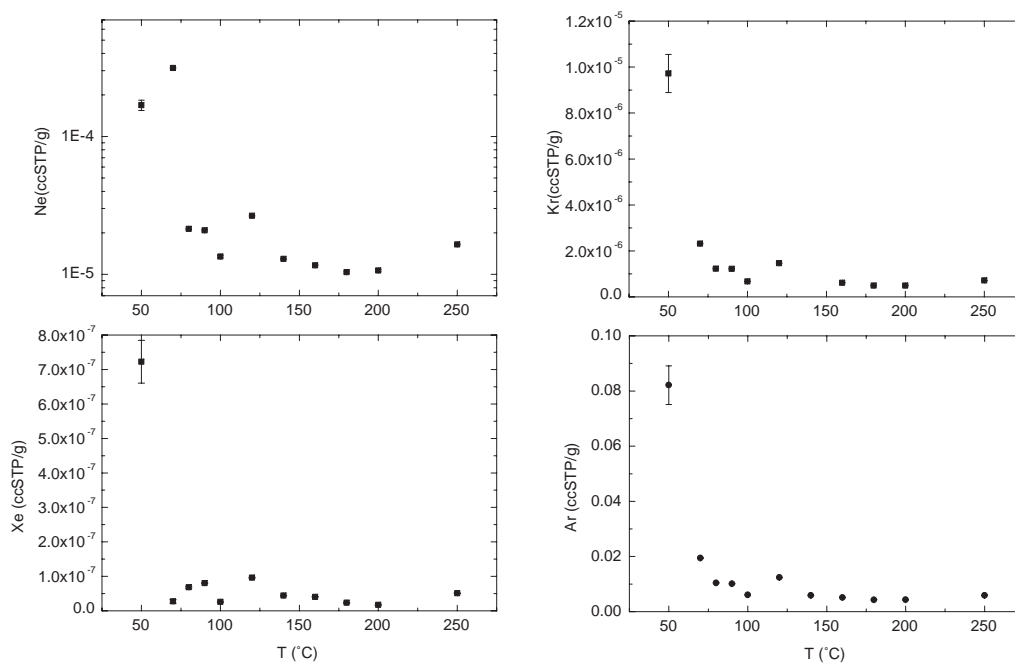


Figure 3.38: Noble gas concentrations versus extraction temperature for a stepwise heated sample (H12, 1.14g). All data are background corrected with a hotblank at 100 °C, respectively 200 °C. A minimum is found between 150 °C and 200 °C indicating low contribution of noble gases from air-filled inclusions.

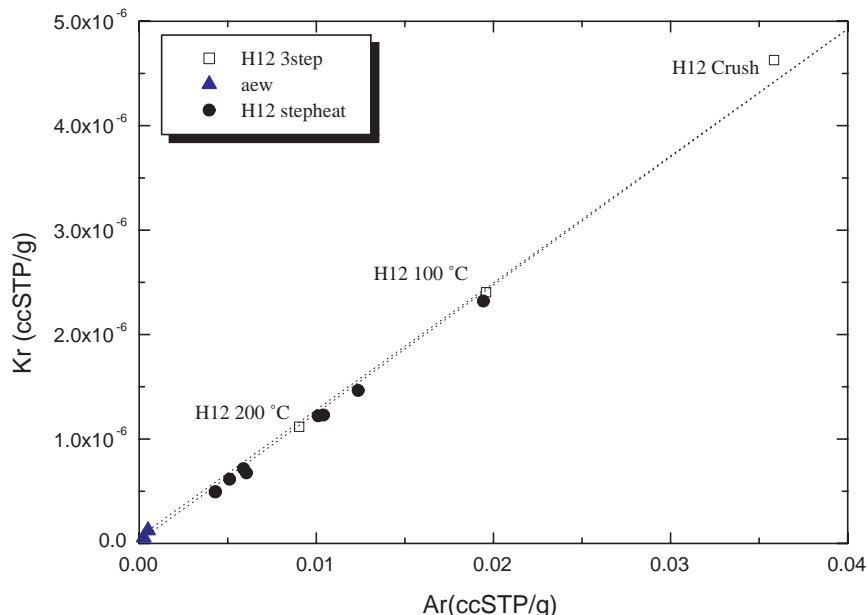


Figure 3.39: Kr versus Ar noble gas concentration for a stepwise heated sample (H12, 1.14g). All data are background corrected with a hotblank at 100 °C, respectively 200 °C. All values plot around the expected results of air-equilibrated water and a certain addition of air.

Neon shows the most pronounced behaviour and exhibits an additional peak at 70 °C, which is not found in case of the other noble gases. This can be explained by a high fraction of gases from air-filled inclusions.

Heating may affect the noble gas pattern as the lighter noble gases show a higher diffusivity. To investigate this effect noble gas concentrations are plotted against each other in Fig. 3.39 and Fig. 3.40. In case of the stepwise heating of an uncrushed sample (black points) no deviation from the expected values of air-equilibrated water with addition of atmospheric air can be detected for Kr vs. Ar. For a sample that was crushed in a first step, then heated to 100°C and finally to 200°C (open squares) also no deviation was found. Similar results were detected for Xe vs. Ne. If we take into account that the H12-samples generally yield a small Ne-offset of about 20 %, the stepwise heating data plots on the expected line (with one exception: thermal decrepitation at 70°C, indicated by an arrow). The three-step extraction using crushing and two heating steps led to the same results. Significant diffusive loss of noble gases can be ruled out, as there is no obvious excess in Kr and Xe compared to the lighter noble gases, even after a set of 11 heating steps at different temperatures on the same sample. Thus, in principle a stepwise heating procedure can be used to reduce sequentially the air-contribution to the total signal.

3.4.3 Combined stepwise procedures

One of the crucial points, the separation of noble gases from air- and water-filled inclusions, may be solved by a combination of several techniques. A combination of crushing with heating turned out to be most promising.

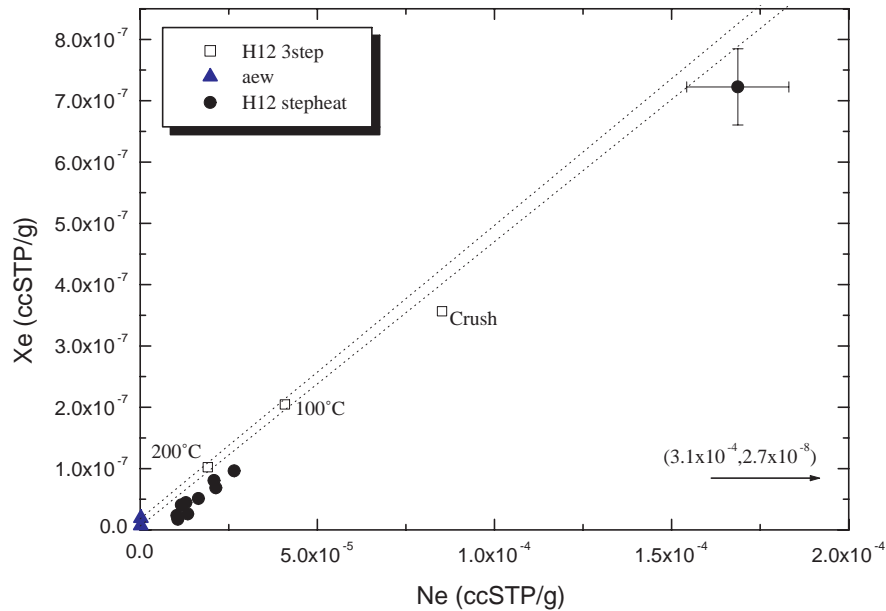


Figure 3.40: Xe versus Ne noble gas concentrations for a stepwise heated sample (H12, 1.14g). All data are background corrected with a hotblank at 100 °C, respectively 200 °C. The systematic shift towards higher Ne-concentrations is due to an intrinsic Ne-surplus of the H12-stalagmite sample.

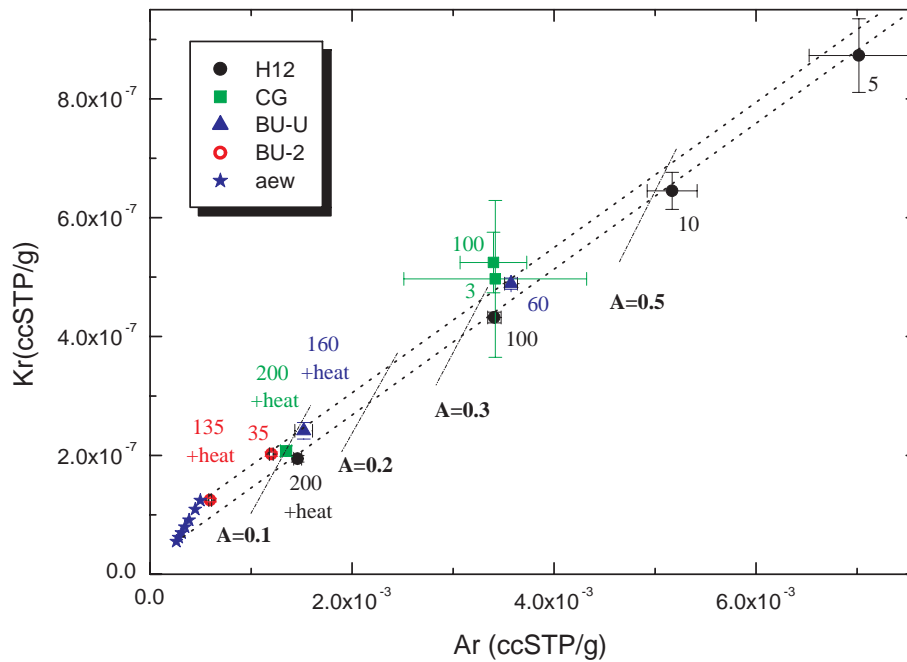


Figure 3.41: Kr versus Ar concentrations for samples extracted by a combined procedure of crushing in the steel cylinder and subsequent heating. The first step always consists of simple crushing, the following steps either of crushing, crushing and heating or a simple heating step. Numbers refer to the total of applied strokes. For comparison the limit for certain A is given.

An analysis of the microwave heating pointed out that this method is not useful with regard to the separation of air- and water-filled inclusions in a single step. However, it was not explicitly tested in a combined stepwise procedure and is therefore not discussed further. We will now focus on crushing in the steel cylinder and thermal heating.

Taking into account the findings with regard to the different extraction methods, a standard stepwise procedure was developed. First, the modified crushing cylinder is heated for at least 8 hours at 150°C to reduce the background. The sample is included at the same time, but exposed to lower temperatures below 70°C. After the initial pumping phase a first crushing step is applied to mainly open the air-filled inclusions. This is attempted by hitting the sample typically 5 times with the steel ball. The gases from this step may be pumped away as they mostly contain noble gases from the air-filled part. We also measure this fraction as we are interested in the radiogenic He. In the subsequent step the principal water fraction is released by crushing the sample 60 times. A higher number of strokes would be associated with a linearly increasing background, but almost no additional water released. As the largest air-filled inclusions are opened in the first crushing step the air/water volume ratio is reduced in the second crushing phase. Another crushing step may be applied if the first two yield high water values ($\geq 0.5 \mu\text{l}$). Otherwise a final heating step is applied to further reduce A . The sample is heated for 60 minutes, respectively 120 minutes at 150°C. Meanwhile, the water is frozen into a cold finger. As mostly the intra-granular inclusions are remaining after the crushing, this mainly water-filled fraction will contribute to the signal. Details of this extraction procedure as well as some results are discussed by Marx (2008). Here we give a short summary of the data.

In Fig. 3.41 some results of samples from the stalagmites H12, CG, BU-U and BU-2 are summarized. H12 was investigated in a 6-step procedure. In the first five steps there was crushing only. The last step consisted of a combination of 100 additional strokes and heating of 2h at 150°C. The CG stalagmite was extracted in six steps, whereof three are displayed. The first data point refers to the extraction by hitting 3 times with the steel ball, followed by the 100 strokes extraction and a combined extraction of 100 additional strokes with 2 hours heating at 150°C in the last step. The BU-2 sample was crushed 35 times in the first step and 100 times more in the second step, which was combined with 2 hours heating at 150 °C. A similar procedure was applied to the BU-U sample, however with 60 hits in the first step. From the Holocene H12 sample only the last four steps are displayed in Fig. 3.41, whereof the results of the higher number of steps always refers to data points increasingly closer to the noble gas concentrations of air-saturated water. The displayed H12 values are all plotting on a line referring to one temperature of air-equilibrated water. Fitting the noble gas concentrations of the last H12-measurement leads to a value of $24 \pm 4 \text{ }^\circ\text{C}$, which corresponds well with the present-day cave temperature.

The CG data shows a larger scatter and higher uncertainties, which are mostly due to the large uncertainties of water determination in consequence of the extremely small water amounts. However, the result of the last step, which is the CG-point with the lowest Ar concentration, shows a strongly reduced air-contribution and therefore allows a temperature calculation with an uncertainty of 1.8 °C. Similarly, the BU-U and the BU-2 samples show a decreased contribution of unfractionated air to the noble gas concentration. In both cases the concentrations of the different extraction steps are shifted parallel to the excess-air line.

In all cases the excess-air contribution could be reduced strongly, so that the last step resulted in values which can be used for meaningful fitting. The calculated temperatures, $4.9 \pm 0.6 \text{ }^\circ\text{C}$ for the 51 000 yr old BU-2, $5.6 \pm 1.8 \text{ }^\circ\text{C}$ for an early Eemian BU-U piece and $24 \pm 4 \text{ }^\circ\text{C}$

for the Oman-stalagmite H12, show that it is possible to obtain reasonable temperatures with acceptable uncertainties even from speleothems or speleothem sections with unfavorable properties.

Unfortunately, the combined stepwise procedure was not successful in all cases. It is always possible to reduce A by about 1 order of magnitude, which works fine for the H12 stalagmite, but which is otherwise not sufficient if the initial A values are above 5 (like in the case of the MA-speleothems). Furthermore, the low water amount in some steps is challenging (CG 0.15 μl at the heating step, 0.08 μl after crushing the H12 sample 5 times, 0.11 μl during the heating step of BU-U). Thus, further development is necessary balancing the demand of air-reduction and precise water and noble gas determination.

3.4.4 Summary

The temperature determination gets feasible, if noble gas amounts and the corresponding water can be measured sufficiently precise and if the contribution of air is sufficiently small. To accomplish these constraints, a combined stepwise procedure is most suitable. The air/water volume ratio can be reduced in each step and, furthermore, the water and gas amounts are still rather precisely measurable in the presented three-step procedure. In general a reduction of A in the order of one magnitude can be achieved. Tests on pieces from H12, BU-U and BU2 showed the efficiency of the stepwise procedure and yielded reasonable temperature results with acceptable uncertainties.

However, in the case of samples with a very unfavourable A (≥ 1) the stepwise procedure has to be extended by additional crushing and heating steps. Unfortunately, not each time useful data will be obtained as water as well as gas amounts get increasingly smaller. There, more work has to be done and a modified procedure has to be found in order to achieve meaningful results.

3.5 Mass spectrometry

This section is focused on the technical point of view with regard to the preparation, separation and measurement of the noble gases. The general procedure is orientated at current methods developed for water and gas samples in a common range (about 1 ccSTP of ambient air) as it is described by Friedrich (2007). The preparation procedure itself was developed according to the system of Beyerle et al. (2000). A special calibration standard enables the determination of absolute gas amounts. The reproducibility of the standard gives a measure for typical uncertainties. Finally, the sensitivity is investigated and blank values of our extraction and measurement line are given in comparison with literature values.

3.5.1 Gas separation and purification

The sample gases are frozen into two cold traps after being released from the speleothem. The first trap, a bare steel volume, is cooled to 25 K, which enables the freezing of the heavy noble gases (Ar, Kr, Xe). After 20 minutes the second trap, a charcoal-trap held at 10 K, is opened to condensate Ne and retain the He. This two-step freezing procedure needs altogether about 40 minutes to quantitatively freeze the noble gases.

Subsequently, they are released from the traps and admitted to different line volumes for purification and splitting, if necessary. At the beginning, the charcoal trap is heated to 42 K to release the He, but not the Ne. From this fraction a small aliquot is taken for a control measurement in a quadrupol mass spectrometer. According to this result a splitting of the total He amount is performed in order to obtain a He signal in a well measurable range.

Before the gas inlet into the sector-field mass spectrometer (GV 5400), the He is purified by a cold SAES AP 10N getter for 120 s and again 120 s during the inlet. To release the Ne from the charcoal the trap temperature is raised to 90 K. The rest of the procedures is the same as for He, except the purification time, which is increased to 180 s before the gas inlet into the mass spectrometer and to 150 s during the inlet.

The heavy noble gases are prepared in a different way. They are released altogether from the bare steel trap at 130 K. In this case not only Ar, Kr and Xe are admitted to the system, but also N₂ (boiling point: 77 K), O₂ (90 K) and other gases like methane (111 K). Therefore, purification becomes an important point. In a first step, the whole gas amount is admitted to a hot SAES GP50 W2F getter for 10 minutes to remove the reactive gases. Subsequently, the remaining fraction is processed to the cold SAES AP 10N getter for further purification. This step lasts 240 s before the inlet into the mass spectrometer and 210 s during the inlet. In contrast to water samples no splitting is applied; all the gas from the naked steel trap is used.

3.5.2 Measurement sequences

This section presents the measurement procedure for a typical speleothem sample. Furthermore the changes and differences with regard to water samples are explained.

A measurement run consists of sample, calibration and blank measurements. Each of these types is subdivided into the sample gas measurement and an according fast-calibration measurement ("fastcal"), which is performed to correct short-time electronics or ion source changes. According to the gas release from the cryogenic traps, He, Ne and Ar-Kr-Xe are measured subsequently. Thus, a sample, calibration or blank measurement consists of a sample-He, fastcal He, sample Ne, fastcal Ne, sample Ar-Kr-Xe and fastcal Ar-Kr-Xe measurement.

The water samples that are usually processed on the preparation line have a weight of about 20 g, which is 20 000 times more than the water extracted from 1 g of stalagmite with a water content of 0.1 %wt. Due to the air-inclusions of the speleothems, the signals of the light noble gases (He, Ne) are actually only 5 000 to 10 000 times smaller. In the case of the combined Ar-Kr-Xe measurement the difference between the signals of the speleothems and water samples is even much smaller, because the corresponding fraction from the water samples is split by taking a small aliquot of about 0.5 cm³ from a 2000 cm³ expansion volume (Friedrich, 2007). This procedure was developed by Beyerle et al. (2000) in order to measure Ar on a Faraday cup and Kr-Xe on an ion multiplier in a single measurement. For stalagmite samples, the expansion volume is bypassed, leading to comparable gas amounts in the mass spectrometer as in the case of water samples.

The signals of the isotopes ⁴He, ²⁰Ne, ²²Ne, although much smaller than for water samples, where they are measured on a Faraday detector, can still easily be measured on an ion-multiplier (MasCom SEV MC-217). Typical count rates in the case of speleothems are 10³ to 10⁴ cps for ⁴He, 10⁴ to 10⁵ cps for ²⁰Ne, and 10³ to 10⁴ cps for ²²Ne. ³⁶Ar and ⁴⁰Ar are measured on the Faraday cup with a 10¹¹Ω resistor with typical signals of 10⁻³ to 10⁻² V for ³⁶Ar and 0.5 to 10 V for ⁴⁰Ar. ⁸⁴Kr and ¹³²Xe are measured by the multiplier with typical count rates of 10³ to 10⁴ respectively 10² to 10³ cps. In order to achieve maximum precision and to reduce variations due to the ion source, the source tuning is normally not changed during the whole speleothem measurement run. This provides maximum stability of the ion source.

The fast calibrations, consisting of pure He, Ne or Ar-Kr-Xe volumes, are normally performed after the according sample and calibration measurement. Therewith we want to obtain a background as low as possible for sample measurements. As the mass spectrometer is pumped only 6 minutes after each measurement, a small fastcal gas amount may rest in the system after the pumping time.

The He fast calibration is measured before the sample, because enough time is available while the gases are frozen into the traps for separation purposes. As He is the noble gas which can be pumped the fastest, the pumping time between fast calibration and sample is assumed to be long enough (≥ 5 min). Blank measurements show that the influence of the residual gas of the He fastcal is negligible.

The fast calibrations of He and Ne for speleothem measurements as well as for the diluted standards are prepared in a special way. They are also diluted to values in the order of typical sample or diluted standard values by using a splitting volume. The fastcal for Ar, Kr and Xe is prepared as for water samples and the undiluted standard. It is taken from a volume with a rather pure Ar, Kr and Xe mixture and admitted to the mass spectrometer after an initial purification step.

The mass-spectrometric noble gas measurement starts with the gas inlet into the spectrometer. At first one or more peak centerings are performed to determine the precise peak position. Then, baseline measurements are performed at 0.5 atomic mass units difference to the isotope peak. Subsequently, the signal is integrated alternately at the isotope masses determined during the peak centering. The measurement value corresponds to the baseline-corrected intercept value, which is the back-calculated signal at the time of gas inlet into the spectrometer.

3.5.3 Calibration

The noble gas measurement is based on a comparison of the sample signal with a standard signal. The standard signal refers to a gas volume with a known composition. For normal water and gas samples a standard was prepared with ambient air at precisely known conditions. From this standard volume certain pipettes (0.2148 cc and 0.9989 cc) are taken to calibrate the signals. In the whole measurement procedure the standards are handled in the same way as the samples to achieve maximum precision and comparability.

With regard to speleothem samples the gas amounts are strongly reduced, typically to about 10 000 times smaller than for a 20 ml groundwater sample. Therefore, the normal standard can not be used for calibration of the speleothem signals. For speleothem samples we prepared a diluted standard by using one big pipette (0.9989 cc) of the normal air standard and expanding it under precisely known conditions into a volume of 6.37 l. In this case we were able to generate a calibration curve for the nonlinearity correction which expands over the range of typical speleothem samples. The gas amounts in the case of one small pipette of the diluted standard are shown in Table 3.5.

Processing one big pipette (about 1cc) of the diluted standard produces about 14 000 cps for ^4He , 107 000 cps in the case of ^{20}Ne and 9 800 cps for ^{22}Ne . The Faraday measurement of Ar yields about $2.75 \cdot 10^{-2}$ V for ^{36}Ar and 8.2 V for ^{40}Ar . The heavier noble gases are less abundant and therefore generate a smaller number of counts, of about 650 cps in the case of ^{132}Xe and 16 000 cps for ^{84}Kr . The count rates as well as the measured voltage are taken from run Delta (spring 2008). The values are varying slightly between different runs (some %) according to ion source tuning or gas preparation.

Table 3.5: Noble gas amounts in one small pipette (0.2148 cc) of the diluted standard before dilution by taking aliquots.

isotope	gas amount in ccSTP
^4He	$1.5606 \cdot 10^{-10}$
^{20}Ne	$4.9001 \cdot 10^{-10}$
^{22}Ne	$5.0001 \cdot 10^{-11}$
^{21}Ne	$1.4500 \cdot 10^{-12}$
^{36}Ar	$9.3760 \cdot 10^{-10}$
^{40}Ar	$2.7706 \cdot 10^{-7}$
^{84}Kr	$1.9352 \cdot 10^{-11}$
^{132}Xe	$1.0545 \cdot 10^{-13}$

From the calibration data a curve for nonlinearity corrections can be determined. Calibration signals are measured in different volume sizes, from one small (0.2148 cc) to up to 4 times a big pipette (4 x 0.9989 cc). The fast-calibration corrected sample signal is then transferred into absolute gas amounts using the nonlinearity curve and subsequently into a noble gas concentration through dividing by the water amount.

3.5.4 Reproducibility and uncertainties

A measure for typical uncertainties is given by the reproducibility of the diluted standard. All investigated noble gas isotopes (except the rare ^{21}Ne) show uncertainties below 2 % or about 2% (^{132}Xe). Typical values are summarized in Table 3.6. The reproducibility of the diluted standard was calculated by taking the mean of the 1- σ deviations from the fit function accounting for the non-linearity. The shown data refer to run Beta and are representative for the diluted standard. So far, all speleothem runs confirmed the rather high reproducibility of the calibration data. Furthermore, it was possible to improve the results for He and Ne.

Table 3.6: Typical calibration reproducibilities for all measured noble gas isotopes in the case of the diluted standard and the normal standard. ^{21}Ne has a rather high uncertainty, but is not used for noble gas temperature calculation. The reproducibility of the diluted standard was calculated by taking the 1 σ deviations from the fit function accounting for the non-linearity. The values for the normal standard are taken from Friedrich (2007).

isotope	typical uncertainties	
	diluted standard	normal standard
^4He	1.6 %	0.8 ± 0.7 %
^{20}Ne	1.3 %	0.4 ± 0.2 %
^{22}Ne	1.5 %	0.4 ± 0.3 %
^{21}Ne	5 %	-
^{36}Ar	1.7%	0.8 ± 0.4 %
^{40}Ar	$\leq 1\%$	0.5 ± 0.4 %
^{84}Kr	$\leq 1\%$	0.9 ± 0.7 %
^{132}Xe	2%	1.4 ± 0.7 %

To obtain noble gas temperatures with an uncertainty below 1°C either the air contribution has to be lower than $A = 0.01$ at a total uncertainty of 5% or, if we also want to measure samples with a higher air contribution, the total uncertainty has to be reduced strongly. If it is intended to calculate noble gas temperatures for a speleothem sample with $A = 0.7$ the temperature uncertainty can only be reduced to 2 °C, even if the total analytical error is about 1 %. In consideration of the calibration uncertainties given in Table 3.6 it is totally unrealistic to reduce the total analytical error to a value below 2 %, including the sample measurement

uncertainty, the uncertainty of blank correction, of calibration and the uncertainty of water determination. Under really ideal conditions a total analytical error between 2 and 3 % may be possible. In this case the limit for A is about 0.1, if a temperature uncertainty below 1 °C should be achieved (compare Fig. 2.7). The reproducibility of the diluted standard is similar to the normal undiluted calibrations. In the case of Ne some improvements have been achieved by a modified measurement procedure, which reduces the uncertainty to about 1 % for ^{20}Ne and ^{22}Ne . However, it is unlikely that the analytical error can be reduced further.

The reproducibility of the diluted standard shows that it is possible to measure small gas amounts (e.g., 1 small pipette of the diluted standard corresponds to $3.37 \cdot 10^{-5}$ ccSTP of air) with a rather high precision ($\leq 2\%$). This implies that noble gas temperature calculations with an uncertainty below 1 °C are possible for adequate samples with a low air/water-volume ratio.

3.5.5 Sensitivity

Palaeoclimate studies to investigate rapid changes and short-time events require a temporal resolution as high as possible. Therefore, the sample size has to be reduced and consequently less gas is available. The limit in sample size is given by the counting statistics and the maximum tolerable uncertainty. A high mass spectrometric sensitivity can push down the lower limit of measurable samples.

The sensitivity of two runs in 2007, run Beta and the subsequent run Gamma, is summarized in Table 3.7. In run Gamma the ion source tuning was modified for the He and Ne measurements. With regard to the heavy noble gases a splitting step was removed, so that the sensitivity was strongly increased. The numbers for typical water samples at the same system and from a high precision laser microprobe noble gas mass spectrometric system are given for comparison (data from Böhlke and Irwin, 1992a).

Table 3.7: Mass spectrometer sensitivity. Run Beta and Run Gamma refers to a speleothem measurement series, the water samples are measured using a standard procedure as described by Friedrich (2007), microprobe refers to a highly sensitive system of Böhlke and Irwin (1992a).

reference	sensitivity in 10^3 atoms per cps				
	He	Ne	Ar	Kr	Xe
run Beta	1 600	665	482	2 300	4 000
run Gamma Ar tuning	1 600	665	69	280	440
run Gamma He tuning	77	65	69	280	440
water samples HD	150	920	1 850 000	3 920 000	6 580 000
microprobe MS	-	-	107	146.6	156.2

Measurements using He tuning turned out to be of no use, because of high background values in the case of He. A line blank, including only the pathway of the calibrations to the mass spectrometer, yields already about 70 % of the total He signal caused by one small pipette. Fluctuations in the blank values can therefore provoke unacceptably high uncertainties for calibrations as well as for sample signals. In the case of Ne the blank contribution to the signal of one small calibration is about 10 %, which is lower, but still too high to achieve a confidently low uncertainty at lower sample count rates. Furthermore, the Ne signal is strongly influenced by twofold ionized Ar atoms. The Ar value increases permanently after closing the pumping valve due to degassing from the spectrometer walls, which is an effect caused by the memory of larger water samples. Test series showed that 19.7 % of the Ar get double ionized in the case of He tuning. If the ion source is changed to Ar tuning, only about

1 % of the He-signal and about 3% of the Ne signal of one small calibration are due to the line blank. Thus, in the subsequent measurements and in run Gamma the ion source was set to Ar tuning.

0.1 μl of water-filled fluid inclusions at 10 °C contain about $3.5 \cdot 10^{-13}$ ccSTP ^{123}Xe , which corresponds to about $35 \cdot 10^6$ atoms of Xe. Thus, we can expect about 80 counts per second, which is well measurable. Assuming a water content of 0.2 ‰ would mean that a sample size down to 0.5 g is adequate, if the setting of run Gamma is used.

3.5.6 Blank values

Due to the small gas amounts the background control becomes very important. Several types of blanks are determined depending on the extraction and measurement procedure.

The calibration data are corrected by a line blank which excludes the extraction part. Prior to each sample a blank of the extraction line including the pumped sample was performed. Sample crushing measurements are corrected with this value. Furthermore, crushing blanks of the empty copper tubes respectively crushing cells have been measured to determine the difference between empty untreated crushing devices and the background of the extraction process. Additionally a hotblank was determined to investigate the influence of the background on the signal in the case of thermal decrepitation. Moving of the steel ball also produces a certain background. Its value has been examined in an experiment using "de-gassed" stalagmite powder (prepared from inclusion-poor calcite by crushing several 100 times and heating >150 °C during pumping). Similarly, a blank is produced by squeezing of empty copper tubes (chapter 3.3.3).

In Table 3.8 a summary of different measurements is given. Unfortunately, the types are not directly comparable as they have been measured using different settings. However, it is clearly visible that the simple crushing mechanism does have little influence on the signals in case of the steel cylinder. Squeezing of an empty copper tube releases in contrast much more Xe compared to the unsqueezed tube. Heating creates in all cases strongly elevated values in the first heating step, which are extremely pronounced using copper tubes.

A comparison with the laser microprobe noble gas spectrometer of Böhlke and Irwin (1992a) reveals that it is possible to achieve lower blanks applying an adequate preparation. Our system yields blanks up to one order of magnitude higher.

A comparison of our hotblank values shows, that it is unrealistic to achieve useful results with the copper tube extraction. The hotblank obtained in the steel cylinder during 2 h heating at 150 °C is in general significantly lower, especially for the heavy noble gases. Systematic experiments with varying pumping periods and heating temperatures revealed an exponentially decreasing background for increasing pumping times and temperatures (Marx, 2008). Compared to the blank values achieved in other laboratories our values are rather good for the light noble gases, but show some potential for improvement in the case of the heavy noble gases (Table 3.9). The results of the "cold" steel crusher at 70 °C constitute a lower limit for the achievable blank. As this value is up to three orders smaller than the heating blank at 150 °C it is possible to reduce the hotblank by special treatments prior to the measurement. So far, preheating was performed at medium temperatures of about 150 °C and rather short time periods of < 24 h. Increasing the temperature and prolongating pumping time reduces the hotblank values (Marx, 2008). This is an essential requirement for the further developments in stepwise extraction methods as well as the sophisticated water collection and determination.

Table 3.8: Typical blank values of different background measurements. The microprobe system blank refers to a highly sensitive system of Böhlke and Irwin (1992a) and is given for comparison. He, Ne, Kr and Xe blanks are given in counts per second. Ar is given in Volt except the microprobe blank (cps). The values of the copper tube and steel cylinder measurements are hardly comparable as they have been determined in different runs with different settings.

type	He	²⁰ Ne	⁴⁰ Ar	⁸⁴ Kr	¹³² Xe
copper tube	150	1100	$4 \cdot 10^{-3}$	12	1
copper tube squeezing (empty)	38	410	$6.9 \cdot 10^{-3}$	16	15
copper tube heating (empty, 100 °C)	-	1400	0.2	600	600
steel cylinder (empty, 70 °C)	100-200	1500	0.01	20	2
steel cylinder (empty, 150 °C)	730	2500	0.06	130	11
steel cylinder crushing (empty, 300 strokes)	300	3300	0.01	20	1.3
steel cylinder crushing (calcite, 100 strokes)	6110	1030	0.03	80	8
steel cylinder crushing (calcite, 300 strokes)	17700	1600	0.08	220	24
microprobe system blank	-	-	1900 - 3600	0.3 - 0.4	0.13-0.18

Table 3.9: Typical blank values of different background measurements in ccSTP. 'hotblank Tokio' refers to a system for geological applications (e.g., Podosek et al.1980) as well as the 'hotblank Kobe' (Matsubara et al., 1988), which was determined at 1500 °C. 'hotblank Heidelberg' has been determined at 800 °C, respectively at 1700 °C and refer to data published by Trieloff et al. (2001). 'hotblank Houston' (Copeland et al., 2007) was derived from several long duration (≥ 16 h) hotblank measurement at 400 °C. 'blank manchester' refers to extraction blanks described by Turner and Bannon (1992). Values are given in ccSTP.

type	⁴ He (10^{-10})	²⁰ Ne (10^{-11})	⁴⁰ Ar (10^{-8})	⁸⁴ Kr (10^{-12})	¹³² Xe (10^{-13})
copper tube heating (empty, 100 °C)	-	≈ 0.5	≈ 1	≈ 10	≈ 200
steel cylinder heating (empty, 70 °C)	0.01	0.08 - 0.8	0.001 - 0.01	0.001 - 0.01	0.001 - 0.01
steel cylinder heating (empty, 150 °C)	0.7	4	3	4	2
steel cylinder crushing (calcite, 60 strokes)	1.7	0.5	0.31	0.29	1
hotblank Tokio	1.5	50	30	20	30
hotblank Kobe	8.9	0.66	-	0.45	1.5
hotblank Heidelberg	210 - 230	-	-	0.01-0.07	-
hotblank Houston	0.3 - 1.2	-	-	-	-
blank Manchester	-	-	0.1 - 0.01	-	-

3.5.7 Measurement automation

After manually extracting the noble gases from the speleothems, the whole gas separation and measurement process is run automatically. Software and control tools (Prepline 5400) developed by R. Friedrich and K. Träumner are used. For each type of sample (water, gas or speleothem samples) a special script can be written, which corresponds to the specific requirements. The scripts can open and close the valves, control the temperature of the cryo gas traps for subsequent gas separation, check the gas amount in a quadrupol before the inlet into the mass spectrometer as well as start and stop the measurement in the mass spectrometer. Furthermore, the details of peak centering, the scanning sequences as well as the time-scales of the measurement can be determined by the individual scripts.

We developed three different speleothem scripts for background, sample and calibration. Apart from the extraction process, the gas separation and purification as well as the measurement in the mass spectrometer is completely identical for the three sample types. In the case of the background measurement only the line part between pipettes and traps is included, the extraction part itself is closed off. These values are used for the correction of the calibration and are named with B for automatic data evaluation.

The calibrations use the same line parts as the blanks. In this case the extraction part is also closed off. These measurements are marked with C for the data processing with the evaluation program Calc5400.

The sample measurements are split into two parts, although the same scripts are used for both. Before each sample measurement a blank is made for the line, including the extraction part and the sample. Subsequent to the blank measurement the sample is processed using the same script. It is marked with an S with regard to automatic evaluation.

3.6 Mass spectrometric procedures and data evaluation

In this section, the measurement of the different noble gases is discussed in detail. Due to the low signals and the strong non-linear behaviour of the electron-multiplier special routines have been developed for the He as well as the Ne measurement. The magnet-stability is the major problem for the measurement of the heavy noble gases. Due to hysteresis the peak moves after jumps to other masses and therefore provokes to fail the peak maximum. Different blank contributions require the development of a sophisticated data evaluation which is presented at the end of this section.

3.6.1 He and Ne measurement

The signal interpretation was most difficult for He and Ne. The signals are about 10 000 times smaller as for typical water measurements. In contrast to this, the heavy noble gases yield signals, which are comparable because a big splitting volume for water samples is not used for stalagmites.

The measured signals include several parts: the real signal due to the sample, a memory contribution due to the Ne memory of the mass spectrometer and a contribution of double ionized ^{40}Ar in the case of ^{20}Ne (Fig. 3.42 c, d). For He the measured signal is composed of the sample signal, but furthermore influenced by a contamination peak (Friedrich, 2007).

As the Ne signal is rather large in case of water samples (some V, corresponding to some $100 \cdot 10^6$ cps), a remarkable Ne memory has built up in the mass spectrometer during several years of use. If the pumping of the mass spectrometer is stopped, the neon atoms are released from the walls and are leading to an increasing signal for all Ne isotopes (measured: ^{20}Ne ,

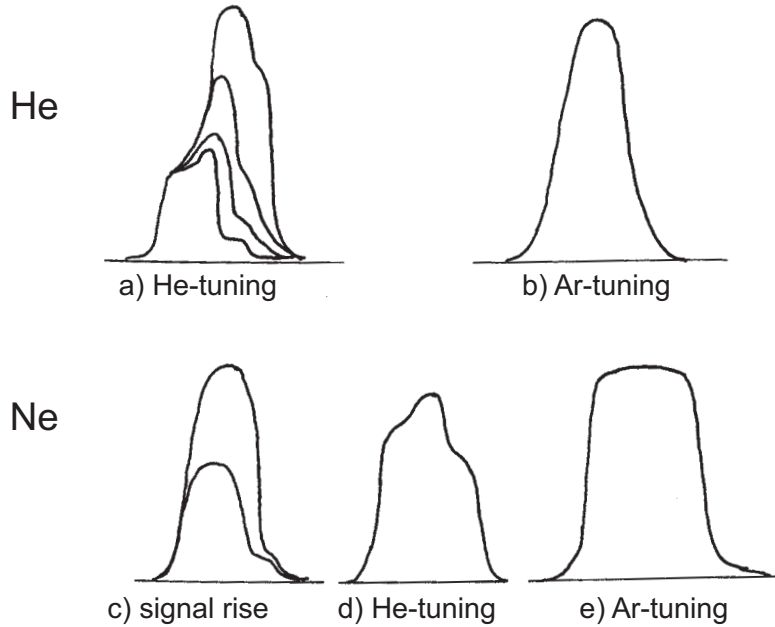


Figure 3.42: Signal forms of He and Ne using different tuning parameters. He tuning yields a better ionisation efficiency but furthermore produces multiple ionisation, which affects the peaks (a,d). a) and c) show the increasing signal due to the He, respectively Ne memory of the mass spectrometer. b)d) and e) displays the peaks for typical sample gas amounts.

^{21}Ne , ^{22}Ne). This background contribution is assumed to be constant in time, that means for the same time the same number of atoms are outgassing. ^{20}Ne to ^{22}Ne ratios (s. Table 3.12), which are not deviating extremely from atmospheric values even in the case of line blanks, indicate that this is the dominating part of the signal background.

The contribution of double ionized ^{40}Ar was calculated by special measurement series. A pure heavy noble gas composition, containing only Ar, Kr and Xe isotopes, was investigated. Mass 20, 22 and 40 were recorded in each measurement using Ar tuning. The experiment was repeated 10 times to achieve higher statistical significance (s. Table 3.10).

In none of the measurements a significant ^{22}Ne signal was visible, however a well measurable ^{20}Ne value. As the ^{20}Ne signal was about $3.9 \cdot 10^{-2}$ V, we would expect a signal of about

Table 3.10: Measurement series for the check of double ionized ^{40}Ar isotopes which influences the ^{20}Ne results. A pure heavy noble gas composition containing only Ar, Kr and Xe isotopes was used for this experiment. The measurement was performed using Ar tuning.

measurement no.	isotope signals			mass 20/40 ratio (in %)
	Ar-40 (V)	mass 20 (V)	mass 22 (V)	
10434	2.3086	$3.8446 \cdot 10^{-2}$	negative	1.665
10435	2.3428	$3.9305 \cdot 10^{-2}$	negative	1.678
10436	2.3471	$3.9344 \cdot 10^{-2}$	negative	1.676
10437	2.3521	$3.9149 \cdot 10^{-2}$	negative	1.666
10438	3.3507	$3.9454 \cdot 10^{-2}$	negative	1.678
10439	2.3505	$3.9735 \cdot 10^{-2}$	negative	1.690
10440	2.3514	$3.9687 \cdot 10^{-2}$	negative	1.688
10441	2.3510	$3.9554 \cdot 10^{-2}$	negative	1.682
10442	2.3496	$3.9568 \cdot 10^{-2}$	negative	1.684
10443	2.3480	$3.9131 \cdot 10^{-2}$	negative	1.667

Table 3.11: Measurement series for the check of double ionized ^{40}Ar isotopes with He tuning. A pure heavy noble gas composition containing only Ar, Kr and Xe isotopes was used for this experiment.

measurement no.	isotope signals			mass 20/40 ratio (in %)
	Ar-40 (V)	mass 20 (V)	mass 22 (V)	
12956	8.5891	1.7329	negative	20.17
12957	8.4722	1.6737	negative	19.76
12958	8.3729	1.6511	negative	19.72
12959	8.3596	1.6332	negative	19.54
12960	8.3156	1.6223	negative	19.51
12961	8.3046	1.6109	negative	19.40

$3.9 \cdot 10^{-3}$ V for ^{22}Ne . This signal is easily measurable with the Faraday cup, which exhibits a lower limit of about $2 \cdot 10^{-4}$ V. Thus, it can be assumed that there is no Ne in the gas. Otherwise 10 % of the ^{20}Ne values should be visible at mass 22. Therefore, the signal at mass 20 was caused by double ionized ^{40}Ar . Taking into consideration all 10 measurements (1.677 ± 0.009)% of the argon get ionized twice.

The experiment was repeated with He tuning, which yields a higher electron energy for ionisation. Instead of about 62 eV the ion-source produces electrons with about 71 eV. This difference is sufficient to increase the amount of double ionized ^{40}Ar significantly to about (19.7 ± 0.3)% (Table 3.11). We tested the double-ionisation as we wanted to measure Ne and also He in the He tuning. This would result in a higher ionisation efficiency and enables the ^{20}Ne detection with the Faraday Cup. We intended to avoid the use of the multiplier for high count rates above some 10 000 cps as the sensitivity increases very strongly in the first minutes at high count rates. However, the high ionisation efficiency of the He tuning provokes also the double ionisation of memory- ^{40}Ar and a background at mass 4, e.g. a line blank yields 80 000 cps for ^4He , whereas about 200 000 cps have been counted for a Fastcal at the same isotope. The line blank accounts for 50% of the sample signal in the case of 1 small pipette of the undiluted standard and still about 9 % in the case of 2 big pipettes of the undiluted standard. The contribution is smaller for Ne, about 10 % in the case of 1 small pipette and 2 % in the case of 2 big pipettes. However, the varying background leads to large uncertainties in the final gas amounts. Therefore, we rejected the measurement with the He tuning. Additionally, the signals become more stable because the tuning of the ion-source is not changed during the whole measurement series.

A neon measurement takes about 27 minutes if ^{20}Ne , ^{22}Ne and ^{21}Ne are measured. The mass 40 value subsequent to the neon measurement was about $2.9 \cdot 10^5$ cps (s. Table 3.13) after 30 minutes and is rather constant. Therefore only about 4400 cps in the neon measurement are due to the ^{40}Ar using the Ar tuning for 27 min. In the case of the line blanks the total signal is about $1.5 \cdot 10^4$ cps at the end of the measurement. This means that the contribution of the double ionized argon to the total signal is at most 35 %. Most samples have some 100 000 cps and more, so that the ^{40}Ar contribution is in the low % range and can be corrected according to the subsequent argon measurement. Actually, this is rather difficult and charged with high uncertainty, as we need to extrapolate the background data to the beginning of the sample measurement. However, the double ionized ^{40}Ar is a constant offset for all Ne measurements and thus no correction for the sample as well as the calibration was performed. Furthermore, if the concentration is above $4 \cdot 10^5$ cps the argon contribution to the neon signal is below 1 % and can therefore be neglected.

Analysis of the $^{20}\text{Ne}/^{22}\text{Ne}$ ratio shows, that the double-ionized ^{40}Ar leads to an increased ratio in the raw data (Table 3.12). ^{22}Ne is affected neither by the multiple ionized argon nor by the low number of atoms at mass 44. Therefore, the $^{20}\text{Ne}/^{22}\text{Ne}$ ratio is above 10, but

Table 3.12: Neon isotope ratios in the case of different calibrations, calculated from raw data. The size of the calibrations is comparable to that of the speleothems. The neon ratios are constant and not dependent on the size, except the (line)blank. For comparison the $^{20}\text{Ne}/^{22}\text{Ne}$ ratio of blank-corrected sample data (mean of 50 measurements) is given.

measurement	ratio		
	Ne-20/Ne-22	Ne-20/Ne-21	Ne-21/Ne-22
line blank	11.20	375	33.7
Cal 0.2 cc	10.38	376	35.6
Cal 0.4 cc	10.34	358	35.1
Cal 0.6 cc	10.32	369	35.4
Cal 0.8 cc	10.26	362	34.8
Cal 1.0 cc	10.27	365	34.9
Cal 2.0 cc	10.30	359	34.9
Cal 3.0 cc	10.30	360	34.9
Cal 4.0 cc	10.33	367	34.9
theory atmosphere	9.80	338	34.5
mean samples run Delta	9.74	-	-

Table 3.13: Ar and CO₂ background for different sample sizes. This values have been determined subsequent to the sample-Ne measurement.

measurement	Ar-40 (10 ⁵ cps)	CO ₂ (cps)
line blank	2.07	204
Cal 0.2 cc	2.51	207
Cal 0.4 cc	2.50	214
Cal 0.6 cc	2.69	213
Cal 0.8 cc	3.00	212
Cal 1.0 cc	3.17	214
Cal 2.0 cc	2.81	211
Cal 3.0 cc	2.20	207
Cal 4.0 cc	2.40	205

relatively constant over the whole range of the calibrations. Similarly, the $^{20}\text{Ne}/^{21}\text{Ne}$ ratio is elevated, as ^{21}Ne is not affected by multifold ionized atoms in contrast to ^{20}Ne . Furthermore, the $^{21}\text{Ne}/^{22}\text{Ne}$ ratio is very close to the expected values, even in the case of the line blank and the uncorrected calibration data. Blank correction and comparison of the sample signals with calibration signals yield the expected ratios. The mean calculated from about 50 single measurements in run Delta resulted in a ratio of 9.74 and shows the correctness of the data evaluation including the background correction and the calibration procedure.

In addition to the sample value, the ^{40}Ar background and the Ne memory, the signal is influenced by attrition due to the ion source. As the double ionized Ar plays a minor role for the signal evolution of ^{20}Ne by using Ar tuning we neglect this contribution in the following. The signal change of ^{20}Ne can be described by the following differential equation:

$$\frac{dN}{dt}(t) = R_{\text{Ne}} - z \cdot N(t) \quad (3.2)$$

R_{Ne} describes the constant outgassing of Ne from the walls and $-z \cdot N(t)$ is the attrition of Ne by the ion source. For the factor z it is assumed, that the attrition is proportional to the

amount of Ne in the system. A solution according to Bronstein et al. (2000) is:

$$N(t) = N_0 \cdot \exp(-zt) + \frac{R_{\text{Ne}}}{z} \cdot (1 - \exp(-zt)) \quad (3.3)$$

$$= \left(N_0 - \frac{R_{\text{Ne}}}{z} \right) \cdot \exp(-zt) + \frac{R_{\text{Ne}}}{z} \quad (3.4)$$

$(N_0 - \frac{R_{\text{Ne}}}{z}) \cdot \exp(-zt)$ is the attrition term with $(N_0 - \frac{R_{\text{Ne}}}{z})$ negative for most cases ($N_0 \leq 10^6$ cps), $\frac{R_{\text{Ne}}}{z}$ gives the end member by balancing of attrition and outgassing, N_0 is the signal due to ^{20}Ne amount extracted from the sample.

The typical signal evolution in time is plotted in Figure 3.43. The evolution is strongly dependent on the initial neon concentration N_0 . If this value is higher than the limit $R_{\text{Ne}}/z \approx 10^6$ cps then only an exponential decrease can be seen. The turning point between increase and attrition was found by analysis of all measured data sets. Up to some 100 000 cps a linear increasing trend is dominating, between 10^5 and 10^6 cps an inverse exponential decay is visible and at $1.0 \cdot 10^6$ cps the signal is constant. Above this point the values are exponentially decreasing.

For typical stalagmite samples the count rate is about some 100 000 counts or even lower. Then the difference $(N_0 - \frac{R_{\text{Ne}}}{z})$ is very large and the signal is strongly increasing for the first time after the gas inlet. Therefore the equation can be simplified by series expansion for a short time scale after the gas inlet:

$$\left(N_0 - \frac{R_{\text{Ne}}}{z} \right) \exp(-zt) + \frac{R_{\text{Ne}}}{z} = \frac{R_{\text{Ne}}}{z} + \left(N_0 - \frac{R_{\text{Ne}}}{z} \right) \cdot (1 - (zt) - (zt)^2/2 - \dots) \quad (3.5)$$

$$= \frac{R_{\text{Ne}}}{z} + \left(N_0 - \frac{R_{\text{Ne}}}{z} \right) - zt \left(N_0 - \frac{R_{\text{Ne}}}{z} \right) + \dots \quad (3.6)$$

$$= N_0 + R_{\text{Ne}} \cdot \left(1 - \frac{N_0}{R_{\text{Ne}}} \cdot z \right) t + \dots \quad (3.7)$$

$\frac{N_0}{R_{\text{Ne}}} \cdot z$ is a very small number for small gas amounts ($\leq 10^5$ cps) as R_{Ne} is about 10^6 cps and z about 10^{-2} s^{-1} . Therefore, we expect a linearly increasing count rate for a small gas amount according to the following equation derived by simplification from the above formulas:

$$N(t) = N_0 + R_{\text{Ne}} \cdot t \quad (3.8)$$

Comparison with measurements confirm the theoretically derived signal evolution for small sample gas amounts (see for example Figure 3.44).

If the signal is larger (10^5 to 10^6 cps), no longer a linear trend can be expected, because the difference to the equilibrium value gets smaller. The slope decreases very fast and an inverse exponential decay curve is found, as it was deduced theoretically. Several measurements have been recorded by their peak centre values at the beginning. These plots (see Fig. 3.45) show this behaviour quite well. According to this result the fitting routines have been adapted to this data. Evidently, a linear fit does lead to wrong data, only the exponential curve gives reasonable results.

Recapitulatory it can be said, that up to 100 000 cps the neon data is fitted linearly. Between $1 \cdot 10^5$ and $3 \cdot 10^5$ cps the last cycles showing the exponentially decreasing slope are deleted and the rest is fitted linearly. Above 300 000 cps the data is fitted according to the inverse exponential decay curve.

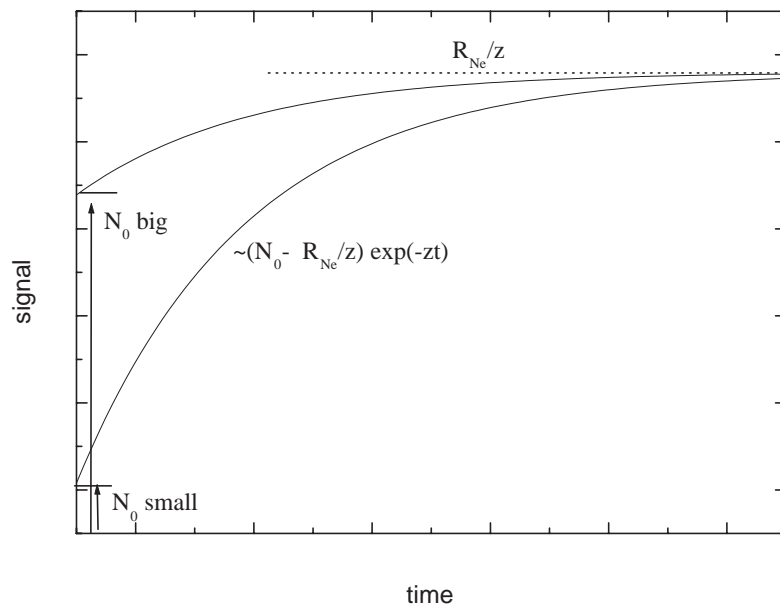


Figure 3.43: Time dependent evolution of the ^{20}Ne signal due to attrition by the ion source and the increase by the memory effect.

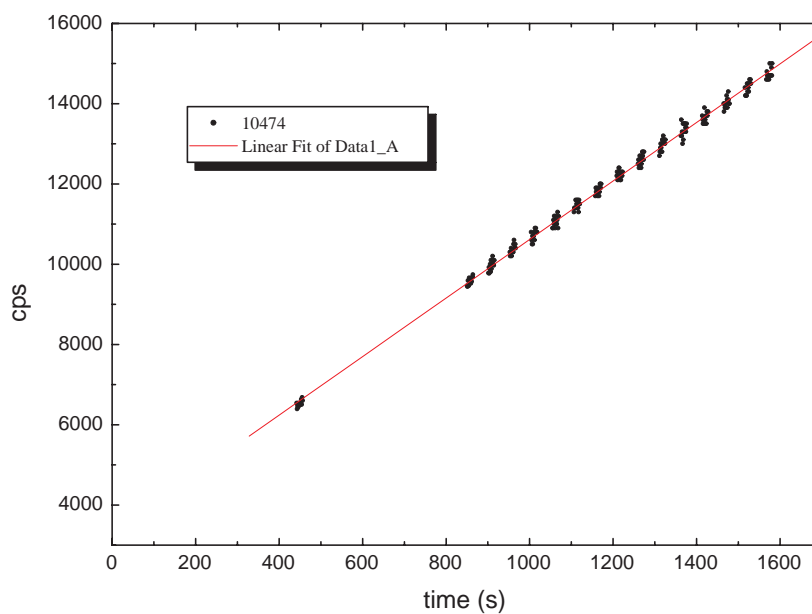


Figure 3.44: Ne signal for a sample with a low count rate. The trend is totally linear, as the outgassing of Ne due to the memory effect is strongly dominating.

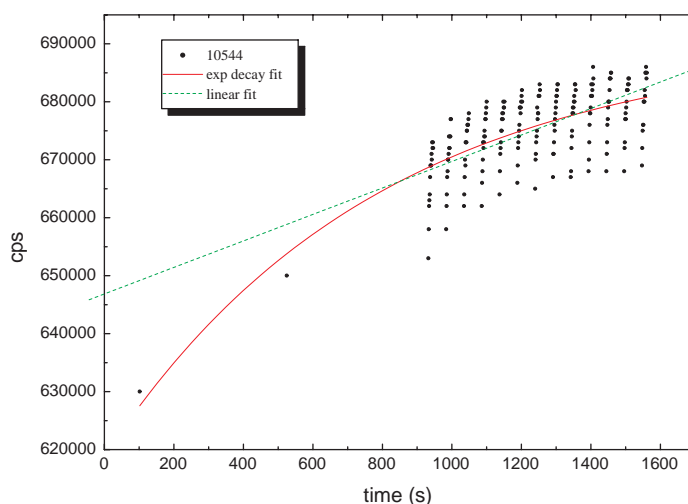


Figure 3.45: Ne signal for a sample with a high count rate. The trend is non-linear, as the signal is influenced not only by outgassing but also by attrition from the ion source. A linear fit leads to much too high intercept values, whereas the exponential fit can reproduce the peak center values and therefore will give a reasonable intercept value.

The He and Ne measurements on the multiplier are furthermore complicated by its sensitivity change. In the case of relatively high count rates (above some 10 000 cps) the sensitivity increases rapidly if the ion-beam constantly hits the multiplier (Fig. 3.46, right diagrams). After a certain time the sensitivity for both He and Ne stabilises. For He this takes about 100 to 120 s. To solve the problem concerning the multiplier sensitivity change, we extended the measurement cycle of He to about 10.5 min. For small gas amounts the trend is totally linear with a correlation coefficient R of 0.995 (Fig. 3.46, lower left diagram).

If the count rates are in a higher level and thereby influencing sensitivity, this has to be taken into account. The first data points can not be used for fitting due to this effect. We rejected mostly the first 10 measurement points and performed a linear fit through the remaining points. Using this technique the intercept value of e.g. the He measurement in Fig. 3.46 (lower right diagram) can be determined with an uncertainty of 2 ‰. The maximum deviation of the 2 big pipettes calibration from the linear trend is 2.7 ‰ for the very first measurement readback.

In the case of ^{20}Ne much larger effects are obvious. Already one small pipette of the diluted standard is in the same signal range than He in the case of 2 big pipettes. However, for Ne the sensitivity increase is most pronounced above 100 000 cps. In contrast, one small pipette leads to an almost totally linear increase of the count rate (Fig. 3.46, upper left diagram). At some 100 000 cps the signal is nearly completely dominated by the multiplier sensitivity leading to an increase of about 3.7 ‰ in few seconds (Fig. 3.46, upper right diagram). Thus, it is not useful to integrate over the ^{20}Ne -peak for a longer time, but rather changing between ^{20}Ne and ^{22}Ne . After each peak jump the same, or at least a similar effect of increasing sensitivity occurs. Using a minimum of 3 peak jumps a linear fits gets possible. The intercept value can be determined with an uncertainty of less than 5 ‰ using this technique.

In all examples shown in Fig. 3.46 the signal increase due to the memory effect is visible. The interplay with the attrition is not as important as displayed in Fig. 3.45 due to the reduction of the measurement time and is hardly visible in the upper right diagram of Fig. 3.46.

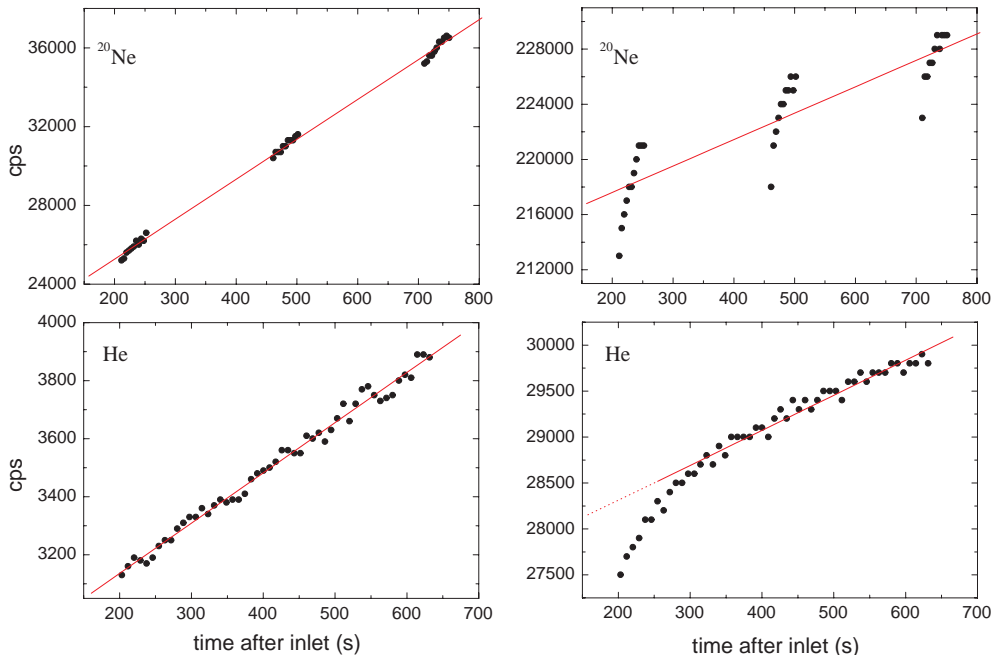


Figure 3.46: Ne and He signal trends for different count rates. The upper figures refer to ^{20}Ne , the lower ones to ^4He . On the left side, samples with low gas amounts and on the right side measurement results with higher signals are displayed. The linear fit in the lower right figure was performed without the first 10 data points.

In summary, the precise determination of absolute Ne and He gas amounts is possible using a long He-measurement and a Ne-measurement consisting of at least three peak jumps. An extension of the Ne measurement with one or two additional peak jumps and reduced measurement iterations on the same peak may further reduce the intercept uncertainties. However, for long measurement times the effect of attrition in combination with the memory effect has to be taken into account.

3.6.2 Argon measurement

In general, the argon signal is significantly above the memory values (0.005 V) during the measurement cycles for calibrations (one small pipette: ≈ 1.6 V) as well as for samples. As the equilibrium value between attrition and outgassing for $t \rightarrow \infty$ is approximately 0.01 V, the outgassing of argon due to the memory does not play a role and is neglected in the following. However, the attrition has to be taken into account. The argon amount changes by:

$$\frac{dN}{dt} = -z \cdot N \quad (3.9)$$

Integration leads to the following time dependent signal:

$$N(t) = N_0 \cdot \exp(-zt) \quad (3.10)$$

where N_0 is the argon amount at inlet time and the z the attrition factor.

In Figure 3.47 a typical ^{40}Ar signal evolution is shown. The exponential fit has a significantly lower uncertainty and fits better to the signal evolution. The linear fit is an approximation which leads to an underestimation of the intercept value of about 1 % compared to the exponential result. As the exponential behaviour is physically based and leading to a better fit, this routine was used in run Beta. In general, the linear approximation can also be

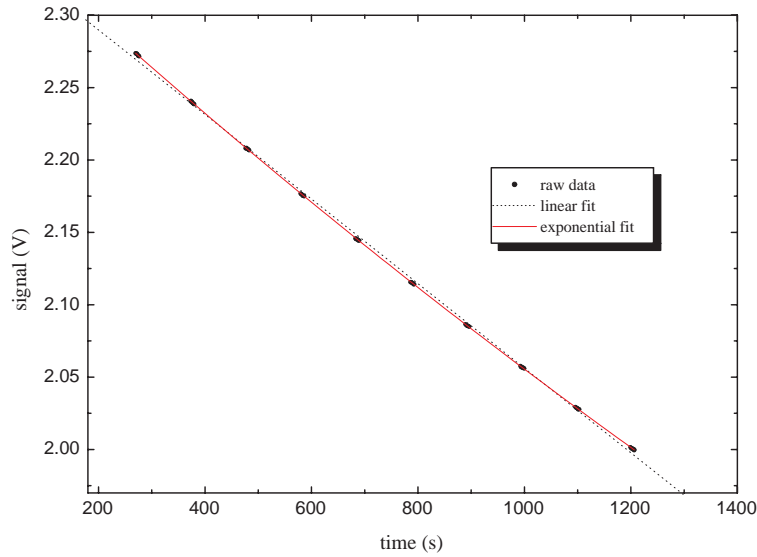


Figure 3.47: ^{40}Ar signal during a typical measurement. Ar shows exponentially decreasing values due to attrition. Therefore the linear fit underestimates the gas at inlet time by $\approx 0.7\%$.

Table 3.14: $^{40}\text{Ar}/^{36}\text{Ar}$ ratios. The calibration data are not line blank corrected.

measurement	$^{40}\text{Ar}/^{36}\text{Ar}$	no. of samples
samples run Delta	296 ± 4	28
Cal 0.2 cc	299 ± 5	17
Cal 0.8 cc	299.2 ± 0.8	12
theory	295.5	-

used if the same fit is applied to all measurements. Therefore, we evaluated our data in the subsequent runs with a linear fit. The investigation of sample $^{40}\text{Ar}/^{36}\text{Ar}$ ratios proves the argon measurements and data evaluation to be accurate (Table 3.14). The sample ratios agree within the uncertainty with the theoretically expected values. The ratios of the calibrations are independent of the gas amount, but more precise for the larger calibrations due to less scattering.

3.6.3 Magnet stability and implications for data evaluation

The behaviour of the magnet is a further complication in the measurement procedure as well as in the data evaluation. As the peaks are quite sharp, the multiplier measurement depends strongly on the precision of the deflection magnet. If the magnet setting for the peak measurement changes a bit, the multiplier will be off the peak. As in all measurements (except for He) more than one isotope is recorded, the magnet has to jump between different masses.

Magnetic fields are known to be influenced by the behaviour of the material which is used to increase the magnitude of the magnetic field. The ferromagnetic material between the copper coils leads to hysteresis and therefore the return point after a peak jump is not exactly the same. The magnet is provided with a Hall probe to achieve the desired magnetic field. However, in the first measurement cycles drifts are clearly visible despite the Hall probe

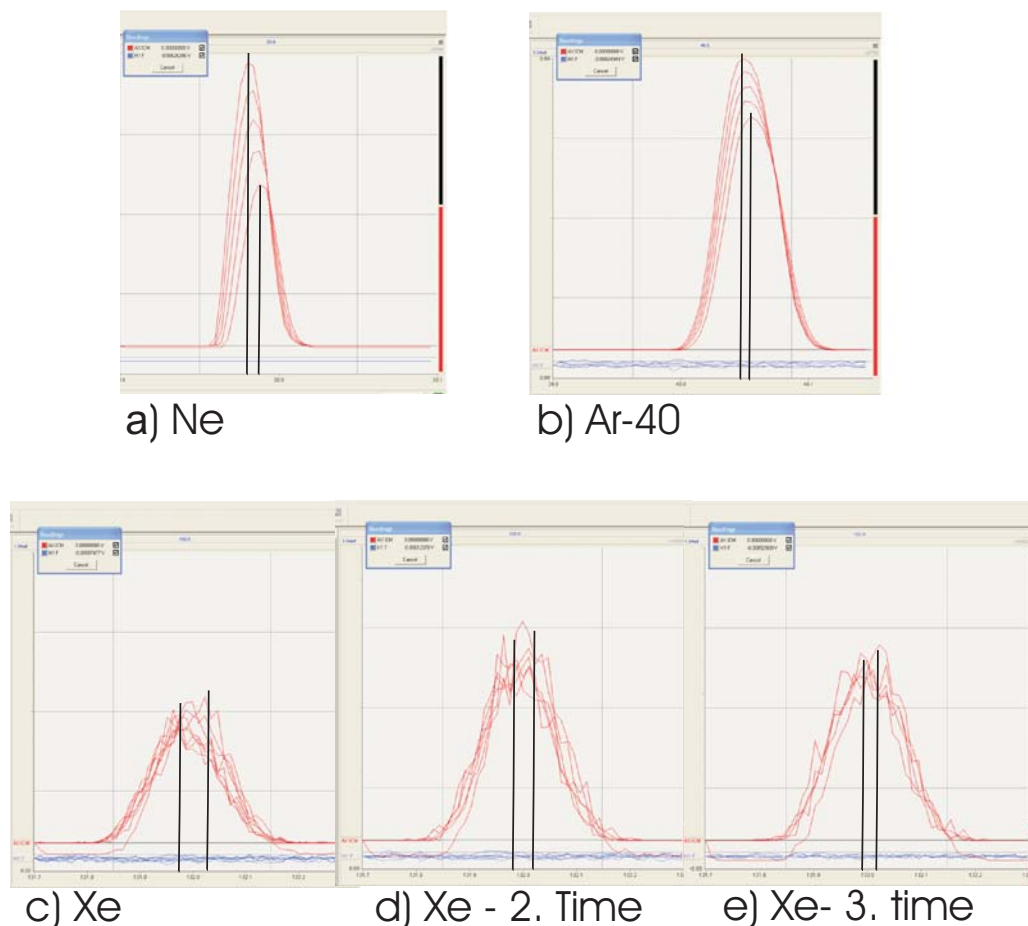


Figure 3.48: The five screen prints show typical examples for the effects of hysteresis on the data. Evidently, a drift in the peak center position occurs (indicated by vertical black lines). The peak center moves to lower masses in subsequent scans. a) refers to ^{20}Ne after a jump from mass 4, b) to ^{40}Ar after a jump from mass 4 and c) d) e) to ^{132}Xe after a jump from mass 40.

measurements (Fig. 3.48). Peak scans show drifts for all masses, which are most pronounced for the heavier gases after a large peak jump (Ne: mass 4 to mass 20, Xe: mass 40 to mass 132). The deviation between the first peak scan and the last recorded cycles in Fig. 3.48 are 0.0076 amu for ^{20}Ne , 0.0081 amu for ^{40}Ar , and 0.054 amu for ^{132}Xe after the first jump from mass 40 to 132. In the second and third step at Xe the drift is reduced with a value of 0.039 amu and 0.026 amu, respectively. As it is obvious in Fig. 3.48 the peaks stabilise at a little bit lower mass compared to the first peak scan. Thus, the measurement occurs in general at too high masses and provokes the risk of wrong readback values. For Ne and Ar the drift is not important as the peaks are normally rather wide. The peaks of Ne and Ar in Fig. 3.48 refer to the outgassing due to the memory. However, the Xe values in the same figure refer to a fastcal AKX and correspond to typical signal levels. Such large drifts can lead to measurements at wrong positions and even missing of the peak.

To stabilise the magnet several techniques have been developed, e.g a precycling is performed before the measurement and additionally a second peak center is done after the baseline measurements. Despite these procedures the effect of hysteresis can not be avoided totally. Consequently, we attempted to prevent peak jumps. A typical measurement procedure for the heavy noble gases Ar, Kr and Xe is composed of a long Xe measurement (5 min) followed

by a Kr measurement of about 1 min. The procedure starts with Xe to get the intercept value as precise as possible. Subsequent to the combined ^{36}Ar and ^{40}Ar measurement, the cycle starts again with Xe and is repeated once. Finally, an additional Xe measurement is performed to raise the precision of the curve and the intercept value. This technique is very sensitive to the order of investigated masses. Changes in the sequence provoke that the peaks of Kr and Xe are not found any more. Furthermore, the magnet has to be stabilized also between one measurement of the same element (especially ^{132}Xe) even if no peak jump occurs. Without precycling, ^{132}Xe was lost after the third or fourth recording period in the first cycle. Therefore, the magnet current is changed slightly after each single measurement to mimic adequate small peak jumps to antagonize hysteresis effects. Due to this method a rather stable signal could be achieved with low variations for Ar and Kr and acceptable values for Xe. However, the procedure has to be optimized further with regard to the ^{132}Xe measurement as in some cases the Xe signal is not as stable as expected.

3.6.4 Data evaluation

The raw data is evaluated by WinCalc, which is used for discarding of outliers and fitting the intercept values. For further data processing always the fitted intercept value including the resulting uncertainty is used. Subsequently, the data is evaluated automatically with the program Calc5400, which was developed by Friedrich (2007).

Firstly, the data is fastcal-corrected to remove sensitivity changes. The raw data from the calibration S_C , blank S_B and sample measurement S_S is divided by the dilution-corrected fastcal signal S_F^* :

$$SE_C = \frac{S_C}{S_F^*} \quad (3.11)$$

$$SE_B = \frac{S_B}{S_F^*} \quad (3.12)$$

$$SE_S = \frac{S_S}{S_F^*} \quad (3.13)$$

$$(3.14)$$

Then, the fastcal-corrected blank values are subtracted from the calibration as well as from the sample data. Afterwards, the background corrected calibration values $SE_C - SE_B$ are dilution corrected, as the gas amount in the standard containers are reduced every time by taking a calibration pipette:

$$SE_{C-B}^* = \frac{SE_C - SE_B}{\prod_{i=1,2} d_i^{n_i}} \quad (3.15)$$

d_i dilution factor for pipette i , n_i total number of portions taken from pipette i .

The sample values are converted into absolute gas amounts by comparison with a fit function, which accounts for the nonlinearity of the fastcal-, background and dilution-corrected calibration values SE_{C-B}^* . Due to non-linearity effects a curve has to be established by calibration measurements of different sizes, which cover the range of typical speleothem samples. Therefore, the so-called inverse sensitivity $Sens_c^{\text{inv}}$ is calculated:

$$Sens_c^{\text{inv}} = \frac{V_c}{SE_{C-B}^*} \quad (3.16)$$

V_c gas amount of one pipette of the diluted standard before taking aliquots, representing the initial value.

The inverse sensitivity $Sens_c^{inv}$, which represents a gas amount per signal, is fitted with a suitable function $f(SE_{C-B})$. Absolute gas amounts M_S for the samples, as well as for the different extraction blanks (extraction line blank M_{extr} , crushing blank M_{crush}) can be calculated from the signals using this function $f(SE_{C-B})$:

$$M_S = SE_{S-B} \cdot f(SE_{C-B})|_{SE_{S-B}} \quad (3.17)$$

SE_{S-B} represents the fastcal- and background-corrected sample signal $SE_S - SE_B$. The value of the fitting function is taken at the position SE_{S-B} .

The program Calc5400 executes the presented steps and delivers absolute gas amounts for the speleothem samples as well as the extraction blanks. The absolute sample gas amount M_S is corrected by the extraction blank gas amount M_{extr} , and depending on the extraction procedure also by other factors, like the contribution of the crushing itself (M_{crush}). For calculation of noble gas concentrations c the resulting absolute gas amount is divided by the released water amount m_w :

$$c = \frac{M_S - (M_{extr} + M_{crush} + \dots)}{m_w} \quad (3.18)$$

The uncertainty is calculated by using the error propagation of the different contributions. The most important part is generally the uncertainty of the water determination, which is in the range of 2 to 3%. For small samples also the uncertainty of the noble gas measurement, especially in the case of Xe, gets significant.

The data evaluation for speleothems is discussed in detail by Marx (2008).

3.7 Test of the measurement procedure with an artificial standard

To test extraction, measurement and data evaluation, an artificial standard with a known noble gas content would be ideal. At first glance the glass capillaries, used for calibration of the water amount - gas pressure curve, could provide the desired properties. A well known amount of equilibrated water can be inserted and additionally the excess-air contribution can be adjusted by the melting-controlled closing.

Seven samples have been prepared (Table 3.15) with an appropriate water and air content to cover a certain range of real speleothem samples. The water was taken in glass capillaries from a drum with equilibrated water at about 24 °C, respectively from a small bowl which was filled before with tap water at 25.5 °C. The glass capillaries were prepared as for the water vapour-pressure curves and were measured in the same way as speleothem samples.

In the three isotope plot (Fig. 3.49) all samples are approximately located on a line, even though the water sources have been different. In general, they show a much too high noble gas content for all gases. This can not be assigned to the fact that tap water was used, which was probably not perfectly equilibrated with ambient air. Otherwise the samples prepared with equilibrated water should show a different behaviour, which is not the case.

In general, He, Kr, and Xe are strongly enriched, whereas Ne and Ar are depleted relative to the expected values (Table 3.16). The absolute offset respectively deficit decreases with the air amount in the capillary. The highest absolute offset was found in the sample with only 1.129 μl water and $6.52 \cdot 10^{-3}$ ccSTP air, whereas the capillary with 6.13 μl water and $1.81 \cdot 10^{-3}$ ccSTP air shows the lowest value. Therefore, it is unlikely that the deviations from the expected data are caused by changes in the solubility as for example by negative pressure

Table 3.15: Artificial standard samples. The first 5 samples have been prepared with tap water from a small bowl, the last two with equilibrated water from a large ton. Extraction 'at line' means the sample is prepared directly at the line of the mass spectrometer, 'external' stands for extraction in a separate line (Fig. 3.14), from where only the gases are transferred to the measurement line with a special sample container after the extraction.

no.	water amount (μl)	air volume (10^{-3}cc)	extraction
274	1.42	6.52	at line
275	4.06	3.87	at line
276	2.48	5.45	at line
281	1.13	6.81	at line
282	3.26	4.71	at line
330	6.13	1.81	external
331	6.19	1.74	external

Table 3.16: Absolute offset (in ccSTP/g) of the artificial samples compared to the expected values according to the inserted water and the additional air amount. Sample no.331 shows a deviation from the overall trend, which can be assigned to the fact, that the sample container for the gas transfer was not pumped properly before. No. 281 was affected by splitting problems.

no.	water amount (μl)	He (10^{-6})	Ne (10^{-5})	Ar (10^{-3})	Kr (10^{-6})	Xe (10^{-7})
281	1.129	9.65	-1.88	4.15	6.13	6.44
274	1.420	-	-1.39	-10.28	2.68	3.39
276	2.484	5.57	-0.63	-4.02	1.67	2.02
282	3.258	3.73	-0.55	-2.99	1.49	1.73
275	4.064	3.64	-0.30	-1.73	0.83	1.02
330	6.129	-1.29	-0.22	-0.69	0.22	0.32
331	6.194	1.58	-0.30	-1.11	0.93	0.94

due to the capillary effect (e.g. Mercury et al., 2004). The dependency of the offset on the enclosed air volume implies a major effect of the air. The reason for this result could not be figured out. It is possible that the flame sealing causes a fractionation and removes especially Ne and Ar, or that the blowpipe gas may be a source with a non-atmospheric gas composition containing a large fraction of heavy noble gases.

Although a clear trend from atmospheric air towards air-saturated water can be detected with an increasing amount of water in the glass capillaries, the data is far away from the expected noble gas concentrations. Therefore, it is not possible to use them as an artificial standard for measurement, extraction and the data evaluation process. However, the overall measurement uncertainties of typically about 1% show the general possibility of high precision measurements in the low-level noble gas mass spectrometry.

Modification of the flame sealing may enable the use of capillaries as artificial standards. After the water is filled in and moved in the middle of the glass capillary, the ends are closed with an appropriate material (e.g. rubber). In this case contact with the blowpipe gas can be avoided during flame sealing. It may also be possible to create small steel volumes, which are closed by squeezing and opened in the same way as copper tube diffusion samplers. Further tests should show the applicability of these ideas. The development of an artificial standard was not pursued further as the data from the diluted calibration standard suggest a reliable measurement and data evaluation procedure.

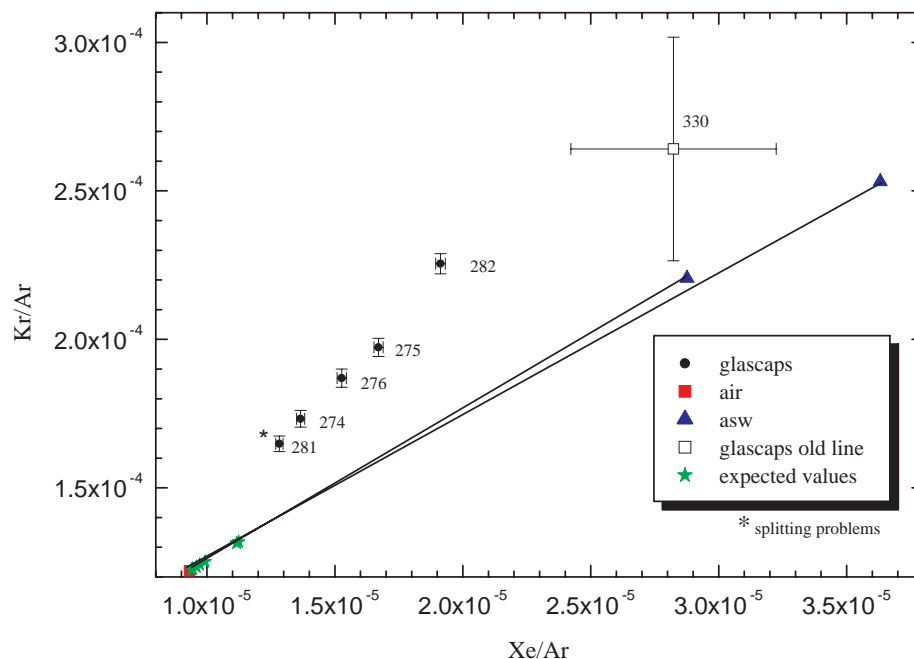


Figure 3.49: Results of the artificial samples in the three isotope plot. On the lower end of the two excess-air lines the theoretical values of the glass samples are plotted. The measurement no. is given for referencing.

A similar idea was used by Böhlke and Irwin (1992a). They applied air-filled capillaries with a special technique. One end was sealed, cooled at room temperature, then the other end was sealed while immersed partially in water. Shorter segments have been produced by halving the remaining parts. With this procedure they achieved results which are scattering around the expected line of various amounts of unfractionated air. Although the number of counts was very small in the case of ^{132}Xe and ^{84}Kr the uncertainty is impressively low. As an additional micro standard they used a synthetic basalt glass with a known noble gas content, which yields values similar to air. However, the variability and uncertainty in this case was higher. Furthermore, they prepared synthetic fluid inclusions of a special optical quartz to demonstrate that it is possible to measure noble gases in microscopic samples of trapped fluids.

Recently precipitated calcite from the last decades may also be used as a standard sample as well as artificially produced calcite precipitates. Speleothems can be grown in special experiments under very well known controlled conditions. Thus, this samples may provide the highest potential for control and calibration measurements. However, they have not been tested with regard to NGTs and unfortunately it is not known, if they provide the required properties as e.g. low air content and sufficiently high water amount. Laboratory experiments may furthermore be an important source to fully understand the conditions which lead to high water content and which also control the air/water volume ratio.

Chapter 4

Results

4.1 Cave air and dripwater measurements

The first section is focused on the cave and its environment. Deriving temperatures from noble gas concentrations by inverse modelling requires the knowledge of the noble gas mixing ratios in the air. In a first approach we can assume the noble gas composition of the cave air to be simply atmospheric. However, in some cases, as e.g. in badly ventilated caves, deviations may occur. To put this important factor on a solid scientific basis, we collected air and dripwater samples in three caves, which were investigated in the framework of the DFG-group Daphne and from which the most important speleothems were taken.

4.1.1 Investigation of the cave air

Noble gas temperatures are calculated from noble gas concentrations by inverse modeling using the temperature dependence of the equilibrium concentration (as well as taking into account the addition of air and fractionation, s. Aeschbach-Hertig et al., 2000). The equilibrium values depend at a certain temperature on the mixing ratio in the air. With regard to the application of the method on speleothems, the composition of the cave air has to be tested prior to the data evaluation and interpretation. If the cave is scarcely ventilated, the noble gas mixing ratio could be changed by terrigenic or radiogenic production of some elements. To prove or revise this assumption we took air samples in two caves in the Sauerland (51°22' N, 7°40' E).

One site, Bunker Cave, is monitored in the framework of the DFG research group DAPHNE. Most of the later discussed speleothem samples, which could be measured with a simple technique and which resulted in reasonable data, derive from this cave. It is situated in the north-western part of Germany near Bochum (20 km). The surrounding geology is dominated by Devonian Massive Limestones. Above the cave there are 10 m to 20 m of rock with few soil (about 1 m), which is covered by small trees and scrubs. The cave air sampling points are marked in Fig. 4.1 with white stars.

Altogether five samples have been taken at two different dates. In January 2007 two cleaned and evacuated 100 ml stainless steel cylinders were filled inside the cave at the indicated sampling points by opening the vacuum-valve for some minutes. Additionally, two small copper tubes were used for collecting the cave air at the same locations. They were closed airtight by special pliers. In November 2007, again cave air samples were taken at the same places by using an evacuated steel cylinder. It was placed on the ground and opened for 10 to 15 minutes.

Additionally, the radon values have been monitored during the sampling in January 2007 to

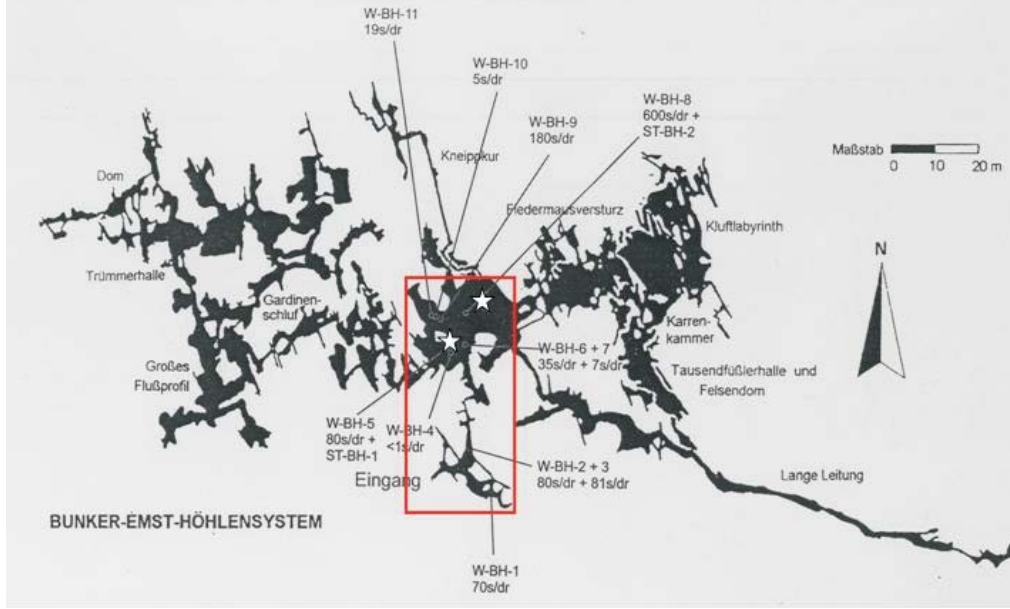


Figure 4.1: Map of the Bunker cave, modified from Grebe (1993). Sampling points are indicated by white stars. The entrance is located at the lowerleft part of the red rectangle. Subsequent a very narrow part is following, which disables the air flow.

control the ventilation and to estimate the influence of the inflowing air. A radon monitor (RAD 7, Durrige Company) was carried through the cave for continuous activity measurements (Fig. 4.2). The first data point indicates the activity concentration outside the cave ($\leq 40 \text{ Bq/m}^3$). Passing a long narrow part (about $50 \text{ cm} \times 50 \text{ cm}$), the radon activity increases rapidly to a steady value of about 1800 Bq/m^3 . Going back to the entrance area after sampling in the inner cave chambers, the activity concentration drops after passing the crawling passage. In the entrance area a lower, but compared to the outside air significantly elevated Rn-level of $330 \pm 30 \text{ Bq/m}^3$ is found. As the differences between the radon concentration outside and inside the cave are large, even small mixing events with atmospheric air or small inflow can be traced (Hakl et al., 1999, 1997, 1996). However, it is difficult to determine Rn-fluxes or calculate the amount of inflowing air. The activity concentration in a cave chamber A_c is determined by an advective component F_{ad} through fractures and passages with cross-section S_f , the diffusive flux F_{diff} from the rock surface S and the decay of radon in the chamber volume. In the case of steady state conditions this can be used for quantitative calculations:

$$(F_{ad} \cdot S_f + F_{diff} \cdot S) - \lambda_{Rn} \cdot V \cdot A_c = 0 \quad (4.1)$$

The advective component consist of the influx $Q_{in} \cdot A_{in}$ and the outflow $Q_{out} \cdot A_c$. The outflowing air masses are equal to the inflowing volume due to mass conservation. Thus, $F_{ad} = Q \cdot (A_{in} - A_c)$ is negative and reduces the activity concentration in the cave chamber. Two parameters are unknown, the advective volume flux Q and the diffusive flux. The last component may be estimated from a badly ventilated cave chamber by neglecting the advective term. Subsequently, the advection can be calculated for other cave parts in a first order approximation by assuming the diffusive flux to be constant allover. In the case of the Bunker Cave this calculation was not possible, as no measurement in highly unventilated parts has been performed. Moreover, Rn measurements at different places inside the cave can show the signal development in the case of fresh air intrusion. This can also be used for estimation of underground airflow velocities and chamber volumes (Hakl, 1997).

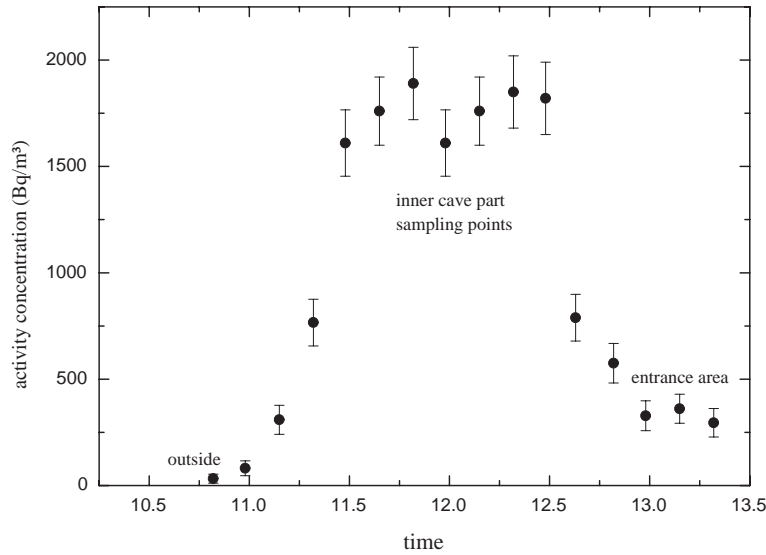


Figure 4.2: Radon activity concentration in different parts of the Bunker cave. The activity is plotted against the time, as the measurement was continuous. The investigation started at quarter to 11 in front of the cave entrance. Then the monitor was carried through the cave. The high values have been detected after a narrow part, where the activity had increased rapidly.

The noble gas air samples have been taken in the part of the cave, where the highest radon activity was measured, so that a small contribution of ambient air can be assumed. According to the sample type, a slightly different measurement procedure was used. The gas from sample containers was measured by taking pipettes of about 0.41 cc. The pressure as well as the temperature were recorded for each pipette. The copper tube samples are inserted completely in a cracker system where they are opened under vacuum. In this case, all the gas is transferred to the mass spectrometer and the temperature, humidity as well as the pressure at the sampling point is used for calculation of the noble gas mixing ratio in the cave air. The measurement results are compared to a set of laboratory air measurements using calibrated pipette volumes of atmospheric air. The lab air pipettes reproduce very well, e.g. in run 33 (January 2007) the standard deviation is $\leq 0.4\%$ for ^4He , ^{20}Ne , ^{22}Ne , ^{40}Ar and ^{84}Kr , and $\leq 1\%$ for ^{36}Ar and ^{132}Xe . The standard deviation for the cave air sample container C, measured in the same run, is comparable. The standard deviation is about 2% for repeated measurements of laboratory air with copper tube samples.

The noble gas measurements of the air samples in the copper tubes show no systematic deviation of the noble gas mixing ratios from the atmospheric values (Table 4.1). The sample containers taken in January show a slightly elevated noble gas concentration, except for He. The sample container C, filled with cave air in November, is closer to atmospheric values, except for He. Calculating the mean of all Bunker Cave measurements, the noble gas concentrations are marginally above the atmospheric values. In case of Xe its in the range of the measurement uncertainty. The standard deviation of the mean values indicates that at least Xe, Kr and Ar are comparable to atmospheric values. Only Ne is 2σ above the air concentration. He seems to be a special case. All samples from the first campaign in January did not show an excess in He. However, the value of the sample-container C is significantly above atmospheric values, which could be confirmed by a duplicate measurement. The elevated He concentration can be caused by a lower degree of ventilation at the time of sampling. Unfortunately, no radon concentrations have been measured at this time.

Table 4.1: Deviation of the noble gas mixing ratios of the Bunker cave air samples compared to atmospheric standard values prepared by lab air pipettes. The precision of the noble gas measurement is about 1 % for all noble gases except xenon, where it is about 2-3%. SD mean refers to the standard deviation of the mean values. Dripwater refers to the mean of four dripwater measurements and indicates the difference to the model expectation. It is given for comparison.

sample	sampling date	deviations from atmospheric ngc in %				
		$\Delta^4\text{He}$	$\Delta^{20}\text{Ne}$	$\Delta^{40}\text{Ar}$	$\Delta^{84}\text{Kr}$	$\Delta^{132}\text{Xe}$
Coppertube sample 1	23.1.07	-1.1	2.0	0.8	0.7	1.4
Coppertube sample 2	23.1.07	-2.3	0.7	-0.5	-1.5	-2.1
Sample ContainerA-I	23.1.07	-0.3	3.4	2.0	2.9	6.6
Sample ContainerA-II	23.1.07	-0.0	2.8	2.2	3.7	3.9
Sample ContainerB-I	23.1.07	0.2	3.1	2.3	4.2	1.5
Sample ContainerB-II	23.1.07	-0.4	2.2	2.2	2.8	5.1
Sample ContainerC-I	28.11.07	16.9	1.7	1.7	0.9	-1.7
Sample ContainerC-II	28.11.07	14.9	1.7	2.1	0.8	1.4
mean all	-	3.5	2.2	1.6	1.8	2.0
SD mean	-	4.6	1.0	1.2	2.2	3.2
dripwater (mean)	23.1./24.4.07	-1.1	-0.5	-1.6	1.1	0.6

Additionally, water samples have been taken from dripwater inside the cave. Fitting of the obtained noble gas concentrations did not show systematic deviations from the model, which is based on typical atmospheric mixing ratios for the equilibrium concentration. Significant deviations of the cave air from atmospheric mixing ratios would result in systematic shifts in the noble gas concentrations of water equilibrated with the cave atmosphere, as e.g. of dripwater which before had been in contact with the cave air.

If we disregard the He values, we can conclude from the Ne, Ar, Kr and Xe results of the cave air measurements and the dripwater concentrations that the air inside the Bunker Cave has most likely atmospheric composition. Water included in speleothems from this cave should therefore possess typical noble gas concentrations of water in equilibrium with the atmosphere.

For comparison and as a test of the representativeness of the Bunker Cave data, a second cave was investigated. The second site is the adjacent B7 cave (Niggemann, 2000), which is a larger system (5100 m) with about 50 m of rock covering above the galleries where air samples have been taken. These galleries are also characterized by a stable cave climate, which indicates low ventilation. In the beginning of 2008, samples were taken at 4 different places and by using two methods, filling of evacuated steel cylinders and enclosing of cave air in copper tubes by squeezing. The sampling points are indicated in Fig. 4.3.

Unfortunately, the measurement of the largest part of the copper tube samples failed. Possibly due to the difficult transport through the cave small leaks had been generated, which made the measurement impossible. Furthermore, problems during sample opening and gas extraction lead to the loss of additional samples. However, one copper tube sample in combination with the measurement of equilibrated water from a cave pond and several dripwater samples (chapter 4.1.2) provide reliable information about the atmosphere in different cave parts.

The Ne, Ar, Kr and Xe mixing ratios of the copper tube sample can not be distinguished from the ambient air (Table 4.2). Similarly, the water samples show negligible deviations from the model indicating that the dripwater as well as the the water in the cave pond was equilibrated with air possessing typical atmospheric noble gas mixing ratios. Calculating the mean of the deviation from the atmospheric mixing ratio for the copper tube sample as well as the water samples, no significant values can be found for Ne, Ar and Kr. Xe seems to have a small uncertainty, but typical measurement errors are rather 1 to 2 % and thus the

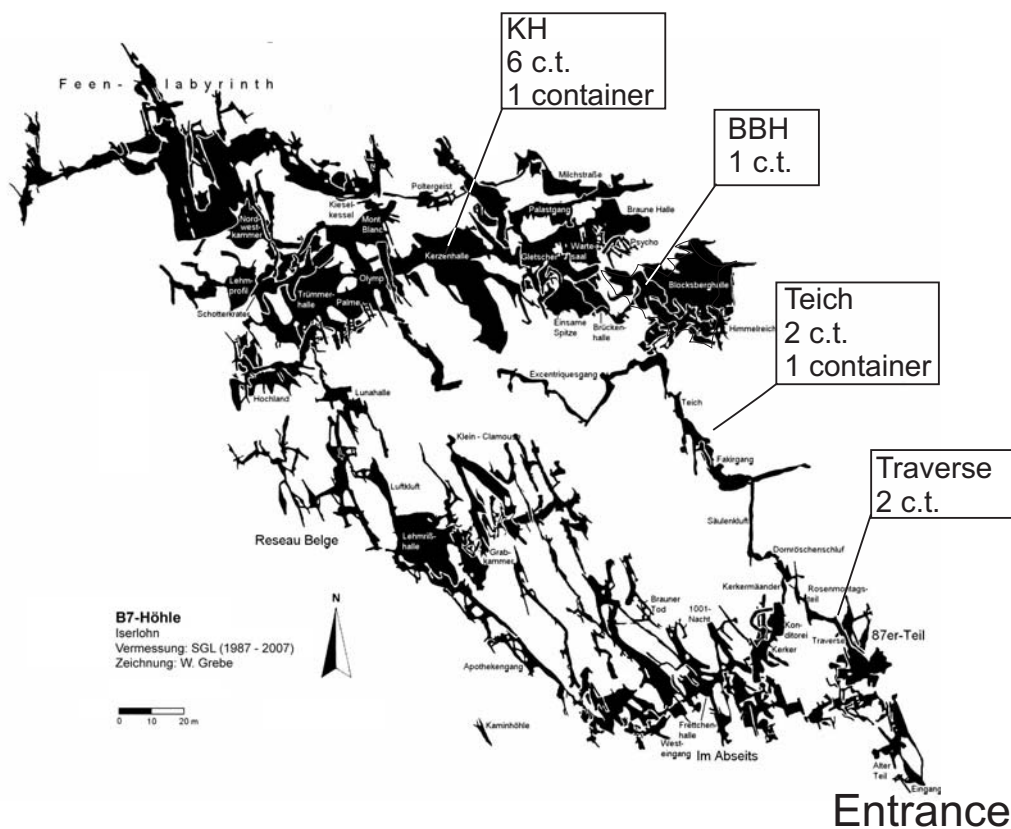


Figure 4.3: Map of the B7 cave, modified from Grebe (1998). Sampling points are indicated by arrows. c.t. refers to air enclosed in copper tubes, container indicates sampling in 100 ml steel cylinders.

Table 4.2: Deviation of the noble gas mixing ratios of the B7 cave air samples compared to atmospheric standard values. WS refers to water samples from the cave pond, respectively from corresponding stalactite drip sites. In these cases the numbers describe the deviation from the model. SD refers to the standard deviation of the mean values of water and air samples.

sample	sampling date	deviations from atmospheric ngc in %				
		$\Delta^4\text{He}$	$\Delta^{20}\text{Ne}$	$\Delta^{40}\text{Ar}$	$\Delta^{84}\text{Kr}$	$\Delta^{132}\text{Xe}$
Container Teich-I	2.2.08	not yet measured	-	-	-	-
Container KH-I	2.2.08	not yet measured	-	-	-	-
C.t. Teich	2.2.08	2.3	-0.0	-0.3	-0.6	1.6
WS Teich	2.2.08	2.2	-1.0	0.0	1.7	1.0
C.t. Traverse	2.2.08	failed	-	-	-	-
C.t. BBH	2.2.08	failed	-	-	-	-
WS BBH I	2.2.08	2.5	0.0	0.0	0.5	1.3
WS BBH II	2.2.08	3.0	0.0	0.0	0.9	0.8
C.t. KH-I	2.2.08	failed	-	-	-	-
mean B7 cave	2.2.08	2.5	-0.3	-0.1	0.6	1.2
S.D B7 cave	2.2.08	0.4	0.5	0.2	1.0	0.4

Xe can hardly be distinguished from expected atmospheric values. However, He has a lower uncertainty and perhaps shows a certain enrichment of He in this deeper and less ventilated cave.

Several measurements of the cave air in the shallow Bunker cave and the deeper B7 cave using different methods could prove the cave air to be atmospheric with regard to Ne, Ar, Kr and Xe. Thus, the NGT calculation is well based on atmospheric concentrations for the two investigated caves and is not influenced by strange cave atmospheres. This result is additionally confirmed by the measurement of water from a large cave pond. The deviations from the expected noble gas concentrations in equilibrium with atmospheric air are negligible. Furthermore, dripwater measurements in the B7 cave as well as the Bunker cave yielded similar results. However, He concentrations may be elevated, as found in the copper tube air and the water samples from the B7 cave. Fortunately, this does not affect the temperature calculation, but can be of importance for dating by radiogenic He.

4.1.2 Dripwater measurements

Karstified sites and especially caves constitute a unique environment as they contain calcite precipitates which provide interesting insights into climate history. Stalagmite trace element concentrations and also stable isotope profiles can be used to determine climatological events on multi-annual, annual or even seasonal scale (Mattey et al., 2008). However, to combine isotope signals with seasonal or multi-annual forcings, it is important to understand the drip hydrology (Baldini et al., 2006) and to know how long the water needs to travel through the overlying structure. The question of the residence time is in particular interesting for the detection of strong short time scale events as severe droughts and extremely warm or cold seasons. A shift of several years will be significant in interpretation. Furthermore, information about the percolation time may be useful for water resources management.

Simple observation of the drip intervals and the drip behaviour may be misleading. Even if an immediate response of the drip rate to precipitation changes were detected, as found by Baker et al. (1997), the water may need significantly longer from the rain event at the surface to the dripping point. Immediate response can be caused by changes in the height of the water column in fissures above the drip site or the water content of the unsaturated zone. Furthermore, threshold controlled flow can be present, which can be established by e.g. an overflow of a cave pond above the dripping site during rain events with sufficient precipitation. Moreover, a direct connection of the dripping site with cracks (fractured flow) is also possible.

A better solution is a multi-tracer approach to determine the time span of water staying in the rock cover and the overlying soil. For young waters an age estimation can be derived by combined ^3He and tritium measurements (see chapter 2.3.3). ^3He is built up in the flow path due to the decay of the tritium contained in the precipitation. An important constraint for this gas-tracer dating technique is the closing-off from the atmosphere. If the water flowing through the underground outgases, like in cracks or cavities, then only the equilibrium component of ^3He or at least a reduced fraction will present in the water sample. A certain amount of the surplus helium, including the radiogenic component, will be lost. Beyond this, a possible excess air component has to be subtracted from the ^3He -signal, which is due to the inclusion of small bubbles in the water. This correction is performed using Ne, Ar, Kr and Xe in an inverse modelling routine ("Noble", Peeters et al., 2003) by applying the CE Model. As the whole data-set of noble gases is measured, also a noble gas temperature is calculated, which can be used for fitting control.

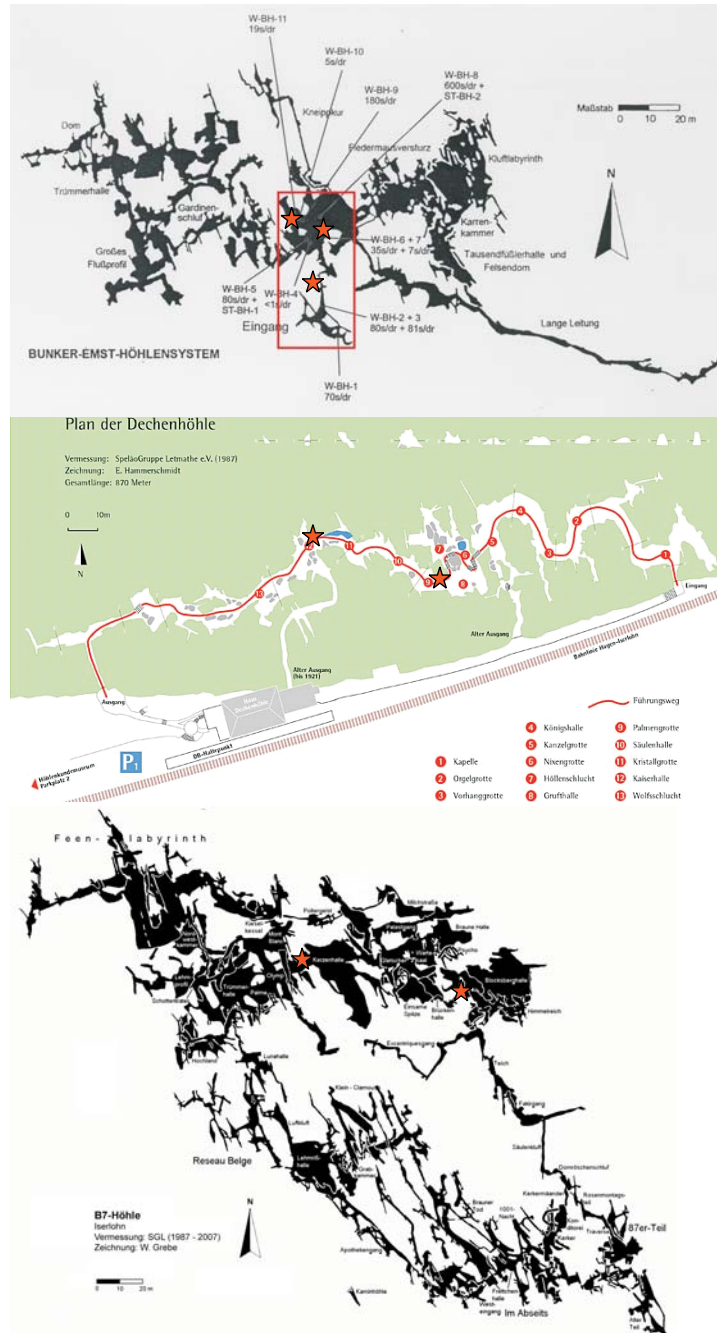


Figure 4.4: Maps from the three investigated caves. On the top Bunker Cave, below Dechen Cave and on the bottom B7 - cave. The sampling points are marked with red stars. The pictures are adapted from Grebe (1993, 1998) and E. Hammerschmidt.

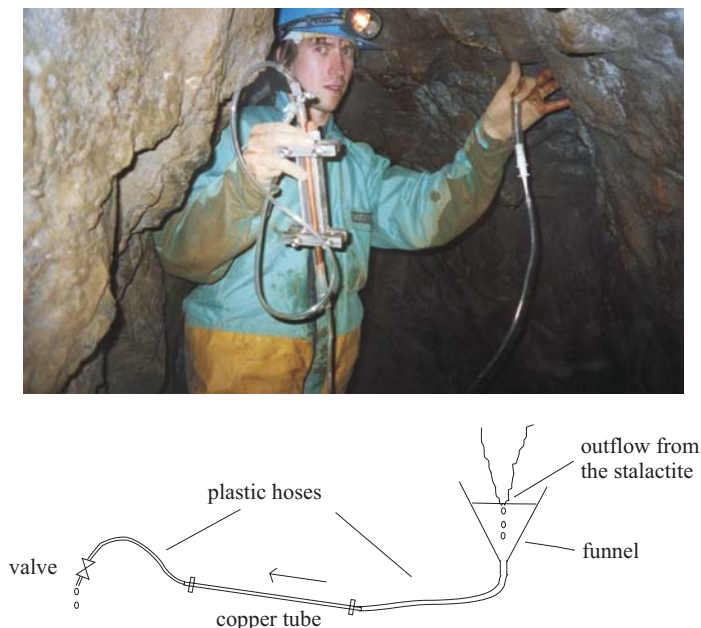


Figure 4.5: Dripwater sampling in the cave. In the picture it is shown how sampling under field conditions looks like. In the scheme below the typical setup, consisting of a copper tube, plastic hoses and a funnel, is illustrated.

In addition to the ^3H - ^3He approach, the stable oxygen isotopes as well as the tritium may be used for dating purposes. From the stable isotope data and possibly also from tritium values an age estimation for very young waters can be derived by comparing the seasonally influenced precipitation data. Tritium shows a pronounced seasonal signal with low values in winter and significantly higher values in summer (Fig.4.6) and varies in the Bunker Cave region between 4 TU in winter and 14 TU in summer (Fig.4.7), whereas the $\delta^{18}\text{O}$ values are oscillating between -6 and -12‰ VSMOW in this region. Thus, the precipitation is imprinted by a clear seasonal signal, which can be used for an age estimation.

Dripwater sampling technique

Similar to groundwater noble gas measurements, we have taken copper tube samples from drip sites in three adjacent caves. As the available water amount is significantly smaller than for groundwater wells, we reduced the sample amount to about 6 ml and used a modified sampling technique (Fig. 4.5). Hoses can not be attached to the soda straws or other dripping sites, because they mostly stop dripping after attaching them. Thus, we are forced to hold the hoses and a small funnel closely below the dripping point. The water is collected until the level in the funnel is above the dripping point to prevent or at least to reduce instantaneous degassing. Subsequently, the water flows slowly through the attached plastic hoses, which are smaller (inner diameter 4.8 mm) than in the case of groundwater sampling to reduce the necessary water amount. The copper tubes are closed by clamps after flushing several times combined with knocking for removal of attached air-bubbles. Only stalactites, which are dripping from inside, have been used. If the water flows on the outside of the speleothem the degassing can not be prevented and therefore too small gas ages have to be expected.

Site description

In the vicinity of Bochum in North-Western Germany, two shallow and one deeper cave have been investigated. The two shallow caves, Bunker Cave and Dechen Cave, bear about 10 to 20 m soil or rock cover. The sampling points in the adjacent deeper cave, B7 Cave, are covered by about 50 m of rock and soil. The three caves are located 180 m asl. Today, Bunker Cave shows a mean temperature of about 10.5 °C, which is comparable to the values in the two other caves. The caves are described in more detail by Niggemann (2000) and Hammerschmidt et al. (1995). Most investigated drip sites are seasonal drips with a medium discharge (≤ 15 ml/min). The drip site B7 BBH is a rather constant drip site with a relatively high discharge (≥ 50 ml/min) and thus belongs to the seepage flow regime. Samples have been taken from the three caves in three different sample campaigns, from Dechen cave at 23.1.2007 and 24.4.2007, from Bunker cave at 23.1.2007 and 24.4.2007 and from B7-Cave at 25.4.2007 and 2.2.2008. Sampling places are marked in the maps with white stars (Fig. 4.4).

Results of the first sampling in January 2007

In January 2007 we made the first attempt to sample dripwater. As we have not been confronted before with the sampling conditions in a cave and were not used to the sampling of dripping stalactites, the sampling was rather difficult and challenging. During sampling a certain contact with the atmosphere could not be prevented. Altogether the sampling time for one copper tube was about 10 - 15 min corresponding to the drip rate. Therefore some outgassing could have occurred, which may have influenced the age calculation and led to wrong ages because of the gas loss. Additionally, small air bubbles could have been included due to the sampling. Two samples from the campaign in January show a rather high excess-air value (see Table 4.3). In this case it is likely that this is caused by inclusion of small bubbles.

The fitting results show acceptable χ^2 -values together with very low temperature uncertainties. The calculated temperatures are in the range of the mean cave values. The cave temperature is about 11 °C in Dechen Cave and 10.5 °C in Bunker Cave. The fitting results indicates that the water has equilibrated in the soil at the mean annual soil temperature. The calculated temperature from Bunker Cave is a little bit elevated, perhaps due to re-equilibration during the longer lasting sampling.

The tritium results are quite low, but fitting well to the tritium values in the winter precipitation (compare Fig. 4.6 and Fig. 4.7). As the samples have been taken in January, they could therefore reflect winter precipitation of the current year, but the ^3He excess requires a longer travel time through the soil. At the time of the first sample run the mass spectrometric measurement of ^3He was not perfect, so it can not be excluded that measurement problems have caused deviations in the signals and therefore influenced the resulting ages. Furthermore, the uncertainty of the ^3He measurement was high, so that the age error had risen similarly to significant values. Therefore, it was not possible to derive a definitive conclusion from the measured data which motivated a second sampling.

Results of the second sampling in April - 24.4 - 25.4.07

To check the results of the first campaign in January, the same drip sites have been sampled for noble gases and tritium. In Bunker cave the drip site was dry, so we were forced to use another place. Additionally, three samples have been taken in the much deeper and larger cave B7. Furthermore water was filled into 40 ml glass bottles for radon analysis in the case of sufficiently fast dripping stalactites.

Table 4.3: Data for dripwater samples. Age, T, χ^2 and ΔNe are obtained by fitting T and excess-air to the noble gas concentrations using the CE-model (Aeschbach-Hertig et al., 1999, 2000). Rn and tritium values are determined from additional samples. If no age is given, a ^3He deficit was existent. The noble gas results have been corrected by an extraction dependent offset. The abbreviations are BH Bunker Cave, DH Dechen Cave and B7 for B7 Cave. TS, BBH or names indicate the dripping site. Duplicate samples are numbered by I or II. B7 Teich is a reference sample of a cave pond.

sample	Rn (Bq/l)	results of fitting with noble 90				
		TU	Age (years)	ΔNe (%)	T ($^{\circ}\text{C}$)	χ^2
BH TS4 (23.1)	-	6.3 ± 1.1	13 ± 14	220	12.3 ± 0.4	0.2
BH TS1-I (24.4)	3.3 ± 0.9	8.4 ± 0.9	0.9 ± 2.0	0	9.3 ± 0.3	15.1
BH TS1-II (24.4)	3.3 ± 1.6	8.4 ± 0.9	2.5 ± 1.8	0	9.4 ± 0.3	4.5
BH TS7 (24.4)	-	7.4 ± 1.0	5.8 ± 1.9	0	12.4 ± 0.2	8.1
DH Grufthalle(23.1)	-	7.4 ± 1.0	-	0	10.8 ± 0.3	3.6
DH Grufthalle(24.4)	5.9 ± 1.5	8.6 ± 1.0	4.8 ± 1.7	0	10.0 ± 0.3	11.2
DH Kristallg.(23.1)	-	5.0 ± 1.0	0.9 ± 5.2	71	10.2 ± 0.3	1.1
DH Kristallg.(24.4)	7.6 ± 1.7	6.7 ± 0.9	-	0	10.1 ± 0.3	9.4
B7 BBH-I (25.4)	17.5 ± 2.2	6.0 ± 0.9	2.7 ± 2.6	9.0	10.0 ± 0.3	2.4
B7 BBH-II (25.4)	17.5 ± 2.2	6.0 ± 0.9	2.3 ± 2.7	9.1	10.3 ± 0.3	3.8
B7 BBH-I (2.2.08)	-	7.2 ± 1.0	-	8.6	9.7 ± 0.1	0.2
B7 BBH-II (2.2.08)	-	7.2 ± 1.0	2.5 ± 5.9	10.2	9.7 ± 0.1	0.3
B7 Kerzenhalle(25.4)	-	-	0.1 ± 2.6	0	14.6 ± 0.3	58
B7 Teich (2.2.08)	-	8.4 ± 1.0	1.9 ± 3.9	0	9.6 ± 0.1	17.3

The noble gas data were analysed with noble 90 and are also displayed in Table 4.3. The χ^2 looks slightly worse, but this is mainly an effect of the relatively small analytical errors. The maximum deviation from the models is in case of the B7 samples BBH-I and BBH-II smaller than 1.4 %. The rest of the samples show deviations from the models of 3 % at maximum. Only the sample B7-Kerzenhalle is really a badly fitted sample, Ne is 6% lower than the model and Xe 4 % higher. Therefore this result can hardly be used further. The elevated temperature indicates that this sample has re-equilibrated during sampling, which has taken about 15 min or even longer and additionally, there have been few drips per minute. As there is a degassing pattern visible (He most depleted and Xe most enriched compared to the models, other noble gases accordingly between), gas loss during the time of sampling might have occurred.

A second slowly dripping site - BH-TS7 has a slightly elevated temperature. In this case, sampling took also 15 minutes, so a loss of noble gases can not be excluded. However, there is no pronounced degassing pattern visible, the ^3He values are quite high. As the ^3He determination via mass spectrometer was not completely stable, the resulting age has to be handled with care.

The two duplicate samples TS1-I and TS1-II from Bunker cave are reproducing quite well. Their mean temperature is 9.35°C , which is close to the mean annual air temperature in the cave area. They did not show any excess air. Therefore, it can be assumed that the water did equilibrate within the soil in the unsaturated zone. The calculated age is charged with a high uncertainty. It is not possible to derive an age with the $^3\text{H} - ^3\text{He}$ method in this case. However, a glance on the monthly collected tritium data from rain and dripwater (Fig. 4.7) shows that the ^3H values may follow the typical annual cycle with some delay indicating a residence time of about 6 months. Unfortunately, the measurement precision for the ^3H of the dripwater is not high enough and therefore interpretation is difficult. Higher resolution is required to better constrain the tritium results. Assuming the ^3H value from February to be actually the tritium peak in the dripwater, the trend is similar to the stable isotopes (Fig. 4.8).

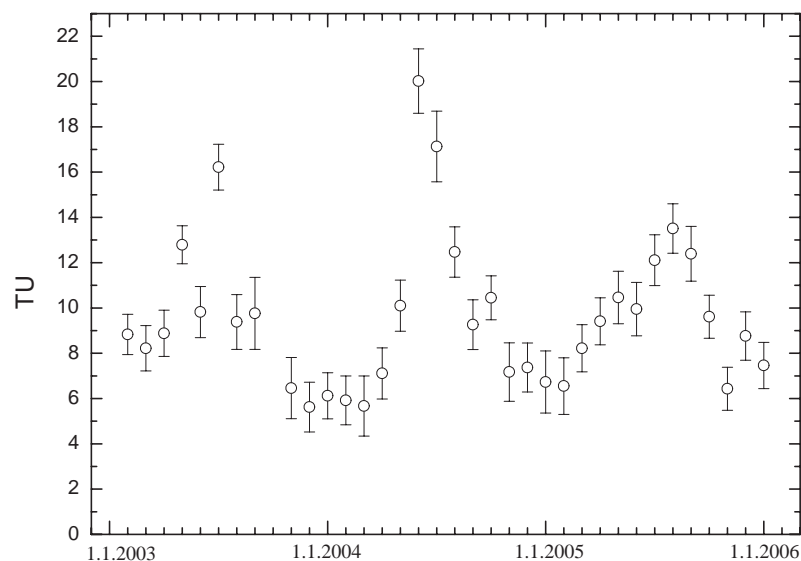


Figure 4.6: Tritium measurement of monthly collected rain water from Hof (Bavaria) from 1.1.2003 to 1.1.2006, showing a typical annual cycle. High values are found in the summer rain and low activities in winter precipitation. Samples have been provided by the German Weather Service and were measured in the Heidelberg tritium laboratory.

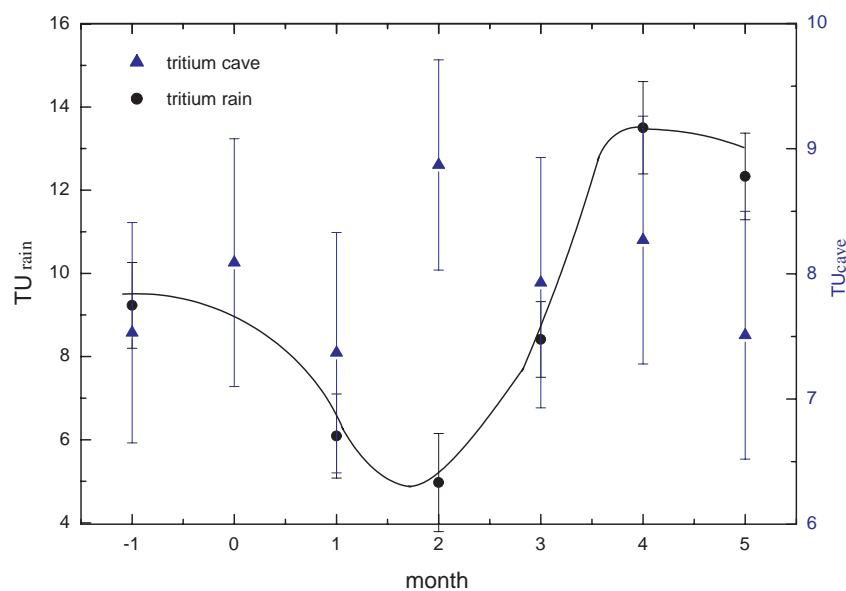


Figure 4.7: Seasonal tritium cycle at the Bunker Cave site. Samples were taken of rain and dripwater on a monthly basis and were measured in the Heidelberg tritium laboratory. Month 1 refers to January 2008.

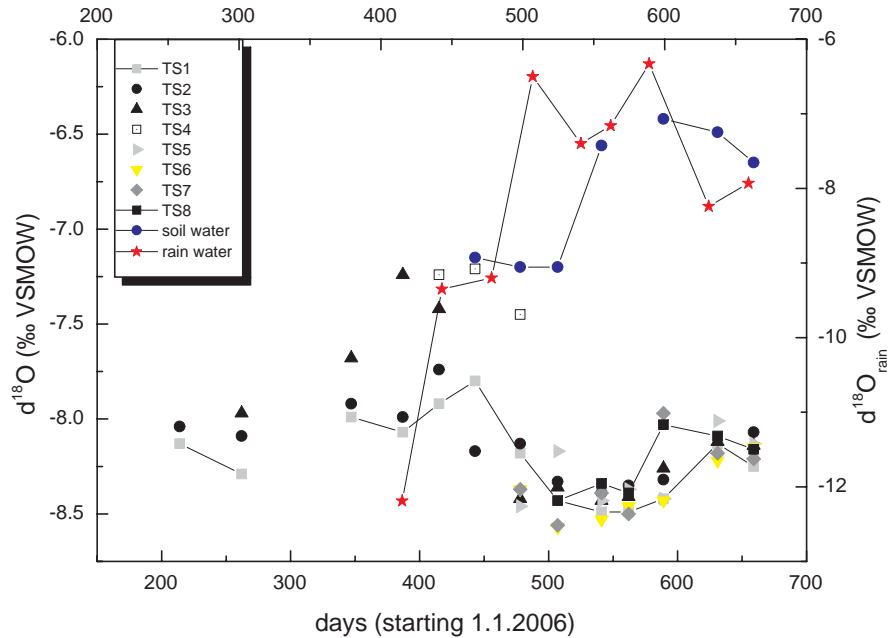


Figure 4.8: Stable isotope data from rain and dripwater at/in Bunker cave. TS1 to TS8 refers to dripping places inside the cave. Soil water and dripwater is plotted in the same diagramm (scale on the left side). The rainwater (taken from the cave vicinity) refers to the numbers on the right. Take notice of the different scales. The stable isotope data has been provided by C. Spötl from the University of Innsbruck.

The results from Dechen Cave are more complex. The sample Kristallg. from 23.1.2007 has a high excess air value, which indicates problems during sampling by inclusion of bubbles. The calculated age seems to be a little bit high. All other samples from Dechen Cave have no excess air and similar fitted temperatures with a mean of 10.3°C , which is about 0.5°C higher than the mean annual air temperature. The temperature may be elevated because Dechen Cave is a public cave, which is illuminated by lots of spotlights. Temperature measurements of the cave air showed a mean value of 10.6°C (Pflitsch et al., 2000). Again the determination of the age is difficult with the ^3H - ^3He method, because of the high uncertainties in the ^3He -measurements and the young ages. The radon samples show activity concentrations which are some orders of magnitude higher than it would be expected in the case of equilibrium. 7.6 kBq/m^3 in water at 11°C would require an activity concentration of 22.5 kBq/m^3 in air. Test measurements in the less ventilated Bunker Cave (Fig. 4.2) showed a maximum activity concentration in the air of 1.8 kBq/m^3 , which corresponds to about 0.6 kBq/m^3 in equilibrated water at 10°C . Thus the water stays at least some weeks in the unsaturated zone with suppressed gas exchange. Due to similar soil cover and geological settings as in the case of the Bunker Cave and similar ^3H - ^3He results, the residence time can be estimated to at least 6 months.

B7 Cave is a large cave with a considerable soil cover above the sampling points (50 to 60 m). Three samples have been taken, duplicate samples from a fast dripping stalactite and one from a very slowly dripping soda straw. As mentioned before, the fitting was bad for this sample, which can likely be due to a degassing. The duplicate samples BBH-I and BBH-II reproduce very well with similar temperatures, excess-air values and even ages. As the sampling had taken place under ideal conditions the excess air was not caused by bubbles, but is rather due to the water itself and therefore reflects typical excess air. As all parameters are reliable, a mean residence time derived by the ^3H - ^3He method for this dripwater is about 2.5 years. However, the uncertainty of a single measurement is rather high (2.6 and 2.7 yr).

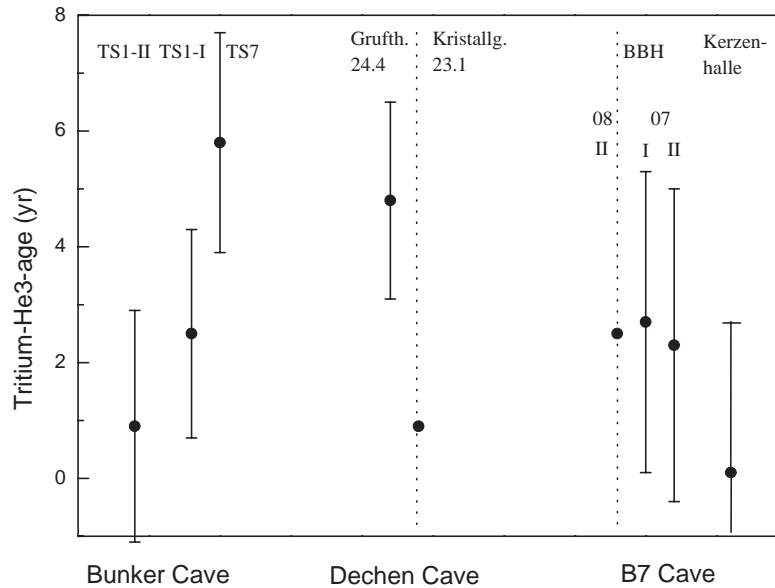


Figure 4.9: Summarized result of the ^3H - ^3He -measurements. Two samples of Dechen Cave and one sample from B7 Cave yield a small deficit in ^3He , one sample from Bunker Cave a high uncertainty and are therefore not displayed.

Results of the third sampling in February 2008

Again we took samples from the deeper B7 chambers for validation of the already obtained results, three from the fast dripping stalactite in chamber BBH and some samples from a pond (Teich) for comparison. One sample from the cave pond and two samples from the drip site were measured. The χ^2 is very well for the two dripwater samples and somewhat worse for the cave pond water, but this being mainly an effect of the relatively small analytical errors. The maximum deviation of Ne, Ar, Kr and Xe from the model is in this case smaller than 1.7 %. The two dripwater samples show similar excess-air values of 8.6 % and 10.2 % compared to the previous measurements from April 2007. As expected, the cave pond water possesses no excess-air component and should therefore be water equilibrated with the cave air. The fitted NGTs of all three measured samples are very similar at about 9.7 °C. For BBH-I (2.2.2008) no age could be calculated as the sample yielded a small deficit in ^3He . The second sample from this site resulted in an age of about 2.5 yrs, which corresponds well to the data obtained in April 2007. The apparent age of the single measurement from the cave pond should be interpreted carefully as the measurement uncertainty of ^3He was quite high. The measurement of the remaining duplicate samples can decide the question of tritiogenic ^3He in the cave pond water in future using an improved ^3He measurement procedure.

Discussion

Only six of the 13 copper tube samples of dripwater show a measurable excess-air value. The high values of two samples (BH TS4, DH Kristallg.) taken in the first campaign indicate inclusions of some bubbles. The rest, except multiple samples from a deep B7 cave part (B7 BBH), show no excess-air. This may be explained by the hydrological situation as there is no typical aquifer with a saturated zone. At some points a perched layer with quasi-saturated conditions may be present, which can be an explanation for the excess-air values from the B7 samples (BBH samples from 25.4.2007 and 2.2.2008).

Radon measurements in the Bunker Cave showed an air activity concentration of about 1 800 Bq/m³ corresponding to an equilibrium value in water of 630 Bq/m³ at 10 °C. Spot tests of the dripping water revealed significantly higher activity concentrations. This implies that the copper tube samples do not represent re-equilibrated water at least (correct sampling provided), but furthermore preserve a large fraction of the original gas composition of the dripwater.

All noble gas samples from the second campaign (24.4.07 and 25.4.07) contain no radiogenic ⁴He, but rather show a very small deficit. However, most have a tritiogenic ³He component (except DH Kristallg., DH Grufthalle and B7 BBH-I from 2.2.2008). Therefore it was possible to calculate ³H-³He ages from the noble gas measurements and the corresponding tritium value. For B7 Kerzenhalle no tritium data was available, thus the same value as for B7 BBH-I was assumed.

The results for the Bunker Cave (BH) are scattering over a large scale. Two samples overlap with young water, whereas the other two indicate ages above 1 year up to 8 years. Two of the Dechen Cave samples could not be evaluated due to the ³He-deficit. One sample yields a high uncertainty and one an age between 3 and 7 years. The results from the B7-Cave are more uniform. The multiple samples from the dripsite BBH are reproducing well and are resulting in a mean age of 2.5 ± 0.2 years, which is reasonable if we take into account the 50 m thick overlying structure of rock and soil. The sample B7 Kerzenhalle agrees with these results within the uncertainty, even though the sample seems to be partially re-equilibrated at least. Unfortunately, the measurement uncertainty of ³He was relatively high during the first measurements. This could be reduced in the second campaign. However, the uncertainty has to be further reduced to achieve reliable and useful data. For constraining the results, the stable oxygen isotopes can be used for young waters. Precipitation values are varying strongly on a seasonal scale (s. Fig. 4.8). Isotope values of the dripwater can be compared to the seasonality of the rain water. Shifts between the two water types can be used for the estimation of the travel time. In the case of the Bunker Cave a shift of 50 days can be found between rain water and soil water and an additional shift of 50 to 100 days between soil water and dripwater. Altogether, the dripwater is shifted by about 100 to 150 days compared to rain water, which implies a travel time of about 4 to 5 months. This result is reasonable for the shallow Bunker Cave, but only more precise ³H-³He data can decide, if the water needs 4 to 5 months or rather 1 year and 4 months. Niggemann (2000) found only small influence of the seasonal rain isotopic signal on the dripwater in the B7 cave due to attenuation of the signal. Tritium can be used as an additional tracer for the water percolation time through the aquifer for shallow caves or short time scales. The tritium values in the rain water show a similar or even more pronounced seasonality than the stable oxygen isotopes (Fig. 4.6). A comparison of dripwater with rain water, as e.g. displayed in Fig. 4.7 can give an estimate for the timescales. Assuming the highest tritium value in the dripwater (in February) to be the seasonal peak, a similar shift between rain and dripwater than for the stable oxygen isotopes occurs. Due to the signal attenuation the resolution for the tritium has to be improved to <0.5 TU to achieve unambiguous results.

We tried to date the dripwater to gain important information with regard to the palaeoclimatic interpretation of speleothem tracer data. Using ³H-³He it was possible to derive gas ages for dripwater from sites in three different caves. These gas ages have to be a lower limit for the percolation time, as we can not expect conditions like in a normal aquifer. Degassing may occur in the mostly unsaturated parts of the aquifer. However, excess-air found in the dripwater of a deeper cave part indicates a perched aquifer, which may provide similar conditions as in normal groundwater sampling. Radon samples from some drip sites showed a large excess in comparison with the cave air activity and proved, that the investigated

parts are not in equilibrium with the cave atmosphere and, therefore, can be used for gas-age estimation. As a further complication, a diffusive exchange of certain tracers with the rock matrix is possible (Cook et al., 2005). E.g. He may be released from the quasi-immobile water in the matrix and therefore can provoke an apparent higher concentration. Inversely, a retention of, for instance, the stable isotopes or tritium can occur and influence the age estimation. Therefore, a multitracer approach seems to be most suited for age determination as diverse tracers are affected in a different extent by the interaction with the porous rock parts. With regard to the dripwater dating, the seasonal signals of oxygen stable isotopes and tritium can also be useful for constraining the noble gas results. They are less affected by degassing, but are rapidly smoothed. In the shallow Bunker Cave the seasonal signal was found to be present in the dripwater with a shift of 100 to 150 days compared to the rain. In the deeper B7 cave it was not possible to relate the signals of drip and rain water.

Combining all results of ^3H - ^3He , stable isotopes and tritium, a residence of 4 - 6 months for Bunker Cave and Dechen Cave, and about 2.5 years for the deeper B7 cave seems to be most likely.

In summary, dating of water from karstified aquifers seems to be feasible by the use of ^3H - ^3He , as e.g. shown by Yamada et al. (2008). However, the application has to be limited due to some constraints:

- highly fractured and karstified sites enable the equilibration of the percolating water with ambient air in fractures. Thus, a too low age has to be expected. In this case stable isotopes or tritium may be better suited. A perched aquifer as found most likely above the drip site BBH in the B7 Cave provides conditions for determination of reliable ages. Shallow caves are thus commonly not well suited for the method, whereas deeper caves may exhibit perched aquifers. However, only spot checks focused on the excess-air and the tritiogenic ^3He can decide about the applicability.
- degassing during sampling should be minimized. This implies the improvement of sampling with regard to the gas exchange. The sampling should not take longer than five minutes, otherwise the degassing will make the results senseless with regard to age determination. Thus, the drip rate should be high enough. Furthermore, it should be aimed to apply the method also to slower dripping sites, which are also of importance for the palaeoclimatic investigations.
- the sample size has to be adequate so that the ^3He can be measured with sufficient precision in the range of months to few years. If the uncertainty of the ^3He measurement is too high, the error of the age calculation will make the results irrelevant. 6 ml water samples seem to be a good trade-off between sampling time and sampling size.
- the water flow should not be too high, rather reduced by a thick soil cover above the cave. Residence times in the order of some weeks or months could hardly be detected by ^3H - ^3He . However, tritium data and a comparison with the annual tritium cycle can help to estimate an age even for residence times of weeks.

4.2 Extraction

4.2.1 Sample selection

One measurement of a speleothem sample takes at least one day or more for preparation, pumping and cleaning. It consists of 4 hours blank measurement, up to three times 4 hour-lasting sample measurements due to the stepwise procedures and a certain time for data evaluation. If the sample is not adequate for our purpose, namely calculation of noble gas temperatures, all time spent and the effort were useless. Therefore, it is very helpful to select in advance the best and most promising samples.

A porous stalagmite (as e.g. MA2 with mean A of 10.6) with a large amount of holes can be excluded in advance from the measurement. Due to the large air inclusions the noble gases from this parts will make it impossible to derive the noble gas fraction from the water-filled inclusions with the needed precision. In contrast, compact and whitish speleothems with no visible holes and fractures show a very low air fraction. E.g. the whitish stalagmite CG from Cuba with large columnar crystals has a mean A of 0.9, and the the milky-whitish stalagmite BU-U from Bunker Cave even 0.16. Thus, in a first step, samples can be chosen due to their obvious structure and colour. Porous ones should be excluded and the whitish, compact speleothems prepared for the next step.

Using thin sections it is possible to check the distribution of water and air-filled inclusions. Furthermore the homogeneity of the material and the dimension of the different inclusions can be observed. At first, surface effects due to the preparation process should be distinguished from real structure. Using transmitted and reflected light, this differentiation is possible and the main focus can be on the different inclusion types. Water-filled inclusions can be identified by light reflection or bubbles inside. In general they are roundish and relatively small, but more irregular shapes can not be excluded. Air-filled inclusions are in general larger, more diffuse and irregular in their shape. Mostly, they appear between calcite grains, whereas water-filled inclusions are often inside the crystals (Scheidegger et al., 2007a).

Again, very large air-filled inclusions are a good argument to exclude the according sample from further processing. However, if very few and additionally small water-filled inclusions are present, it is also a challenge to achieve good results. The CG stalagmite shows a low fraction of air-derived noble gases, but as it also yields few and only μm -sized water-filled inclusions, the released water amount is in general too small to determine meaningful temperatures. Similarly, we found a low A -value in the case of a translucent sinter piece with very large columnar crystals. The water content was larger (about 0.2 %wt), but not comparably large as in the case of the milky whitish stalagmites BU-U and BU-1 from the Bunker cave.

The most promising samples with a small fraction of air-filled inclusions and a large water amount seem to be speleothems with a whitish colour and columnar crystals.

4.2.2 Water determination and water content

A reproducible and precise water measurement in the μl -range could be established using the water vapour pressure. The comparison with a calibration curve, prepared by using known water quantities, enables determination of the water amount from the resulting pressure.

The preparation of the calibration curve as well as the determination of the fluid inclusions follow the same procedure. After the crushing, respectively the release of a known water amount from calibrated capillaries, the line is heated to about 100 °C, whereas the crusher itself is heated to about 70 °C. The released water is frozen into a dry-ice cooled cold-finger for 20 minutes. Subsequently, it is closed off from the system and warmed to room-temperature, which is stabilized by an air-conditioning system to $(23 \pm 0.5)^\circ\text{C}$. After at least waiting 40 minutes, the water vapour is admitted to different volumes (s. Fig. 3.12) for pressure

Table 4.4: Uncertainty of the water determination in the case of different quantities. error (cal-...) refers to the uncertainty, which is due to the fitting error of the calibration in the according volume. * refers not to the line, but to the first expansion volume.+ corresponds to the first expansion volume, "Error averaging" gives an impression of the typical deviations of the determined water amounts in the different volumes.

water amount (μl)	used volume	error (cal-vol 2)	error (cal-line)	error (averaging)
3 μl	Exp.vol 2	1.1 %	-	-
2 μl	Exp.vol 2	1.2 %	-	-
1 μl	Exp.vol 1/2	1.6 %	2.3%*	1.0 %
0.5 μl	Exp.vol 1/2	2.5 %	3.0%*	1.2 %
0.1 μl	Exp.vol 1/2/Line	10%	5 %	3.4 %
0.03 μl	Exp.vol 1/Line	32% ⁺	16 %	20 %

determination with a compact capacitance pressure gauge (CMR 263, Pfeiffer). In each volume it remains for five minutes until the pressure is recorded.

The overall error for different water amounts is displayed in Table 4.4. If we use all the available expansion volumes and average the results, even water amounts down to 0.1 μl can be determined with an error of $\approx 3\%$. The water amount calculated from the pressure in the different volumes is scattering much less than would be expected from the fitting uncertainties. We use an average value and the corresponding uncertainty which takes into account the typical scattering. This scattering is about 1 % for water amounts larger than 0.5 μl . However, the uncertainty increases rapidly for smaller samples. Similarly, the scatter between different volumes rises drastically and reaches 20 % at 0.03 μl . Thus, the lower limit of water determination with total uncertainties below 10 % is at about 0.05 μl .

An interesting property of the speleothems is their water content, which is discussed more detailed in chapter 4.2.4. As the samples are always weighed before the extraction, the water content in % of the total speleothem weight can be calculated by dividing the released water amount by the calcite mass. A summary is given in Fig. 4.10.

A piece of the BU-1 stalagmite yields the highest value with a water content of 6.6 %₀wt. The lowest value was measured in the case of a CG-sample and was about 0.0012 %₀wt, which is 6 000 times less. Despite this very large difference most of the samples vary between 0.1 and 1 %₀wt. Furthermore, the water content seems to be characteristic for the various speleothems. The milky whitish BU-1 has a mean value of 2.88 %₀wt, the whitish, but more crystalline BU-U 0.44 %₀wt. The mean values of two soda straws and also from a sample of BU-2 are in a similar range. They are also crystalline with a whitish colour. H12 shows a highly layered structure consisting of an alternation of broad milky white with small brownish layers. The thin-section analysis revealed a high number of large water- (and also air-) filled inclusions, which is reflected in the high water content. MA2 and the flowstone as well as the samples from the Spannagel cave and the sinter from Bunker cave range between at 0.1 to 0.2 %₀wt. They show either a more translucent crystalline structure (sinter, Spa) or an alternation of relatively dark layers with few whitish parts (flowstone). The stalagmite with the lowest water content shows a milky colour. However, the cut samples look very crystalline and translucent. On thin-sections, a large number of inclusions could be found, however, only very small and μm -sized. This may be related to the growth conditions in the cave. The sample was taken from a chamber, which is at least 1.3 km distant from any entrance and with some 100 metres of rock cover above (J.M. Pajón, personal communication). Therefore, the growth was presumably less influenced by temperature and drip interval changes and also less affected by organics in the dripwater. This may cause the growth of ideal crystals and prevent the development of large inclusions.

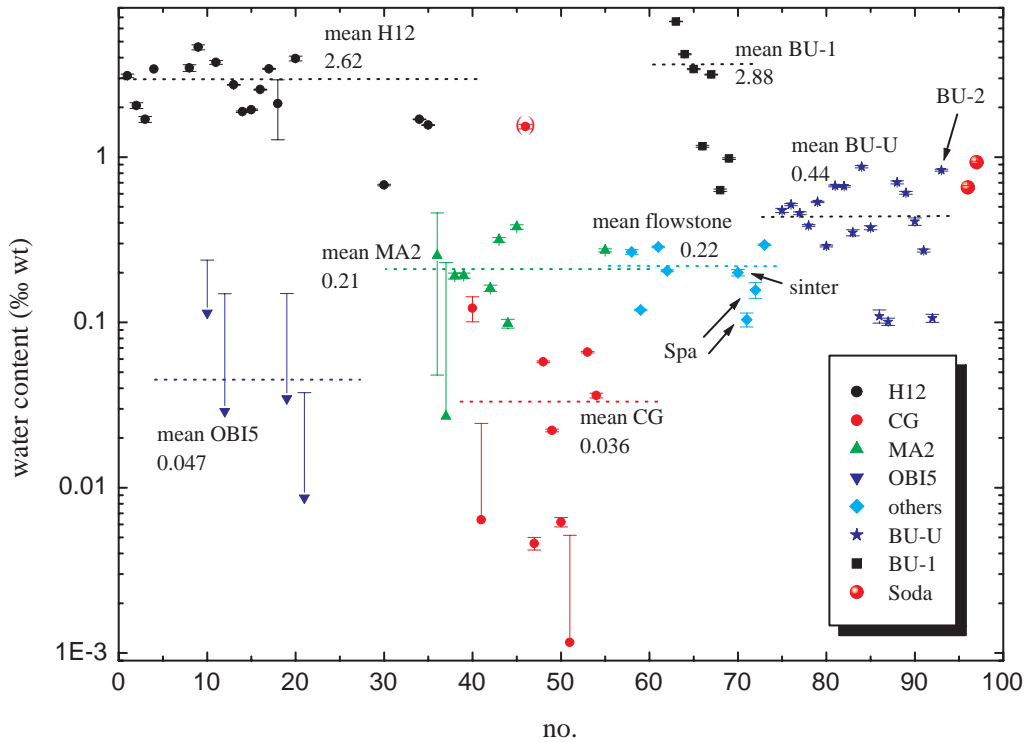


Figure 4.10: Water content in ‰ of the total speleothem weight. The water content has been calculated by summarizing the results of the crushing and heating steps.

4.2.3 Air/water volume ratio

For the determination of temperatures from noble gas concentrations in fluid inclusions it is necessary to subtract the air-derived part from the total noble gas signal as it does not contain any temperature information. The contribution of noble gases from the air-filled inclusions is one of the most decisive points. If their amount is too high, i.e. the air/water volume ratio is above 0.3 (Fig. 2.7), no meaningful results can be achieved. About 100 times more He and between 5 to 10 times more Xe is contained in air compared to the same volume of water. If we have an uncertainty of 1 % in the magnitude of the air-fraction the uncertainty gets much larger for the remaining water part due to the subtraction process.

If the noble gases are extracted by a simple crushing method the results are strongly dependent on the stalagmite type and structure. The investigated samples cover a wide range of some magnitudes (Fig. 4.11). In the worst case, the speleothems MA2 and MA1 from Chile, an A of 42 in maximum and a mean of 10.6 was reached. In this case the air inclusions are dominating. The H12-Oman samples have a mean of 1.8 and scatter between 0.4 and 7.8, which is clearly lower than for the Chilean stalagmite. Already half of the mean of the H12 stalagmites is achieved with samples from Cuba. There a mean value of 0.9 with a scatter between 0.05 and 4.1 was measured. For the BU-U stalagmite from the Bunker cave even lower values have been achieved. The mean is 0.16 with a scatter between 0.026 and 0.44 in maximum. The lowest values have been measured for a soda straw from the same cave. It reveals an air/water-volume ratio of 0.002, which is comparable to a typical groundwater sample. This provides ideal conditions for the NGT calculation. Therefore, at least some samples from the stalagmite CG and of the speleothems from Bunker cave are in a suitable range and theoretically enable meaningful NGT calculation using a simple extraction procedure instead of a stepwise method.

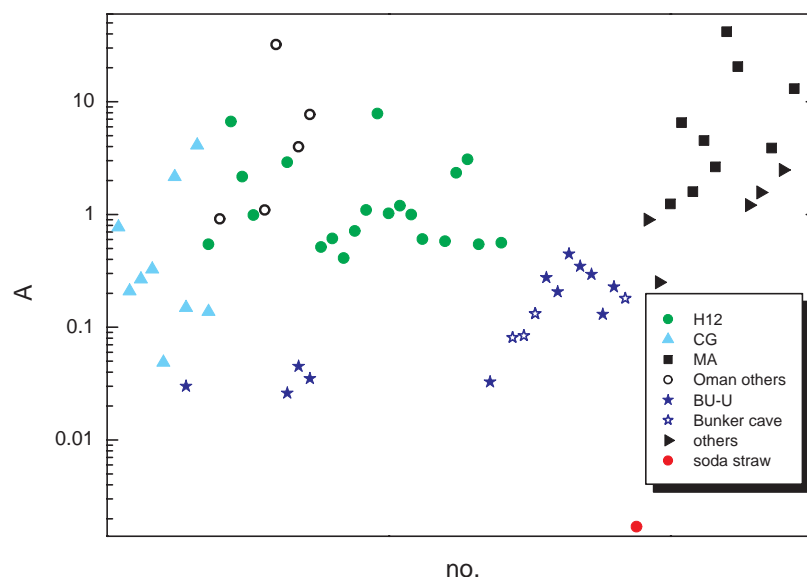


Figure 4.11: Air/water volume ratio for different stalagmite samples on a logarithmic scale. The results show a large scatter, even for different pieces from the same stalagmite. Nevertheless, clustering of results from certain stalagmites is visible. Only the Cuban stalagmite CG and the speleothems from Bunker Cave (BU-U, BU-1, BU-2, soda straw) theoretically enable meaningful noble gas temperature calculation using a simple extraction procedure instead of a stepwise method.

4.2.4 Applications

One interesting application beyond noble gas measurements on fluid inclusions may be the quantification of the entrapped water and its spatial distribution along the growth axis. Brook et al. (1999) approved a relationship of inclusion concentrations with stalagmite growth and precipitation. They found inclusion-rich layers in the case of fast calcite precipitation and inclusion-poor calcite in the case of slow growth. Genty and Quinif (1996) interpreted couplets of dark and light laminae as annual cycles caused by differences in the water excess. They suggested the compact type of columnar crystals to be an indicator for higher drip rate. Frisia et al. (2000) investigated fabrics in speleothems in Alpine and Irish caves and found relations to the growth conditions. Columnar fabrics grow during wet phases, which implicates the speleothems to be continuously wet. Furthermore they grow in the case of low supersaturation, from fluids at near-equilibrium conditions, which also can be related to wetter conditions. Dendritic fabrics are related to high supersaturation and periodic dry conditions. Fairchild et al. (2007) also stated the occurrence of couplets to be related to changes in the dripwater composition and flow rate. The milky white part of these couplets is supposed to contain a large number of water-filled inclusions. In the following, we will discuss the relation of speleothem parts with a high water content with precipitation and growth conditions based on our own data.

In the case of the BU-1 stalagmite a highly variable water content was found. The values fluctuate between 0.6 and 6.6 %wt. An investigation of the calcite structures shows in the most measured parts columnar crystals, only at two places dendritic fabrics. The sample pieces yield a highly different amount of inclusions, less in the dendritic part and a rather large number in the sections with columnar crystals. This has to be related to the growth conditions, such as temperature, precipitation, CO₂-level in soil and cave, drip rate and water film on the speleothem. In the case of BU-1 temperature changes can be ruled out for explanation, as the mean annual air temperature has not changed significantly in this region

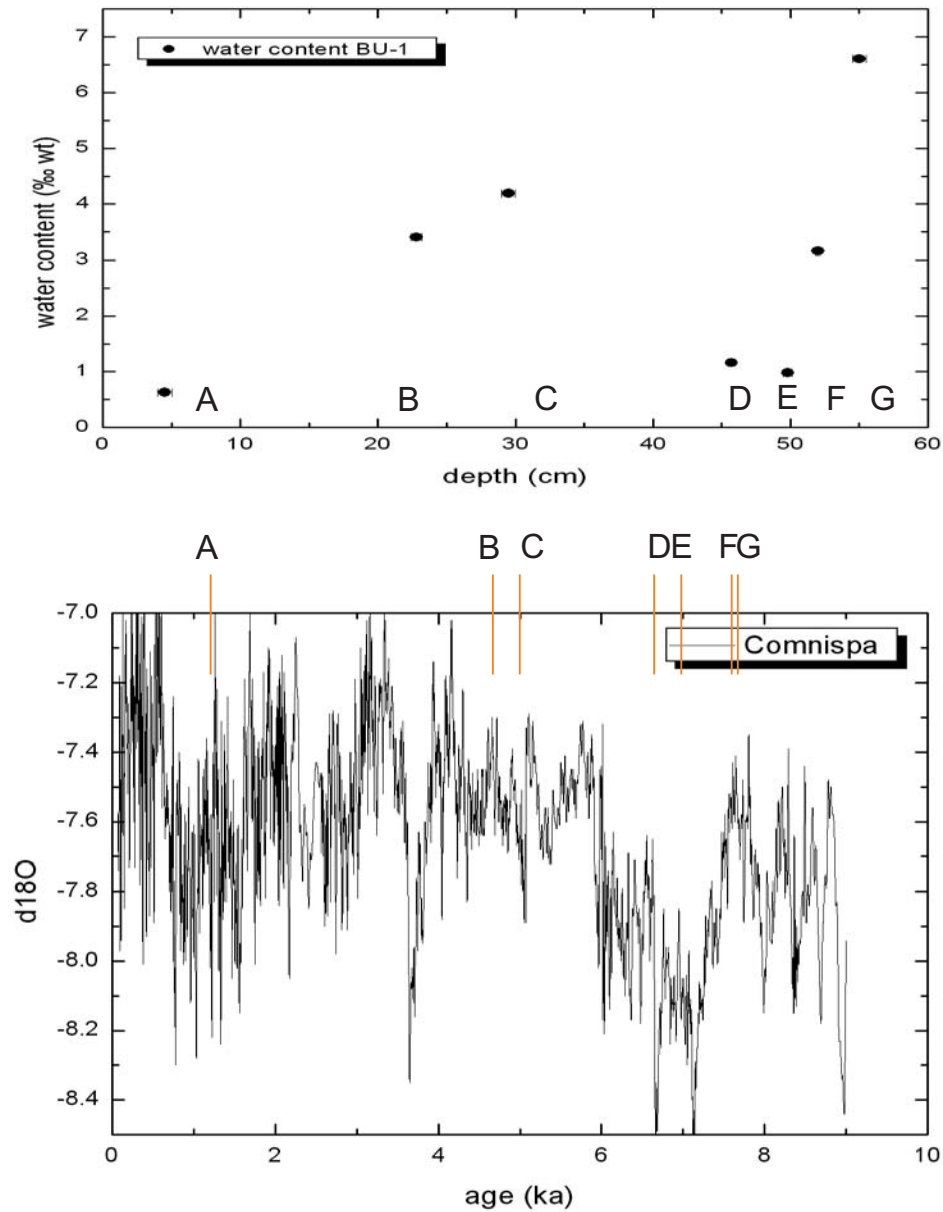


Figure 4.12: Water content of BU-1 in ‰ of the total speleothem weight, measured along the growth axis (upper panel). The water content has been calculated by summarizing the results of the crushing and heating steps. For comparison the $\delta^{18}\text{O}$ -values of the Comnispas-record (Vollweiler et al., 2006) are displayed in the lower panel. The BU-1 results (characters) are allocated to the the Comnispas record using the ages obtained by U/Th measurements along the BU-1 growth axis.

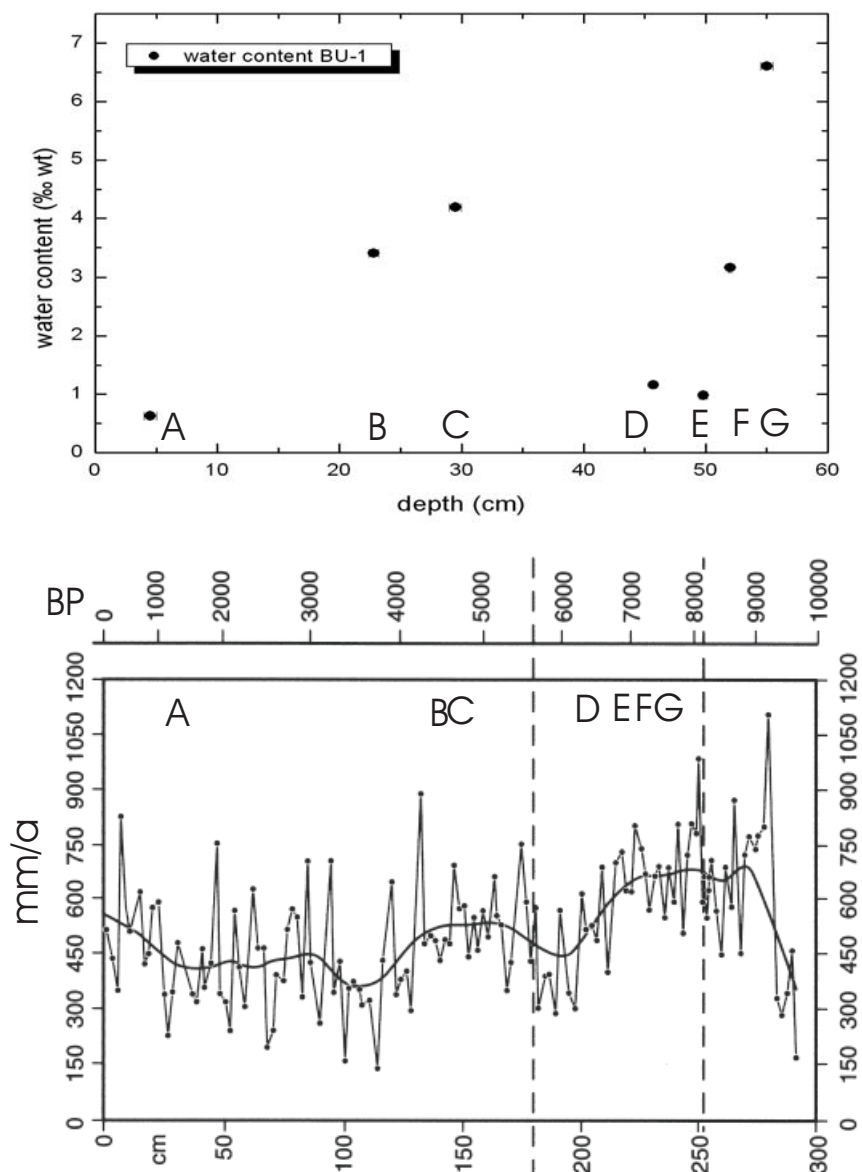


Figure 4.13: Water content of BU-1 in ‰ of the total speleothem weight, measured along the growth axis (upper panel). The water content has been calculated by summarizing the results of the crushing and heating steps. For comparison the reconstructed precipitation of a Scandinavian Pollen record (Seppä and Birks, 2001) is displayed in the lower panel. The BU-1 results (characters) are allocated to the pollen record using the ages obtained by U/Th measurements along the BU-1 growth axis.

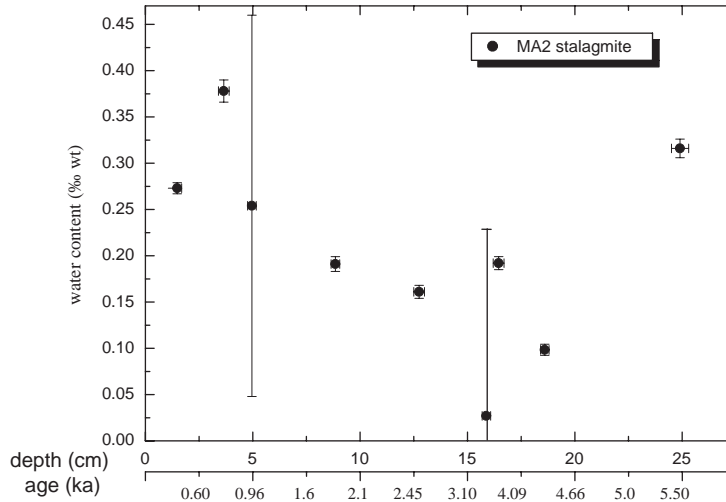


Figure 4.14: Water content in ‰ of the total speleothem weight, measured along the growth axis of the Chile stalagmite MA2. The water content has been calculated by summarizing the results of the crushing and heating steps. Note that the age scale is not linear.

over the last 8 kyr (Davis et al., 2003). Therefore, the water film on the growing stalagmite may have played the dominating role.

In Fig. 4.12 the water content is compared to the $\delta^{18}\text{O}$ -values of the Comnispá record. This record reflects changes in precipitation and temperature. Despite the high-frequency fluctuations it is obvious that the BU-1 water content is related to the $\delta^{18}\text{O}$ -values. Periods with more depleted $\delta^{18}\text{O}$ correspond to an extremely low water content, whereas high water content is observed in periods with less negative $\delta^{18}\text{O}$. Higher lake levels during phases with less negative $\delta^{18}\text{O}$ (Vollweiler et al., 2006) suggest this to be related to a larger amount of precipitation.

A comparison with reconstructed data from a pollen record, derived from lake sediments in northern Finland, shows a certain agreement. Although the amplitudes are different, the general trend is the same. Periods of high precipitation correspond to a high water content, lower precipitation to a reduced amount of water-filled inclusions. Consistently, the pollen record, Comnispá $\delta^{18}\text{O}$ as well as the water content in BU-1, show, that the periods around 5 kyr B.P. and 7.5 to 9 kyr B.P. are affected by a higher amount of precipitation. In contrast the period around 6 to 7 kyr B.P. is most likely a period of reduced humidity in large parts of Europe. In summary, the agreement of the BU-1 water content with precipitation-related proxies indicates that the water content may be a useful tool for a qualitative estimation of palaeo-humidity and precipitation.

As an interesting application we investigated the water content of MA2. Along the growth axis 9 samples have been taken and measured. With exception of two extremely small pieces (0.148 g and 0.146 g) the error in the water content is small enough to derive significant trends. The temperature during the growth period of the stalagmite is assumed to be rather stable. However, the precipitation may have changed considerably, as the cave is located at the southern margin of the Westerlies in Chile.

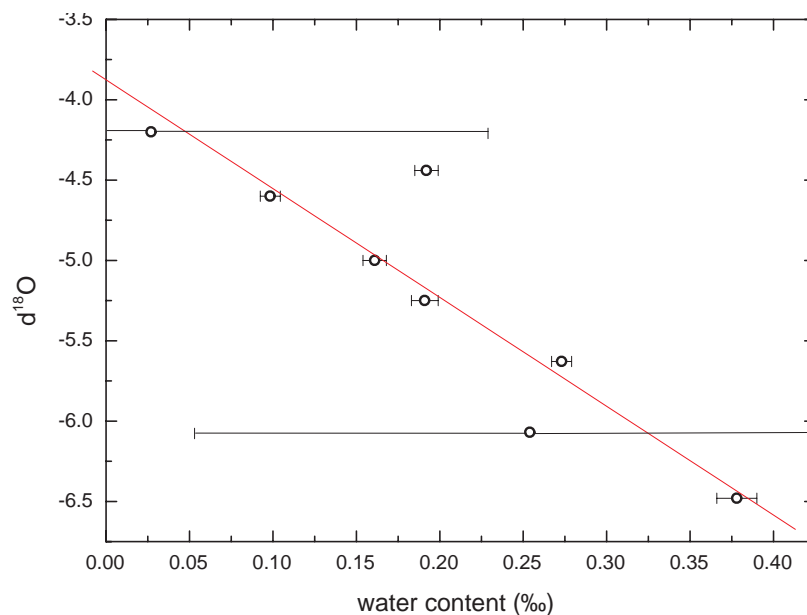
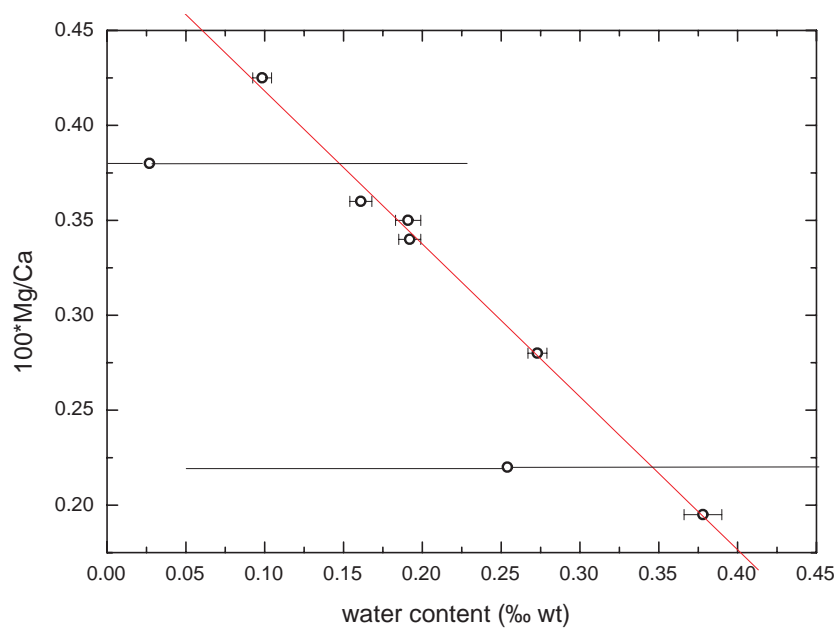


Figure 4.15: $\delta^{18}\text{O}$ values against water content of the same pieces from the stalagmite MA2. The red line represents a linear fit of the 8 data points with a correlation coefficient R of -0.91.

Figure 4.16: $100*\text{Mg}/\text{Ca}$ against water content of the same pieces from the stalagmite MA2. The red line represents a linear fit of the 6 most reliable data points with an R of -0.997, the two measurements with large uncertainties have been discarded for fitting, but agree with the fitted line taking into account the errors.



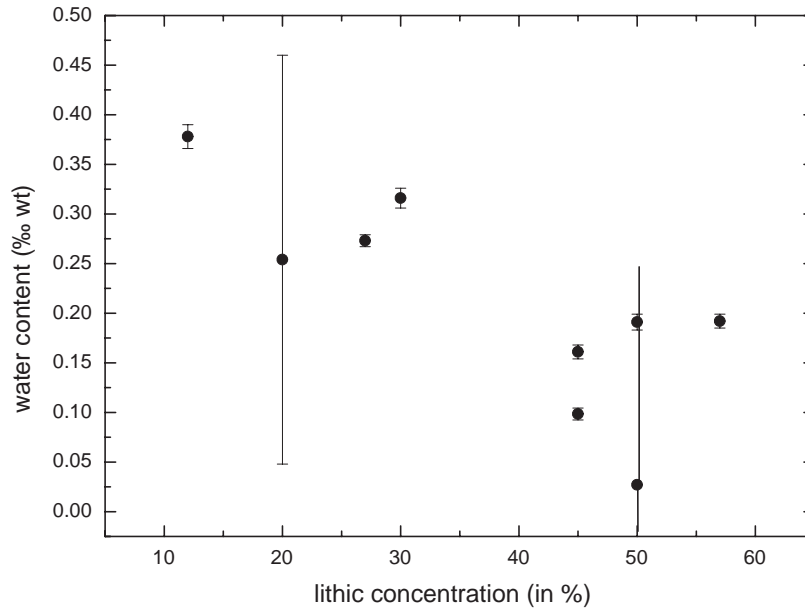


Figure 4.17: Comparison of the MA2 water content with an ENSO related marine sediment core. The sediment core data are taken from (Rein, 2007).

The water content suggests a general trend of increasing precipitation beginning from 5 000 or 4 500 yr BP towards present day values (Fig. 4.14). Unfortunately, no pollen data or sediment core from this region with sufficient information about the precipitation is available to constrain this hypothesis. However, we can compare the water content with the $\delta^{18}\text{O}$ value and the Mg/Ca ratio of the same stalagmite (Fig. 4.15 and Fig. 4.16). The location of the samples for water content measurements are somewhat uncertain (± 0.5 cm), especially in the deepest section (25 cm from top). However, this does not affect the general trends of $\delta^{18}\text{O}$ and Mg/Ca against the water content. Both are correlated inversely with the water content. An increasing water content corresponds to a more depleted $\delta^{18}\text{O}$ value and a decreasing Mg/Ca ratio. If we interpretate the more depleted values in the $\delta^{18}\text{O}$ as a result of the amount effect due to increased precipitation, the higher water content indicates a higher rainfall amount. A low Mg/Ca ratio corresponds to a higher recharge into the karstic aquifer, as the calcite precipitation in the unsaturated zone above the cave decreases during high recharge. A high Mg/Ca ratio is an indication for low recharge (Cruz et al., 2007). A high water content in the stalagmite is related to a low Mg/Ca ratio and vice versa. As in the case of the stable oxygen isotopes a high water content is related to an increased precipitation. This corresponds to our interpretation from the Bunker Cave stalagmites.

Interestingly, a certain inverse correlation with the precipitation at the northern margin of the southern Westerlies can be found. The precipitation record of Heusser et al. (1981), derived from pollen contained in lake sediments at 42° S and 73° W at least partially shows an anti-correlation to the suggested precipitation pattern from southern Chile. Both precipitation records can be reconciled by a south- respectively northward shift of the Westerlies. A northward shift would reduce the precipitation in South Chile and increase the rain fall in the northern part and vice versa.

If we compare the water content with a laminated marine sediment core from Peru (Rein, 2007), which is a proxy for ENSO triggered flood events, a certain correlation can be found (Fig. 4.17). The water content of the MA2 stalagmite is related to the concentration of lithic grains in the marine sediment using the age model established by U/Th dating. High concentrations of lithic grains are an indicator for strong El Niño events, leading to heavy

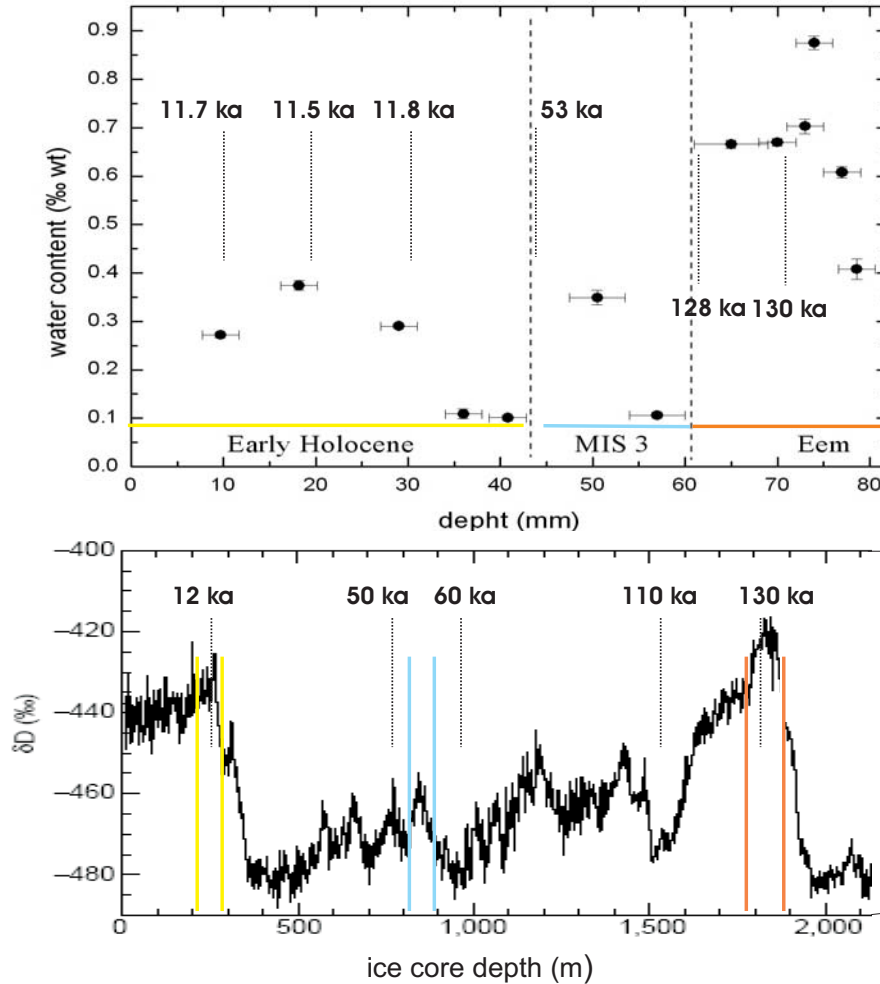


Figure 4.18: Water content in ‰ of the total speleothem weight, measured along the growth axis of BU-U (upper panel). The water content has been calculated by summarizing the results of the crushing and heating steps. U-Th-dated pieces are indicated by the according age, the uncertainty is about 3 to 4 %. For comparison the δD values of the Vostok ice-core are displayed (Petit et al., 1999) in the lower panel. Corresponding parts are marked in colour.

precipitation and floods in Peru. If we assume high water content in the stalagmite to be related with high precipitation, then the periods with stronger El Niño events are connected to decreased precipitation in southern Chile. Vice versa, low El Niño activity is related to stronger precipitation in the southern Chile region. This may be induced by changed circulation patterns due to the ENSO phenomenon (Kilian et al., 2008). Furthermore, sediment cores from a Bolivian lake show a pronounced dry period between 6.2 and 2.3 kyr BP and than an increase in precipitation towards present day values (Abbott et al., 2000). This may indicate general drier periods during the mid Holocene as Baker et al. (2001) found also corresponding dry periods in tropical South America. Clement et al. (2000) claim largely arid coastal regions in the mid-Holocene to be caused by a relatively cool eastern equatorial Pacific. However, the relationships between the different forcings as well as the influences on the circulation patterns are highly controversial. Thus, it is not possible to constrain the interpretation of the water content of MA2 definitively. Based on the common interpretation of the Mg/Ca ratios, and the $\delta^{18}\text{O}$ signal in terms of the amount effect, the water content is closely related to precipitation. A likely interpretation of speleothem sections with increasing water content suggest increasing recharge and precipitation.

The stalagmite BU-U expands over some periods of the last 130 kyr in its top 75 mm. We measured 13 pieces along the growth axis. The calculated water content varies in the order of one magnitude from about 0.10 to 0.88 ‰wt. The first five data points belong to the early Holocene (10.5 to 12.0 kyr), which corresponds to the fastest growth period of the whole stalagmite (top 4 cm). The mean water content of the first three samples is about 0.31 ‰wt. The water content of the two subsequent pieces, which were extracted from a more translucent layer, is low and about 0.1 ‰wt. The next growth period of about 2 cm corresponds to a warmer interstadial (MIS 3, D/O-events 14-17, compare Dansgaard et al., 1993) at about 53 kyr BP. The interstadial at 53 kyr is reflected by a higher value in the water content and a denser calcite. This corresponds also to the fact, that other stalagmites (BU-2) show rapid growth during this phase, whereas no growth is found in other periods during the Glaciation. The next part with low water content is a rather translucent layer of about 8 mm. Unfortunately, no U-Th-dating is available for this period. Subsequent to the MIS3 period in BU-U a dark brownish layer with macroscopic detritus particles (clay minerals) is visible, which indicates a hiatus. This period may refer to MIS 4 and MIS 5a-d from 60 to 120 kyr BP. The following larger growth layer refers to MIS 5e and is milky white with one small brownish layer. The uppermost sample dated in this larger growth layer was found to be about 128 kyr old. Below the dark layer of MIS4 the water content rises rapidly to 0.67 ‰wt and peaks finally at 130 kyr BP with 0.88 ‰wt. The older samples then show a decline in the water content. The layer from MIS 5e is followed by an extremely dark brown layer (undated).

A comparison of the water content with the Vostok ice-core (Petit et al., 1999) shows an astonishing agreement of the general trend. The warm periods with less depletion in δD compares with the periods with a high water content in the stalagmite. In contrast, colder phases in the ice core with strong depletion in δD correspond to slowly growing parts with low water content. The most striking feature is the good replication of parts of the Eemian peak in the water content. In the case of BU-U the water content seems to be closely related to temperature. However, warmer periods may additionally be connected with a more humid climate and thus the primary factor influencing the water content is most likely the precipitation. In consideration of the BU-1 and especially the MA2 results, the water content seems to be related to precipitation. In the following, we discuss the empirically found correlation on a more theoretical approach.

4.2.5 Theory of fluid inclusion origin and frequency

In the precedent section some examples of water content curves along the growth axis have been shown. They reveal correlations with precipitation and possibly also with temperature. To use this interesting information in a less speculative way, it is necessary to know the origin of this feature.

Lamination with an alternation between inclusion-poor and inclusion-rich layers are a common feature (Mattey et al., 2008; Frisia et al., 2003; Brook et al., 1999). However, theories about the origin are scarce (Frisia et al., 2003; Genty and Quinif, 1996; Kendall and Broughton, 1978). Kendall and Broughton (1978) suggest changes in the environmental conditions, especially in the drip rate, to be responsible for the layering. Similarly, Fairchild et al. (2007) and Genty and Quinif (1996) interpreted couplets of dark and light laminae as annual or multi-annual cycles caused by differences in the water excess or the dripwater composition. By review of the literature and our own investigation and experiences, a hypothesis of fluid inclusion origin was developed (s. schematic drawing on page 125).

Three main environmental conditions can influence the amount of inclusions: precipitation, temperature and the CO₂-level of soil and cave. High soil-CO₂ values lead to a high amount

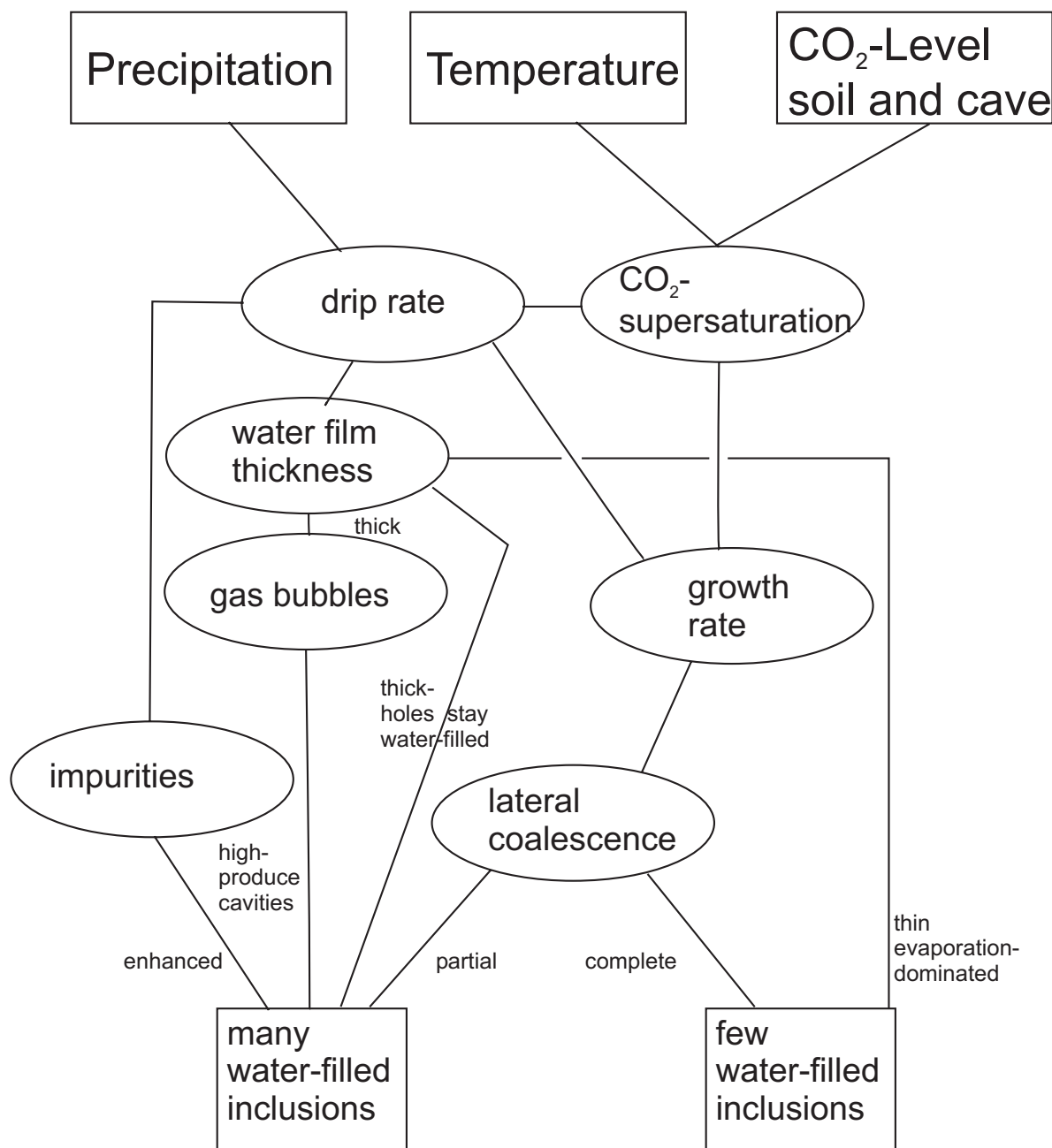


Figure 4.19: Factors influencing the amount of water-filled inclusions.

of H_2CO_3 (see equation 2.1), which in turn increases dissolution of calcium carbonate from the soil and the host rock. The CO_2 -level in the cave influences the precipitation of calcite. A rather low cave- CO_2 -value induces a higher supersaturation of the dripwater, which favors the calcite precipitation and thus speeds up the growth. A higher growth rate leads to an elevated amount of partial lateral coalescence. In the case of partial lateral coalescence the elongated imperfections are fluid inclusions and may be water-filled (Kendall and Broughton, 1978).

The growth-rate is also influenced by temperature. Higher temperatures lead to changes in the chemical reactions and reduce the solubility of CO_2 . A faster CO_2 degassing in turn accelerates the calcite precipitation. Therefore, the faster growing speleothem is expected to yield more imperfections due to the partial lateral coalescence of the single crystals resulting in a larger number of fluid inclusions.

The growth rate can also be changed by the precipitation, which modulates the dripwater supply. A constant drip site, which does not dry out over the year, increases the growth, compared to a seasonally dripping site. In contrast, slower growth favours complete lateral coalescence, which results in inclusion-poor calcite.

Precipitation is supposed to have the largest influence on fluid-inclusion occurrence. The precipitation governs the drip rate, which directly controls the crystal growth by the variation in the lateral coalescence, and changes also the water film thickness as well as the amount of impurities washed into the cave. Kendall and Broughton (1978) also speculate the water film thickness to have an important influence on the crystal growth. Low drip rate and a thin water film leads to enhanced drying of the speleothem surface. Therefore, the cavities, which are occurring less often due to a lower growth rate and complete lateral coalescence, are most likely not water-filled. In contrast, a thicker water film enables the cavities to be water-filled all the time and thus impedes the appearance of only air-filled inclusions. By splashing, tiny air bubbles may form, which can adhere on the growing speleothem surface and disturb the growth (Kendall and Broughton, 1978). Taylor and Chafetz (2004) also detected holes presumably provoked by adhesion of bubbles. The occurring spherical cavities may be (partially) water-filled later on. Another reason for an elevated number of small water-filled inclusions could be impurities in the dripwater. Strong precipitation and enhanced water flow in the karstic aquifer can transport organics as well as tiny minerals. Deposited on the speleothem surface they can influence the growth and impede or slow down crystal development at the affected parts. Possibly, they are the explanation for skeleton-like features found in the Bunker Cave (Fig. 2.6). In contrast, laboratory experiments with similar growth conditions, but clean dripwater resulted in perfect crystals (Fig.2.3). The impurity derived cavities may be water-filled and overgrown. This hypothesis can be verified by the occurrence of a high number of very small inclusions in the μm -range (BU-U stalagmite, s. Fig. 3.5) , which fits to the size and distribution of holes in the SEM image from Bunker Cave (Fig. 2.6).

The argumentation can be turned around for the palaeoclimatic interpretation of the speleothem water content. Inclusion-poor layers are related to complete lateral coalescence or a thinner water film. This may be related to a smaller growth and also to a reduced drip rate. Finally, a reduced precipitation or lower temperatures can account for this feature.

To disentangle the different effects, temperature estimates from independent proxies or from NGT-determination on speleothems as well as the growth rates, derived from an age-model, established by U-Th dating or ^{14}C -measurements, can be used. Furthermore, thin-sections can give an insight into the crystal growth history and help to decide if lateral coalescence or other effects caused the existence of the water-filled fluid inclusions.

The measurements on BU-U expand over more than 130 kyr. Therefore, temperature as well as precipitation changes may be responsible for the observed water content variations. In this case it is not possible to separate the effects. Most likely a warmer climate is related to elevated precipitation. Therefore the inclusion-rich parts are related to a rather fast growth, whereas the inclusion-poor layers, reflecting the cold glacial periods, hardly exhibit any growth (some mm in 30-40 kyr).

The Holocene stalagmite BU-1 is not supposed to reflect significant temperature changes (compare Davis et al., 2003). However, we revealed high variations in the water content. In retrospect to the presented theory this can be explained by precipitation effects, whereas the larger water film thickness, the higher drip rate and possibly the elevated content of washed out organics have played the major role. Elongated ellipsoidal inclusions as indicators for partial coalescence have been found in nearly all sections of the stalagmite, however in different magnitudes. Despite the difficulties to calculate a growth rate from the age stratigraphy, parts of higher water content coincide mostly with a higher growth rate. In turn, this reflects the water supply and finally the precipitation, as under drier conditions the stalagmite surface dries out and the growth slows down. Similarly, Genty and Quinif (1996) detected a high correlation of laminae thickness with water excess and thus precipitation.

The variation in the water content for the MA2 stalagmite are smaller, but significant. As again temperature changes are not supposed to be that large in the last 6 kyr, the changes in water content have to reflect variations in the precipitation pattern. Correlations with the stable isotopes suggest an increasing water content to be related to an also increased precipitation. Although the cave is located in a super-humid climate (3 500 - 5 000 mm per year) changes in precipitation are influencing the content of water-filled inclusions, most likely by the increased input of detritus or potentially by bubble influenced cavity formation. The latter factor can be of importance especially for this stalagmite as we found in general an extremely high amount of air-filled inclusions. The amount of air-filled inclusions decreased with a higher water content perhaps due to enhanced water flow removing the bubbles partially. The growth rate did not change substantially over the whole stalagmite growth period.

In summary, the comparison of the water content in BU-U, BU-1 and MA-2 with other proxy data from either the same stalagmites or from sediment and ice cores has shown that this value can deliver precious information about the past precipitation regime. A higher water content is correlated in all investigated samples with a higher precipitation. This can be explained by theoretical considerations about the growth conditions.

4.3 Separation techniques

Noble gases from air-filled inclusions can contribute significantly to the total signal. E.g., in air about 100 times more Ne is abundant compared to the same volume of water. As the temperature information is only contained in the water-derived component, it is necessary to subtract the noble gases of the air-filled inclusions from the total signal. In the case of a significant amount of air-filled inclusions ($A > 0.3$), even a small uncertainty in the air-water volume ratio can cause a large error in the remaining noble gas amount after subtraction. This part is used for temperature determination and thus can only deliver meaningful temperatures if the air contribution is sufficiently small ($A < 0.3$).

Unfortunately, only a small number of stalagmites fulfil this criterion in a simple extraction procedure consisting of a single step (compare Fig. 4.11). Stepwise procedures may overcome this problem by subsequent opening of different inclusions. The idea is based on findings from

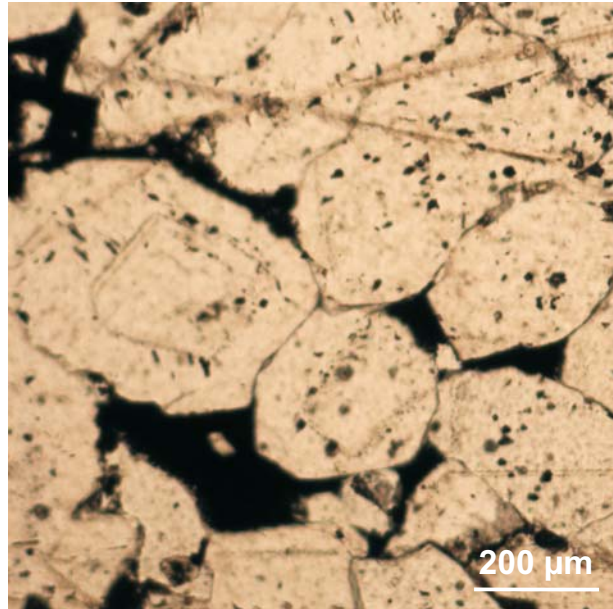


Figure 4.20: Thin-section of a piece from the H12 stalagmite. Between the calcite crystals large air-filled inclusions are visible. The inclusions within the crystals are significantly smaller and are supposed to be mostly water-filled.

thin section analysis (Fig. 4.20). Large air-filled inclusions are located between the calcite crystals. Inside the grains the inclusions are in general smaller (some μm in diameter) and predominantly water-filled. Badertscher (2007) conducted intensive studies on fluid inclusion characterization. She found the large inclusions between the crystals to be always air-filled and water-filled inclusions to appear only inside the crystals.

Using this knowledge we developed special stepwise procedures which consist of crushing, heating or a combination of both extraction methods. The first crushing predominantly opens the air-filled parts, whereas the subsequent steps increasingly extract the gases from water-filled inclusions. The results of stepwise crushing experiments are displayed in Fig.4.21. In all cases A is reduced in subsequent steps; if crushing only is applied a linear trend on the double-logarithmic scale is visible. Crushing up to 200 times can reduce A by a factor of 3. A further heating step enables additional reduction of the air contribution. In summary, the air-water volume ratio can be reduced by about 1 order of magnitude by application of several crushing steps in combination with a final heating step.

These results indicate that the first crushing opens actually the largest (air-filled) inclusions. Studies at ETH Zurich confirm this finding. They achieved also good results with a stepwise procedure consisting of a precrushing step followed by a main-extraction using thermal decrepitation (Scheidegger et al., 2008).

The stepwise procedure may have influences on the obtained noble gas pattern. Mechanical crushing may produce micro-fractures, which enable exchange with the atmosphere. In this case it is supposed that especially the light and mobile noble gases He and Ne would be affected. However, in some cases we found e.g. an excess in Xe in the first crushing step of samples from BU-1 (Fig. 4.22). This is in contradiction to the expectations and can not be explained by the extraction method. The sample is crushed few times with the steel ball and all the gases from this step are transferred to the cryo traps and further to the mass spectrometer. If micro-fractures had arisen from the crushing, a clear Ne-excess should be visible. On the other hand, the treatment prior to the extraction can have an influence. Due to the sampling of the stalagmite, subsequent transport and the cutting of

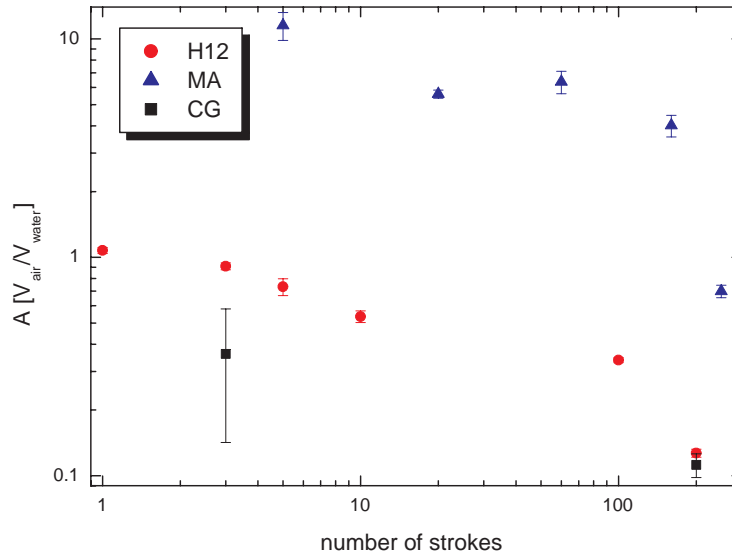


Figure 4.21: Development of the air-water volume ratio A using stepwise extraction procedures. A is plotted against the total number of strokes. The values at 200 strokes are achieved by a combination with heating at 150 °C. The data point of MA2 at the highest stroke number refers to a pure heating step.

small pieces, small micro-fractures may emerge. Possibly they enable the exchange of the inter-granular inclusions with the atmosphere and a certain re-equilibration. The heavy noble gases as Xe are suppressed in the exchange due to their larger atomic diameter ($2.18 \cdot 10^{-12} \text{m}$, He: $1.28 \cdot 10^{-12} \text{m}$) and diminished kinetic behaviour. Furthermore the Ne may get lost in the initial pumping step, whereas the heavier noble gases stay mainly inside the calcite. This may be an explanation for the deviations in the Xe-Ne plot towards Xe-excess. In the subsequent crushing steps only smaller inclusions inside the calcite crystals are opened which are hardly affected by the precedent extraction. Therefore, the noble gas concentrations are within the expected range and follow the line of decreasing air-addition towards equilibrated water at a certain temperature for all subsequent extraction steps beside the first crushing. This can be observed in the shown examples of BU-1 for the 60 hits step towards the combined 110 hits and heating step (Fig. 4.22). In stepwise procedures generally the noble gas concentrations evolve along the line of air-equilibrated water with a constantly decreasing addition of unfractionated air in higher extraction steps (Fig. 3.41). In the very first steps the mentioned deviation may occur. Thus, the stepwise crushing under vacuum may help to overcome not only the problem of high air addition, but also to reduce and minimize influences of micro-fractures. The Xe excess may also be explained by another reason. Adsorption is more effective for heavier gases. Thus, the Xe excess in the first step can also be due to removal of superficially adsorbed Xe. As we observed also Ar excess in the first step this assumption alone is not able to explain the noble gas pattern completely. A more detailed discussion about the deviations from expected values is given in the following subsection.

Another important point concerns the released water amount. For meaningful temperature determination from noble gas concentrations a water amount with small errors ($<5\%$) is essential. This can not be achieved with a liberated water amount $<0.1 \mu\text{l}$. Measurements on a very inclusion-rich stalagmite (BU-1) showed a decreasing trend in the released water

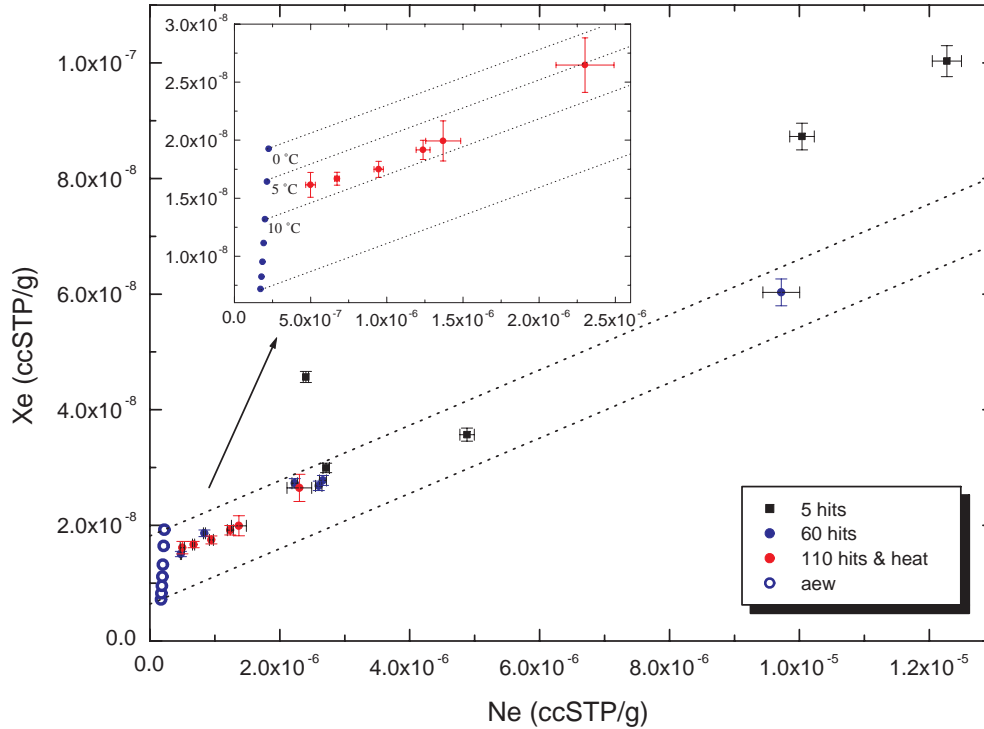


Figure 4.22: Reduction of the air-addition by stepwise methods, shown exemplary for the BU-1 stalagmite. Each sample is first crushed 5 times, than 60 times and finally 110 times in combination with 2 hours heating at 150 °C. The insert shows the result for the last step. The heating measurements are not hotblank-corrected.

amount per step. The strongest decline can be found from 60 to 100 hits. Thus, with the first 60 strokes most inclusions, at least the larger ones are opened. The remaining μm -sized inclusions can not provide such large amounts, even if they are more abundant than the big inclusions. A stalagmite with medium high water content (H12) did not show a significant trend. The amount of released water scatters mostly between 0.1 and 0.3 μl in one step, which is in an acceptable range for water determination. A different behaviour was found for the CG stalagmite. There, we only have few and in addition very small inclusions. They are opened primarily after the stalagmite is milled to fine powder and especially by thermal decrepitation. Thus, the optimum procedure depends on the stalagmite type and its inclusions.

In summary, the stepwise procedure enables the reduction of the air contribution to the total noble gas signal. A moderate number of strokes combined with a heating step yield in general enough water at the end of the stepwise extraction for precise water determination and finally the calculation of temperatures from noble gas concentrations.

4.4 Noble gas fractionation and enrichment

As mentioned in the precedent section, some speleothems show deviations from the expected atmospheric mixing ratio. Xe can be enriched in the first crushing step (Fig. 4.22), which may be caused either by the differential pumping due to micro-fractures (Ne most affected) or the release of superficially adsorbed Xe. Furthermore, extremely high values of Ar are sometimes found in the first crushing step (Fig. 4.24). This can neither be explained by adsorption (the deviation should tend towards Kr) nor by differential pumping (Ar should be depleted).

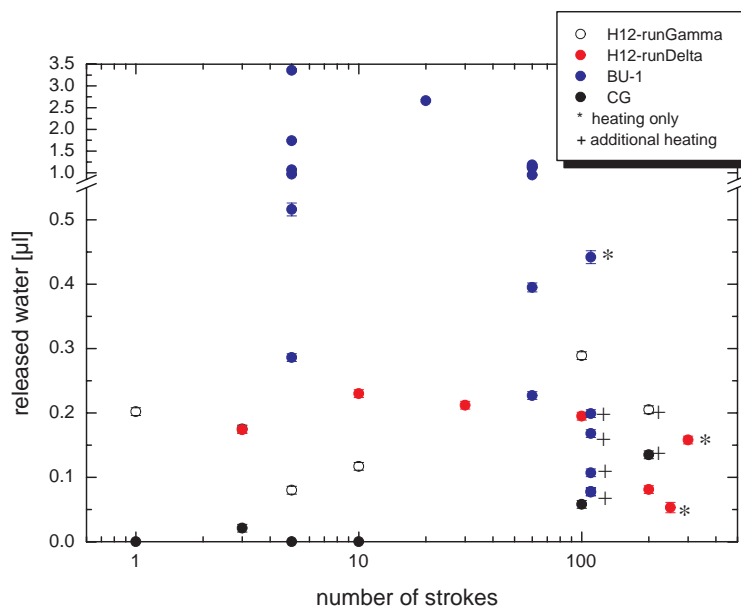


Figure 4.23: Water amounts released during the stepwise extraction. The samples at 110 and 200 strokes are additionally heated for 2h at 150 °C.

Even a combination of both effects can hardly account for the observed signal. Turner and Bannon (1992) also found excess Ar in quartz and fluorite samples and suggested dissolution of adsorbed atmospheric gases from sediments through which the fluids flow as a possible source. Furthermore, they explained a high ^{40}Ar concentration by a possible emplacement of sill. However, in the case of the speleothems the Ar-excess remains an open question. To get a hint with regard to the origin of this deviation, the main gas components (O_2 , N_2) as well as the major trace gases (CO_2 , CH_4) should be recorded as well.

It is important to mention, that the deviations from the excess-air line are only found in the first step or steps. At higher step numbers little or no deviations from the expected line are found, as it can clearly be seen in Fig. 4.24 and Fig. 4.22. Only the 5 hit-points are distant from the line, all 60-hit points as well as the 110-hit points are inside the area of air-equilibrated water with a different contribution of atmospheric air. An interesting result is in both cases the very good correspondence of the heating results with regard to the temperature. They refer to a Holocene stalagmite (<8 kyr) and should therefore not show large differences in temperature. The results of the heating step can affirm this expectation.

A systematical analysis of all measured data can provide a better insight into unexpected effects. At first, the measurements with bad fits are rejected ($\chi^2 > 10$) as they may have been influenced by technical problems during extraction and measurements. Then, the residuals between measurement and model are calculated and summarized according to each stalagmite (see Table 4.5). The major part of the investigated stalagmites show no significant deviation from the expected concentration for any noble gas. E.g. the deviation of the BU-1 samples from the model is in general smaller than 1%. However, the H12 stalagmite from Oman clearly stands out. Using Ne for temperature calculation always delivered bad results and strange temperatures. After detecting the Ne excess to be not a systematical measurement problem, but a property of the stalagmite, Ne was not used further for fitting. Subsequently,

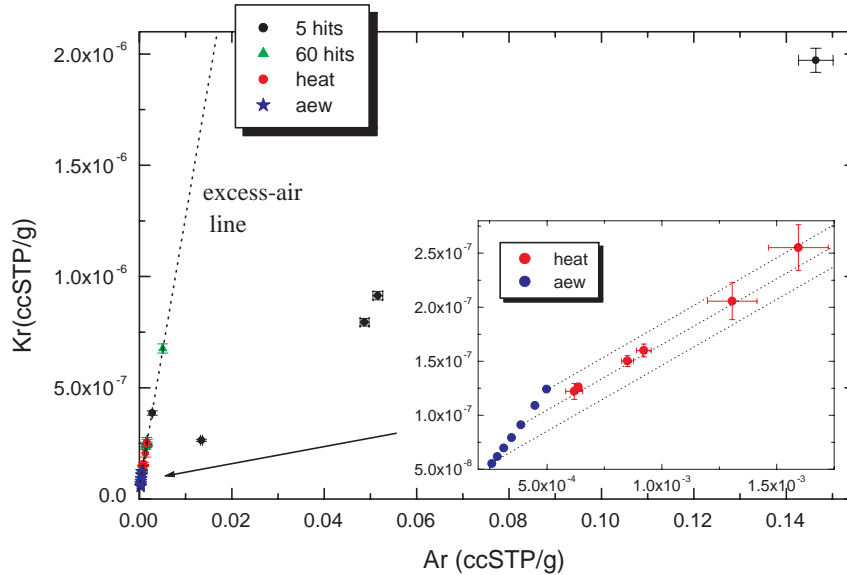


Figure 4.24: Deviations from expected signals at BU-1. The first extraction step resulted in high Ar concentrations. None of the subsequent steps did provide similar deviations. The insert shows the results for the last step of each sample. The heating measurements are not hotblank-corrected.

the temperature values got more reasonable and in general better fitting results have been achieved. Ar, Kr and Xe show no significant deviation from the models, whereas the Ne concentration is more than 2σ away from air-equilibrated water with atmospheric air.

It is difficult to explain this unexpected effect. An explanation for the Ne excess may be an enrichment of noble gases in some relatively undisturbed and badly ventilated caves, perhaps in some way related to the findings of Podosek et al. (1980), who discovered enrichment patterns towards heavier noble gases and also an enrichment of Ne in sedimentary rocks. Assuming a certain ventilation of the cave chambers it is at least in shallow caves unreasonable, but can not be excluded in deeper caves with long and narrow passages. Our own measurements confirm that in the shallow Bunker Cave no significant deviation from the atmospheric mixing ratio exists. Air samples from deep and less ventilated chambers in the B7 cave show also no significant deviation from the atmospheric mixing ratios of Ne, Ar, Kr and Xe. Thus, it is less likely that the Ne excess is caused by an excess in the cave atmosphere.

Another reason may be a diffusive isotope exchange of the inclusion fluids with the noble gases from the host calcite and sedimentary particles in it, as known from the stable isotopes Wilkinson (2001). A cross section of the stalagmite H12 along the growth axis (Badertscher, 2007; Neff, 2001) reveals a pronounced layering consisting of brownish, red and white layers. The white layers are related to a larger amount of water-filled inclusions, whereas the brownish and especially the red layers may be due to depositions of sedimentary mineral grains. The deposition of extrinsic material in the H12 stalagmite is also manifested in the high detritus values (mean $c(^{232}Th) \approx 14,1$ ng/g, Neff, 2001).

However, the Ne excess seems not to be dependent on the air-water volume ratio or on the extraction procedure (Fig.4.25). The deviations from the expected model values do not decrease or increase with the fraction of noble gases from the air-filled parts. Only 5 out of 30 samples exceed the 1σ deviation from the mean Ne excess, but show no systematics. Furthermore, even stepwise measurements and microwave extraction yield a similar Ne excess compared to model values. Thus, this Ne excess is not generated by extraction or measurement procedures, but has to be an intrinsic property of the stalagmite. Interestingly, other studies also revealed Ne excess for samples from the same region (Scheidegger et al., 2008).

Table 4.5: Noble gas excesses in different samples. The given numbers refer to the residuals between measurement and model (UA-model, fit-parameter: T , A). "Number of samples" indicates how many measurements have been used for the calculation of the mean. The uncertainty refers to the 1σ -deviation of all used measurements. The displayed samples have been selected by the χ^2 -values. Results with bad χ^2 (>10) have been rejected. H12 was fitted without Ne.

sample	deviations from model (in %)				number of samples
	Ne	Ar	Kr	Xe	
BU-U	1.9 ± 2.0	-1.5 ± 1.3	-0.1 ± 1.1	0.9 ± 1.3	16
BU-1	0.5 ± 1.4	-0.6 ± 1.7	-0.2 ± 0.8	0.6 ± 1.4	7
BU-2	1.8 ± 2.0	-3.1 ± 3.2	-0.4 ± 2.1	2.4 ± 3.9	2
CG	-6.7 ± 2.3	4.9 ± 3.8	6.6 ± 4.1	-3.2 ± 2.2	4
H12	22.3 ± 8.7	0.5 ± 2.1	-0.9 ± 3.2	0.3 ± 1.1	30
MA2	2.9 ± 7.8	-0.8 ± 3.2	-0.4 ± 3.3	-0.2 ± 2.4	6

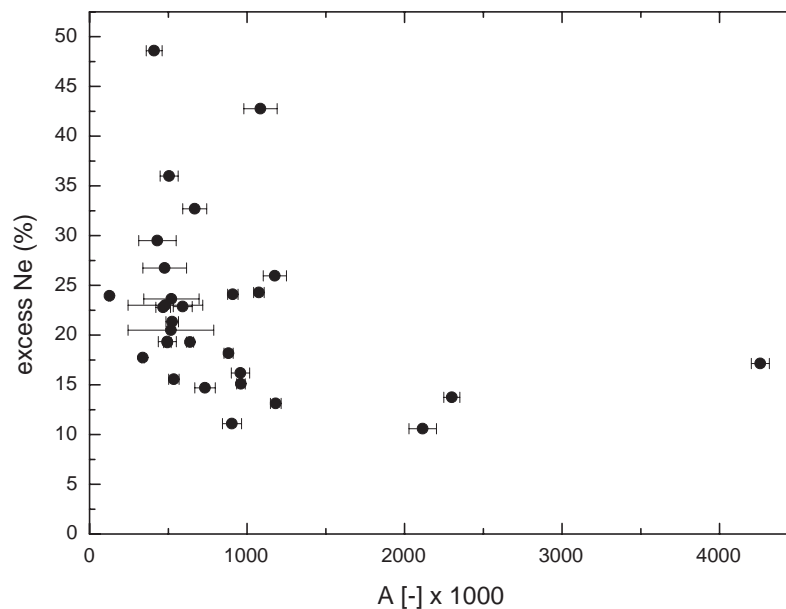


Figure 4.25: Excess-Ne of the H12 samples plotted against the air-water volume ratio A . Here, excess-Ne does not refer to air addition, but to the deviation of the measured values from model expectation based on fits to Ar, Kr and Xe. The mean Ne excess is given in Table 4.5. Three outliers (highest Ne excess) refer to early measurements and may therefore be influenced by extraction and measurement problems.

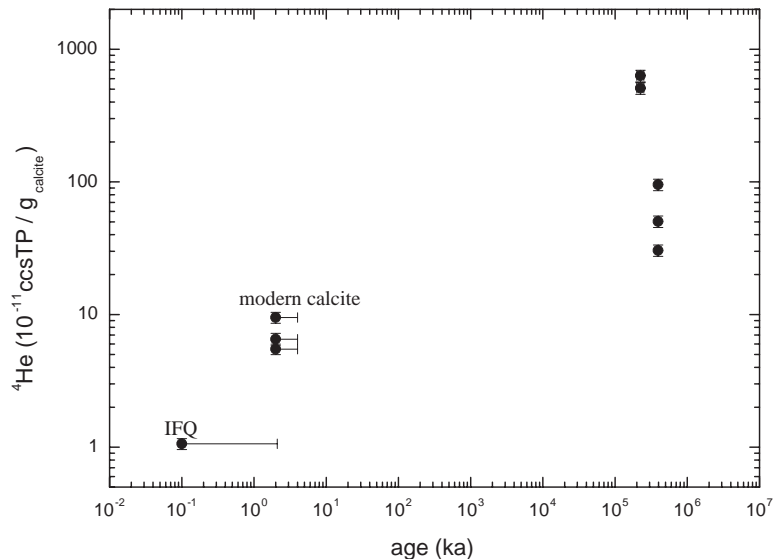


Figure 4.26: He-content measured by Stuart and Turner (1992). He is given in 10^{-11} ccSTP per g of calcite. IFQ is given for comparison and refers to an inclusion-free quartz with unknown age. Modern calcite refers to the samples BB, YB and Carl-1 from the same paper. The data includes He from air- and water-filled inclusions and also the radiogenic fraction.

The CG stalagmite from Cuba also shows a significant deviation in the Ne values. However, this result is not as robust as in the case of H12 as it is based on only 4 fitted samples. Additional measurements may substantiate this first result.

In summary, most speleothems yield a noble gas concentration which corresponds to the theory. The total noble gas concentration obtained from a calcite sample is composed of a component from air-equilibrated water and unfractionated atmospheric air. In rare cases systematic deviations can occur (H12, Oman). However, we found only systematic shifts for Ne so far. Consequently, also for these samples reasonable temperature calculation with acceptable errors has been possible by using the unaffected Ar, Kr and Xe concentrations.

4.5 Dating via Helium

Stalagmites are usually dated using the uranium-thorium method (Richards and Dorale, 2003). In the case of old stalagmites ($\geq 300\,000$ yr) it gets difficult to date precisely using the U/Th disequilibrium. The results can be charged with high uncertainty or it will be even impossible to date if the speleothem is older than 500 000 years. For such stalagmites U/Pb dating can yield an age (Richards et al., 1998; Walker et al., 2006; Hellstrom et al., 2008; Polyak et al., 2008). Additionally, helium may help to estimate a reasonable age, if no U/Pb data are available.

First indications that He in speleothems can be useful for age estimation can be drawn from the data of Stuart and Turner (1992). Even though they claim to find very low He contents, a remarkable difference between modern calcite and rather old precipitates (some 100s of Myr) can be observed (Fig. 4.26). They did not perform data fitting to disentangle the different contributions to the signal. Additionally, the 395 Myr Rhynie chert showed lower He content

than the younger triassic authigenic quartz minerals. Furthermore, the sample preparation may have affected the results due to baking out of the extraction set at 200 °C for 36 hours. However, an increasing He content can be observed for increasing age.

The recent study of Scheidegger (2005) stated that radiogenic He must be abundant due to high He/Ne ratios above air or equilibrated water values. A comparison of radiogenic He contents from a stalagmite of the Qunf-Cave with radiogenic He and age data from the H12-stalagmite yields reasonable ages for the Qunf stalagmite. She concluded from this results that U/Th-He dating should principally be possible.

With respect to our own experiments, the investigation of U/Th-He age determination was motivated by missing U/Th data. The first stalagmite with reliable noble gas concentrations was dated some time after the noble gas measurements. To immediately compare the calculated noble gas temperature with an expected value a rough age estimation was necessary and was performed using the helium data.

Helium accumulates in the stalagmite due to the radioactive decays in the ^{238}U , ^{232}Th and ^{235}U decay chains (Table 4.6). As it can be assumed that the calcite is closed for the noble gases at typical temperatures (≤ 30 °C) and timescales (Copeland et al., 2007), the over time accumulated helium will be a measure of the age. Furthermore, we assume that the air-filled inclusions contain a gas composition equal to the atmospheric mixing ratio and the water-filled inclusions a noble gas component which is equilibrated at cave temperature. The radiogenic helium component C_{rad} can therefore be calculated by subtracting the excess-air C_{air} and the equilibrium component C_{eq} from the total gas amount C_{tot} :

$$C_{\text{rad}} = C_{\text{tot}} - (C_{\text{eq}} + C_{\text{air}}) \quad (4.2)$$

The equilibrium component C_{eq} can be determined using the known amount of released water and the equilibration temperature from data fitting. The excess-air component is derived by inverse modelling from all noble gas data except He.

The radiogenic component is built up inside the calcite matrix and is, therefore, dependent on the uranium $C_{\text{U}238}$, $C_{\text{U}234}$, $C_{\text{U}235}$ and the thorium concentration $C_{\text{Th}232}$, given in $\mu\text{g U (Th)}$ per g of calcite. To establish a first-order approximation, we assume that initially there are no daughter elements to the mentioned isotopes. In general this assumption will not limit the calculation as the half-lives of the daughter elements are in general very low. Thus a secular equilibrium is established in the centennial scale.

However, exceptions are ^{226}Ra with a half-life of 1602 a, ^{231}Pa with a half live of 32 760 a and ^{230}Th with a half-life of about 75 400 a. With regard to old samples (some 10 000 years) the initial Ra will not play a significant role in the case that Ra is not strongly concentrated at the beginning. Gainon et al. (2007) reported that radium is adsorbed efficiently due to iron or manganese-hydroxides under oxidizing conditions. Therefore, the typical radium activity concentration in groundwater and springs is rather low. E.g. in Austria > 90% of more than 380 wells are below 20 Bq/m³ (BMLFUW, 2002). Fanale and Kulp (1961) reported a Ra content in a calcite sample to be $3.6 \cdot 10^{-15}$ g Ra per g of calcite. Based on the activity concentration in groundwater of <20 Bq/m³, which is also valid for the cave dripwater, the radium content would be smaller than $5.4 \cdot 10^{-16}$ g per g water. Compared to the result of Fanale and Kulp (1961) no extreme enrichment of radium in the precipitated calcite occurs. If we assume $3.6 \cdot 10^{-15}$ g Ra per g of calcite and an age of 10 000 years, we obtain about $5.7 \cdot 10^7$ α 's from the decay of this initial Ra. This is low compared to the results of ^{238}U . Using an ^{238}U content of 1 ppm we obtain about $3.9 \cdot 10^9$ α -particles alone from the decay of ^{238}U in the same timescale. The contribution of initial Ra can be of importance in the case of low U content (<0.1 ppm) and ages below 10 kyr (Fig. 4.27). However, this consideration is based on the measurements of Fanale and Kulp (1961). Different Ra contents due to e.g.

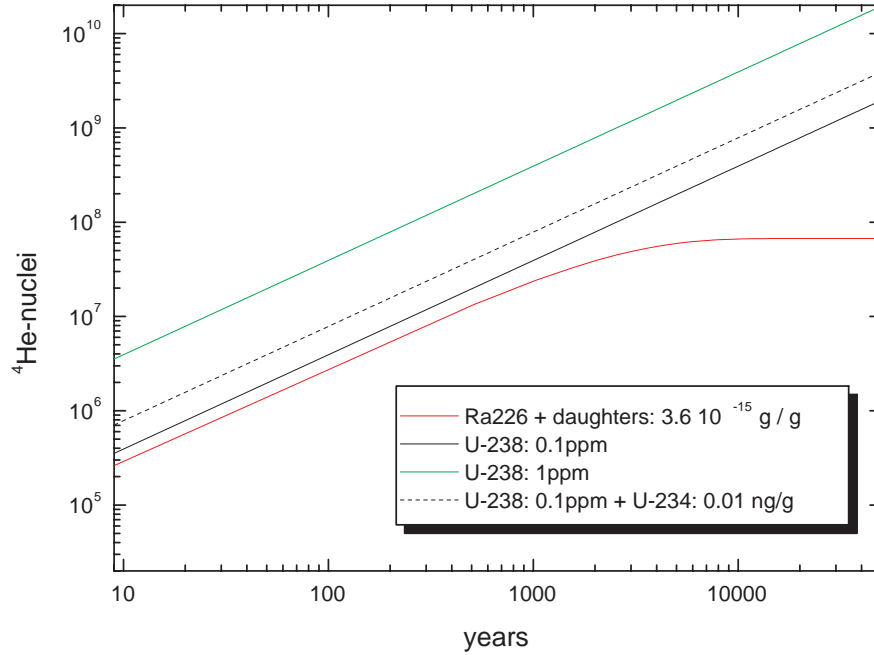


Figure 4.27: Comparison of α -particles produced by ^{238}U and ^{226}Ra . The red line refers to the initial Ra concentration of $3.6 \cdot 10^{-15}$ g/g calcite. After about 8 kyr no further contribution of the initial Ra to the total number of the α -particles occurs, as most of the Ra is already decayed.

detritus may change these values. In the case of older speleothems the contribution gets less significant with age as the initial Ra is almost completely decayed after 8 kyr.

The ^{231}Pa in the ^{235}U decay chain should be low. The estimated oceanic abundance is about $5 \cdot 10^{-17}$ g per g water (TJlab, 2008). Furthermore, ^{231}Pa measurements on carbonates (corals) showed that no initial Pa-231 is abundant in the samples (Edwards et al., 1997). Thus, initial ^{231}Pa is neglected in the following.

The initial ^{230}Th in the calcite is in general rather low as Th is hardly soluble and thus not contained in the dripwater. However, it is particle reactive and can be included in the calcite with detritus such as clay minerals. The initial ^{230}Th is calculated using the detritus correction based on a fix relation between ^{232}Th and detritical ^{238}U (Wedepohl, 1995). Assuming decay equilibrium between the detritical components, the initial ^{230}Th can be inferred:

$$N_{230} = N_{238, \text{det}} \cdot \frac{\lambda_{238}}{\lambda_{230}} = \frac{N_{232}}{3.8} \cdot \frac{\lambda_{238}}{\lambda_{230}} = N_{232} \cdot 4.44 \cdot 10^{-6} \quad (4.3)$$

For calculation of the total number of α particles the ^{235}U decay chain is of minor importance because of the low abundance of ^{235}U :

$$C_{\text{U}235} = 0.0072527 \cdot C_{\text{U}238} \quad (4.4)$$

The content of ^{238}U and ^{232}Th can be assumed to be constant over the investigated time scale of less than one million years. However, for the other relatively long lived isotopes (^{234}U , ^{230}Th) the initial concentration and the change over time has to be calculated. In the ^{238}U decay chain a total of 8 α particles, in the ^{232}Th decay chain 6 α 's and in the ^{235}U decay chain 7 α 's are produced.

Table 4.6: Thorium, uranium-actinium and uranium-radium decay series. Plotted are the main decay channels. In summary 8 α 's are produced in the U-238 series, 7 in the U-235 and 6 in the thorium decay series.

nuclide	decay	half life	nuclide	decay	half life	nuclide	decay	half life
thorium			U-238			U-235		
Th-232	α	$1.405 \cdot 10^{10}$ yr	U-238	α	$4.47 \cdot 10^9$ yr	U-235	α	$7.03 \cdot 10^8$ yr
Ra-228	β	5.75 yr	Th-234	β	24.1 d	Th-231	β	25.5 h
Ac-228	β	6.15 h	Pa-234	β	6.7 h	Pa-231	α	32760 yr
Th-228	α	1.91 yr	U-234	α	$2.46 \cdot 10^5$ yr	Ac-227	β	21.7 yr
Ra-224	α	3.66 d	Th-230	α	$7.54 \cdot 10^4$ yr	Th-227	α	18.7 d
Rn-220	α	55.6 s	Ra-226	α	1602 yr	Rn-223	β	23.2 min
Po-216	α	0.145 s	Rn-222	α	3.82 d	Fr-223	β	22 min
Pb-212	β	10.64 h	Po-218	α	3.05 min	Ra-223	α	11.43
Bi-212	α, β	60.5 min	Pb-214	β	26.8 min	Rn-219	α	3.96 s
Po-212	α	10^{-7} s	Bi-214	β	19.9 min	Bi-215	β	7.6 min
Ti-208	β	3.1 min	Po-214	α	0.164 μ s	Po-215	α	1.78 ms
Pb-208	-	-	Bi-214	β	19.9 min	Pb-211	β	36.1 min
			Ti-210	β	1.3 min	Bi-211	α	2.14 min
			Pb-210	β	22.3 yr	Ti-207	β	4.77 min
			Bi-210	β	5.01 d	Pb-207	-	-
			Po-210	α	138 d			
			Pb-206	-	-			

To correctly assess the amount of He generated inside the speleothem, the calculation for the decays in the ^{238}U decay chain has to be performed in a stepwise order as shown by Farley et al. (2002).

$${}^4\text{He} = 6 \cdot C_{\text{Th}232} \cdot \left(1 - e^{-\frac{t}{\lambda_{232}}}\right) \quad (4.5)$$

$$+ C_{\text{U}238} \cdot \left(1 - e^{-\frac{t}{\lambda_{238}}}\right) \quad (4.6)$$

$$+ 7 \cdot 0.007257 \cdot C_{\text{U}238} \cdot \left(1 - e^{-\frac{t}{\lambda_{235}}}\right) \quad (4.7)$$

$$+ \left[C_{\text{U}238} \cdot \left(1 - e^{-\frac{t}{\lambda_{238}}}\right) + C_{\text{U}234} \right] \cdot \left(1 - e^{-\frac{t}{\lambda_{234}}}\right) \quad (4.8)$$

$$+ 7 \left[\left(C_{\text{U}238} \cdot \left(1 - e^{-\frac{t}{\lambda_{238}}}\right) + C_{\text{U}234} \right) \cdot \left(1 - e^{-\frac{t}{\lambda_{234}}}\right) + C_{\text{Th}230} \right] \cdot \left(1 - e^{-\frac{t}{\lambda_{230}}}\right) \quad (4.9)$$

$$+ 5 \cdot C_{\text{Ra}226,i} \cdot \left(1 - e^{-\frac{t}{\lambda_{226}}}\right) \quad (4.10)$$

Equation (4.5) states the alpha decay from ^{232}Th within the time t , equation (4.6) the decay of ^{238}U , (4.7) of ^{235}U and equation (4.8) the decay of ^{234}U including the fraction of ^{238}U which decays in the same time to ^{234}U . Equation (4.9) summarizes all α 's from the subsequent isotopes and the initial ^{230}Th (which should be zero due to the chemical behaviour, but can yield values above zero due to detritus contribution) including the Th amount which was built up in time t due to the decay of ^{238}U and ^{234}U . Equation (4.10) is the term including the contribution of initial ^{226}Ra .

This theory was applied to six speleothem samples from the Bunker cave stalagmite BU-U. In this case all noble gases have been measured, so that the calculation of the three He components (equilibrium, air and radiogenic component) was possible. Additionally, the released water amount and the sample weight was measured. Results are listed below in Table 4.7. The isotope content of U and Th was determined in the context of the U-Th-dating. The radiogenic He was calculated from all He released in the crushing and the subsequent heating step using equation (4.2). This value was then converted to a radiogenic

Table 4.7: Exemplary calculation of the expected radiogenic He for the mean of six samples of a growth layer of BU-U. The radiogenic He is calculated by summarizing the α particles of all decay chains. He_{rad} indicates the mean amount of the measured radiogenic He per gram of calcite. α 's are summarized from all expected decays within the measured U/Th-age of 10 800 years and converted into gas amounts per gram of calcite.

parameter	value
$C_{\text{U}238}$	108.79 ng/g
$C_{\text{U}234}$	0.00919 ng/g
$C_{\text{Th}232}$	0.46 ng/g
$C_{\text{Th}230}$	0.000263 ng/g
$C_{\text{Th}230,\text{initial}}$	$2.02 \cdot 10^{-6}$ ng/g
He_{rad}	$3.0 \pm 2.2 \cdot 10^{-10}$ ccSTP/g
U/Th-He age	16 500 yr (+7700 yr, -10100 yr)
U/Th age	10 500 - 12 100 yr
α 's (theoretical)	$2.15 \cdot 10^{-10}$ ccSTP/g

He amount per gram of calcite and afterwards the mean of the six investigated pieces was determined (s. Table 4.7).

From the known isotope content and the age (10 800 a) the α particles are calculated. From the ^{232}Th -decay $7.93 \cdot 10^6$, from ^{235}U $3.09 \cdot 10^8$, from ^{238}U $9.58 \cdot 10^8$, from ^{234}U $1.49 \cdot 10^9$ α -particles are produced including the additional contribution of already decayed ^{238}U . The subsequent daughter decays to the stable ^{206}Pb account for additional $3.03 \cdot 10^9 \alpha$ s. In total, we get $5.79 \cdot 10^9$ He nuclei, which corresponds to $2.15 \cdot 10^{-10}$ ccSTP He. With consideration of the dating error of the stalagmite sample of 300 years, the radiogenic He value is located between $2.08 \cdot 10^{-10}$ and $2.48 \cdot 10^{-10}$ ccSTP. In this calculation the uncertainties of the isotopic content of the calcite are not included, but should result in minor deviations.

A comparison of the He amount derived by decay calculation and the mean determined by noble gas measurement show an agreement within the uncertainty. However, the scatter of the measurement data is large. The mean value is about $3.00 \cdot 10^{-10}$ ccSTP/g_{Carb}, whereas the standard deviation is $2.2 \cdot 10^{-10}$ ccSTP/g. The scatter of the measured values can at least partially be attributed to the extraction process. Not only different methods have been used, but also small deviations in the extraction procedure have occurred which influenced the efficiency. This can be verified by a closer look to the obtained grain size distribution (Marx, 2008). A larger fraction of big grains can explain a lower amount of extracted He and vice versa. Additionally, not all samples yield the same ages, even if they are extracted nearby. The corresponding growth layer expands over the period from 10 500 yr BP to 12 100 yr BP. The U/Th-He age was determined by inverse modelling. The age is calculated according to the known U and Th content by using time as fitting parameter and by comparing the measured radiogenic He amount with the mathematically derived α decays.

The results indicate that the measured amount of radiogenic helium is comparable to the theoretically expected values. Turning around this statement an age estimation via inverse modelling using the known U and Th content may be possible. Although we have to keep in mind the not totally reproducible and uniform extraction process, at least the accumulation of radiogenic helium may be used to give a rough estimation of the speleothem age.

In the case of very old samples (≥ 1 Myr) the helium - uranium dating had already been used, not yet for speleothems, but for instance for corals (Bender, 1973), apatite (Wolf et al., 1996) or other minerals (s. summary of Farley, 2002). An important requirement is that the He is retained quantitatively in the calcite, which can be assumed with regard to the diffusion data recently given by Copeland et al. (2007).

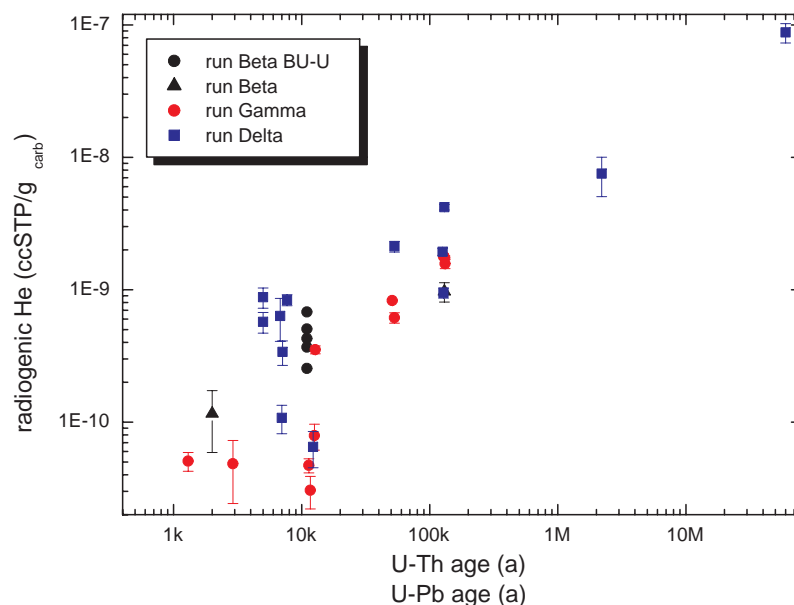


Figure 4.28: Compilation of radiogenic He data for stalagmites with different ages. They refer to different measurement runs. The radiogenic He per g of calcite is plotted against U-Th ages, respectively U-Pb ages. The sample with the highest radiogenic He value has not been dated so far by U-Pb and is only arranged according to the trend.

During the duration of the project not only stalagmites from different locations have been measured, but also speleothems covering a certain age scale. A summary of these samples is given in Fig.4.28. There, the absolute amount of radiogenic He is normalized to the sample weight and given per g of calcite. The youngest sample is dated by U/Th to about 1 300 years, the oldest one dated by U/Pb to about 2.2 Myr. The different measurement runs are displayed in distinct colours. Obviously there is a trend of increasing radiogenic He with age. Despite some deviations in the case of samples extracted in run Gamma, a rather linear relation between age and radiogenic He can be inferred from this diagram. Furthermore, in all runs a similar linear trend can be found. However, the total amount of released gases depends on the extraction efficiency. Compared to Run Delta and Run Gamma, Run Beta seems to yield a generally lower efficiency. The other two runs are comparable. It is important to mention that the scatter in the obtained radiogenic He is remarkable and can reach up to one order of magnitude, even though samples with similar ages are used.

The differences in the magnitude of the measured radiogenic He can already be used to deduce a reasonable age interval for some samples. Based on the data shown in Fig. 4.28 a linear fit was created. The outliers of run Gamma have been rejected for this purpose. Using the remaining 27 data points a fit with a correlation coefficient R of about 0.82 was obtained (Fig. 4.29).

The relationship was used for age determination of the sample BC1-4 from Northern Canada. It refers to a stalagmite from the Bear Cave in the Bear Cave Mountains in the Yukon Territories (66°25'N, 139°20'W). Today the mean annual air temperature is about -8.9 °C. The measurement on a piece of BC1-4 revealed an extremely high amount of radiogenic He, which is about one order of magnitude above all other samples measured so far. The adjustment of the age to the fit using the radiogenic He results in a mean age of about

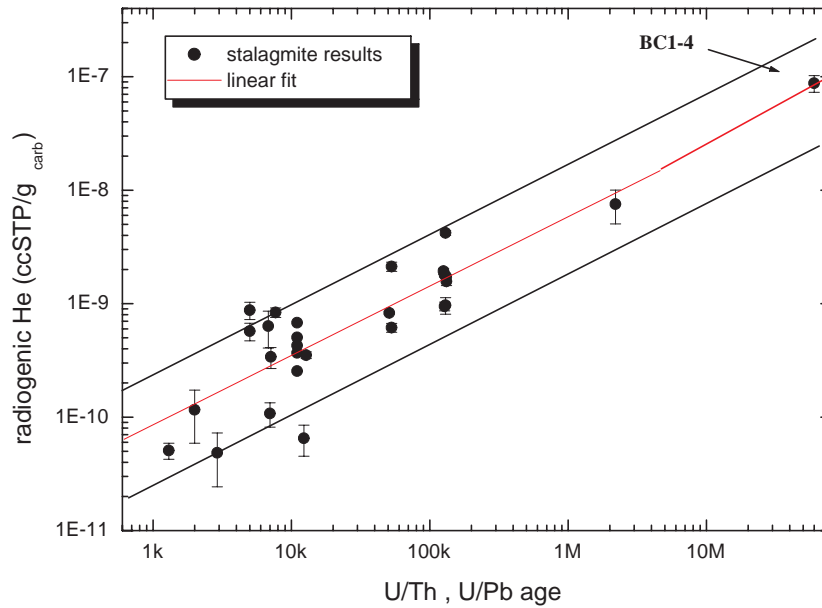


Figure 4.29: Correlation between U/Th age and radiogenic He. The data displayed in Fig.4.28 have been used for fitting a linear relationship. The sample BCI-4 was not included for fitting and is adjusted to the linear fit.

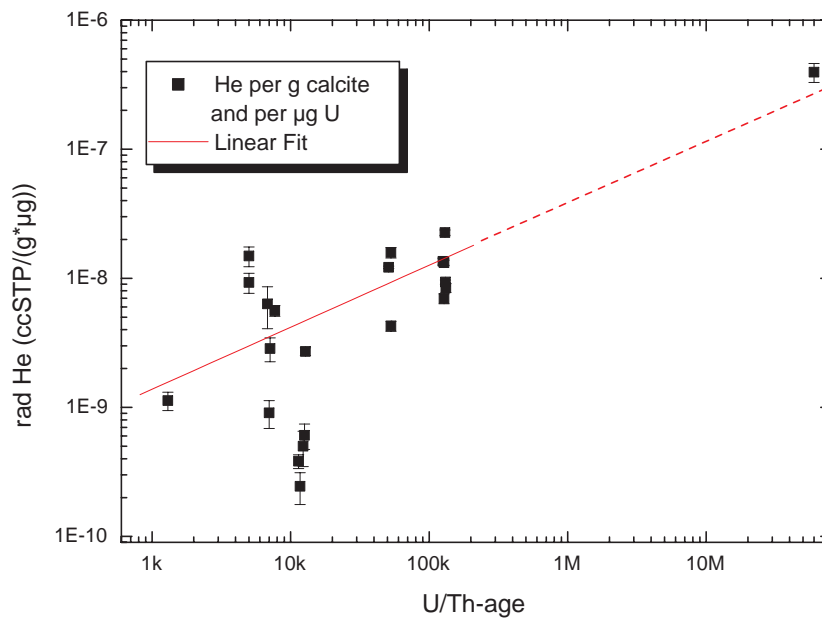


Figure 4.30: Correlation between U/Th ages and normalised radiogenic He. The radiogenic He is referred to 1 g calcite and an uranium content of 1 μg U per g calcite. Again the highest value is only adjusted to the fit. The dashed line indicates extrapolation of the linear relationship.

60 Myr. Assuming the uncertainty to be given by the typical scatter of the other speleothem measurements, BC1-4 could be between 15 Myr in the minimum case and maximum 250 Myr old. Information about growth conditions and U/Th data can help to constrain the result from the radiogenic He. U/Th measurements revealed the sample to be out of the dating range, i.e. older than 500 kyr. Taking into account that today no speleothem growth can be observed due to the low mean annual air temperature, the stalagmite has most likely grown in a warmer period. Even 5 °C above the present-day temperature would not be sufficient to enable stalagmite growth. Thus, the stalagmite can not originate from the Pleistocene, but from the Miocene, which was the last warmer period. The mean age of about 60 Myr, derived from radiogenic He, suggests the stalagmite to have grown in the Paleocene, which was a significantly warmer period, especially during the Paleocene/Eocene transition (55 Myr ago), (Norris and Röhl, 1999). Another very warm period was the Cretaceous, which is also a reasonable period for the investigated speleothem. During this time the sea level was higher (Haq et al., 1988) and the tropical as well as the polar sea temperatures had been elevated. The tropic sea ranged between 27 and 32 °C and the polar sea above 0 °C up to 15 °C (Barron, 1983). The lack of cold-water fauna as well as of any permanent ice and the occurrence of a large palaeo flora at the coast of Northern Alaska (420 species) additionally confirm warm conditions in the far north. Thus, it would not be unreasonable that the investigated speleothem sample has grown during this period, which was one of the warmest in Earth's history.

The age of the BC1-4 sample is additionally constrained by the use of normalized He data. The amount of accumulated He is strongly dependent on the uranium and to a smaller extent on the thorium content. A summary of the normalized data is given in Fig.4.30, where the radiogenic He is calculated per g calcite and μg of ^{238}U . Fitting the data by a linear function leads to a similar relation as in the case of the non-normalized He content. The correlation coefficient R is not that good (0.61) because no data have been discarded and the total sample number was smaller (n=21). For some samples the U content was not known and thus they could not be used for fitting the normalised data. However, the radiogenic He fits to a similar age as inferred from Fig. 4.29, but with a higher mean of about 130 Myr. This result would again correspond to the warm Cretaceous period.

Thus, the age estimation with radiogenic He is not unreasonable, but has first to be constrained by U/Th or U/Pb dating. Additionally, a uniform and reproducible extraction with constant efficiencies has to be developed to reduce uncertainties and to finally enable more precise quantitative results. Furthermore, the theoretical calculations have to be arranged with the experimental data. Fitting the liberated radiogenic He of BC1-4 to the theoretically expected α - decays during time, we would obtain an age of about 1.5 Myr. This is one to up to two orders of magnitude less compared to the age inferred from Fig. 4.29 and Fig. 4.30 and may be due to a low extraction efficiency. Preliminary data obtained from U/Pb dating of the sample BC1-4 resulted in an age of ~ 5 Myr (unpublished, personal communication Nicholas Utting), which suggests the dating attempts with U/Th-He to be in a similar order of magnitude.

In summary, our data, the exemplary application as well as the low diffusivity of He are encouraging and suggest this technique to be possibly useful as a dating tool for very old speleothems.



Figure 4.31: Halves of the stalagmite BU-U. The left side was used for U/Th dating, the missing part between the two halves was used for isotope, trace-element and noble gas measurements. The red rectangle refers to the measurement of six subsamples from the according growth layer. The brownish layers indicate hiatuses. Below the first hiatus the stalagmite has grown during MIS 3 and then in the Eemian. The layers below the subsequent extremely dark parts have not been dated and investigated.

4.6 Case studies

In the first subsection a set of samples is presented, which demonstrates the general possibility for noble gas temperature determination via fluid inclusions in speleothems. Reproducible values from one growth layer covering the Early Holocene (11 - 12 kyr BP) show the robustness of the data. Furthermore, a comparison with a pollen study approves the determined temperature difference of 4 °C between the Early Holocene and the Early Middle Ages to be a reasonable result.

Encouraged by these first useful data we tried to establish a temperature record along the growth axis of the same stalagmite (BU-U). The results are presented briefly in the following subsection and discussed in comparison with independent studies. The determined temperature differences between Holocene, Glacial values (mainly Marine Isotope Stage 3 - MIS3) and the Eemian are in agreement with expectations and reveal the Eemian maximum to be possibly warmer than present-day climate. Similarly, a preliminary temperature record was established for a completely Holocene stalagmite (BU-1) from the same cave. Based on several samples along the growth axis hardly a significant temperature variation can be found in the last 8 kyr in central Europe.

4.6.1 Reproducibility and uncertainties

The first indication for successful temperature determination from speleothem fluid inclusions by noble gas measurements came from one small piece from the stalagmite BU-U (Fig.4.31), which was measured in spring 2007. To substantiate this encouraging results, six pieces from the according growth layer of this stalagmite and a small soda straw were prepared (Table 4.8). Additionally, a small piece was cut out of the younger stalagmite BU-1. All of these samples derive from the Bunker Cave in Northwest Germany (Sauerland). BU-U exhibits very large columnar crystals (up to a length of some cm, Fig. 4.32) in the uppermost growth layer belonging to the Early Holocene.

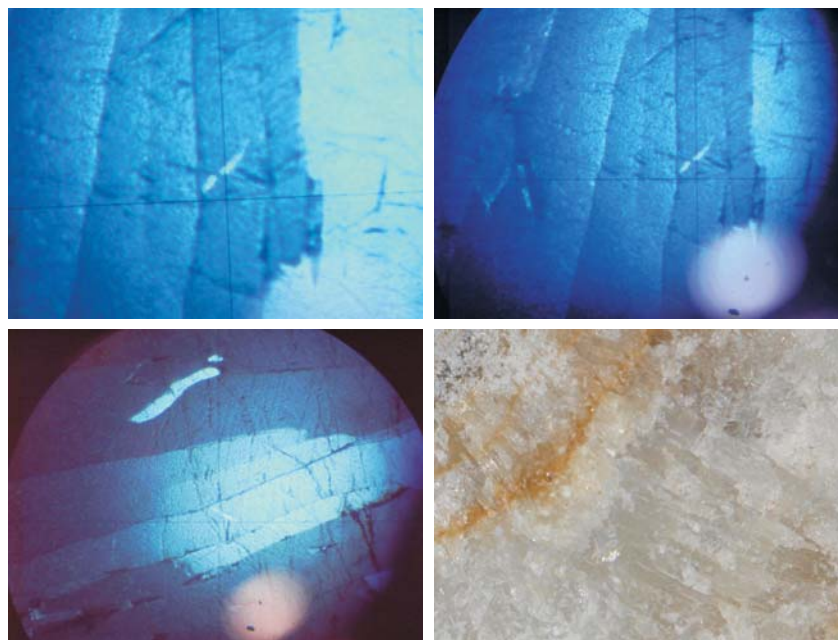


Figure 4.32: The uppermost part of BU-U on a closer view. The three bluish pictures are photos taken from microscope analysis using polarized light. Unfortunately, no exact scale bar was available, but the displayed details shows columnar crystals in the order of one cm. These crystals are already visible by eye as it can be seen in the lower right picture. The growth axis tends there to the lower right edge.

Table 4.8: Total sample weight, released water amount, apparent gravimetric water content, and applied extraction method for different Bunker Cave speleothems

Sample	weight (g)	water amount (μl)	water content % wt	crushing device
BU-Ua	2.748	1.31 ± 0.04	0.48	copper tube
BU-U0	1.084	0.159 ± 0.006	0.15	copper tube
BU-U1	1.001	0.516 ± 0.007	0.52	steel cylinder
BU-U2	1.069	0.49 ± 0.01	0.46	copper tube
BU-U3	1.064	0.411 ± 0.005	0.39	steel cylinder
BU-U4	1.428	0.765 ± 0.007	0.54	steel cylinder
BU-1	1.424	0.899 ± 0.015	0.63	steel cylinder
Soda Straw	1.140	0.669 ± 0.006	0.59	steel cylinder

From the six BU-U sub-samples, three were extracted by squeezing in copper tubes and three by crushing in the steel cylinder accompanied by mild heating at 50 °C. The soda straw was cut into small pieces, which were crushed in the steel cylinder. Similarly, the BU-1 sample was extracted by crushing in the steel cylinder. The further noble gas purification, separation and measurement procedure as well as the water determination follows the sequences described above and is presented also in detail by Kluge et al. (2008). Most samples had a total weight of about 1 g and yielded a well-measurable water amount of around 0.5 μl (≈ 0.5 mg). The water content was thus quite uniform at nearly 0.5 % wt (Table 4.8). The clearly lower value of sample BU-U0 is due to incomplete crushing in a copper tube. When the tube was opened after the measurement, a comparatively large fraction of coarse grains was found for this sample.

The speleothem pieces of BU-U and the soda straw from Bunker Cave produced relatively high noble gas signals, which together with the quite precisely determined water amounts yield well-defined noble gas concentrations (Table 4.9). With the exception of sample BU-U0,

which yielded small gas amounts because of incomplete extraction, and the Xe measurement in the case of sample BU-U2, the relative uncertainties of the concentrations are about 3 % or less. Comparatively large errors occurred for small Xe amounts from samples crushed in copper tubes due to a significant blank correction in this case.

Table 4.9: Apparent dissolved noble gas concentrations in ccSTP/g , i.e. total measured gas amounts (in ccSTP) per released water amount (in g), for different Bunker Cave speleothems.

Sample	He (10^{-7})	Ne (10^{-7})	Ar (10^{-4})	Kr (10^{-7})	Xe (10^{-8})
BU-Ua	6.56 ± 0.50	10.1 ± 0.4	8.30 ± 0.25	1.57 ± 0.05	2.06 ± 0.68
BU-U0	5.54 ± 0.26	11.0 ± 1.1	8.56 ± 0.39	1.65 ± 0.08	2.57 ± 0.07
BU-U1	14.3 ± 0.4	9.68 ± 0.26	8.27 ± 0.11	1.63 ± 0.03	2.12 ± 0.08
BU-U2	6.84 ± 0.21	8.67 ± 0.28	7.54 ± 0.17	1.50 ± 0.04	2.16 ± 0.24
BU-U3	10.5 ± 0.3	7.88 ± 0.22	7.16 ± 0.08	1.44 ± 0.02	2.00 ± 0.07
BU-U4	6.05 ± 0.14	7.41 ± 0.19	6.86 ± 0.06	1.39 ± 0.02	1.92 ± 0.03
BU-1	5.55 ± 0.12	17.1 ± 0.31	11.3 ± 0.19	1.87 ± 0.04	2.17 ± 0.04
Soda Straw	1.46 ± 0.04	2.40 ± 0.07	4.28 ± 0.04	1.01 ± 0.01	1.60 ± 0.06

In a plot comparing two measured noble gas concentrations, e.g. Kr vs. Ar (Fig. 4.33) or Xe vs. Ne (Fig. 4.34), the relative contribution of noble gases from air-filled inclusions can be estimated. The open circles indicated in these figures represent concentrations of AEW at temperatures between 0 and 30 °C (from top to bottom). The lines leading from these points to higher concentrations represent the effect of air addition. The more distant a sample plots from the AEW points, the more noble gases are contributed by air-filled inclusions. Projecting a sample along an excess air line onto the curve connecting the AEW points yields its equilibration temperature based on the two plotted noble gases. Fig. 4.33 and Fig. 4.34 show that all the samples scatter in the range between 0 and 5 °C, except the soda straw, which lies around 6 °C and the BU-1 piece at about 7 °C.

The final NGTs obtained by the fitting procedure (Table 4.10) slightly differ from the values indicated by Figures 4.33 and 4.34, as they take the information from all four atmospheric noble gases into account. The optimal model parameters T and A are obtained by minimising the sum of the error-weighted squared deviations between measured and modeled concentrations, denoted as χ^2 . The goodness of fit can be assessed by the χ^2 -value, which for 2 degrees of freedom (4 measured concentrations and 2 free parameters) has an expectation value of 2 and a probability of 0.99 to be smaller than 9.2. Only one of the 8 samples yields a slightly larger χ^2 (BU-U4 with $\chi^2 = 9.3$, Table 4.10), the others are well described by the simple UA model of equation (2.9) (chapter 2.3.2) within the limits of the experimental errors. This result confirms the assumption that unfractionated air is present in the stalagmites in addition to an AEW component.

A surprising result obtained from the soda straw sample is the extremely low fraction of noble gases derived from air-filled inclusions. An air/water volume ratio A of $(1.80 \pm 0.39) \cdot 10^{-3}$ was determined, which provides optimal conditions for the NGT calculation. Therefore, the temperature uncertainty for this sample is only about ± 0.4 °C, showing that is possible to achieve high precision NGTs at least from selected speleothems.

As already observed in Figs. 4.33 and 4.34, the NGTs of all samples from the BU-U stalagmite scatter around the same temperature, whereas the soda straw and BU-1 yield significantly higher values. Even if we do not have completely identical samples and at least small deviations have to be expected, the temperatures of the BU-U samples are astonishingly similar and reproduce within their uncertainty. It is important to mention that the shown results derive from different measurement runs with different ion-source tuning, peak shapes and measurement methods as well as from a different extraction procedure (in copper tubes or

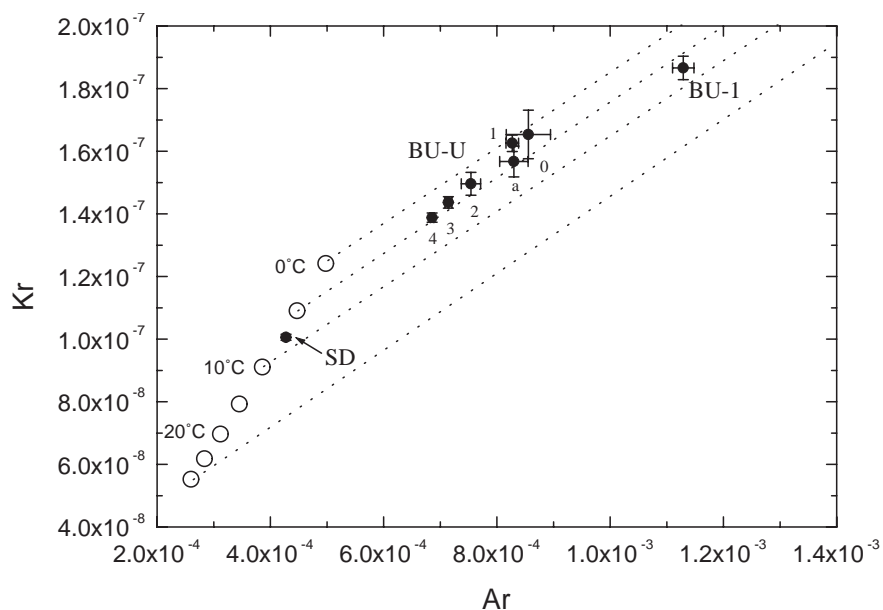


Figure 4.33: Noble gas concentrations in ccSTP per gram of water from fluid inclusions, Kr vs Ar. The open circles on the left hand side represent water equilibrated with atmospheric air (AEW) at temperatures from 0 °C (uppermost point) to 30 °C (lowest point). Samples are shown with error bars, SD: soda straw, the numbers for BU-U indicate the corresponding subsamples. The dotted lines indicate the effect of addition of air to the equilibrated water. As the air component is relatively small, back-extrapolation along such lines yields a well-defined equilibration temperature for each pair of measured noble gas concentrations.

in the steel cylinder) and with different preparation and pumping procedures. Furthermore, measurements of pieces from the same layer in a subsequent run yielded also temperatures in agreement with the older results, even if the extraction procedure was changed (different number of strokes and steps), the preparation was done more sophisticated (baking out of the new steel crusher at 150 °C overnight) and the measurement scripts and procedures have been replaced or written completely new. In between also the filament of the ion-source was changed. This surprising reproducibility underlines the robustness of the obtained results for all subsamples from this growth period and gives a certain confidence in the obtained results. However, to assess whether the NGTs and the temperature differences are plausible, a comparison with present-day temperatures as well as with results of other palaeoclimate studies is necessary.

The BU-U sub-samples give a mean temperature of (2.9 ± 0.7) °C, about 7 °C cooler than the modern cave and air temperatures. The recent mean annual air temperature in the region of Bunker Cave is about 9.5 °C (1961 - 1990 mean of the station Hagen-Fley of the German weather service DWD). The cave temperature is measured since 2006 in the framework of a monitoring program and shows a mean of about 10.5 °C. The single soda straw sample from the Bunker Cave yields a NGT of 6.4 ± 0.4 °C, about halfway between the cold temperatures indicated by the stalagmite samples and the warm modern cave temperature. The young BU-1 sample resulted in a similar temperature of 7.1 ± 0.8 °C.

To assess whether the derived NGTs and temperature differences are plausible, the age of the samples has to be considered. U/Th measurements on the same growth layer of the stalagmite BU-U led to an age of 10 800 - 11 700 years, which indicates that the measured BU-U parts are from the end of the Younger Dryas or the beginning of the Holocene (Preboreal). Because the whole soda straw was needed for noble gas measurements, there was no material

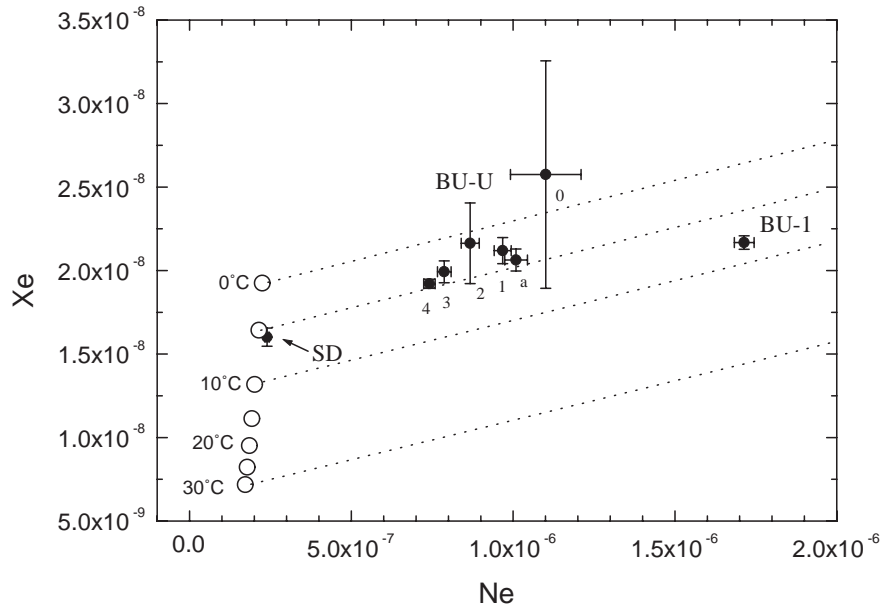


Figure 4.34: Noble gas concentrations in ccSTP per gram of water from fluid inclusions: Xe vs Ne. The open circles on the left hand side represent water equilibrated with atmospheric air (AEW) at temperatures from 0 °C (uppermost point) to 30 °C (lowest point). Back-extrapolation along the excess-air lines yield a well-defined equilibration temperature for each pair of measured noble gas concentrations.

left to determine a U/Th age. Therefore, we considered the use of radiogenic He to estimate its age (Table 4.10). As discussed in the precedent section, the feasibility of using He for quantitative dating of stalagmites certainly needs further investigation. However it seems possible to derive some qualitative statements. The mean concentration of radiogenic He per weight of carbonate is around $2.6 \cdot 10^{-10} \text{ cm}^3 \text{ STP g}_{\text{carb}}^{-1}$ in the case of the stalagmite BU-U. The radiogenic He content of the six samples scatters considerably around this mean value, which can be related to the extraction efficiency. Since the soda straw sample was extracted by relatively efficient milling in the steel cylinder, its low radiogenic He concentration of $5.3 \cdot 10^{-11} \text{ cm}^3 \text{ STP g}_{\text{carb}}^{-1}$ indicates a younger age compared to the stalagmite if we assume a similar U content. The 1 300 yr old BU-1 sample contains $5.1 \cdot 10^{-11} \text{ cm}^3 \text{ STP g}_{\text{carb}}^{-1}$ radiogenic He, which is very similar to the soda straw result. Using the empirically found relation between radiogenic He per g of calcite and the speleothem age, the soda straw is most likely of Holocene origin with an age between some 100 years and at most 3 kyr. Assuming the same U and Th content than for the BU-U stalagmites an age of about 4 400 yr is obtained based on the equations (4.5) - (4.10).

Several studies applying the noble gas thermometer in groundwater indicate that the last glacial maximum in central and northern Europe was at least 5 °C and up to 9 °C colder than the Holocene (Andrews and Lee, 1979; Stute and Deák, 1989; Beyerle et al., 1998; Loosli et al., 2001). 7 °C colder than present temperatures are therefore plausible for the Pleistocene including the Younger Dryas, but may seem rather low for the Preboreal. On the other hand, Kloppmann et al. (1998) reported up to 8 °C cooler than present NGTs in groundwater of the Paris Basin that was dated in the Early Holocene. Thus, the substantially cooler than present NGTs from the BU-U stalagmite are not unreasonable. Additionally, as we only have few dating points for this growth layer, the samples may originate from the latest part of the Younger Dryas. Taylor et al. (1997) reported the transition time span to be from 11 700 to 10 200 B.P. using the $\delta^{18}\text{O}$ from the GSIP2 ice core.

Table 4.10: Fitting results for the Bunker Cave speleothems. The age is determined for BU-U and BU1 by the U/Th method. Noble gas (equilibration) temperature (NGT), air/water volume ratio (A), and total radiogenic He amount were derived by inverse modeling using the program "noble" (Peeters et al., 2003). Pressure was fixed according to the altitude of the cave of 180 m asl and zero salinity was assumed. χ^2 is the sum of the error-weighted squared deviations between model and data (Aeschbach-Hertig et al., 1999).

Sample	Age (years)	NGT ($^{\circ}\text{C}$)	$A(-)$	$\chi^2 (-)$	radiogenic He (10^{-10} ccSTP)
BU-Ua	10 800 - 11 700	3.2 ± 0.9	0.043	1.1	5.04
BU-U0	10 800 - 11 700	2.4 ± 2.9	0.045	1.2	0.43
BU-U1	10 800 - 11 700	1.7 ± 0.7	0.040	2.6	6.09
BU-U2	10 800 - 11 700	3.6 ± 1.1	0.035	2.3	2.22
BU-U3	10 800 - 11 700	3.3 ± 0.7	0.030	5.2	3.47
BU-U4	10 800 - 11 700	3.5 ± 0.9	0.026	9.3	3.19
BU1	1300	7.1 ± 0.8	0.081	4.9	0.72
Soda Straw	holocene	6.4 ± 0.4	0.0018	4.8	0.61

As the soda straw sample is assumed to be considerably younger than the BU-U stalagmite samples, it makes sense that it yields a significantly higher NGT. Furthermore, its value is in agreement with the result of BU-1. It seems to indicate a significant warming for the Late Holocene relative to the Early Holocene represented by the older stalagmite samples. Yet, compared to the present day cave temperature, the NGTs of the soda straw and the BU1 sample seem rather low.

Comparisons between NGTs and modern cave or air temperatures should be interpreted with some caution. The NGTs derived from speleothem fluid inclusions are expected to correspond to cave temperatures, but we have not yet been able to demonstrate this with samples from the period of instrumental temperature records. Even if we had a recent stalagmite sample, only mean annual air temperatures would be available for comparison, which probably differ slightly from cave temperatures. For similar reasons, noble gas studies in groundwater usually rely on temperature differences between NGTs from different periods and compare NGTs of modern samples with air or soil temperatures only to support the validity of the method (Andrews and Lee, 1979; Stute et al., 1992, 1995).

The reconstruction of European temperatures based on pollen data from over 500 sites of Davis et al. (2003) indicates that major warming in western central Europe took place around 11 kyr BP. As the BU-U samples may be older than 11 kyr, their substantially cooler than present NGTs are not unreasonable.

The NGT of the sample from BU-1 with an estimated U/Th age of $1\,300 \pm 300$ years is more than 2°C lower than the modern air temperature. Indeed, the period around 700 AD probably was relatively cool. The multi-proxy temperature reconstruction for the northern hemisphere by Moberg et al. (2005) indicates 0.2 to 0.4°C lower temperatures for this period compared to 1961 - 1990. However, both regionally and episodically, temperatures may have been substantially cooler. E.g., Holzhauser et al. (2005) report a major glacier advance in the Alps during the time of 500 to 700 AD. Nevertheless, the NGT of the sample from BU-1 appears rather low. The absolute accuracy of NGTs from fluid inclusions remains to be tested with modern speleothem samples and direct comparison with cave temperatures. Small offsets between NGT and cave temperature, e.g. due to unknown effects influencing the noble gas composition in speleothems, or even to systematic analytical errors as e.g. an underestimation of the released water amount, can presently not be ruled out completely. Marx (2008) revealed crushed calcite to be a very efficient adsorbent for water vapour, which may have reduced the detected water amount.

The relationship between cave and air temperature also needs to be studied for each cave.

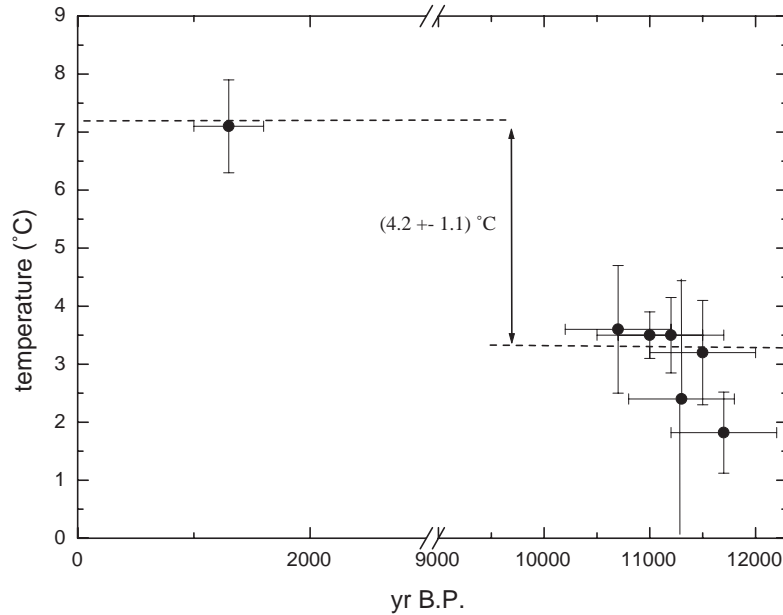


Figure 4.35: Temperature differences for Bunker Cave in western central Europe between the Early Holocene and Early Middle Ages as derived from noble gases in fluid inclusions. The BU-U samples are arranged in the time interval between 10 800 and 11 700 yr BP according to their radiogenic He content.

Yet, the differences between NGTs obtained from individual samples from the same cave should be less affected by such complications. Hence we consider the difference of $(4.2 \pm 1.1) \text{ }^\circ\text{C}$ between the 1 300 yr old BU-1 sample and the ≈ 11 kyr old BU-U samples to be the most reliable palaeoclimatic result of this part of the study (Table 4.35). This result is in good agreement with the temperature reconstruction of Davis et al. (2003), which indicates about $4 \text{ }^\circ\text{C}$ cooler temperatures before 11 kyr compared to recent values in western central Europe, where our site is located.

The most surprising result from this set of measurements is the highly reproducible temperature value of a growth layer from the stalagmite BU-U. Another indication for reasonable temperature determination via noble gas measurements on fluid inclusions is the good agreement of the obtained temperature difference with a high resolution pollen study. Furthermore, the low uncertainty for a soda straw sample of only about $\pm 0.4 \text{ }^\circ\text{C}$ shows that it is possible to achieve high precision NGTs at least from selected speleothems. The precision of the NGTs calculated from the BU-U stalagmite are mostly close to $\pm 1 \text{ }^\circ\text{C}$, which is easily sufficient to resolve glacial-interglacial temperature changes and should, if a sufficient number of samples is available, allow the detection of major temperature shifts within the Holocene. In the following we tried to apply the method on different stalagmites to obtain temperature records along the growth axis.

4.6.2 Case study BU-1

In a first case study we focused on the stalagmite BU-1, which also originates from the Bunker Cave. Due to its generally milky white appearance, we supposed a high water content and a comparably low air contribution. A first test piece did approve this assumption and yielded a precise temperature (s. precedent chapter). Therefore, we tried to measure more points on this Holocene stalagmite and investigated it with regard to temperature changes during the growth period.

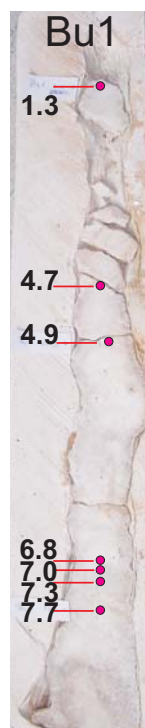


Figure 4.36: Half of BU-1. Locations of sampling for NGT determination are marked with a red circle and anoted with an age in kyr.

BU-1 is a relatively large (67 cm), but rather thin stalagmite ($\approx 5 - 7$ cm) with a candle-stick type shape. Most of the speleothem consists of large columnar crystals. In some periods, which are supposed to have been considerably drier, also dendritic fabric occurs. The stalagmite has grown between 1 kyr and 8 kyr BP with an Eemian part at the bottom (darker layers, s. Fig. 4.36). One hiatus is found between 1.8 and 4 kyr, which is located in the very thin top part of the stalagmite. We extracted 7 samples, one above the hiatus, two in the period of very fast growth at about 5 kyr, and 4 samples between 7 and 8 kyrs, and measured them in two different runs. All samples are extracted by crushing in the steel cylinder using a stepwise procedure consisting of some crushing steps and an optional heating step. Details about the extraction procedure, sample weight and water content are given in Table 4.11.

An interesting feature is the high water content of almost all pieces from BU1. Furthermore the large differences in the released amount of water as well as the water content raise the question about the origin of these deviations. A working hypothesis is discussed in chapter 4.2.5. We will now focus on the temperature information obtained from noble gases in fluid inclusions. The fitting results are summarized in Table 4.12.

Using a stepwise procedure we have been able to reduce the air contribution in each step to values of A of about 0.1 or significantly less (Fig 4.22). This low A was obtained in the heating measurements. Fitting the noble gas concentrations of the heating extraction measurements resulted in a quite good χ^2 of mostly below 1. For 5 of the 7 samples the temperature uncertainty is about 1.5 °C or better. However, this data is not hotblank corrected. It was not possible to measure the hotblank during the measurement run. Thus, we performed a set of totally 5 blank measurements at 150 °C using different steel crushers. Unfortunately, the blank values are scattering strongly by about a factor of 5. Furthermore, the pumping time varied in the case of the speleothem samples between at least 8 hours and 2 or 3 days on week-ends. Therefore, the afterwards measured heating-blanks with a pumping time of generally less than 1 day cannot precisely represent the values in the case of the real samples.

Table 4.11: Total sample weight, released water amount, apparent gravimetric water content, and applied extraction method for the BU-1 stalagmite.

Sample	weight (g)	water amount (μl)	water content % wt	extraction steps
BU1-5	1.424	0.899 ± 0.015	0.63	3 strokes
BU1-22	0.690	2.351 ± 0.023	3.40	5, 60 strokes, heat
BU1-29	0.561	2.352 ± 0.023	4.19	5, 60 strokes, heat
BU1-46	0.514	0.590 ± 0.011	1.15	5, 60 strokes, heat
BU1-49	1.012	0.987 ± 0.014	0.98	5, 60 strokes, heat
BU-51	0.885	2.794 ± 0.026	3.16	5, 60 strokes, heat
BU-55	1.151	7.603 ± 0.052	6.61	5, 20, 60 strokes, heat

Table 4.12: Fitting results for the BU-1 stalagmite. The age is determined from an age model established by the U/Th method. Noble gas (equilibration) temperature (NGT) and air/water volume ratio (A) were derived by inverse modeling using the program "noble" (Peeters et al., 2003). Pressure was fixed according to the altitude of the cave of 180 m asl and zero salinity was assumed. χ^2 is the sum of the error-weighted squared deviations between model and data (Aeschbach-Hertig et al., 1999). The first NGT-, A - and χ^2 -value refers to the not hotblank-corrected heating extraction. The second NGT (NGT-C) was obtained by combinations of the according extraction steps and application of the blank corrections. The mean value refers to the arithmetic mean.

Sample	Age (years)	NGT ($^{\circ}\text{C}$)	$A(-)$	$\chi^2 (-)$	NGT-C ($^{\circ}\text{C}$)	used steps	$\chi^2 (-)$
BU1-5	$1\ 300 \pm 300$	-	-	-	7.1 ± 0.8	3	4.9
BU1-22	$4\ 700 \pm 300$	7.1 ± 1.1	0.036	0.3	3.8 ± 1.1	60, heat	1.5
BU1-29	$4\ 900 \pm 300$	8.6 ± 1.5	0.054	0.6	7.3 ± 1.4	60, heat	1.7
BU1-46	$6\ 800 \pm 600$	4.1 ± 3.9	0.107	0.1	9.8 ± 5.6	60, heat	0.9
BU1-49	$7\ 000 \pm 500$	6.4 ± 2.9	0.061	4.6	7.9 ± 1.6	all	0.3
BU1-51	$7\ 300 \pm 200$	7.7 ± 1.6	0.017	0.4	9.0 ± 1.1	60, heat	0.7
BU1-55	$7\ 700 \pm 300$	7.5 ± 0.8	0.024	0.3	5.9 ± 0.8	60, heat	0.3
mean	holocene	6.9 ± 1.5	0.050	1.1	7.3 ± 2.0	-	1.5

The most reliable results with low temperature uncertainty and good χ^2 stem from the heating measurements of BU1-22, BU1-51 and BU1-55. They are very close or equal to the temperature obtained in the very first measurement of a BU1-piece, even if they represent different periods within the Holocene. Another NGT with good χ^2 refers to BU1-49. Putting together the noble gases of all extraction steps of BU1-49 resulted in a temperature value of 7.9 ± 1.6 $^{\circ}\text{C}$. Calculating the arithmetic mean of these four samples and BU1-5 results in a temperature of 7.5 ± 0.4 $^{\circ}\text{C}$. This is the most reliable result of this case study as it refers to data points with best fitting results and lowest uncertainties.

Using the not-hotblank corrected data is justified by the similarity of their values. They correspond to the corrected data within their uncertainty (except BU1-22, Table 4.12, Fig. 4.37). Similarly, the mean values calculated from both data sets are astonishingly consistent. However, in most cases the result of the combined fitting, including the 60 strokes and heating measurement, is slightly worse than the χ^2 of the hot extraction. This may be mainly due to the applied blank correction in the case of the combined fitting. The hotblank correction seems to be a little bit too strong, as in the case of tiny samples the resulting gas amounts become negative. Furthermore, the uncertainty of the correction is quite large, which leads to increased temperature uncertainties for the combined data set.

Although some more measurements have to be done in the future on this stalagmite, first interpretations are possible using the most reliable data points (BU1-5, BU1-22, BU1-49, BU1-51, BU1-55). They result in an arithmetic mean value of 7.5 ± 0.4 $^{\circ}\text{C}$ and exclude temperature variations larger than 2 $^{\circ}\text{C}$ within the last 8 kyr of the Holocene, at least in the investigated periods. Ojala et al. (2008) found minor temperature variations for the high latitudes in Eu-

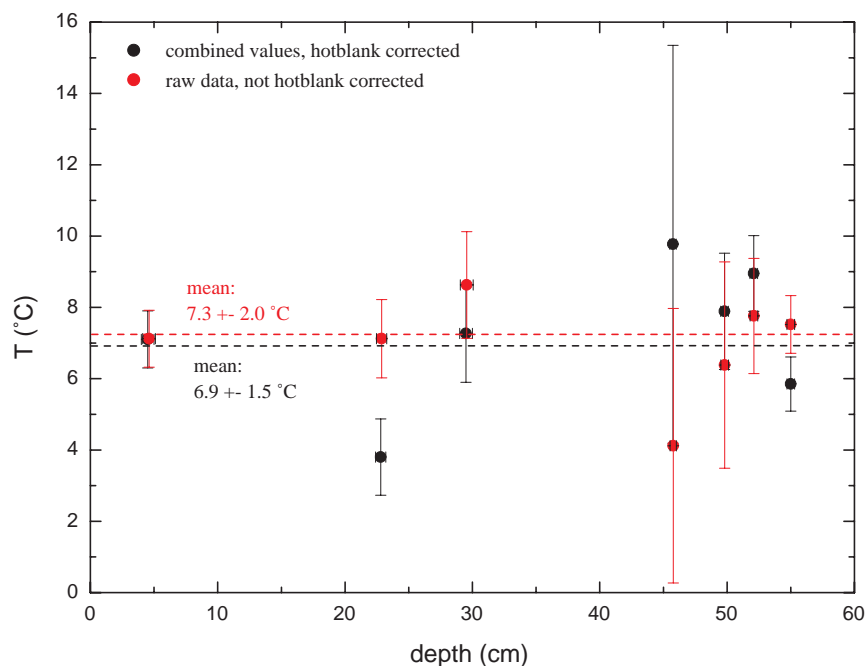


Figure 4.37: NGT from BU-1 samples. Red points refer to the results of the heating measurements (not hotblank corrected), the black points to the fitting results of combined steps. The dotted line indicates the mean values for each case.

rope during the last 8 kyr with variations of less than 1 °C from the mean annual temperature in this period. Nevertheless, systematic trends are detected for summer temperatures as well as for mean annual values from pollen- and varve-based reconstructions. This findings may be only of regional importance. However, Viau et al. (2006) report on mean July temperature anomalies in Northern America on the order of only 0.2 °C in the last 8 kyr based on more than 750 fossil pollen records. The Holocene optimum July temperatures are found between 6 kyr and 3 kyr BP. Similarly, Ojala et al. (2008) stated the warmest period in Northern Europe to be between 8 kyr and 4 kyr BP. Unfortunately, we can until now not resolve such small temperature variations of some tenth of degrees, but all the mentioned studies suggest temperature variations to be <1 °C during the Holocene growth period of BU-1. This is also in agreement with the interpretation of the $\delta^{18}\text{O}$ values from two Greenland ice cores. Grootes et al. (1993) interpreted the small variations in the $\delta^{18}\text{O}$ signals (1-2‰) to be an indication for a remarkably stable climate during the Holocene. On a regional scale Davis et al. (2003) investigated the temperature anomalies during the Holocene throughout Europe and found especially in the region of the Bunker Cave very small changes in the last 7 kyr (± 0.3 °C). From 7 to 8 kyr BP they suggest a temperature decrease of about 1 °C. Comparing the results of these studies with our own measurements, a rather good correlation can be observed. The most reliable NGTs suggest the temperature to have been stable during the investigated period. Nevertheless, variations in the range of ± 1 °C can not be excluded due to the relatively large uncertainties of the single measurements.

Particularly interesting is a closer view on the stable isotope data and the comparison with NGTs as well as with the water content as supposed precipitation proxy. The stable carbon and oxygen isotope curves of BU-1 are displayed in Fig. 4.38. Apart from high frequency fluctuations in the BU-1 stable isotope curve also a longterm trend can be found. One maximum is located at the top at ≈ 1 kyr BP, the second at 6 kyr BP (~ 40 cm from top) and the last at 8 kyr BP (~ 60 cm from top). A similar trend is obvious in the $\delta^{13}\text{C}$ values.

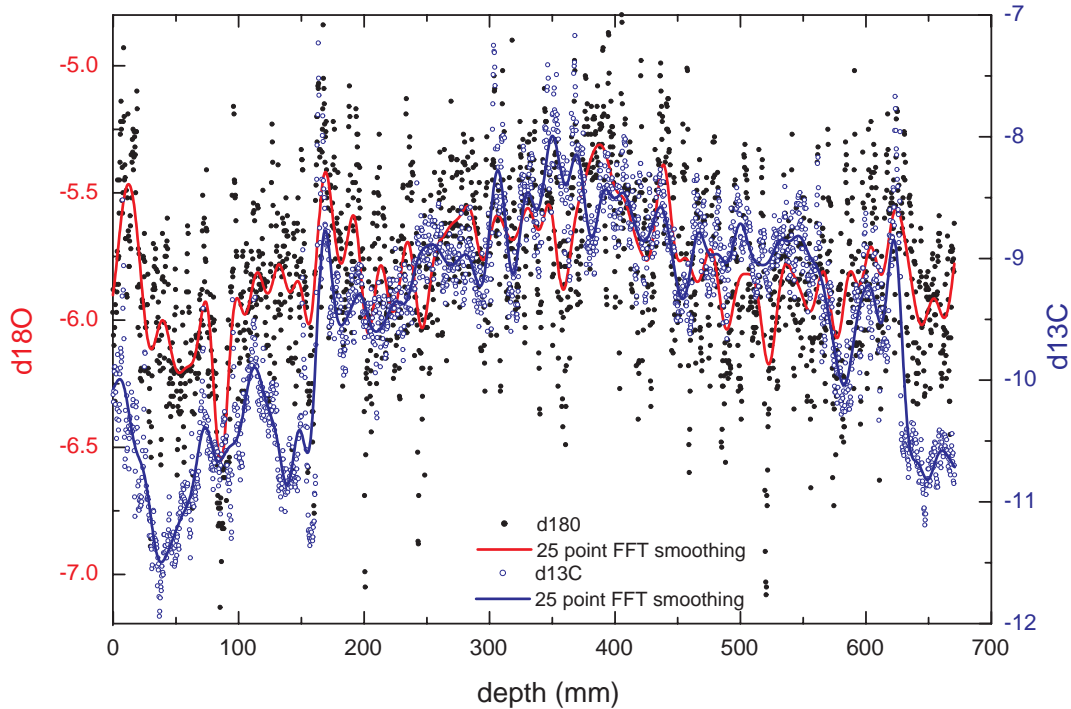


Figure 4.38: Stable oxygen and carbon isotope data of BU-1. Based on the single measurements a curve has been fitted applying 25 points FFT smoothing. Each 300 μm isotopes have been measured. The data have been measured in the framework of the DAPHNE-project and were provided by C. Spötl.

The major question is related to the origin of these fluctuations. In $\delta^{18}\text{O}$ the variations are small and in maximum only about 1 ‰. If we transferred this into temperature, as it has been done e.g. by Friedman and O’Neil (1977) (-0.24 ‰ per $^{\circ}\text{C}$), it would indicate a temperature change of about 4 $^{\circ}\text{C}$ from maximum (5 kyr) to minimum (1.3 kyr). The most reliable NGT results, belonging to maxima as well as to minima periods of $\delta^{18}\text{O}$, can certainly exclude such large temperature variation. The stable isotope signals are influenced by different effects (s. e.g. McDermott (2004)) and are therefore difficult to interpret without additional information. $\delta^{18}\text{O}$ in the calcite is influenced by changes in the precipitation source and amount and may additionally be altered by different kinds of fractionation during calcite precipitation (equilibrium vs. kinetic fractionation). Furthermore, the $\delta^{18}\text{O}$ of the rain is temperature dependent and can change also the oxygen isotopy of the calcite. However, the temperature dependence can be site-specific and may have changed in the past. Therefore it cannot be used to determine unambiguous temperatures only with the isotope information. However, $\delta^{18}\text{O}$ shows in some cases an interesting link to precipitation (Niggemann et al., 2003; Fleitmann and Burns, 2004; Cruz et al., 2005; Wang et al., 2008). As the temperature variations were expected to be small during the growth period of BU-1 it is not unreasonable, that the isotope signal of BU-1 was strongly influenced by precipitation. The periods with a more positive $\delta^{18}\text{O}$ also may be warmer periods, but coincide well with wetter phases reconstructed from pollen (Seppä and Birks, 2001). Similarly, the interpretation of the water content as a proxy for precipitation confirms this assumption (Fig. 4.13). A low water content is found for the more negative $\delta^{18}\text{O}$ and significantly higher values in the case of the less depleted oxygen. Even if this interpretation is not well constrained at the older stalagmite part, the general agreement encourages the additional use of the speleothem water content. The less depleted $\delta^{18}\text{O}$ is possibly caused by a change in the atmospheric circulation pattern, delivering precipitation not only from a different source but also in a higher quantity.



Figure 4.39: Pieces cut out from the growth-axis of BU-U. A darker brownish layer separates the Early Holocene from Marine Isotope Stage 3 (MIS3) and another dark layer MIS3 from the Eemian. The pieces are numbered for referencing. The total length from sample no.1 to no.15 is about 77 mm.

Combining all results can provide a meaningful interpretation of the climate of the last 8 kyr in Northwestern Germany. Most likely, the temperature variations have been smaller than 2 °C. Thus the enhanced signal variations in $\delta^{18}\text{O}$ may be provoked by changes in the precipitation pattern and the atmospheric circulation. This examples show the importance of reasonable temperature calculations via noble gases in fluid inclusions. Using the NGTs it is possible to constrain the hypothesis or to exclude some possibilities, as e.g. in the case of BU-1, temperature changes by 4 °C within the Holocene.

4.6.3 Case study BU-U

Noble gas measurements on BU-1 revealed rather stable temperatures during certain periods of the Holocene. The determined NGTs agree with the expectations. As the assumed variations are quite small within the Holocene, it is rather difficult to confirm the small changes with NGTs. However, the difference between Holocene and Glacial values should be easily detectable. Therefore, we made a set of measurements on the stalagmite BU-U, which cover the Early Holocene, Marine Isotope Stage 3 and also the Eemian (Fig. 4.31). The stalagmite was cut into two halves, one for U/Th dating and one for stable isotope, trace element and noble gas measurements. The latter have all been measured on one small slice (5 mm x 10 mm) cut out near the growth axis (Fig. 4.39). In summary, we extracted 15 samples, seven from the Early Holocene, two from the period of Marine Isotope Stage 3, and six samples from the Eemian and measured them in two different runs. All samples were extracted by crushing in the steel cylinder using a stepwise procedure consisting of some crushing steps and an optional heating step. Details about the extraction procedure, sample weight and water content are given in Table 4.13.

We will now focus on the temperature information gained from the noble gas measurements. A summary of temperature values and the air-water volume ratios is given in Table 4.14. In some cases the temperature uncertainty is quite high, which is due to background correction and also due to tiny samples (mostly < 1 g, down to 0.4 g) as well as influenced by medium air/water volume ratios. However, about half of the samples yield well defined temperatures with an uncertainty below 2 °C. In general, the model fits quite well to the measured noble gas concentrations and therefore the χ^2 is about 1 or even better. Only regarding one measurement the obtained temperature is unlikely, as the χ^2 is about 25 and indicates a bad fit. The background correction for this sample was very strong for some noble gases and perhaps led to an over-correction. Except of one speleothem piece, all samples resulted in realistic temperatures above 0 °C. To assess whether the results are reasonable, we have to take into account the age of the growth periods. To get an impression of the temperature development along the growth axis, the fitted temperatures are summarized in Fig. 4.40.

Table 4.13: Total sample weight, released water amount, apparent gravimetric water content, and applied extraction method for the BU-U stalagmite

Sample	weight (g)	water amount (μl)	water content % wt	extraction steps
BUU-2	1.401	0.381 ± 0.008	0.27	50 strokes, 100 + heat
BUU-3	0.776	0.290 ± 0.008	0.37	60 strokes, 100 + heat
BUU-4	1.750	0.509 ± 0.010	0.29	7, 60, 160 strokes
BUU-5	0.587	0.064 ± 0.006	0.11	60 strokes, 100 + heat
BUU-6	0.795	0.080 ± 0.004	0.10	60 strokes, 100 + heat
BUU-8	0.885	0.218 ± 0.013	0.25	5, 60 strokes, heat
BUU-9	1.331	0.141 ± 0.008	0.11	60 strokes, 100 + heat
BUU-10	1.123	0.748 ± 0.012	0.67	7, 60, 160 strokes
BUU-11	1.134	0.759 ± 0.012	0.67	7, 60, 160 strokes
BUU-12	0.619	0.435 ± 0.009	0.70	60 strokes, 100 + heat
BUU-13	0.680	0.507 ± 0.011	0.75	5, 60 strokes, 50 + heat
BUU-14	0.727	0.442 ± 0.008	0.61	60 strokes, 100 + heat
BUU-15	0.397	0.162 ± 0.008	0.41	60 strokes, 100 + heat

Table 4.14: Fitting results for the BU-U stalagmite. The age was determined by the U/Th method on several points within the different growth layers. Noble gas (equilibration) temperature (NGT) and air/water volume ratio (A) were derived by inverse modeling using the program "noble" (Peeters et al., 2003). Pressure was fixed according to the altitude of the cave of 180 m asl and zero salinity was assumed. χ^2 is the sum of the error-weighted squared deviations between model and data (Aeschbach-Hertig et al., 1999). NGTs were obtained by combinations of the according extraction steps.

Sample	Age (years)	$A(-)$	NGT ($^{\circ}\text{C}$)	used steps	$\chi^2 (-)$
BUU-2	10 800 - 11 700	0.106	1.0 ± 0.9	all	0.2
BUU-3	10 800 - 11 700	0.131	4.2 ± 1.3	60 strokes	0.0
BUU-4	10 800 - 11 700	0.076	3.2 ± 1.4	60, 160 strokes	0.7
BUU-5	10 800 - 11 700	0.272	0.0 ± 6.8	60 strokes	0.4
BUU-6	10 800 - 11 700	0.204	$< 0^{\circ}\text{C}$	60 strokes	0.2
BUU-8	$52\,900 \pm 1\,300$	0.102	4.0 ± 4.1	all	0.1
BUU-9	$52\,900 \pm 1\,300$	0.227	0.9 ± 3.8	60 strokes	0.5
BUU-10	125 000 - 134 000	0.236	6.0 ± 2.3	60, 160 strokes	1.4
BUU-11	125 000 - 134 000	0.255	11.1 ± 3.0	60, 160 strokes	1.5
BUU-12	125 000 - 134 000	0.0	5.0 ± 1.7	heat	25.1
BUU-13	125 000 - 134 000	0.667	8.7 ± 5.3	all	0.3
BUU-14	125 000 - 134 000	0.281	5.6 ± 1.8	all	5.7
BUU-15	125 000 - 134 000	0.293	2.5 ± 4.0	60 strokes	0.3

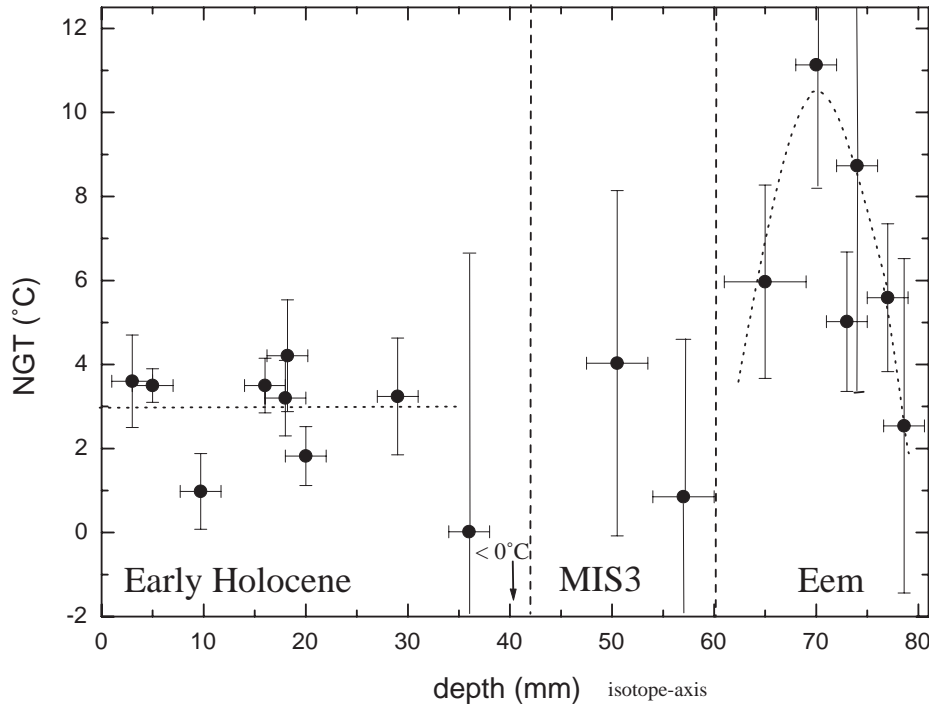


Figure 4.40: NGTs derived from the growth axis of BU-U. In the early Holocene part samples are added from the first measurement campaign focused on this single layer (chapter 4.6.1).

The Early Holocene is characterized by a mean temperature of about 3 °C. Only BUU-2 and BUU-6 are significantly lower. BUU-5 also shows a low temperature, but can not be distinguished from the mean due to the large uncertainty. Taking into account the previous measurements on this growth layer (s. chapter 4.6.1) the arithmetic mean value is $(2.9 \pm 1.0)^\circ\text{C}$. For this calculation the NGT below 0 °C (BU-6) as well as BU-5 were discarded. The temperatures from MIS3 can not be distinguished from values from the Early Holocene due to the rather large uncertainties. This is also reflected in the mean value of $(2.5 \pm 2.2)^\circ\text{C}$. The Eemian differs totally from the other two periods. There we did not find constant temperatures, but rather a temperature evolution with its highest value at ~ 130 kyr BP.

Until now we have not been able to demonstrate that the determined temperatures are exactly identical with the expected temperatures during growth, as we have not yet examined recent calcite precipitates. The mean annual air temperature in the region around the Bunker Cave was 9.5 °C (1960 to 1990). Today, a temperature of about 10.5 °C is measured in the cave. Several measurements on the stalagmite BU-1 resulted in a mean value of about 7 °C. Many studies suggest only minor temperature variations during the growth of BU-1 (the last 8 kyr). Thus, our relatively low NGTs from BU-1 compared to the cave temperature indicate a systematic deviation from the expected values. Recent tests lead to the assumption that incomplete water collection due to adsorption on the crushed stalagmite is responsible for this deviation. However, as we did not substantially change the extraction process a similar systematic offset should occur for all samples. Thus, the temperature differences between the growth periods of BU-U are the most reliable results.

As a Holocene reference temperature we use the NGT of $(7.5 \pm 0.4)^\circ\text{C}$ (chapter 4.6.2). Assuming that the 1960-1990 period to be representative for the Holocene, the systematic deviation of the speleothem NGT to annual air temperatures is $(2.0 \pm 0.6)^\circ\text{C}$. With regard to the

palaeotemperatures from the Bunker Cave speleothems, the Early Holocene is $(4.6 \pm 1.1) ^\circ\text{C}$ cooler than present day values, that means at about $(4.9 \pm 1.1) ^\circ\text{C}$. This is in good correspondence with pollen data from Central Europe (Davis et al., 2003). Using the two data points from Marine Isotope Stage 3, this period was $(5.0 \pm 2.3) ^\circ\text{C}$ cooler than today, resulting in a mean annual air temperature of $(4.5 \pm 2.5) ^\circ\text{C}$. Due to few samples from this part and their unfavorable properties, the temperature uncertainty is quite high and thus the mean can not be distinguished from the Early Holocene values. Another stalagmite from the same cave, BU-2, has a larger growth layer corresponding to MIS3. From this layer (about 51 kyr old) we measured one piece, resulting in a NGT of $(4.85 \pm 0.57) ^\circ\text{C}$. This is warmer than the NGT mean of the two samples from BU-U. As the MIS3 layer of BU-U was very small, the single values may have been affected by a mixture with other layers. However, taking into account the large uncertainty of $2.2 ^\circ\text{C}$, the BU-2 value is in agreement with the BU-U mean ($2.5 ^\circ\text{C}$). Swann et al. (2005) investigated diatoms, C/N ratios and organic carbon isotope ratios in lake Baikal and detected that the period between 54 and 51.5 kyr BP to had relatively warm interstadial conditions. This corresponds to the interstadial 14 (GIS 14), detected also in a high alpine stalagmite, which was dated to last between 54.2 and 51 kyr BP (Spoetl and Mangini, 2002). They state the GIS 14 to have been the longest D/O warm phase during MIS3. As the stalagmite originates from a high alpine cave (≈ 2165 m asl) with an interior present-day cave temperature of $2.3 ^\circ\text{C}$, temperatures during GIS 14 should not have been significantly below contemporary values, at least not significantly below $0 ^\circ\text{C}$, to enable speleothem growth. Cabioch and Ayliffe (2001) detected relatively high sea levels at about 50 kyr BP from coral sample measurements. They estimate the sea level to have been only 30 - 60 m below contemporary values, in contrast to 110 to 130 m below present-day values in the last glacial maximum. Similar features have also been found in the stable oxygen isotope record of Greenland ice cores (Johnsen et al., 2001). Converting the ice-core data into temperature the GIS 14 is about $7 ^\circ\text{C}$ cooler than Holocene values. The difference to the last glacial maximum is about $20 ^\circ\text{C}$. In Central Europe the last glacial maximum was $5 - 9 ^\circ\text{C}$ cooler (Andrews and Lee, 1979; Stute and Deák, 1989; Beyerle et al., 1998; Loosli et al., 2001). Using a mean value of $7 ^\circ\text{C}$ and assuming a similar relation for the GIS 14, the downscaling of the Greenland temperature differences suggested the GIS 14 temperature to be $2.5 ^\circ\text{C}$ cooler compared to present-day values in Central Europe. This value corresponds to the mean of the two BU-U pieces from the GIS14 taking into account the large uncertainty. However, it would fit perfectly to the measurement on a single piece of the BU-2 stalagmite, which suggests a temperature of $(2.6 \pm 0.8) ^\circ\text{C}$ below present-day values. Again, the stalagmite NGTs show the possibility to better constrain the continental climate and especially the temperature. Despite the rather few measurements with relatively large uncertainties, the NGT range of the GIS14 can be fixed to $4.1 - 5.3 ^\circ\text{C}$ calculating the weighted mean of the two values from BU-U and the measurement of BU-2. Taking into account the systematic offset between NGT and mean annual air temperature, the mean air temperature value for GIS 14 in the Bunker cave region is $(7.2 \pm 0.8) ^\circ\text{C}$.

Another very interesting palaeoclimatic epoch is the Eemian period, which is also contained in stalagmite BU-U. There we found considerably higher temperatures compared to GIS 14 and the Early Holocene (Fig.4.40). The temperature values of the three periods contained in BU-U follow the expected temperature trend during the last Glaciation known e.g. from ice core data (Petit et al., 1999; Kawamura et al., 2007). Assuming the two uppermost points to be representative for the Eemian maximum the temperature is $(10.5 \pm 2.6) ^\circ\text{C}$ calculated via a weighted mean of NGTs. Unfortunately, so far we only have few NGTs to better constrain this value indicating a $\approx 3 ^\circ\text{C}$ warmer Eemian period (absolute value: $12.5 ^\circ\text{C}$) compared to contemporary values. Kukla et al. (2002) stated the Eemian to have been at least as warm as the present climate, based on coral, deep-sea sediment, ice-core, speleothem and pollen data.

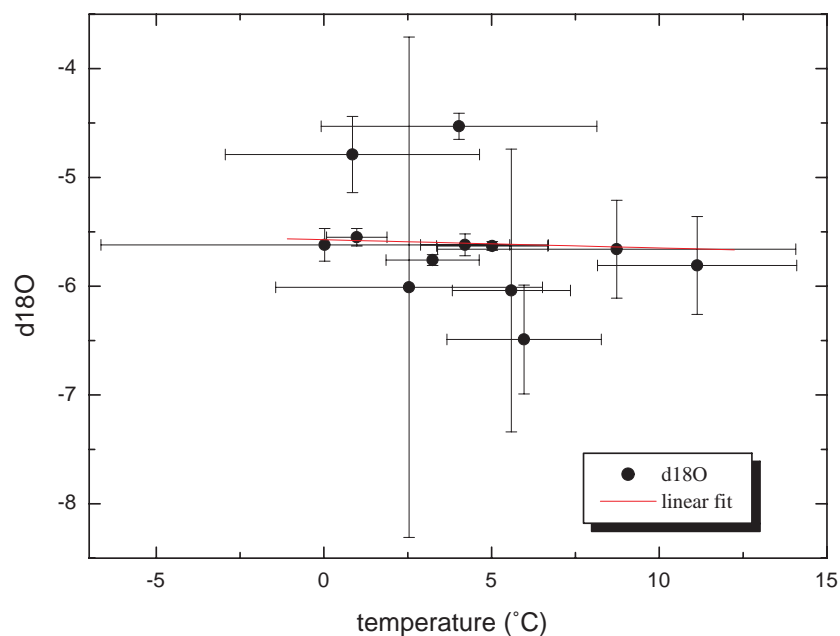


Figure 4.41: NGTs from the growth axis of BU-U compared to averaged $\delta^{18}\text{O}$ -values. The $\delta^{18}\text{O}$ was calculated by averaging the isotope values in the range of the corresponding NGT sample. The uncertainty in $\delta^{18}\text{O}$ was determined by variation of the interval in consideration of the uncertainty in the location of the NGT sample (typically 2 mm).

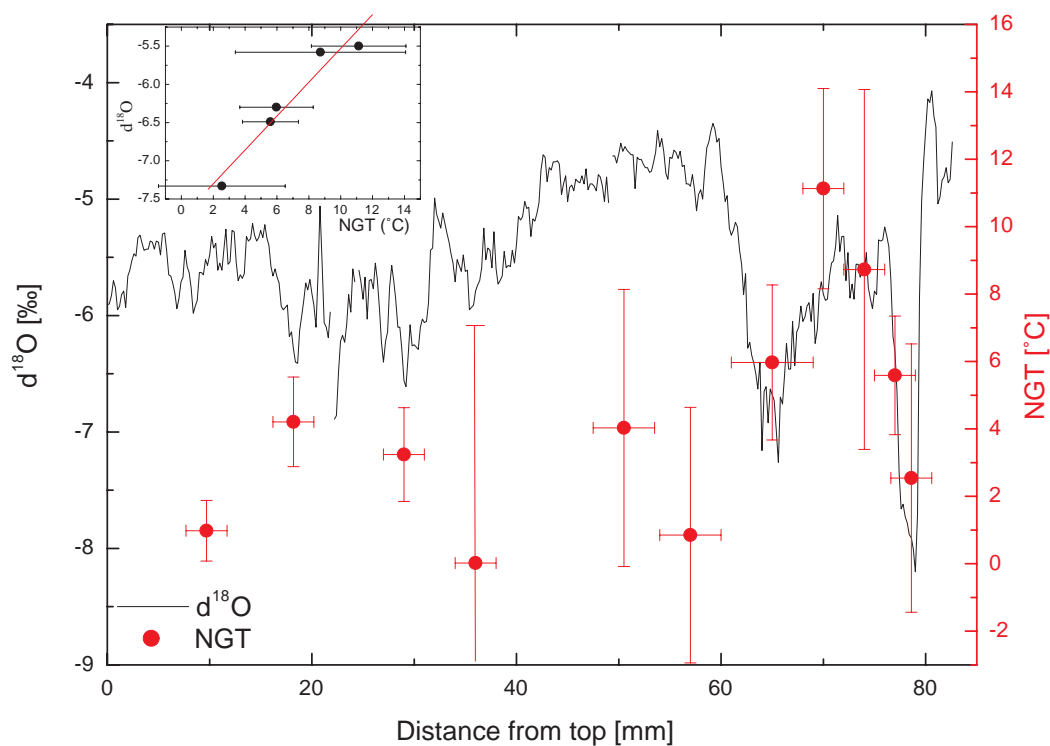


Figure 4.42: NGTs from the growth axis of BU-U compared to the continuous $\delta^{18}\text{O}$ record. In the insert the correlation between the NGT and $\delta^{18}\text{O}$ in the Eemian period is displayed.

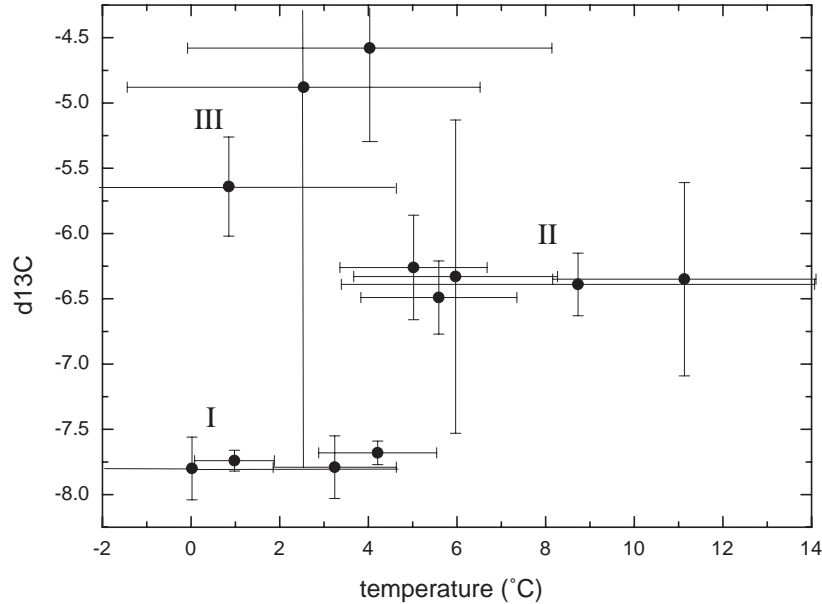


Figure 4.43: NGTs from the growth axis of BU-U compared to $\delta^{13}\text{C}$ -values. The $\delta^{13}\text{C}$ was calculated by averaging the isotope values in the range of the corresponding NGT sample. The uncertainty in $\delta^{13}\text{C}$ was determined by variation of the interval in consideration of the uncertainty in the location of the NGT sample (typically 2 mm). The data points of section I refer to the Early Holocene, II to the Eemian and III to GIS 14, respectively the beginning of the Eemian.

For the western Central Europe Zagwijn (1996) stated the winter maximum to be 3 °C and the summer maximum to be 2 °C above present day values in this region. This fits very well to our speleothem measurements and the determined NGTs. Furthermore, the interpretation of the pollen data with regard to precipitation correspond also to the interpretation of the water content in BU-U. Zagwijn (1996) claims the beginning of the Eemian to have been relatively dry with increasing precipitation and later a generally rather oceanic climate with higher precipitation than in the Holocene. A nicely corresponding trend can be drawn from the water content, including significantly higher precipitation in the Eemian maximum compared to early Holocene values (Fig. 4.18). Klotz et al. (2003) detected from pollen reconstruction in the northern alpine foreland also a more oceanic climate with warmer and more humid periods in the Eemian. Similarly, Aalbersberg and Litt (1998) inferred from pollen data that the summer temperatures were several degrees higher in Southern England than present-day values. Felis et al. (2004) used coral records in combination with a coupled atmosphere-ocean circulation model to infer the influence of the North Atlantic Oscillation during the last interglacial period. The climate model produced for the Bunker Cave region a winter temperature with little deviation from modern values, but up to 1.5 °C warmer summer values. In summary, a warmer Eemian (in comparison with Holocene temperatures) as derived from NGTs of the Bunker Cave speleothem BU-U is reasonable and shows similar trends like other climate proxies.

Using the temperature information from the noble gas measurements on the fluid inclusions, we are now able to better interpret the stable isotope curves (Fig. 4.44). Comparing the NGTs with the $\delta^{18}\text{O}$ -values of the same periods does not reveal any significant correlation with temperature in the Early Holocene and GIS 14 (Fig. 4.41). The two results from GIS 14 are slightly separated from the rest (two uppermost points). Focusing only on the Eemian period a correlation between $\delta^{18}\text{O}$ and temperature is visible (Fig. 4.42). Higher temperatures

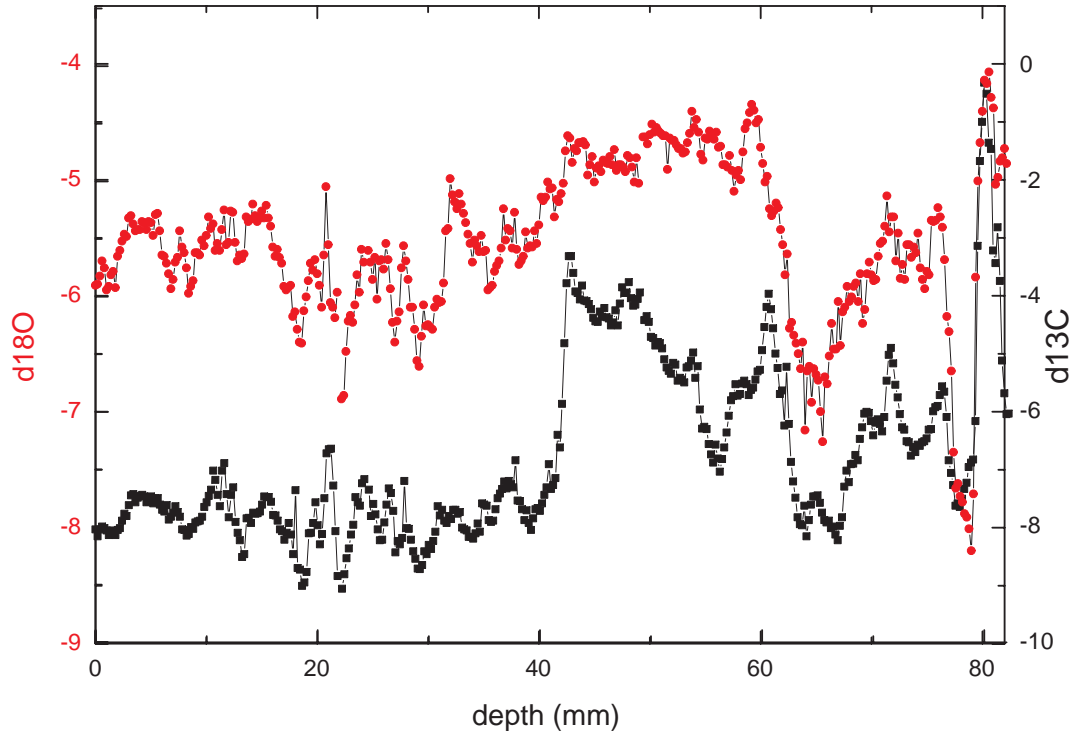


Figure 4.44: $\delta^{13}\text{C}$ and $\delta^{18}\text{O}$ values along the growth axis of BU-U. The stable isotopes have been provided by Dr. C. Spötl.

refer to a less depleted oxygen value, whereas lower temperatures are correlated with a more negative $\delta^{18}\text{O}$ value. Calculating a mean $\delta^{18}\text{O}$ value for the periods covered by the NGT samples and comparing them with the temperature values suggest a high correlation for this epoch with a correlation coefficient of $R=0.97$. The slope of this relation is $0.22 \pm 0.03 \text{ ‰ per } ^\circ\text{C}$. A clearly distinct pattern can be found in the case of the $\delta^{13}\text{C}$ -values. Although, again there is no simple relationship with temperature, the points are arranged according to the corresponding growth period: I Early Holocene, II Eemian and III intermediate points from GIS 14 and the beginning of the Eemian. It looks like a step function with two different stable states. Between 4.2 and $4.5 \text{ }^\circ\text{C}$ the system jumps between the two states. The Early Holocene is characterized by a mean value of $-(7.75 \pm 0.06)\text{‰}$ and the Eemian by $-(6.36 \pm 0.08)\text{‰}$. The reason for such pronounced differences is most likely a change of vegetation above the cave. The $\delta^{18}\text{O}$ -values seems, in some periods, to correlate very well with temperature (Fig. 4.42), but can furthermore show a certain agreement with the trend in the water content. In summary, combined studies with determination of NGTs from fluid inclusions and additional stable isotope measurements can help to establish reasonable climate reconstructions from speleothem data.

Chapter 5

Summary and outlook

Summary

Before summarizing the results of the main objective, temperature determination via noble gas concentrations, the major advances in the related topics will be discussed.

As a first step, we investigated different methods to select suitable samples in advance. Using microscopic analysis, information about the inclusion size and distribution as well as about the fabric can be obtained. We found speleothems with the best properties to be of milky white appearance. This type of speleothem yields a high number of water-filled inclusions and rather few air-filled ones.

For the extraction of water and noble gases from the speleothems we tested several methods: squeezing in copper tubes, milling in a steel crusher and microwave treatment in evacuated vials. The microwave based extraction is not yet investigated in all details, but the first tests did not fulfil the expectations. Squeezing in copper tubes is not as efficient as crushing in a steel cylinder and, furthermore, not completely reproducible. The best results can be obtained using the steel crusher with a magnetically movable steel ball. This setup enables also stepwise extraction, which is of high importance for a large group of speleothems. Adapted to the extraction in the steel cylinder we constructed a special extraction line, including a setup for ultra-high vacuum preparation, pressure recording in different ranges (10^{-9} -10 mbar), to control the sample preparation, noble gas extraction and the water determination via pressure, and three inlets with parallel pumping lines for higher sample throughput (at least one sample per day). Based on the results of the methodological tests, we extracted the samples in the steel crusher using different steps, e.g. 5 strokes followed by 60 strokes and an optional heating step. The water liberated from the sample was then frozen into a cold finger and determined via measurement of the water vapour pressure in different volumes. The noble gases were measured in a static sector-field mass spectrometer by comparison with a diluted air standard. The achievable precision was 2 % in the case of the water determination, 1 % for the He, Ne, Ar and Kr measurement and 2% for the Xe measurement.

We applied the described extraction method to a set of speleothems from Bunker Cave, but also to stalagmites from Chile, Canada, Cuba, Oman and Austria. The most precise results have been achieved for the speleothems from the Bunker Cave. Multiple measurements on one growth layer of BU-U yielded temperatures (mean 2.9 °C) agreeing within their uncertainties. Furthermore, the typical uncertainty was only about 1 °C. The NGT of an undated soda straw from the Bunker Cave even was only charged with an uncertainty of 0.4 °C due to the very low air contribution to the noble gas signal. Several pieces from the younger Holocene stalagmite BU-1 resulted in coinciding noble gas temperatures of about 7 °C. From the stalagmite BU-2 the measurement of a single piece resulted in a reasonable noble gas temperature of about

5 °C for the according growth period (GIS 14). The NGTs obtained along the growth axis of BU-U revealed an interesting pattern, which is in agreement with the trend of the polar ice cores as well as marine and continental cores (pollen), and shows the high potential of this method. However, most of the other investigated speleothems yielded far too high contributions of noble gases from air-filled inclusions. They mask the temperature signal and make it difficult or impossible to obtain reasonable temperatures from a simple extraction method. Large air-filled inclusions are located between the grain boundaries. Therefore, it is possible to reduce the fraction of air-derived noble gases by stepwise crushing. Mainly, the inter-granular inclusions were opened in the first steps, in the subsequent steps the smaller water-filled inclusions were increasingly affected. Applying this technique to a speleothem from Oman (H12) with a high air-water volume ratio using simple extraction, a reasonable temperature (24 °C) in agreement with the cave temperature (23 °C - 26 °C) and an uncertainty of 4 °C was achieved. Further developments suggest the possibility to extend the method to samples with unfavourable properties and to further reduce the uncertainty.

The water content seems to reflect a certain correlation with precipitation and may deliver in some cases information about the palaeo-humidity. Based on published literature and own measurements a working hypothesis is presented for this correlation, namely that higher drip rates and faster stalagmite growth lead to more water-filled inclusions. Additionally, the radiogenic He can help to constrain the age estimates for very old speleothems. The low diffusivity ($2.4 \cdot 10^{-25} \text{ m}^2/\text{s}$ at 30 °C) supposes that quantitative extraction and measurement of He may enable the U/Th-He dating for calcite. Preliminary data showed an encouraging correlation between age and radiogenic He content.

In summary, a large set of successful gas extractions and measurements on speleothems proved the possibility of NGT determination using fluid inclusions in speleothems. All temperature differences obtained from different stalagmites from the Bunker Cave agreed with temperature changes stated in other studies. Not only the changes from the glaciation to interstadials correspond to the expected temperatures, but also the NGTs within the Holocene. They constrain the expected climatic stability in the last 8 kyr and give an upper limit for temperature changes of $\pm 2 \text{ °C}$ from the value of the 1960-1990 reference period. Even though this project was started only three years ago, already a large set of palaeoclimatically interesting conclusions can be drawn, also some beside the NGT information as e.g. of the water content. Improving this methods will certainly help to deliver new insights into the past climate, especially in combination with the stable isotope and trace element data.

Outlook

In the next measurement run tests with recent calcite precipitates or artificial speleothems should be performed. They could help to investigate the absolute accuracy of the NGTs from fluid inclusions in speleothems. Subsequently, a high resolution record may be established on a stalagmite or a set of speleothems covering the Holocene as well as glacial periods. The combination with stable isotopes and trace elements will not only help to disentangle different effects, which cause the changes in the stable isotope values, but furthermore deliver a more complete and also more precise picture of the past climate.

Some effort has to be made to further reduce the background in case of the hot extractions. However, the combination of this step with precedent crushing is supposed to be most promising. Optimization of pumping times as well as baking out of the crushing cell may help to diminish the disturbing background signal.

First analysis of the water content suppose this value to be a proxy for palaeo-humidity. Intensive measurement of other stalagmites has to be performed to verify this assumption. To establish the radiogenic He as a dating tool, the extraction procedure has to be modified towards a complete release of all noble gases. This may be achieved by a strong heating step at temperatures above 600 °C.

This work intended to investigate the feasibility of NGT determination on speleothem fluid inclusions. Summarizing all results shows that NGT calculation is possible and can yield low uncertainties down to values like in groundwater studies. This conclusion should encourage further work in this exciting field which, in all probability, will deliver important data for palaeoclimate studies.

Bibliography

- Aalbersberg, G. and Litt, T.: Multiproxy climate reconstructions for the Eemian and Early Weichselian, *Journal of Quaternary Science*, 13(5), 367–390, 1998.
- Abbott, W., Wolfe, B. B., Aravena, R., Wolfe, A. P., and Seltzer, G. O.: Holocene hydrological reconstructions from stable isotopes and paleolimnology, Cordillera Real, Bolivia, *Quaternary Science Reviews*, 19, 1801–1820, 2000.
- Aeschbach-Hertig, W.: *Helium and Tritium as Tracers for Physical Processes in Lakes*, Ph.D. thesis, Swiss Federal Institute of Technology, Zurich, 1994.
- Aeschbach-Hertig, W. and Kluge, T.: On the feasibility of applying the noble gas thermometer to fluid inclusions in speleothems, *Workshop Daphne, Innsbruck*, abstract, 2006.
- Aeschbach-Hertig, W., Peeters, F., Beyerle, U., and Kipfer, R.: Interpretation of dissolved atmospheric noble gases in natural waters, *Water Resources Research*, 35(9), 2779–2792, 1999.
- Aeschbach-Hertig, W., Peeters, F., Beyerle, U., and Kipfer, R.: Palaeotemperature reconstruction from noble gases in ground water taking into account equilibration with entrapped air, *Nature*, 405, 1040–1044, 2000.
- Aeschbach-Hertig, W., Stute, M., Clark, J. F., Reuter, R. F., and Schlosser, P.: A paleotemperature record derived from dissolved noble gases in groundwater of the Aquia Aquifer (Maryland, USA), *Geochimica et Cosmochimica Acta*, 66(5), 797–817, 2002.
- Alley, R. and Ágústsdóttir, A.: The 8k event: cause and consequences of a major Holocene abrupt climate change, *Quaternary Science Reviews*, 24(10-11), 1123–1149, 2005.
- Alley, R., Mayewski, P., Sowers, T., Stuiver, M., Taylor, K., and Clark, P.: Holocene climatic instability; a prominent, widespread event 8200 yr ago, *Geology*, 25(6), 483–486, 1997.
- Andrews, J. N. and Lee, D. J.: Inert gases in groundwater from the Bunter Sandstone of England as indicators of age and paleoclimatic trends, *Journal of Hydrology*, 41, 233–252, 1979.
- Andrié, C., Jean-Baptiste, P., and Merlivat, L.: Tritium and helium 3 in the northeastern Atlantic ocean during the 1983 Topogulf cruise, *Journal of Geophysical Research*, 93(C10), 12 511–12 524, 1988.
- Auer, A., Böhm, R., and Schöner, W.: Austrian long-term climate 1767 to 2000: Multiple instrumental climate time series from Central Europe, *Österreichische Beiträge zu Meteorologie und Geophysik*, Heft 25, Publ. 397, Zentralanstalt für Meteorologie und Geodynamik, Vienna, Austria, 2001.

- Badertscher, S. V.: Charakterisierung von Einschlüssen in Stalagmiten zur Bestimmung der Paläotemperatur, diploma thesis, Swiss Federal Institute of Technology, Zürich, 2007.
- Badertscher, S. V., Scheidegger, Y., Leuenberger, M., Nyfeler, P., Fleitmann, D., Wieler, R., and Kipfer, R.: Trace gas content in air inclusions in speleothems as new paleoenvironmental archive?, *Geophysical Research Abstracts*, 9, 06 252, 2007.
- Baker, A. and Smart, P. L.: Recent flowstone growth rates: Field measurements in comparison to theoretical predictions, *Chemical Geology*, 122, 121–128, 1995.
- Baker, A., Barnes, W. L., and Smart, P. L.: Variations in the discharge and organic matter content of stalagmite drip waters in Lower Cave, Bristol, *Hydrol.Process*, 11, 1541–1555, 1997.
- Baker, A., Genty, D., Dreybrodt, W., Barnes, W. L., Mockler, N. J., and Grapes, J.: Testing theoretically predicted stalagmite growth rate with recent annually laminated samples: Implications for past stalagmite deposition, *Geochimica et Cosmochimica Acta*, 62(3), 393–404, 1998.
- Baker, P. A., Seltzer, G. O., Fritz, S. C., Dunbar, R. B., Grove, M. J., Tapia, P. M., Cross, S. L., Rowe, H. D., and Broda, J. P.: The History of South American Tropical Precipitation for the Past 25,000 Years, *Science*, 291, 640–643, 2001.
- Baldini, J. U. L., McDermott, F., and Fairchild, I. J.: Spatial variability in cave drip water hydrochemistry: Implications for stalagmite paleoclimate records, *Chemical Geology*, 235, 390–404, 2006.
- Ballentine, C. J. and Burnard, P. G.: Production, Release and Transport of Noble Gases in the Continental Crust, In: Porcelli, D., C.J. Ballentine, R. Wieler(Eds) *Noble gases in geochemistry and cosmochemistry*, vol. 47, pp. 481–538, 2002.
- Ballentine, C. J. and Hall, C.: Determining paleotemperature and other variables by using an error-weighted, nonlinear inversion of noble gas concentrations in water, *Geochimica et Cosmochimica Acta*, 63(16), 2315–2336, 1999.
- Barrer, R. M., ed.: *Diffusion in and through solids*, Cambridge University Press, 1941.
- Barron, E. J.: A Warm, Equable Cretaceous: the Nature of the Problem, *Earth-Science Reviews*, 19, 305–338, 1983.
- Bender, M. L.: Helium-uranium dating of corals, *Geochimica et Cosmochimica Acta*, 37, 1229–1247, 1973.
- Beyerle, U., Purtschert, R., Aeschbach-Hertig, W., Imboden, D., Loosli, H. H., Wieler, R., and Kipfer, R.: Climate and groundwater recharge during the last glaciation in an ice-covered region, *Science*, 282, 731–734, 1998.
- Beyerle, U., Aeschbach-Hertig, W., Imboden, D. M., Baur, H., Graf, T., and Kipfer, R.: A mass spectrometric system for the analysis of noble gases and tritium from water samples, *Environmental Science and Technology*, 34, 2042–2050, 2000.
- BMLFUW: Bundesministerium für Land- und Forstwirtschaft, Umwelt und Wasserwirtschaft: Jahresbericht 2002 für die Wassergüte in Österreich, Wien, 2002.
- Bodnar, R. J. and Zolensky, M. E.: Fluid inclusions in meteorites. Are they useful, and why are they so hard to find?, *Meteoritics and Planetary Science*, 35, A29–A30, 2000.

- Böhlke, J. K. and Irwin, J. J.: Laser microprobe analyses of noble gas isotopes and halogens in fluid inclusions: Analyses of microstandards and synthetic inclusions in quartz, *Geochimica et Cosmochimica Acta*, 56, 187–201, 1992a.
- Böhlke, J. K. and Irwin, J. J.: Brine history indicated by argon, krypton, chlorine, bromine, and iodine analyses of fluid inclusions from the Mississippi Valley type lead-fluorite-barite deposits at Hansonburg, New Mexico, *Earth and Planetary Science Letters*, 110, 51–66, 1992b.
- Brázdil, R., Pfister, C., Wanner, H., Von Storch, H., and Luterbacher, J.: Historical Climatology In Europe, The State Of The Art, *Climate Change*, 70(3), 363–340, 2005.
- Bronstein, I. N., Semendjajew, K. A., Musiol, G., and Mühlig, H., eds.: *Taschenbuch der Mathematik*, vol. 5, Verlag Harri Deutsch, 2000.
- Brook, G. A., Rafter, M. A., Railsback, L. B., Sheen, S., and Lundberg, J.: A high-resolution proxy record of rainfall and ENSO since AD 1550 from layering in stalagmites from Anjohibe Cave, Madagascar, *The Holocene*, 9(6), 695–705, 1999.
- Brunauer, S., Emmet, B. H., and Teller, E.: Adsorption of gases in multimolecular layers, *Journal of the American Chemical Society*, 60(2), 309–319, 1938.
- Buhmann, D. and Dreybrodt, W.: The kinetics of calcite dissolution and precipitation in geologically relevant situations of karst areas - 1.open systems, *Chemical Geology*, 48, 189–211, 1985.
- Bunnell, D.: http://en.wikipedia.org/wiki/Image:Labeled_speleothems.jpg, 2006.
- Burnard, P. G., Stuart, F., and Turner, G.: C-He-Ar variations within a dunite nodule as a function of fluid inclusion morphology, *Earth and Planetary Science Letters*, 128, 243–258, 1994.
- Burns, S. J., Fleitmann, D., Matter, A., Neff, U., and Mangini, A.: Speleothem evidence from Oman for continental pluvial events during interglacial periods., *Geology*, 29(7), 623–626, 2001.
- Cabioch, G. and Ayliffe, L. K.: Raised Coral Terraces at Malakula, Vanuatu, Southwest Pacific, Indicate High Sea Level During Marine Isotope Stage 3, *Quaternary Research*, 56, 357–365, 2001.
- Cable, J. E., Bugna, G. C., Burnett, W. C., and Chanton, J. P.: Application of ^{222}Rn and CH_4 for assessment of groundwater discharge to the coastal ocean, *Limnology and Oceanography*, 41, 1347–1353, 1996.
- Clement, A. C., Seager, R., and Cane, M.: Suppression of El Niño during the Mid-Holocene by Changes in the Earths Orbit, *Paleoceanography*, 15(6), 731–737, 2000.
- Clever, H. L., ed.: *Krypton, xenon and radon - gas solubilities. Solubility data series*, vol. 2, Pergamon Press, Oxford, 1979.
- Cook, P. G., Love, A. J., Robinson, N., and Simmons, C. T.: Groundwater ages in fractured rock aquifers, *Journal of Hydrology*, 308, 284 – 301, 2005.
- Copeland, P., Watson, E. B., Urizar, S. C., Patterson, D., and Lapen, T. J.: Alpha thermochronology of carbonates, *Geochimica et Cosmochimica Acta*, 71, 4488 – 4511, 2007.

- Corbett, R., Dillon, K., Burnett, W. C., and Chanton, J.: Estimating the groundwater contribution into Florida Bay via natural tracers, Rn-222 and CH-4, *Limnology and Oceanography*, 45, 1546 – 1557, 2000.
- Crank, J., ed.: *The mathematics of diffusion*, vol. 2, Clarendon Pr., Oxford, 1994.
- Cruz, F. W., Burns, S. J., Karmann, I., Sharp, W. D., Vuille, M., Cardoso, A. O., Ferrari, J. A., Silva Dias, P. L., and Viana, O.: Insolation-driven changes in atmospheric circulation over the past 116,000 years in subtropical Brazil, *Nature*, 434, 63 – 66, 2005.
- Cruz, F. W., Burns, S. J., Jercinovic, M., Karmann, I., Sharp, W. D., and Vuille, M.: Evidence of rainfall variations in Southern Brasil from trace element ratios (Mg/Ca and Sr/Ca) in a Late Pleistocene stalagmite, *Geochimica et Cosmochimica Acta*, 71, 2250 – 2263, 2007.
- Curl, R. L.: Minimum diameter stalagmites, *Bulletin National Speleological Society of America (Nat. Speleol. Soc. Bull)*, 35, 1–9, 1973.
- Dansgaard, W., Johnson, S. J., Clausen, H. B., Dahl-Jensen, D., Gundestrup, N. S., Hammer, C. U., Hvidberg, C. S., Steffensen, J. P., Svelnbrörnsdottir, A. E., Jouzel, J., and Bond, G.: Evidence for general instability of past climate from a 250 kyr ice-core record, *Nature*, 364, 218–220, 1993.
- Davis, B. A. S., Brewer, S., Stevenson, A. C., Guiot, J., and contributors, D.: The temperature of Europe during the Holocene reconstructed from pollen data, *Quaternary Science Reviews*, 22, 1701–1716, 2003.
- Dennis, P. F., Rowe, P. J., and Atkinson, T. C.: The recovery and isotopic measurement of water from fluid inclusions in speleothems, *Geochimica et Cosmochimica Acta*, 65(5), 871–884, 2001.
- DWD: Deutscher Wetterdienst, webpages: s. www.dwd.de, 2008.
- Edwards, R. L., Cheng, H., Murrell, M. T., and Goldstein, S. J.: Protactinium-231 Dating of Carbonates by Thermal Ionization Mass Spectrometry: Implications for Quaternary Climate Change, *Science*, 276, 782–786, 1997.
- Fairchild, I., Frisia, S., A., B., and Tooth, A.: Speleothems, In: Nash, D.J. and McLaren, S.J.(Eds): *Geochemical Sediments and Landscapes*, Blackwells, Oxford, vol. 47, 2007.
- Fanale, F. and Kulp, J. L.: Helium in Limestone and Marble, *The American Mineralogist*, 46, 155–167, 1961.
- Farley, K. A.: (U-Th)/He Dating: Techniques, Calibrations, and Applications, In: Porcelli, D., C.J. Ballentine, R. Wieler(Eds) *Noble gases in geochemistry and cosmochemistry*, vol. 47, 2002.
- Farley, K. A., Kohn, B. P., and Pillans, B.: The effect of secular disequilibrium on (U-Th)/He systematics and dating of Quaternary volcanic zircon and apatite, *Earth and Planetary Science Letters*, 201, 117–125, 2002.
- Felis, T., Lohmann, G., Kuhnert, H., Lorenz, S. J., Scholz, D., Pätzold, J., Al-Rousan, A., and Al-Moghrabi, S. M.: Increased seasonality in Middle East temperatures during the last interglacial period, *Nature*, 429, 164–168, 2004.

- Fleitmann, D. and Burns, S. J.: Palaeoclimatic interpretation of high-resolution oxygen isotope profiles derived from annually laminated speleothems from Southern Oman, *Quaternary Science Reviews*, 23, 935–945, 2004.
- Fontes, J. C. and Garnier, J. M.: Determination of the initial ^{14}C activity of the total dissolved carbon: A review of the existing models and a new approach, *Water Resources Research*, 15, 399, 1979.
- Ford, D. and Williams, P., eds.: *Karst Hydrogeology and Geomorphology*, vol. 1, John Wiley and Sons, Chichester, 2007.
- Ford, D. and Williams, P. W., eds.: *Karst Geomorphology and Hydrology*, Chapman and Hall, London, 1989.
- Franke, H. W.: The theory behind stalagmite shapes, *Studies in Speleology*, 1, 89–95, 1965.
- Frappier, A., Sahagian, D., Gonzales, L. A., and Carpenter, S. J.: El Niño events recorded by stalagmite carbon isotopes, *Science*, 298, 565, 2002.
- Freundlich, H.: Über die Adsorption von Lösungen, *Zeitschrift für physikalische Chemie, Abteilung A*, 54, 385–457, 1907.
- Friedman, I. and O’Neil, J. R.: *Data of Geochemistry*, vol. 47, chap. KK, pp. 1–12, USGS Professional paper 440-KK, US Government Printing Office, Washington D.C., 1977.
- Friedrich, R.: Helium in polaren Eisschilden, diploma thesis, University of Heidelberg, 2003.
- Friedrich, R.: Grundwassercharakterisierung mit Umwelttracern: Erkundung des Grundwassers der Odenwald-Region sowie Implementierung eines neuen Edelgas-Massenspektrometersystems, Ph.D. thesis, University of Heidelberg, 2007.
- Frisia, S., Borsato, A., Fairchild, I. J., and McDermott, F.: Calcite fabrics, growth mechanisms, and environment of formation in speleothems from the Italian Alps and southwestern Ireland, *Journal of Sedimentary Research*, 70, 1183–1196, 2000.
- Frisia, S., Borsato, A., Preto, N., and McDermott, F.: Late Holocene annual growth in three Alpine stalagmites records the influence of solar activity and the North Atlantic Oscillation on winter climate, *Earth and Planetary Science Letters*, 216, 411–424, 2003.
- Gainon, F., Surbeck, H., and Zwahlen, F.: Natural radionuclides in groundwater as pollutants and as useful tracers, in: *Proceedings of the 12th Symposium on Water Rock Interaction, 31 July - 5 August 2007, Kunming, China*, edited by Bullen, T. and Wang, Y., publisher: Taylor and Francis Ltd, 2007.
- Galdenzi, S. and Maruoka, T.: Gypsum deposits in the Frasassi Caves, Central Italy, *Journal of Cave and Karst Studies*, 65(2), 111–125, 2003.
- Gams, J.: Contribution to morphometrics of stalagmites, *Proceedings of the 8th International Congress of Speleology, Bowling Green, Kentucky*, 8, 276–278, 1981.
- Gascoyne, M.: Paleoclimate determination from cave calcite deposits, *Quaternary Science Reviews*, 11, 609–632, 1992.
- Genty, D. and Quinif, Y.: Annually laminated sequences in the internal structure of some Belgian stalagmites-importance for paleoclimatology., *Journal of Sedimentary Research*, 66, 275–288, 1996.

- Genty, D., Baker, A., and Vokal, B.: Intra- and inter-annual growth rate of modern stalagmites, *Chemical Geology*, 176, 191–212, 2001.
- Genty, D., Plagnes, V., Causse, C., Cattani, O., Stievenard, M., Falourd, S., Blamart, D., Ouahdi, R., and Van-Exter, S.: Fossil water in large stalagmite voids as a tool for palaeo-precipitation reconstruction and palaeotemperature calculation, *Chemical Geology*, 184, 83–95, 2002.
- Goldstein, R. H. and Reynolds, J. T., eds.: *Systematics of fluid inclusions in diagenetic minerals*, SEPM Short Course 31, 1994.
- Gözlhäuser, T.: Laborexperimente zur diffusiven Ausgasung von Helium aus polarem Eis, diploma thesis, University of Heidelberg, 2008.
- Grebe, W.: Die Bunkerhöhle in Iserlohn-Letmathe (Sauerland), *Mitteilung des Verbands der deutschen Höhlen- und Karstforscher, München*, 39(2), 22–23, 1993.
- Grebe, W.: Zur aktuellen Ausdehnung der B7-Höhle, *Speläologisches Jahrbuch - Verein für Höhlenkunde in Westfalen, Iserlohn*, 14, 21–22, 1998.
- Grootes, P. M., Stuiver, M., White, J. M. C., Johnsen, S., and Jouzel, J.: Comparison of oxygen isotope record from the GSIP2 and GRIP Greenland ice cores, *Nature*, 366, 552–554, 1993.
- Gvozdev, V. V. and Tovbin, Y. K.: New method for calculation the adsorption of noble gases on amorphous surfaces, *Russian Chemical Bulletin*, 46(6), 1060–1069, 1997.
- Hakl, J.: Application of radon-222, as a natural tracer in environmental studies, Ph.D. thesis, Lajos Kossuth University Debrecen, 1997.
- Hakl, J., Csige, I., Hunyadi, I., Várhegyi, A., and Géczy, G.: Radon transport in fractured porous media - experimental study in caves, *Environment International*, 22, Suppl.1, S433–S437, 1996.
- Hakl, J., Hunyadi, I., Csige, I., Lénárt, L., and Várhegyi, A.: Radon transport phenomena studied in karst caves - international experiences on radon levels and exposures, *Radiation Measurements*, 28 (1-6), 675–684, 1997.
- Hakl, J., Hunyadi, I., Csige, I., Géczy, G., and Bolner-Takács, K.: Site-specific radon regimes of a cave system, *Il Nuovo Cimento*, 22 C (3-4), 471–474, 1999.
- Hammerschmidt, E., Niggemann, S., Grebe, W., Oelze, R., Brix, M. R., and Richter, D.: Höhlen in Iserlohn, *Schriften zur Karst- und Höhlenkunde in Westfalen*, 1, 1–154, 1995.
- Haq, B. U., Hardenbol, J., and Vail, P. R.: Mesozoic and Cenozoic chronostratigraphy and cycles of sea-level change, In: Wilgus, C. K., Hastings, B. S., Kendall, C. G. S. C., Posamentier, H. W., Ross, C. A., van Wagoner, J. C. (Eds) *Sea-level changes: an integrated approach* SEPM Spec. Publ., 42, 72–108, 1988.
- Harmon, R. S., Schwarcz, H. P., and O’Neil, J. R.: D/H ratios in speleothem fluid inclusions: a guide to variations in the isotopic composition of meteoric precipitation?, *Earth and Planetary Science Letters*, 42, 254–266, 1979.
- Heaton, T. H. E. and Vogel, J. C.: Gas concentrations and ages of groundwaters in Beaufort Group sediments, South Africa, *Water SA*, 5 (4), 160–170, 1979.

- Heaton, T. H. E. and Vogel, J. C.: "Excess-Air" in groundwater, *Journal of Hydrology*, 50, 201–216, 1981.
- Hellstrom, J., Woodhead, J., Drysdale, R., Couchoud, I., and Zanchetta, G.: U-Th, U-Pb and U-U dating of the Corchia Cave speleothems: a continuous 1 Ma chronology, *Geophysical Research Abstracts*, 10, EGU2008–A–11 591, 2008.
- Heusser, C. J., Streeter, S. S., and Stuiver, M.: Temperature and precipitation record in southern Chile extended to $\approx 43'000$ yr ago, *Nature*, 294, 65–67, 1981.
- Hoehn, E. and von Gunten, H. R.: Radon in groundwater - a tool to assess infiltration from surface waters to aquifers, *Water Resources Research*, 25(8), 1795–1803, 1989.
- Holocher, J., Peeters, F., Aeschbach-Hertig, W., Hofer, M., Brennwald, M., Kinzelbach, W., and Kipfer, R.: Experimental investigations on the formation of excess air in quasi-saturated porous media, *Geochimica et Cosmochimica Acta*, 66(23), 4103–4117, 2002.
- Holzhauser, H., Magny, M., and Zumbühl, H. J.: Glacier and lake-level variations in west-central Europe over the last 3500 years, *The Holocene*, 15(6), 789–801, 2005.
- Johnsen, S., Dahl-Jensen, D., Gundestrup, N., Steffensen, P., Clausen, H. B., Miller, H., Asson-Delmotte, V., Sveinbjörnsdóttir, A., and White, J.: Oxygen isotope and palaeotemperature records from six Greenland ice-core stations: Camp Century, Dye-3, GRIP, GISP2, Renland and NorthGRIP, *Journal of Quaternary Science*, 16 (4), 299–307, 2001.
- Jones, P. D. and Moberg, A.: Hemispheric and Large-Scale Surface Air Temperature Variations: An Extensive Revision and an Update to 2001, *Journal of Climate*, 16, 206–223, 2003.
- Kaufmann, G.: Stalagmite growth and palaeo-climate: the numerical perspective, *Earth and Planetary Science Letters*, 214, 251–266, 2003.
- Kawamura, K., Parrenin, F., Lisiecki, L., Uemura, R., Vimeux, F., Severinghaus, J. P., Hutterli, M. A., Nakazawa, T., Aoki, S., Jouzel, J., Raymo, M. E., Matsumoto, K., Nakata, H., Motoyama, H., Fujita, S., Goto-Azuma, K., Fujii, Y., and Watanabe, O.: Northern Hemisphere forcing of climatic cycles in Antarctica over the past 360,000 years, *Nature*, 448, 912–917, 2007.
- Kelley, S., Turner, G., Butterfield, A., and Shepherd, T.: The source and significance of argon isotopes in fluid inclusions from areas of mineralization, *Earth and Planetary Science Letters*, 79, 303–318, 1986.
- Kendall, A. and Broughton, P.: Origin of fabrics in speleothems composed of columnar calcite crystals, *Journal of Sedimentary Petrology*, 48(2), 519–538, 1978.
- Kilian, R., Schimpf, D., Mangini, A., Spötl, C., Kronz, A., and Arz, H.: High resolution precipitation and wind record from the Southern Hemisphere Westerly Zone, based on speleothem proxies., *Geophysical Research Abstracts*, 10, EGU2008–A–10 551, 2008.
- Kloppmann, W., Dever, L., and Edmunds, W. M.: Residence time of Chalk groundwaters in the Paris Basin and the North German Basin: a geochemical approach, *Applied Geochemistry*, 13, 593–606, 1998.
- Klotz, W., Guiot, J., and Mosbrugger, V.: Continental European Eemian and early Wrmian climate evolution: comparing signals using different quantitative reconstruction approaches based on pollen, *Global and Planetary Change*, 36 (4), 277–294, 2003.

- Kluge, T. and Aeschbach-Hertig, W.: Noble gas measurement on fluid inclusions in stalagmites, In: Lippmann-Pipke, J. and Aeschbach-Hertig, W.(Eds) *4th Mini Conference on Noble Gases in the Hydrosphere and in Natural Gas Reservoirs - abstract volume*, doi 10.2312/GFZ.mga.050, GFZ Potsdam, Germany, 2007.
- Kluge, T., Ilmberger, J., von Rohden, C., and Aeschbach-Hertig, W.: Tracing and quantifying groundwater inflow into lakes using radon-222, *Hydrology and Earth System Sciences*, 11, 1621–1631, 2007.
- Kluge, T., Marx, T., Scholz, D., Niggemann, S., Mangini, A., and Aeschbach-Hertig, W.: A new tool for palaeoclimate reconstruction: Noble gas temperatures from fluid inclusions in speleothems, *Earth and Planetary Science Letters*, 269, 407–414, 2008.
- Kolodny, Y., Bar-Matthews, M., Ayalon, A., and McKeegan, K. D.: A high spatial resolution $\delta^{18}\text{O}$ profile of a speleothem using an ion microprobe, *Chemical Geology*, 197, 21–28, 2003.
- Krawczyk, W. E. and Ford, D. C.: Correlating specific conductivity with total hardness in gypsum karst waters., *Earth Surface Processes and Landforms*, 32, 612–620, 2007.
- Kukla, G. J., Bender, M. L., de Beaulieu, J., Bond, G., Broecker, W. S., Cleveringa, P., Gavin, J. E., Herbert, T. D., Imbrie, J., Jouzel, J., Keigwin, L. D., Knudsen, K., McManus, J. F., Merkt, J., Muhs, D. R., Müller, H., Poore, R. Z., Porter, S. C., Seret, G., Shackleton, N. J., Turner, C., Tzedakis, P. C., and Winograd, I. J.: Last interglacial climates, *Quaternary Research*, 58 (1), 2–13, 2002.
- Küster, F.: Beiträge zur Molekulargewichtsbestimmung an "festen" Lösungen, *Zeitschrift für physikalische Chemie*, 13, 445–458, 1894.
- Langmuir, I.: The constitution and fundamental properties of solids and liquids. Part I. Solids, *Journal of the American Chemical Society*, 38(11), 2221–2295, 1916.
- Langmuir, I.: The adsorption of gases on plane surfaces of glass, mica and platinum, *Journal of the American Chemical Society*, 40(9), 1361–1403, 1918.
- Leya, I. and Wieler, R.: Nucleogenic production of Ne isotopes in Earth's crust and upper mantle induced by alpha particles from the decay of U and Th, *Journal of Geophysical Research*, 104, 15 439–15 450, 1999.
- Lippolt, H. J., Leitz, M., Wernicke, R. S., and Hagedorn, B.: (Uranium + thorium)/helium dating of apatite: experience with samples from different geochemical environments., *Chemical Geology (Isotope Geoscience Section)*, 112, 179–191, 1994.
- Loosli, H., Aeschbach-Hertig, W., Barbecot, F., Blaser, P., Darling, W., Dever, L., Edmunds, W., Kipfer, R., Purtschert, R., and Walraevens, K.: Isotopic methods and their hydro-geochemical context in the investigation of palaeowaters, In: Edmunds, W.M., Milne, C.J. (Eds.) *Palaeowaters in Coastal Europe: evolution of groundwater since the late Pleistocene*, vol. 189, pp. 193–212, Geol. Soc. Special Publication, Geological Society of London, London, 2001.
- Lucas, L. and Unterwiesing, M. P.: Comprehensive Review and Critical Evaluation of the Half-Life of Tritium, *Journal of Research of the National Institute of Standards and Technology*, 105(4), 541–549, 2000.

- Marx, T.: Weiterentwicklung des Mess- und Extraktionssystems zur Bestimmung von Edelgastemperaturen aus Speläothemen, diploma thesis, Institute of Environmental Physics, University of Heidelberg, 2008.
- Matsubara, K., Matsuda, J., Nagao, K., Kita, I., and Taguchi, S.: Xe in amorphous silica: A new thermometer in geothermal systems, *Geophysical Research Letters*, 15, 657–660, 1988.
- Mattey, D., Lowry, D., Duffet, J., Hodge, E., and Frisia, S.: A 53 year seasonally resolved oxygen and carbon isotope record from a modern Gibraltar speleothem: reconstructed drip water and relationship to local precipitation, *Earth and Planetary Science Letters*, 269, 80–95, 2008.
- Matthews, A., Ayalon, A., and Bar-Matthews, M.: D/H ratios of fluid inclusions in Soreq Cave (Israel) speleothem as a guide to the eastern Mediterranean Meteoric Line relationship in the last 120 ky, *Chemical Geology*, 166, 183–191, 2000.
- Mazor, E., ed.: *Chemical and isotopic groundwater hydrology - The applies approach*, vol. 2, Dekker, New York, 1997.
- Mazor, E. and Bosch, A.: Helium as a semi-quantitative tool for groundwater dating in the range of 10^4 to 10^8 years., *Consultants meeting on isotopes of noble gases as tracers in environmental studies*, IAEA, Vienna, 305 p., 1992.
- McDermott, F.: Palaeo-climate reconstruction from stable isotope variations in speleothems: a review, *Quaternary Science Reviews*, 23, 2004.
- McDermott, F., Mattey, D., and Hawkesworth, C.: Centennial-scale Holocene climate variability revealed by a high-resolution speleothem ^{18}O record from S.W. Ireland, *Science*, 294, 1328–1331, 2001.
- McDermott, F., Schwarcz, H., and Rowe, P. J.: Isotopes in Speleothems, In: M.J. Leng (Ed.) *Isotopes in palaeoenvironmental research*, Springer Verlag, Dordrecht, 2006.
- McGarry, S., Bar-Matthews, M., Maathews, A., Vaks, A., and Ayalon, A.: Constraints on hydrological and paleotemperature variations in the eastern Mediterranean region in the last 140 ka given by the δD values of speleothem fluid inclusions, *Quaternary Science Reviews*, 23, 901–918, 2004.
- Mercury, L., Pini, D. L., and Zeyen, H.: The effect of the negative pressure of capillary water on the atmospheric noble gas solubility in ground water on palaeotemperature reconstruction, *Earth and Planetary Science Letters*, 223, 147–161, 2004.
- Moberg, A., Sonechkin, D., Holmgren, K., Datsenko, N. M., and Karlén, W.: Highly variable Northern Hemisphere temperatures reconstructed from low- and high-resolution proxy data, *Nature*, 433, 613–617, 2005.
- Munakata, K., Kanjo, S., Yamatsuki, S., Koga, A., and Ianovski, D.: Adsorption of noble gases on silver-mordenite, *Journal of Nuclear Science and Technology*, 40(9), 695–697, 2003.
- Musset, A. E.: Diffusion Measurements and the Potassium-Argon Method of Dating, *Geophys. J. R. astr. Soc.*, 18, 257–303, 1968.
- Neff, U.: *Massenspektrometrische Th/U-Datierung von Höhlensintern aus dem Oman: Klimaarchive des asiatischen Monsuns*, Ph.D. thesis, University of Heidelberg, 2001.

- Neff, U., Burns, S. J., Mangini, A., Mudelsee, M., Fleitmann, D., and Matter, A.: Strong coherence between solar variability and the monsoon in Oman between 9 and 6 kyr ago, *Nature*, 411, 290–293, 2001.
- Newman, B. D., Norman, D. I., Gundimenda, M., and Levy, S. S.: Understanding the genesis of nonmarine calcite deposits through quadrupole mass spectrometric analysis of fluid inclusion gases, *Chemical Geology*, 132, 205–213, 1996.
- Niggemann, S.: Climate related research on late postglacial stalagmites from massive limestone caves in the Sauerland, *Bochumer Geologische und Geotechnische Arbeiten*, 55, 5–129, 2000.
- Niggemann, S., Mangini, A., Mudelsee, M., Richter, D. K., and Wurth, G.: Sub-Milankovitch climatic cycles in Holocene stalagmites from Sauerland, Germany, *Earth and Planetary Science Letters*, 216, 539–547, 2003.
- Norman, D. I. and Musgrave, J. A.: N₂-Ar-He compositions in fluid inclusions: Indicators of fluid source, *Geochimica et Cosmochimica Acta*, 58, 1119–1131, 1994.
- Norris, R. D. and Röhl, U.: Carbon cycling and chronology of climatewarming during the Palaeocene/Eocene transition, *Nature*, 401, 775–778, 1999.
- Ojala, A. E. K., Alenius, T., Seppä, H., and Giesecke, T.: Integrated varve and pollen-based temperature reconstruction from Finland: evidence for Holocene seasonal temperature patterns at high latitudes, *The Holocene*, 18 (4), 529–538, 2008.
- Ozima, M. and Podosek, F. A., eds.: *Noble gas geochemistry*, Cambridge university press, 2nd edn., 2001.
- Pajon, J. M., Curtis, J., Tudhope, S., Metcalfe, S., Brenner, M., Guilderson, T., Chilcott, C., Grimm, E., and Hernández, I.: Isotope records from a stalagmite from Dos Anas cave in Pinar del Rio Province, Cuba. Palaeoclimatic implications, *conference contribution*, NURT-2006. V International Symposium on nuclear and related techniques. Havana, Cuba, April 3-7., 16 pp., 2006.
- Peeters, F., Beyerle, U., Aeschbach-Hertig, W., Holocher, J., Brennwald, M. S., and Kipfer, R.: Improving noble gas based paleoclimate reconstruction and groundwater dating using ²⁰Ne/²²Ne ratios, *Geochimica et Cosmochimica Acta*, 67, 587–600, 2003.
- Petit, J. R., Jouzel, J., Raynaud, D., Barkov, N., Barnola, J.-M., Basile, I., Bender, M., Chappellaz, J., Davisk, M., Delaygue, G., Delmotte, M., Kotlyakov, V. M., Legrand, M., Lipenkov, V., Lorius, C., Pépin, L., Ritz, C., Saltzman, E., and Stievenard, M.: Climate and atmospheric history of the past 420,000 years from the Vostok ice core, Antarctica, *Nature*, 399, 429–436, 1999.
- Pflitsch, A., Piasecki, J., and Niggemann, S.: Untersuchungen zum Einflu von Touristen auf das Höhlenklima in der Dechenhöhle/Iserlohn, *Mitteilungen des Verbands d.dt. Höhlen- und Karstforschung*, 16, 45–48, 2000.
- Plummer, L. N., Wigley, T. M., and Parkhurst, D. L.: The kinetics of calcite dissolution in CO₂-water systems at 5 °C to 60 °C and 0.0 to 1.0 atm CO₂, *American Journal of Science*, 278, 179–216, 1978.
- Podosek, F. A., Honda, M., and Ozima, M.: Sedimentary noble gases, *Geochimica et Cosmochimica Acta*, 44, 1875–1884, 1980.

- Polyak, V., Hill, C., and Asmerom, Y.: Age and Evolution of the Grand Canyon Revealed by U-Pb Dating of Water Table Type Speleothems, *Science*, 319, 1377–1380, 2008.
- Porcelli, D., Ballentine, C. J., and R. Wieler: An overview of noble gas geochemistry and cosmochemistry, In: Porcelli, D., C.J. Ballentine, R. Wieler (Eds) *Noble gases in geochemistry and cosmochemistry*, vol. 47, pp. 1–17, 2002.
- Rein, B.: How do the 1982/83 and 1997/98 El Niños rank in a geological record from Peru?, *Quaternary International*, 161, 56–66, 2007.
- Rice, S. B.: *The Development of a Method for the Extraction and Measurement of Noble Gases from Fluid Inclusions in Samples of Calcium Carbonate*, master thesis, Institute of Environmental Physics, University of Heidelberg, 2004.
- Richards, D. A. and Dorale, J. A.: U-series chronology and environmental applications of speleothems, In: Bourdon, B., Henderson, G.M., Lundstrom, C.C., Turner, S.P. (Eds) *Uranium-Series Geochimistry*, vol. 52, Reviews in Mineralogy, pp. 407–460, 2003.
- Richards, D. A., Bottrell, S. H., Cliff, R. A., Ströhle, K., and Rowe, P. J.: U-Pb dating of a speleothem of quaternary age, *Geochimica et Cosmochimica Acta*, 62 (23/24), 3683–3688, 1998.
- Roeckner, E., Buml, G., Bonaventura, L. Brokopf, R., Esch, M., Giorgetta, M., Hagemann, S., Kirchner, I., Kornbluh, L., Manzini, E., Rhodin, A., Schlese, U., Schultzweida, U., and Tompkins, A.: The atmospheric general circulation model ECHAM5. Part I: Model description, report, *Max-Planck-Inst. F. Meteor.*, 2003.
- Roedder, E.: Introduction to fluid inclusions, In: Roedder, E. (ed) *Reviews in mineralogy - Fluid inclusions*, vol. 12, pp. 1–10, Mineralogical Society of America, Blacksburg, 1984.
- Roedder, E., Ingram, B., and Hall, W. E.: Fluid inclusions. Extraction and quantitative analysis of inclusions in the milligram range, *Economic Geology and the Bulletin of the Society of Economic Geologists*, 58(3), 353–74, 1964.
- Rozanski, K. and Dulinski, M.: Deuterium content of European paleowaters as inferred from isotopic composition of fluid inclusions trapped in carbonate cave deposits, *Isotope Techniques in Water Resources Development*, IAEA, Vienna, 565–578, 1987.
- Scarsi, P.: Fractional extraction of helium by crushing of olivine and clinopyroxene phenocrysts: Effects on the $^3\text{He}/^4\text{He}$ measured ratio, *Geochimica et Cosmochimica Acta*, 64(21), 3751–3762, 2000.
- Scheidegger, Y.: Stalagmiten als mögliche Klimaarchive, diploma thesis, Swiss Federal Institute of Technology, Zurich, 2005.
- Scheidegger, Y., Brennwald, M., Heber, V., Wieler, R., and Kipfer, R.: A first convincing step towards the application of dissolved noble gases in speleothem fluid inclusions to determine local meteorological conditions in caves, *Geophysical Research Abstracts*, 8, EGU06–A–04 832, 2006.
- Scheidegger, Y., Badertscher, S. V., Driesner, T., Wieler, R., Heber, V., and Kipfer, R.: Microscopical speleothem calcite investigations proofing the existence of two different types of fluid inclusions, *Geophysical Research Abstracts*, 9, EGU–2007–A–06 374, 2007a.

- Scheidegger, Y., Kipfer, R., R., W., Badertscher, S., and Leuenberger, M.: Noble gases in fluid inclusions in speleothems., *abstract, Goldschmidt Conference, Köln*, 2007b.
- Scheidegger, Y., Kluge, T., Kipfer, R., and Aeschbach-Hertig, W.: Paleotemperature reconstruction using noble gas concentrations in speleothem fluid inclusions, *Pages Newsletter*, submitted, 2008.
- Schlosser, P., Stute, M., Dörr, H., Sonntag, C., and Münnich, K. O.: Tritium/³He-dating of shallow groundwater, *Earth and Planetary Science Letters*, 89, 353–362, 1988.
- Schwarcz, H. P.: Geochronology and isotope geochemistry of speleothems, In: Fritz, P. and Fontes, J. Ch.(Eds) *Handbook of Environmental Isotope Geochemistry*, pp. 271–303, Elsevier, Amsterdam, 1986.
- Schwarcz, H. P., Harmon, S., Thompson, P., and Ford, D. C.: Stable isotope studies of fluid inclusions of speleothems and their paleoclimatic significance, *Geochimica et Cosmochimica Acta*, 40, 657–665, 1976.
- Seppä, H. and Birks, H. J. B.: July mean temperature and annual precipitation trends during the Holocene in the Fennoscandian tree-line area: pollen-based climate reconstructions, *The Holocene*, 11(5), 527–539, 2001.
- Serefiddin, F., Schwarcz, H. P., and Ford, D. C.: Palaeotemperature reconstruction using isotopic variations in speleothem fluid inclusion water, *Geochimica et Cosmochimica Acta*, 66, 697, 2002.
- Siegenthaler, U., Stocker, T. F., Monnin, E., Lüthi, D., Schwander, J., Stauffer, B., Raynaud, D., Barnola, J., Fischer, H., Masson-Delmotte, V., and Jouzel, J.: Stable Carbon Cycle Climate Relationship During the Late Pleistocene, *Science*, 1313 - 1317, 697, 2005.
- Solomon, D. K., Poreda, R. J., Schiff, S. L., and Cherry, J. A.: Tritium and helium³ as groundwater age tracers in the Borden aquifer, *Water Resources Research*, 28(3), 741–755, 1992.
- Spahni, R., Chappellaz, J., Stocker, T. F., Loulergue, L., Hausammann, G., Kawamura, K., Flückiger, J., Schwander, J., Raynaud, D., Masson-Delmotte, V., and Jouzel, J.: Atmospheric Methane and Nitrous Oxide of the Late Pleistocene from Antarctic Ice Cores, *Science*, 310, 1317–1321, 2005.
- Spoetl, C. and Mangini, A.: Stalagmite from the Austrian Alps reveals Dansgaard Oeschger events during isotope stage 3: Implications for the absolute chronology of Greenland ice cores, *Earth and Planetary Science Letters*, 203, 507–518, 2002.
- Spoetl, C., Fairchild, I. J., and Tooth, A. F.: Cave air control on dripwater geochemistry, Obir Caves (Austria): Implications for speleothem deposition in dynamically ventilated caves, *Geochimica et Cosmochimica Acta*, 69(10), 2451–2468, 2005.
- Stuart, F. M. and Turner, G.: The abundance and isotopic composition of the noble gases in ancient fluids, *Chemical Geology (Isotope Geoscience Section)*, 101, 97–109, 1992.
- Stuart, F. M., Burnard, P. G., Taylor, R. P., and Turner, G.: Resolving mantle and crustal contributions to ancient hydrothermal fluids: He-Ar-isotopes in fluid inclusions from Dae Hwa W-Mo mineralisation, South Korea, *Geochimica et Cosmochimica Acta*, 59 (22), 4663–4673, 1995.

- Stute, M. and Deák, J.: Environmental isotope study (^{14}C , ^{13}C , ^{18}O , D, noble gases) on deep groundwater circulation systems in Hungary with reference to paleoclimate, *Radiocarbon*, 31, 902–918, 1989.
- Stute, M. and Schlosser, P.: Principles and applications of the noble gas paleothermometer, *Climate Change in Continental Isotopic Records*, 78, 89–100, 1993.
- Stute, M. and Sonntag, C.: Paleotemperatures derived from noble gases dissolved in groundwater and in relation to soil temperature., *Isotopes of noble gases as tracers in environmental studies*, Vienna, IAEA, 111–122, 1992.
- Stute, M., Schlosser, P., Clark, J. F., and Broecker, W. S.: Paleotemperatures in the Southwestern United States derived from noble gases in ground water, *Science*, 256, 1000–1003, 1992.
- Stute, M., Forster, M., Frischkorn, H., Serejo, A., Clark, J. F., Schlosser, P., Broecker, W. S., and Bonani, G.: Cooling of Tropical Brazil ($5\text{ }^{\circ}\text{C}$) during the Last Glacial Maximum, *Science*, 269, 379–383, 1995.
- Swann, G. E. A., Mackay, A. W., Leng, M. J., and Dernory, F.: Climatic change in Central Asia during MIS 3/2: a case study using biological responses from Lake Baikal, *Global and Planetary Change*, 46, 1-4, 235–253, 2005.
- Szabo, Z. and Rice, D. E.: Age dating of shallow groundwater with chlorofluorocarbons, tritium/helium 3, and flow path analysis, southern New Jersey coastal plain, *Water Resources Research*, 32(4), 1032–1038, 1996.
- Taylor, K. C., Mayewski, P. A., Alley, R. B., Brook, E. J., Gow, A. J., Grootes, P. M., Meese, D. A., Saltzman, E. S., Severinghaus, J. P., Twickler, M. S., White, J. W. C., Whitlow, S., and Zielinski, G. A.: The Holocene Younger Dryas Transition recorded at Summit, Greenland, *Science*, 278, 825–827, 1997.
- Taylor, P. M. and Chafetz, H. S.: Floating rafts of calcite crystals in cave pool, Central Texas, U.S.A.: crystal habit vs. saturation state, *Journal of Sedimentary Research*, 74(3), 328–341, 2004.
- TJlab: Thomas Jefferson National Accelerator Facility - Office of Science Education, <http://education.jlab.org/itselemental/ele091.html>, 2008.
- Torgersen, T., Kennedy, B. M., and van Soest, M. C.: Diffusive Separation of Noble Gases by adsorption and throat constrictions: Explaining Noble Gas patterns in Sedimentary Rocks, *American Geophysical Union, Fall Meeting 2002*, pp. abstract #V52B–1291, 2002.
- Träumner, K.: Inbetriebnahme, Tests und erste Anwendungen einer neuen Aufbereitungslinie zur massenspektrometrischen Messung von Edelgasen aus Grundwasser- und Stalagmitproben, diploma thesis, University of Heidelberg, 2005.
- Trieloff, M., Kunz, J., and Allègre, C. J.: Noble gas systematics of the Réunion mantle plume source and the origin of primordial noble gases in Earth's mantle, *Earth and Planetary Science Letters*, 200, 297–313, 2001.
- Turner, G. and Bannon, M. P.: Argon isotope geochemistry of inclusion fluids from granite-associated mineral veins in southwest and northeast England, *Geochimica et Cosmochimica Acta*, 56, 227–243, 1992.

- Viau, A. E., Gajewski, K., Sawada, M. C., and Fines, P.: Millennial-scale temperature variations in North America during the Holocene, *Journal of Geophysical Research*, 111, 2006.
- Vollweiler, N., Scholz, D., Mühlinghaus, C., Mangini, A., and Spötl, C.: A precisely dated climate record for the last 9 kyr from three high alpine stalagmites, Spannagel Cave, Austria, *Geophysical Research Letters*, 33, 2006.
- von Antropoff, A.: Untersuchungen über die Adsorption von Gasen von kleinsten bis zu höchsten Drücken, *Kolloid-Zeitschrift*, 137(2/3), 105–108, 1954.
- Walker, J., Cliff, R. A., and Latham, A. G.: U-Pb Isotopic Age of the StW 573 Hominid from Sterkfontein, South Africa, *Science*, 314, 1592–1594, 2006.
- Wang, Y., Cheng, H., Edwards, R. L., Kong, X., Shao, X., Chen, S., Wu, J., Jiang, X., Wang, X., and An, Z.: Millennial- and orbital-scale changes in the East Asian monsoon over the past 224,000 years, *Nature*, 451, 1090–1093, 2008.
- Wedepohl, K. H.: The composition of the continental crust, *Geochimica et Cosmochimica Acta*, 59(7), 1217–1232, 1995.
- Weigel, F.: Radon, *Chemiker-Zeitung*, 102, 287–299, 1978.
- Weiss, R. F.: The solubility of nitrogen, oxygen and argon in water and seawater, *Deep-Sea Research*, 17, 721–735, 1970.
- Weiss, R. F.: Solubility of helium and neon in water and seawater, *Journal of Chemical and Engineering Data*, 16(2), 235–241, 1971.
- Weiss, R. F. and Kyser, T. K.: Solubility of krypton in water and seawater, *Journal of Chemical and Engineering Data*, 23(1), 69–72, 1978.
- Wernicke, R. S. and Lippolt, H. J.: Dating of vein Specularite using internal (U+Th)/4He isochrons, *Geophysical Research Letters*, 21(5), 345–348, 1994.
- White, W.: Cave minerals and speleothems In: Ford, T.D. and Cullingford, C.H. (Eds) *The science of speleology*, pp. 267–327, Academic Press, London, 1976.
- Wilkinson, J. J.: Fluids in hydrothermal ore deposits, *Lithos*, 55, 229–272, 2001.
- WMO: World Meteorological Organization, webpages: s. www.wmo.ch, 2008.
- Wolf, R. A., Farley, K. A., and Silver, L. T.: Helium diffusion and low-temperature thermochronometry of apatite, *Geochimica et Cosmochimica Acta*, 60, 4231–4240, 1996.
- Yamada, M., Ohsawa, S., Matsuoka, H., Watanabe, Y., Brahmantyo, B., Maryunani, K. A., Tagami, T., Kitaoka, K., Takemura, K., and Yoden, S.: Derivation of travel time of limestone cave drip water using tritium/helium 3 dating method, *Geophysical Research Letters*, 35, 2008.
- Yamamoto, J., Kaneoka, I., Nakai, S., Kagi, H., Prikhod'ko, V. S., and Arai, S.: Evidence for subduction-related components in the subcontinental mantle from low $^3\text{He}/^4\text{He}$ and $^{40}\text{Ar}/^{36}\text{Ar}$ in mantle xenoliths from far eastern Russia, *Chemical Geology*, 207, 237–259, 2004.

- Yatsevich, I. and Honda, M.: Production of nucleogenic neon in Earth from natural radioactive decay, *Journal of Geophysical Research*, 102, 10 291–10 298, 1997.
- Yonge, C. J.: Stable isotope studies of water extracted from speleothems, Ph.D. thesis, McMaster University, Hamilton, Ontario, Canada, 1982.
- Zagwijn, W. H.: An analysis of Eemian climate in western and central Europe, *Quaternary Science Reviews*, 15, 451–469, 1996.
- Zhang, R., Schwarcz, H. P., Ford, D. C., Schroeder, F. S., and Beddows, P. A.: An absolute paleotemperature record from 10 to 6 ka inferred from fluid inclusion D/H ratios of a stalagmite from Vancouver Island, British Columbia, Canada, *Geochimica et Cosmochimica Acta*, 72(4), 1024–1026, 2008.
- Zolensky, M. E., Bodnar, R. J., Bogard, D. D., Garrison, D. H., Gibson, E. K., Nyquist, L. E., Reese, Y., Shih, C.-Y., and Wiesmann, H.: Asteroidal water within fluid inclusion-bearing halite in an H5 chondrite, *Science*, 285, 1377–1379, 1999.

Abbreviations

abbreviation	description
<i>A</i>	air/water volume ratio
AEW	air-equilibrated water
amu	atomic mass unit
asl	above sea level
ccSTP	gas amount in cm ³ at standard conditions (temperature $T = 273.15$ K, pressure $p = 1$ atm)
cps	counts per second, refers to the measurement of the electron multiplier
D/O-events	Dansgaard-Oeschger events relatively warm phases during the glacial periods
GIS	Greenland Interstadials
MIS3	Marine Isotope Stage 3
NGT	noble gas temperature
SEM	scanning electron microscope
TU	tritium units 1 TU corresponds to 1 atom of ³ H in 10 ¹⁸ atoms of ¹ H
UHV	ultra-high vacuum
‰ wt	fraction calculated with reference to the total weight 1 ‰ wt water content implies a total of 1 mg water in a calcite sample of 1 g

List of Figures

2.1	Crystal structure of carbonate species and possible ideal configurations	10
2.2	Selection of common speleothem forms	10
2.3	SEM of a calcite crystal grown under lab conditions	12
2.4	Pictures from different speleothem types	14
2.5	Thin section of a sample from the stalagmite H12	16
2.6	SEM image of a single calcite crystal	17
2.7	NGT uncertainty at given analytical error and air/water volume ratio	27
2.8	Molecular diffusion	30
2.9	Diffusion with fixed boundary values	30
2.10	Freundlich, Langmuir and BET isothermes	32
3.1	Location of caves, from which samples have been taken	38
3.2	Thin sections of the stalagmites H12 and OBI5	39
3.3	Thin sections of the flowstone H8Z from Hoti cave	40
3.4	Thin sections of the stalagmite CG from Cuba	41
3.5	BU-U thin section	41
3.6	BU-U thin section on a closer view.	42
3.7	High precision balance	44
3.8	Artificial water samples	45
3.9	Water determination and water collection efficiency	45
3.10	Effects of different handling on the determined weight.	46
3.11	Calibration curve at the extraction line in first extension stage	47
3.12	Pressure-water calibration curve in certain volumes	49
3.13	Limits of water determination by vapour pressure	50
3.14	Extraction line, first versions	52
3.15	Extraction line, final state	53
3.16	Extraction by crushing in a steel cylinder	54
3.17	Grain size distribution of crushing in the steel cylinder and copper tubes . . .	55
3.18	Extraction in copper tubes	57
3.19	Squeezing technique copper tubes	57
3.20	Copper tube squeezing blank	58
3.21	Heating blanks for copper tubes	59
3.22	Extraction by microwave treatment	60
3.23	Vials used for the microwave extraction	61
3.24	Effect of microwave heating - water released by this method	61
3.25	O-ring free System for extraction of microwave treated glass vials	62
3.26	Ar-40 microwave blanks	63
3.27	Three-isotope plot of the first microwave run	64
3.28	Three-isotope plot of the second microwave run	65

3.29	Effect of the heating duration on the air/water-volume ratio.	66
3.30	Stepwise heating experiment applied on a H12 sample	67
3.31	Kr vs. Ar noble gas concentrations of heated samples	68
3.32	Xe vs. Ne noble gas concentrations of heated samples	69
3.33	Influence of heating on different samples in run Beta	70
3.34	Pressure increase due to the water vapour during crushing	71
3.35	Stepwise crushing experiment, conducted with a sample from H12	72
3.36	Ar offset, measured during a stepwise crushing procedure	73
3.37	Xe signal per water amount in the case of stepwise heating	74
3.38	Noble gas concentrations for a stepwise heated sample	74
3.39	Kr-Ar noble gas concentrations for a stepwise heated sample	75
3.40	Xe-Ne noble gas concentrations for a stepwise heated sample	76
3.41	Combined procedure of crushing in steel cylinder and heating	76
3.42	Signal forms of He and Ne using different tuning parameters	86
3.43	Evolution of the neon signal due to different contributions	90
3.44	Neon signal for a sample with a low count rate	90
3.45	Neon signal for a sample with a high count rate	91
3.46	Ne and He signal trends for different count rates	92
3.47	^{40}Ar signal in the mass spectrometer	93
3.48	Magnet stability and impact on data evaluation	94
3.49	Results of artificial sample measurements	98
4.1	Map of the Bunker cave	100
4.2	Radon air activity concentrations in the Bunker cave	101
4.3	Map of the B7 cave	103
4.4	Map of the sampling points for dripwater	105
4.5	Dripwater sampling technique	106
4.6	Recent tritium values in Germany (Hof)	109
4.7	Seasonal tritium cycle at the Bunker Cave site	109
4.8	Stable isotope data from rain and dripwater at/in Bunker cave	110
4.9	Summarized result of the ^3H - ^3He -measurements.	111
4.10	Water content of different stalagmites	116
4.11	Air/water volume ratio from different stalagmite samples using a single step procedure	117
4.12	Water content along the growth axis of BU-1	118
4.13	Water content along the growth axis of BU-1, compared to a pollen record . .	119
4.14	Water content of the Chile stalagmite MA2	120
4.15	Comparison of the MA2 water content with the $\delta^{18}\text{O}$ values of the same sta- lagmite.	121
4.16	Comparison of the MA2 water content with the Mg/Ca value measured at the same stalagmite.	121
4.17	Comparison of the MA2 water content with an ENSO related marine sediment core.	122
4.18	Water content along the growth axis of BU-U	123
4.19	Factors influencing the amount of water-filled inclusions	125
4.20	Occurrence of water- and air-filled inclusions	128
4.21	Development of the air-water volume ratio using stepwise extraction	129
4.22	Reduction of the air-addition by stepwise methods at BU-1	130
4.23	Liberated water during the stepwise extraction	131
4.24	Deviations from expected signals at BU-1	132

4.25	Excess-Ne in the H12 samples plotted against A	133
4.26	He-content measured by Stuart and Turner (1992)	134
4.27	α -particles produced by ^{238}U and ^{226}Ra	136
4.28	Compilation of radiogenic He data for stalagmites with different ages.	139
4.29	Correlation between U/Th age and radiogenic He.	140
4.30	Correlation between U/Th ages and normalised radiogenic He	140
4.31	Stalagmite BU-U	142
4.32	Microscopic analysis of young BU-U part using polarized light	143
4.33	Kr-Ar noble gas concentrations for the Early Holocene BU-U samples	145
4.34	Xe-Ne noble gas concentrations for the Early Holocene BU-U samples	146
4.35	Temperature difference between the Early Holocene and Early Middle Ages	148
4.36	Measurement half of BU-1, sample locations	149
4.37	NGT for samples from BU-1	151
4.38	Stable isotope results for BU-1	152
4.39	measured pieces of BU-U	153
4.40	NGTs derived from the growth axis of BU-U	155
4.41	NGTs from the growth axis of BU-U compared to averaged $\delta^{18}\text{O}$ -values	157
4.42	NGTs from the growth axis of BU-U compared to continuous $\delta^{18}\text{O}$ values	157
4.43	NGTs from the growth axis of BU-U compared to $\delta^{13}\text{C}$ -values	158
4.44	$\delta^{13}\text{C}$ and $\delta^{18}\text{O}$ values along the growth axis of BU-U	159

List of Tables

2.1	Properties of different carbonate species	11
2.2	Atmospheric mixing ratios of noble gases	20
2.3	Noble gas concentrations of equilibrated water	21
3.1	Saturation vapour pressure of water respectively ice at different temperatures.	47
3.2	Blank of squeezing a copper tube once	59
3.3	Mean line blank and sample signals for the two microwave test series.	62
3.4	Samples measured in the second microwave run	63
3.5	Diluted standard - gas amounts	81
3.6	Calibration reproducibilities of the diluted and the undiluted standard	81
3.7	Mass spectrometer sensitivity	82
3.8	Typical blank values	84
3.9	Typical blank values in ccSTP	84
3.10	Double times ionized ^{40}Ar in Ar tuning	86
3.11	Double times ionized ^{40}Ar in He tuning	87
3.12	Neon isotope ratios in the case of different calibrations	88
3.13	Ar and CO_2 background	88
3.14	$^{40}\text{Ar}/^{36}\text{Ar}$ ratio	93
3.15	Artificial standard samples	97
3.16	Artificial standard samples - offset	97
4.1	Cave air mixing ratios in Bunker Cave - deviation from the atmosphere	102
4.2	Cave air mixing ratios in B7 Cave - deviation from the atmosphere	103
4.3	Dating of dripwater - results	108
4.4	Uncertainty of the water determination	115
4.5	Noble gas excess in different samples	133
4.6	The three natural decay chains	137
4.7	Exemplary calculation of the expected radiogenic He	138
4.8	BU-U, BU-1 and soda straw - samples	143
4.9	BU-U, BU-1 and soda straw - noble gas data	144
4.10	BU-U, BU1 and soda straw - results	147
4.11	BU-1 sample data	150
4.12	BU-1 results	150
4.13	BU-U sample data	154
4.14	BU-U results	154

Acknowledgments

Prof. Dr. Werner Aeschbach-Hertig und Prof. Dr. Augusto Mangini möchte ich für das Ermöglichen der interessanten Arbeit und der vielseitigen Unterstützung danken.

Im besonderem Maße möchte ich meinem Betreuer Prof. Dr. Werner Aeschbach-Hertig danken. Er hatte für Fragen immer ein offenes Ohr, bei Unsicherheiten weitergeholfen und in begeisternder Weise in das wissenschaftliche Arbeiten und in die Welt der Forschung eingeführt.

Prof. Dr. Augusto Mangini möchte ich dafür danken, dass er das Zweitgutachten der Arbeit übernahm und darüberhinaus bei fachlichen Fragen immer hilfreich zur Verfügung stand.

Den Mitgliedern der Arbeitsgruppe Aquatische Physik, sowie der "Speläogruppe" unter Prof. Dr. Augusto Mangini danke ich für die schöne Zeit am Institut, für die sehr produktive und angenehme Zusammenarbeit und für das Gefühl jeden Tag gern ins Institut zu kommen.

Dr. Ronny Friedrich, Dr. Laszlo Palscu und Martin Wieser danke ich ganz herzlich für ihre Unterstützung bei der Bedienung des Massenspektrometers und der zugehörigen Software. Darüberhinaus danke ich Martin für seine Bereitschaft an allen Expeditionen teilzunehmen und mich dabei in selbstloser Weise zu unterstützen, ob auf dem Willersinnweiher mit löchrigem Schlauchboot oder in Iserlohn bei 10-stündigen Touren durch schlammige Höhlen.

Im speziellen danke ich Thomas Marx für die hervorragende Zusammenarbeit. Nachdem ich ihn für das Thema interessieren konnte, hat er dem ganzen Projekt einen starken Impuls gegeben. Durch konstruktive, aber auch kontroverse Diskussionen und eine Reihe arbeitsintensiver Messungen sowie einiger interessanter Ideen konnten das Extraktions- und Messverfahren optimiert und eine Reihe erfolgreicher Messungen durchgeführt werden.

Dr. Johann Ilmberger danke ich für seine guten Ideen, seine engagierten Beiträge bei Diskussionen und dafür, dass er bei Fragen und Problemen immer ein offenes Ohr hatte.

Danken möchte ich auch Gerhard Zimnek, der unermüdlich für das Funktionieren der Technik des Massenspektrometers gesorgt und mir darüberhinaus sehr viel Arbeit mit der Bestellung von Ersatzteilen und neuen Komponenten abgenommen hat.

Dr. Ullrich Glasmacher danke ich für seine Unterstützung und die Bereitschaft seine Mikroskope für die Dünnschliffuntersuchungen an Stalagmiten zur Verfügung zu stellen. Darüberhinaus möchte ich H.P. Meyer, sowie J. Fillauer für die Dünnschliffherstellung danken.

Einen besonderen Dank möchte ich an Dr. Stefan Niggemann, sowie Rasmus Dreyer und weiteren Mitgliedern des Höhlenvereins Speläogruppe Letmathe richten. Ohne ihre Unterstützung wären die interessanten Probenahmen in der Dechen-, Bunker- und vor allem der B7-Höhle nicht möglich gewesen.

Dana Riechelmann danke ich für die gute Zusammenarbeit. Durch das Zuverfügungstellen von Messdaten und die Hilfe bei der Interpretation von Dünnschliffen und Kristallformen habe ich einen besseren Einblick in Entstehung und Verteilung von Fluid Inclusions bekommen.

Danken möchte ich allen, die bei der Interpretation einzelner Stalagmitdaten geholfen haben: Claudia Fensterer für das Beschaffen der Monitoring- und Höhlendaten zum Stalagmiten CG, Daniel Schimpf für das Bereitstellen der Isotopendaten, Monitoringwerte und Diskussionen bzgl. der MA-Stalagmiten aus Chile, Prof. Dr. Christoph Spötl für das Messen der Isotope am Stalagmiten BU-U und das Zuverfügungstellen einiger Proben aus der Spannagelhöhle, René Eichstädter und Dr. Dennis Scholz für Datierungen an diversen Stalagmiten und Dr. Stefan Niggemann für die Stalagmitprobe BU-U, die die ersten glaubwürdigen Edelgastemperaturen lieferte.

Für die hilfreichen Diskussionen und dafür, dass sie bei Fragen jederzeit ansprechbar waren, möchte ich mich ganz besonders bei Dr. Christoph von Rohden, Dr. Dennis Scholz und Dr. Andrea Schröder-Ritzrau bedanken. Danken möchte ich auch Daniela Polag für ihre Hilfe bei der Literatursuche und Fragen zur Kalzitherstellung.

Für das Korrekturlesen möchte ich mich bei Dr. Christoph von Rohden, Martin Wieser, Dr. Dennis Scholz und vor allem bei Helga Rietz für die hilfreichen Bemerkungen und Vorschläge bedanken.

Einen besonderen Dank möchte ich an diejenigen richten, die mich motiviert und auch in schwierigen Phasen unterstützt haben, insbesondere Andreas Meyer und Jörg Peschek. Danken möchte ich auch meinen ehemaligen Mitbewohnern aus dem 8.Stock. Sie haben mich motiviert nach der Diplomarbeit weiterzumachen. Außerdem haben sie mir durch die vielen gemeinsamen Aktivitäten geholfen in Phasen der Frustration den Mut nicht zu verlieren.

Im besonderen danken möchte ich auch meinen Eltern, Großeltern und meinem Bruder, die mich während des ganzen Studiums und darüber hinaus in jeder Hinsicht unterstützt haben.